NASA CR-159466
PWA-5558-12

(NASA-CR-159466) INSTRUMENTATION FOR MEASURING THE DYNAMIC PRESSURE ON ROTATING COMPRESSOR BLADES Final Report (Pratt and Whitney Aircraft) 182 p HC A09/MF A01 CSCL 14B G3/35

N79-12418

Unclas
38904

INSTRUMENTATION FOR MEASURING THE DYNAMIC PRESSURE ON ROTATING COMPRESSOR BLADES

by

H. P. Grant and G. A. Lanati

United Technologies Corporation
Pratt & Whitney Aircraft Group
Commercial Products Division

Prepared for

National Aeronautics and Space Administration

NASA-Lewis Research Center
Contract NAS3-20296

U.S. DEPARTMENT OF COMMERCE
National Technical Information Service

N79-12418

INSTRUMENTATION FOR MEASURING THE DYNAMIC PRESSURE ON ROTATING COMPRESSOR BLADES

H. P. GRANT, ET AL

UNITED TECHNOLOGIES CORPORATION
EAST HARTFORD, CONNECTICUT

SEPTEMBER 1978

NASA CR-159466
PWA-5558-12

(NASA-CR-159466) INSTRUMENTATION FOR MEASURING THE DYNAMIC PRESSURE ON ROTATING COMPRESSOR BLADES Final Report (Pratt and Whitney Aircraft) 182 p HC A09/MF A01 CSCL 14B G3/35
N79-12418
Unclas
38904

NASA

INSTRUMENTATION FOR MEASURING THE DYNAMIC PRESSURE ON ROTATING COMPRESSOR BLADES

by

H. P. Grant and G. A. Lanati

United Technologies Corporation
Pratt & Whitney Aircraft Group
Commercial Products Division

Prepared for

National Aeronautics and Space Administration

NASA-Lewis Research Center
Contract NAS3-20296

1. Report No.	2. Government Accession No.	3. Recipient's Catalog No.
NASA CR-159466		

4. Title and Subtitle	5. Report Date
INSTRUMENTATION FOR MEASURING THE DYNAMIC PRESSURE ON ROTATING COMPRESSOR BLADES	September 1978
	6. Performing Organization Code
7. Author(s)	8. Performing Organization Report No.
H. P. Grant and G. A. Lanati	PWA-5558-12
	10. Work Unit No.
9. Performing Organization Name and Address	
United Technologies Corporation Pratt & Whitney Aircraft Group Commercial Products Division East Hartford, Connecticut 06108	11. Contract or Grant No. NAS3-20296
	13. Type of Report and Period Covered
12. Sponsoring Agency Name and Address	Contractor Report
National Aeronautics and Space Administration Washington, D.C. 20546	14. Sponsoring Agency Code

15. Supplementary Notes

Project Manager, D. R. Englund, Airbreathing Engines Division, NASA-Lewis Research Center, Cleveland, Ohio 44135

16. Abstract

To establish the capability for measurement of oscillatory pressure on rotating blades, miniature fast response semiconductor strain gage pressure transducers (2mm x 0.33mm) were mounted in several configurations on thin titanium and steel compressor blades and subjected to pressure cycles from 1 to 310 kPa during static tests and spin tests. Static test conditions included 20°C to 150°C, 0 to 3000 tensile microstrain, -1000 to +1000 bending microstrain and ±650G vibration. The spin test conditions included 20°C to 82°C at 0 to 90,000G. Durability was excellent. Pressure transducer sensitivity changed by only a few percent over this range of environmental conditions. Noise signal due to oscillatory acceleration normal to the diaphragm was acceptable (0.33Pa/G). Noise signal due to oscillatory strain was acceptable (0.5 Pa/microstrain) when the transducer was mounted on a 0.05 mm rubber pad, with a total buildup of 0.38mm on the measure surface. Back mounting or partial recessing to eliminate buildup, increased the strain effect to 1.2 Pa/microstrain. Flush mounting within the blade to eliminate buildup reduced the strain effect, but required development of a special transducer shape. This transducer was not available in time for spin tests.

Unpredictable zero drift ±14 kPa ruled out the use of these mounting arrangements for accurate steady-state (D.C.) measurements on rotating blades.

The two best configurations fully developed and spin tested were then successfully applied in the NAS3-20606 rotating fan flutter program for quantitative measurement of oscillatory pressure amplitudes.

17. Key Words (Suggested by Author(s))	18. Distribution Statement
Rotating instrumentation, Fan instrumentation, Compressor instrumentation, Dynamic pressures, Pressure transducers	

19. Security Classif. (of this report)	20. Security Classif. (of this page)	21. No. of Pages	22. Price*
		174	

* For sale by the National Technical Information Service, Springfield, Virginia 22161

NASA-C-168 (Rev. 10-75)

FOREWORD

This document describes the work accomplished under the National Aeronautics and Space Administration (NASA) contract NAS3-20296 by the Commercial Products Division, Pratt & Whitney Aircraft Group of United Technologies Corporation. This report was prepared in accordance with contract requirements and is assigned the P&WA report number PWA-5558-12.

Appreciation is expressed to Mr. D. R. Englund, NASA Lewis Research Center Project Manager, for his technical advice and guidance. The following P&WA personnel are recognized for their contribution to the program: W. L. Anderson, experience in transducer configurations and design of rotating mechanisms; W. C. Mager, fabrication; and L. A. Davis, assistance in the spin pit tests. The assistance of Mr. John Kicks of Kulite Semiconductor Products, Inc. is also recognized.

TABLE OF CONTENTS

TABLE OF CONTENTS (Cont'd)

LIST OF ILLUSTRATIONS

LIST OF ILLUSTRATIONS (Cont'd)

LIST OF ILLUSTRATIONS (Cont'd)

LIST OF ILLUSTRATIONS (Cont'd)

LIST OF TABLES

SUMMARY

The program goal was to establish the capability for measuring the oscillatory component of pressure on the surface of compressor and fan blades during engine operation, particularly during flutter tests. This goal was accomplished using blade-mounted miniature fast-response (20 kHz) semi-conductor pressure transducers. The useful operating range includes pressures from 1 kPa (0.15 psi) to 310 kPa (45 psi), oscillatory pressure of 1 kPa (0.15 psi) or more, centripetal accelerations up to at least 90,000 G, temperatures up to 150°C (300°F), vibration amplitudes to at least 650 G, and surface strains to 3000 microstrain. Accuracy of measurement of oscillatory pressure is degraded typically by only about ± 3 percent due to the engine environment and noise signals due to oscillatory acceleration (vibration). Oscillatory strains are generally below + 0.1 kPa (± 0.015 psi).

In the first phase of this two-phase program, selected mounting arrangements were used to attach transducers to actual steel and titanium compressor blades which were then subjected to controlled static tensile, bending and vibration tests at a series of known pressures and temperatures. Output zero shift and change in transducer sensitivity due to each variable were determined for each mounting configuration.

In the second phase of the program, two transducer mounting arrangements were used to mount pressure transducers on a spin disk. Transducers were mounted with two different orientations relative to the centripetal acceleration vector. The disk and transducers were spun at selected centripetal accelerations, temperatures and pressures. The data were used to establish the small corrections to be applied to the pressure signals to account for the rotational effects.

All configurations tested were found to be durable. There were no failures at test among fourteen transducers tested, and changes in sensitivity with time were generally small under all test conditions.

The effects of acceleration and temperature on sensitivity were small and generally within predicted performance specifications.

The effects of oscillatory blade surface strains were important. Strain-induced output of hard-mounted transducers was 10 Pa per microstrain. Use of soft rubber mountings reduced this undesired output to levels between 0.2 and 2.0 Pa per microstrain depending on the mounting configuration used. The best strain isolation required a total surface buildup of 0.38 mm on the measured surface (with no machining of the blade surface) or a flush mount in a through hole in the blade. Mounting the transducers in a shallow recess in the measured surface or upside down on the non-measured surface increased the effects of strains. A flush mount in a through hole in the blade was most promising of all in static tests, but further development of the special transducers used in this configuration is required to reduce rejection rate to a reasonable level.

A secondary goal was to define the extent to which the system developed for the oscillatory pressure measurement might be used for steady state pressure measurement. The test program verified that these transducers, when blade mounted, are not suitable for accurate

steady-state pressure measurements because of unpredictable, random, slow, temporary zero drifts on the order of ± 14 kPa (2 psi) under engine operating conditions. This behavior does not affect the accuracy of oscillatory pressure measurements at frequencies above a few Hz.

The two configurations which were spin pit tested were used on fan blades which were operated successfully in an extensive rotating fan flutter program at Pratt & Whitney Aircraft in 1977. Initial results are presented, comparing the performance of the two mounting configurations in flutter and out of flutter.

SECTION 1.0

INTRODUCTION

1.1 PROGRAM OBJECTIVE

The primary goal of the program was to establish the capability for measuring the oscillatory component of pressure on the surfaces of compressor and fan blades during engine operation. A secondary goal was to define to what extent the system developed for oscillatory pressure measurement might be useable for steady state pressure measurement.

1.2 BACKGROUND

The measurement of the oscillatory component of pressure on the blade surfaces is central to the problem of selecting and confirming theoretical models for use in flutter analysis and prediction. Figure 1-1 is an example of some measurements at Pratt & Whitney Aircraft during a fan flutter test in 1975 in which blade-mounted pressure transducers showed oscillatory pressure amplitudes of about 1 kPa at the flutter frequency during a severe flutter. Such measurements could only be regarded as semi-quantitative, since the effects of the rotating environment on the pressure transducer were not well established. For example, the estimated effect of oscillatory G-loading on the transducer (based on theory and some nonrotating vibration tests), shown by the dashed curve in Figure 1-1, represents a considerable fraction of the total signal. The effects of the large centripetal acceleration, oscillatory accelerations due to vibration and steady state and oscillatory surface strains on both the sensitivity and output level were unknown. The present program was undertaken to establish the magnitude of all of these effects for each of several candidate mounting arrangements.

1.3 PREVIOUS DEVELOPMENT AT PRATT & WHITNEY AIRCRAFT

In previous in-house programs, Pratt & Whitney Aircraft had developed promising mounting techniques for strain isolation (Reference 1) and had worked closely with two manufacturers of semiconductor strain-gage pressure transducers beginning in 1971 to achieve improved durability and accuracy in the sensors.

Successful and repeatable qualitative pressure measurements on rotating compressor and fan blades had been obtained in four programs which are summarized in Table 1-I. Several additional programs were planned for 1977 and 1978.

In the latest case shown in Table 1-I, an advanced fan flutter program, the semiconductor strain gage sensors survived 15 hours at centripetal loadings up to 50,000 G on blades vibrating at 660 Hz through a peak-to-peak amplitude of 0.32 mm. Figure 1-2 shows the transducer mounting technique used in this program and Figure 1-3 shows the completed installation of eight semiconductor strain gage pressure transducers on one of the fan blades. Figure 1-4 shows a sample pressure signal during these tests and Figure 1-5 is a series of 68 spectra obtained in quick succession as the fan operating point was gradually changed from normal operation into flutter at constant fan speed. Similar data from a nearby strain gage is also shown in Figures 1-4 and 1-5 during this same time interval. Frequency and phase relationships are readily determined. The importance of even qualitative pressure measurements is clearly illustrated. In order to use these data for quantitative analysis of the detailed flutter mechanism, it is necessary first to translate the recorded information into pressure units and to subtract apparent pressures due to strain, temperature, and accelerations. The state-of-the-art was such that the uncertainty of the strain and acceleration effects was still the same order of magnitude as the oscillatory flutter pressure amplitudes indicated in Figures 1-4 and 1-5.

The effectiveness of several strain-isolation techniques used in mounting sensors was evaluated in simple tests at Pratt & Whitney Aircraft in 1971 (Reference 1). The best technique, shown in Figure 1-2, was thought to reduce the effect of 2000-microstrain - - approaching the yield point of the blade - - to approximately 0.1 kPa indicated pressure. This technique was used in mounting the sensors for the flutter tests, the results of which are shown in Figures 1-4 and 1-5.

In the development program listed in the third column of Table 1-I, an attempt was made to obtain a few definitive measurements of pure acceleration effects. One semiconductor strain gage transducer mounted as shown in Figure 1-2 was subjected to a controlled pressure environment by placing a small sealed housing over the sensor on the rotating surface, attaching a radial tube of adjustable length to the housing, and varying the rotational speed both to vary the pressure (due to centripetal forces) and to vary the centripetal acceleration in the plane parallel to the sensor diaphram. Sensor temperature was monitored during the test. Only one orientation of the sensor was investigated. The pressures were calculated from the equations of fluid mechanics, but were not controlled independently. The results indicated that the effects of acceleration up to 10,000 G were less than the 0.7 Pa per G suggested by the transducer manufacturer. However, the effects of acceleration rose rapidly to extremely high levels at 20,000 G. The experiment was found to be repeatable, but the results were still considered unreliable since neither orientation nor actual pressure used was controlled during the test. Flexing of the mounting fixture and large temperature gradients could easily have accounted for the curious results at the higher speeds.

Some other programs which have demonstrated useful measurements with surface-mounted pressure transducers on rotating or oscillating blades are described in Reference 2 (rotating fan at Hamilton Standard Division of United Technologies Corporation), Reference 3 (oscillating airfoils at United Technologies Research Center), and Reference 4 (oscillating airfoils at Detroit Diesel Allison Division). Quantitative measurements of effects of centripetal accelerations up to 11,000 G on semiconductor strain gage pressure transducers are presented in Reference 5.

1.4 PROGRAM

The specific capabilities desired in a system to satisfy the primary program goal were as follows:

1. Dynamic pressure amplitude (minimum):

   2 kPa (0.3 psi) peak-to-peak

2. Average pressure level:

   50 kPa (7 psia) to 310 kPa (45 psia)

3. Frequency range:

   75 Hz to 5000 Hz

4. Permissable blade surface buildup:

   Measured surface: 0.25 mm (0.010 inch)

   Non-measured surface: 0.50 mm (0.020 inch)

5. Pressure transducers:

   Semiconductor strain-gage type, selected for service at temperatures up to 150°C (300°F)

6. Operating temperature range:

   21°C (70°F) to 150°C (300°F) (transducer temperature)

7. Operating centripetal G loading:

   110,000 G maximum

A two-phase program was carried out, the first phase consisting of static tests (non-rotating) and the second phase consisting of spin tests.

In the first phase (static test) of the program, pressure transducers were mounted on compressor blades and subjected to tensile, bending and vibration tests at selected levels of temperature and pressure. Three different mounting configurations and two different blade materials were included. Since one specimen of each kind was tested, the total number of test items was six. The principal test conditions are summarized briefly in Table 1-II. The static test items, configuration, detailed static test program and procedures are described in Section 2. Some preliminary static tests not listed in Table 1-II were also performed to screen alternative configurations and to evaluate effects of light, chemical vapors, and small alterations in mounting procedure and shelf-life. These tests are also described in Section 2.

In the second phase (spin test) of the program, pressure transducers were mounted on a spin disk and subjected to centripetal loading tests at selected levels of temperature and pressure. Two different mounting configurations and two different orientations were included. A set of four specimens, one of each kind, was mounted on the spin disk. The principal spin test conditions are summarized briefly in Table 1-III. The spin test items and the detailed spin test program and procedures are described in Section 2.

Results of all tests (including some flutter application results) are presented in Section 3. Conclusions and recommendations are summarized in Section 4.

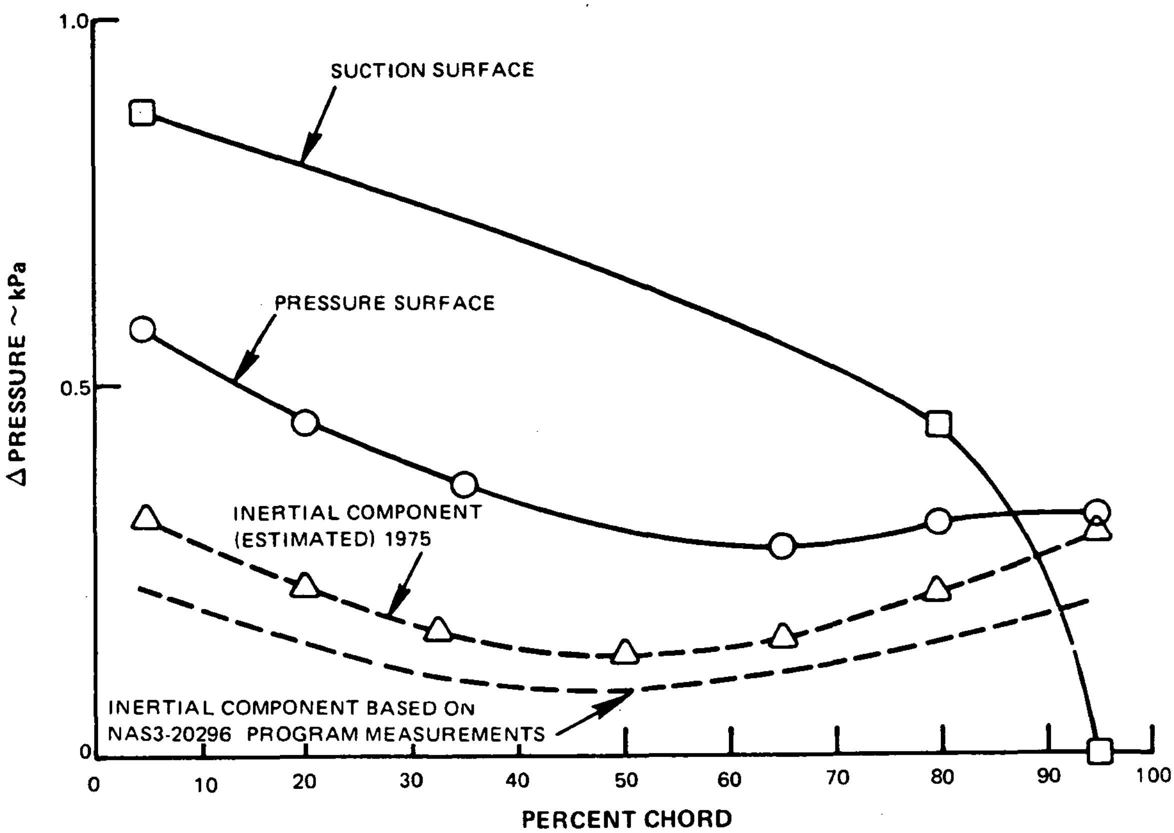

Figure 1-1 *Oscillatory Pressure on Blade Surface – This date was obtained in tests of the TS-22 fan in 1975. Flutter occurred at 70 percent speed.*

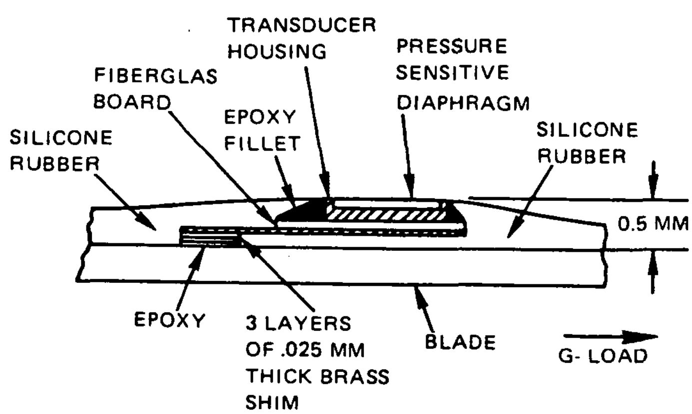

Figure 1-2 *Transducer Mounting Technique Used In Past Programs at P&WA*

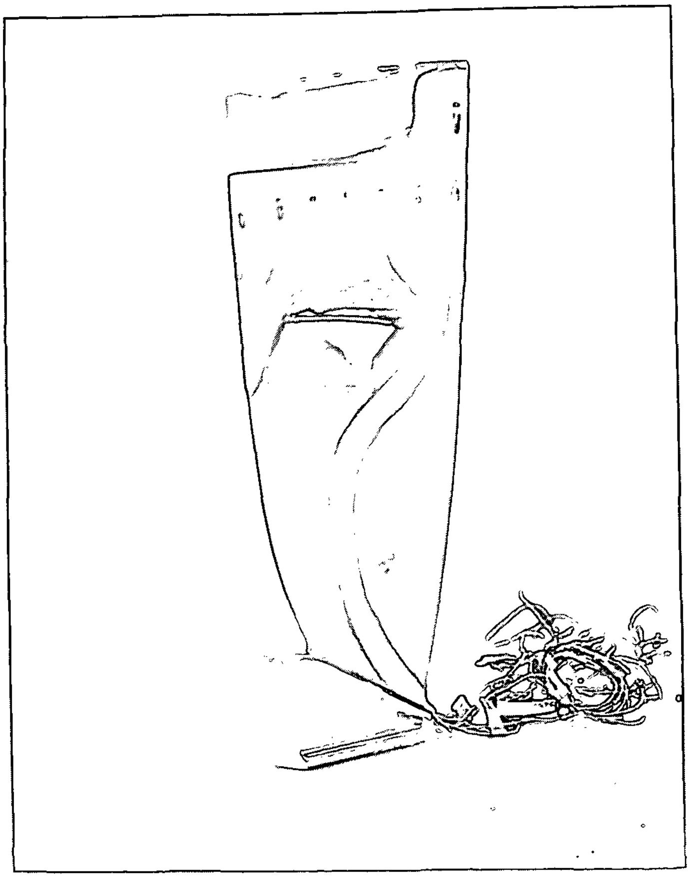

Figure 1-3 *Transducer Installation – Shown here are eight pressure transducers installed on a fan blade.* *(XPN-56103)*

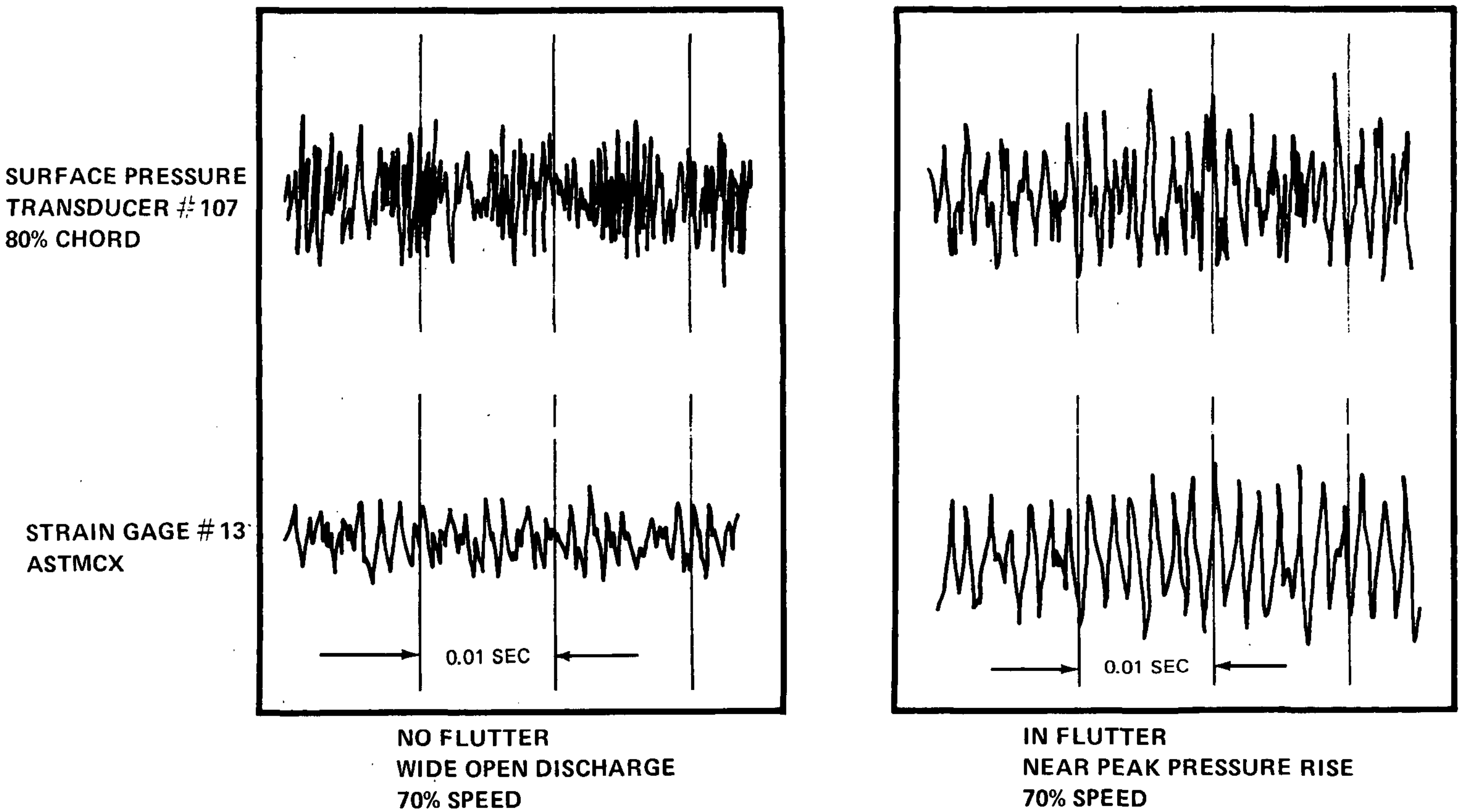

Figure 1-4 *Fan Blade Surface Pressure and Strain Signals – This data was obtained in tests of the TS-22 fan.* *(76-6323)*

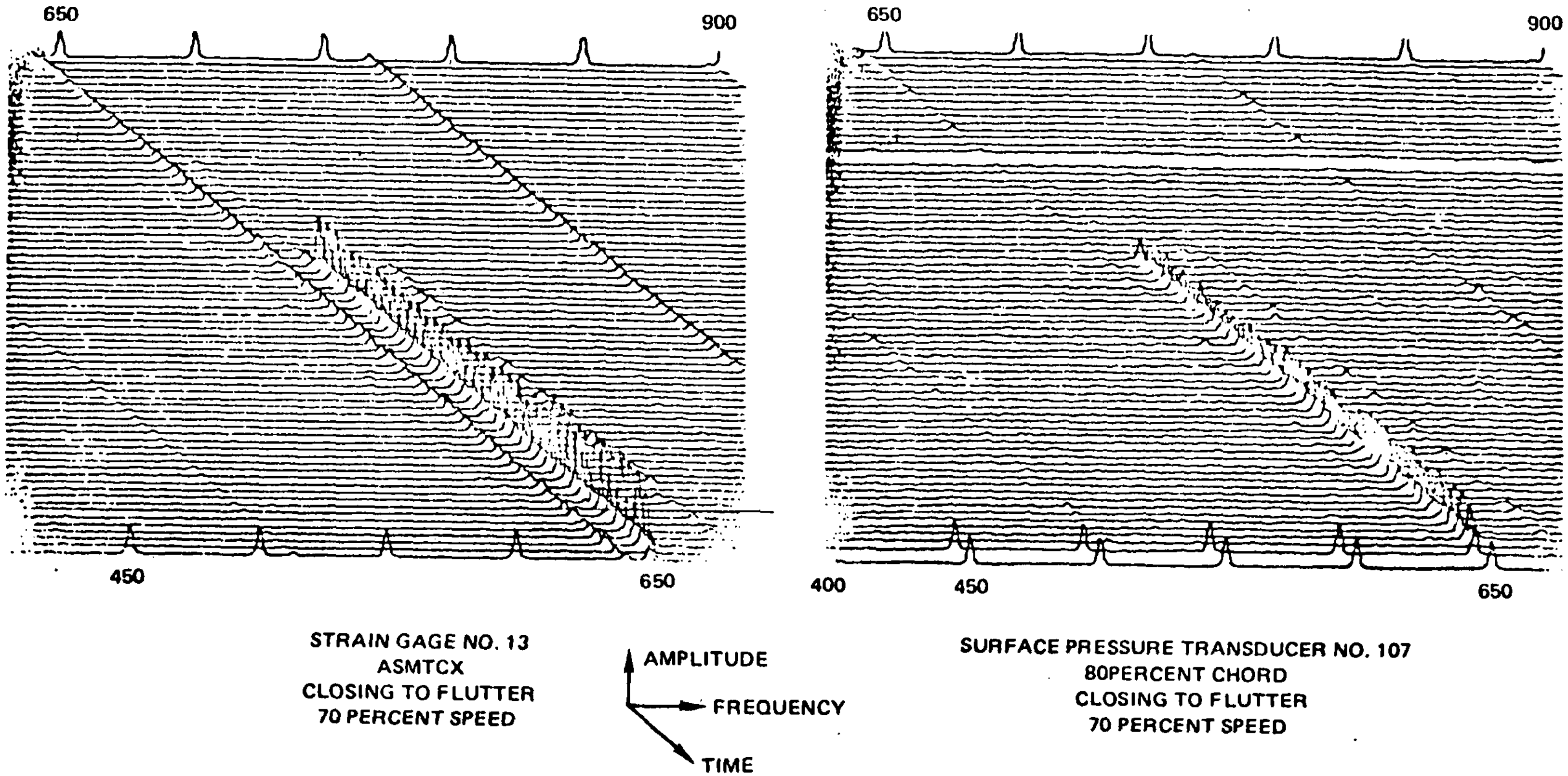

Figure 1-5 *"Carpet Plot" of Fan Blade Surface Pressure and Strain Signals – Shown here is a series of 68 spectra obtained as fan operating point was changed from normal to flutter. (76-6323)*

TABLE 1-I

PRATT & WHITNEY AIRCRAFT
ROTATING PRESSURE MEASUREMENT EXPERIENCE

	Test Program			
	0.57 Scale JT9D Fan	Three-Stage Compressor	Development Program	TS-22 Fan
Year	1971	1973	1974	1975
Centripetal Acceleration (G)	28,000	10,000	20,000	50,000
Temperature (°C)	40	40	40	25
Sensor Diameter (mm)	2.0	2.0	2.0	2.0
Number of Sensors	6	8	2	16
Running Time (hours)	51	50	10	15
Frequency Response* (Hz)	10,000	10,000	10,000	10,000
Minimum Resolution (kPa peak-to-peak)	0.3	0.3	3.0	0.07
Sensor Range (kPa)	175	175	175	175
Rotating Amplifiers	Yes	Yes	No	Yes

*Limited by Recorder

TABLE 1-II

STATIC TEST CONDITIONS

Blade Materials
- (1) Titanium alloy (PWA 1202)
- (2) Steel alloy (CEVRMS 18 Ni-300)

Mounting Configurations
- (1) B
- (2) C
- (3) E

Test Mode
- (1) Tensile
- (2) Bending
- (3) Vibration

Temperature
- (1) 20°C (70F)
- (2) 150°C (300F)

Pressure
- (1) 50 kPa (7 psia)
- (2) 180 kPa (26 psia)
- (3) 310 kPa (45 psia)

Strain
- (1) 0
- (2) Maximum (nominal 1000 mincrostrain)

TABLE 1-III

SPIN TEST CONDITIONS

Base Material
- (1) Titanium alloy (PWA 1202)

Mounting Configurations
- (1) A
- (2) B

Orientation
- (1) 0° relative to radial plane
- (2) 7° relative to radial plane

Temperature
- (1) 20°C (70°F)
- (2) 80°C (180°F)

Pressure
- (1) 7 kPa (1 psia)
- (2) 150 kPa (22 psia)
- (3) 310 kPa (45 psia)

RPM/Centripetal Acceleration
- (1) 0 rpm (0 G)
- (2) 10132 rpm (27500 G)
- (3) 14330 rpm (55000 G)
- (4) 16734 rpm (75000 G)
- (5) 18330 rpm (90000 G)

Radius
- (1) 23.95 cm. (9.430 inches)

SECTION 2.0

EQUIPMENT AND PROCEDURES

2.1 TRANSDUCER SELECTION

2.1.1 Transducer Error Sources

The semiconductor strain gage pressure sensor (Figure 2-1) was the only sensor which was known to have demonstrated high enough sensitivities at high frequencies and small enough size to obtain the desired measurements. These sensors were available from three commercial sources. The sensing element is a thin silicon diaphram on which a semiconductor strain gage bridge array is produced by suitable doping.

Sources of false pressure indication which could affect semiconductor strain gage pressure transducers were:

- Vibration
- Humidity
- Radiation (visible light)
- Erosion
- Temperature
- Accelerations
- Strains in the mounting surface

Vibration sensitivity could be reduced by proper sensor diaphragm design (stiff construction to produce extremely high natural frequency) and humidity sensitivity could be eliminated by selection of appropriate sensor materials (avoidance of hygroscopic materials). Sensitivity to incident light radiation is an intrinsic problem in all semiconductor devices and could be overcome by shielding the sensor from direct sunlight by application of a thin overcoat of opaque material, for example an evaporated metal film. Protection from erosion could be accomplished by applying a thin coating of a resilient material; it was found in Reference 6, for example, that a 0.8 mm coating of RTV silicone rubber on the 0.08 mm thick diaphragm of a strain gage pressure transducer whose resonant frequency was about 10 kHz did not alter its rise time or amplitude response, and it was found in Reference 1 that this type of coating material provided good erosion protection in an actual engine test.

Unpublished reports of sensitivity of semiconductor strain gage pressure transducers to hydrocarbon (and other) vapors suggested that additional precautions should be taken to prevent direct exposure to such atmospheres.

The combined effects of temperature, large centripetal accelerations, and large surface strains represented the most serious source of possible error. The use of a full 4 element strain gage bridge on the transducer diaphragm plus external fixed compensating resistors, reduced error due to temperature alone to a reasonable level (typically 1% per 50°C), in the absence of strains and accelerations, but it remained to be determined whether the temperature compensation adjustment which is correct for this condition is also correct for a blade-mounted transducer subjected to large accelerations and strains.

The effect of acceleration perpendicular to the diaphragm was easily estimated, but the effect of acceleration parallel with a (deflected) diaphragm was not. It remained to determine the effect of parallel accelerations on the order of 100,000 G encountered in gas turbine blade rows.

Finally, it was obvious that the transmission of steady or oscillatory blade surface strains to the transducer diaphragm could easily produce diaphragm deflections equivalent to a considerable fraction of full scale applied pressure; strain isolation of some sort was required.

It is important to observe that oscillatory zero shifts alone constitute apparent oscillatory pressure readings. Therefore, it was necessary to plan to determine the effect of change in each environmental variable (temperature, acceleration, strain) on the zero-shift output level of the transducer, as well as on the sensitivity of the transducer.

2.1.2 Differential vs. Absolute Measurement

The strain gage pressure transducer for this application was selected to have a reasonably high dynamic strain level in the diaphragm at 2 kPa peak-to-peak oscillatory pressure and yet be able to withstand 310 kPa time-average pressure.

A differential pressure transducer referenced to time-average pressure through a controlled leak (pneumatic filter) might be an attractive approach since it would permit the use of an extremely thin diaphragm to attain high sensitivity over a small dynamic pressure range. The thinner diaphragm, however, results in reduced natural frequency and increased fragility and the controlled leak presents dust contamination problems and mechanical complexity.

The diaphragm of the sealed transducer used in previous programs at Pratt & Whitney Aircraft (Table 1-I) is 0.018 mm thick and 1 mm effective diameter. Experience had shown that this design combined durability, excellent sensitivity, and high natural frequency (125 kHz). These dimensions also result in high strength in edgewise buckling, and capability to withstand about 440 kPa differential pressure within the elastic limit, so that the increased complexity of a differential pressure transducer with pneumatic filtering was not required.

2.1.3 Acceleration Environment

An acceleration vector with a large steady-state component and a smaller time-varying component acts upon each surface element of the rotating blade in a fan or compressor due to the combined effects of centripetal acceleration and blade vibration. The time-varying component of acceleration stems partly from the translational accelerations of vibration and partly from the time-varying orientation of the blade surface with respect to the steady-state centripetal acceleration vector, due to bending and twisting during vibration. As an example, Table 2-I lists the accelerations which are experienced at a radius of 25 cm at 20,000 rpm, if the blade surface is at an average inclination of 5 degrees from a radial plane and the blade is vibrating in easywise pure bending at 500 Hz through a 0.25 mm peak-to-peak amplitude. The table lists the values of the three mutually perpendicular components of acceleration parallel to blade surface in the spanwise direction, normal to the blade surface and parallel to the blade surface in the chordwise direction in a circumferential plane.

The transducer is most sensitive to the normal component. From the table, it is clear that in addition to the 250 G time-varying normal component due to vibration, there is superimposed an additional 110 G time-varying normal component due to the time-varying orientation relative to the centripetal field. Torsional vibration and stiffwise bending vibration produce additional contributions to all three time-varying acceleration components. The magnitude of these contributions varies with position on the blade surface.

Reducing the thickness of the transducer diaphragm would proportionately reduce the zero-shift due to normal acceleration, but could increase the effect of parallel acceleration (edgewise buckling). The transducer selected for this program had the thinnest possible diaphragm (0.018 mm) which was consistent with the desired pressure range and buckling strength. The resulting effect of normal acceleration was consistent with the desired pressure range and buckling strength. The resulting effect of normal acceleration was calculated to be about 0.4 Pa/G.* The manufacturer rated the transducer more conservatively at 0.7 Pa/G.

Consideration was given to providing inertial compensation through the use of a second strain gaged diaphragm shielded from the stream pressure. The Franklin Institute Research Laboratories proposed to Pratt & Whitney Aircraft a promising approach along these lines. This approach could reduce th effects of acceleration by a factor of twenty. Since the calculated effect of 0.4 Pa/G for the uncompensated transducer was not excessive, and a major additional program would be required to develop the compensation, the approach was not pursued.

2.2 MOUNTING CONFIGURATION SELECTION

Figure 2-2 shows the five mounting configurations considered. Buildup of blade thickness due to installation of a surface-mounted transducer should ideally be limited to a fraction of the local boundary layer thickness, and should be smoothly faired, whether on the surface to be measured or on the opposite surface of the blade. Both steady-state and flutter aerodynamic characteristics can be altered by a large local surface buildup. On the other hand, removal of material from the blade alters its stress and vibration characteristics. Taking into account the structure and leadwork arrangement of the semiconductor strain gage transducer, and the desirability of minimizing the amount of material machined from the blade, configurations A, B, C, and E of Figure 2-2 were pursued in the program. Previous Pratt & Whitney Aircraft installations have used configuration A, with no machining of the blade and with

*Inertial force per unit area at 1G = ρAt G/A = ρtG. For silicon density ρ = 2.33 gm/cm^3, thickness t = .0018 cm, and G = 980 cm/s^2, force per unit area = 4.1 gm cm/s^{2}cm^2 = 0.4 N/m^2 = 0.4 Pa up to 0.5 mm buildup carefully faired from leading edge to trailing edge of the blade. Reductions of transducer thickness have been achieved by the manufacturers, and a buildup of 0.38 mm was feasible in configuration A. To reduce buildup to 0.12 mm on the measured surface, a small mount of material was machined from the blade locally to achieve configuration C. Configuration B could be achieved with the permissable buildup of 0.5 mm on the non-measured side of the blade without machining. Configuration E required development of a special cylindrical version of the transducer. Configuration D was not pursued, since additional machining of leadwire grooves would be required, and the resulting alteration of flutter mechanical properties of the blade was thought to be too severe.

2.3 STATIC TEST EQUIPMENT AND PROCEDURES

2.3.1 Sensors and Mounting

2.3.1.1 Transducers

For use in configurations A, B and C, the "thin" style of transducers were purchased already mounted (with epoxy cement) on a perforated carrier shim 0.025 mm thick. The perforations were specified in order to enhance adhesion through the pegging action of the cements used in the blade mounting procedures. The complete specification drawing and the description of the purchased item are presented in Figures 2-3 through 2-7. A 1 μm sputtered alumium coating on the diaphragm is specified to reduce light sensitivity. Orientation of transducer strain elements is specified to be the same in all transducers, with the orientation identified within ±2° by means of a scribed line on the carrier shim. Figure 2-8A is a photograph of one transducer as received. It should be remarked that the "thin" transducers purchased for the program met or exceeded specifications as received and the twelve used performed reliably throughout the program of static tests and spin tests, with the exception of one transducer which developed a pressure leak after installation on a spin disk and before spin tests were begun.

For use in configuration E, the transducer was purchased already mounted on the end of a stainless steel cylindrical button 2.0 mm in diameter and 2.0 mm long, with a stiffening plate at the diaphragm end. The complete specifications for this purchased item are presented in Figures 2-9, 2-10, 2-11. The aluminum coating and reference scribe line for orientation are again called out. A photograph is shown in Figure 2-8B. The transducer proved to be extremely difficult to manufacture in this short button form, and there were persistent problems with air leaks in the sealed cavity of some samples of this item, mostly at the leadwire entry, and with adherence of the aluminum coating on the diaphragm. Enough good samples were eventually obtained to perform the desired static test evaluations, but development was completed too late in the program to permit spin tests.

The sealed pressure cavity in each transducer is pressurized by the manufacturer at a pressure of 24 to 28 kPa.

Each transducer was connected through five 36 gage enamel coated copper leadwires 61 cm long to a temperature compensation module supplied by the manufacturer. The temperature compensation module is a cylinder 3.9 mm in diameter and 31 mm long. The temperature compensation module was then connected to the instrumentation power supply and input and output digital voltmeters through five 24 gage teflon coated copper leadwires. The wiring diagram is shown in Figure 2-7.

An excitation of 15.000 VDC was applied to each system at the temperature compensation module throughout the test program (unless otherwise noted). The voltage at the semiconductor strain gage bridge terminals was therefore about 5.0 VDC.

Note that an output proportional to the bridge resistance of the semiconductor strain gage bridge (and therefore to diaphragm temperature) was provided by the arrangement of Figure 2-7 in addition to the bridge unbalance output voltage proportional to pressure. This special output was designated the bridge temperature output.

2.3.1.2 Mounting Configurations

The principal mounting configurations (B, C, and E) adopted, and shown in Figures 2-12, 2-13, 2-14 were designed to isolate the pressure transducers from strains in the fan blade or compressor blade, including strains due to thermal expansion. Pressure was measured on the convex ("suction") surface of the blade in all cases.

Note, in Figures 2-12, 2-13, 2-14, that a small amount of epoxy is used in a region remote from the transducer diaphragm to provide a strong mechanical bond of the transducer assembly to the blade, following the recommendation of Reference 1. In configurations B and C, using the thin transducer shown in Figure 2-1, the carrier shim is cantilevered radially outward along the blade surface from the epoxy-bonded region and floated on soft RTV rubber for maximum strain isolation. In configuration E, utilizing a cylindrical transducer, the isolation is provided in a different way. The diaphragm end of the cylindrical transducer is stiffened with a steel end plate and this end is floated in the soft RTV rubber, so that minimum distortion of the cylindrical transducer body will occur in the critical region near this diaphragm.

The detailed step-by-step mounting procedure for each configuration is presented in Appendix I.

Once a transducer is mounted on a blade, it generally cannot be removed and reinstalled without destroying it. The transducers mounted on the blade specimens were not removed and were still available for further testing at the end of the contract program.

2.3.2 Preliminary Tests

2.3.2.1 Preliminary Tests of Bridge Temperature Output

During initial calibration tests at 21°C and 50°C the bridge temperature output was monitored to determine its usefulness as a substitute for or supplement to other independent temperature measurements. From day to day the difference between the bridge temperature output and the readings of several thermocouples placed in the vicinity of the transducer, in a closed chamber at equilibrium temperature, were found to vary by only about 2°C. However, neither correlated with observed random drifts in transducer pressure output voltage, described later. It was concluded that the bridge temperature output, proportional to total bridge resistance of the semiconductor strain gage bridge on the diaphragm, was not any more useful than the external thermocouples in predicting or explaining transducer calibration drifts and it was not monitored during subsequent tests. It was conjectured that drifts occur in all four arms of the bridge, as a result of changing stress patterns in the diaphragm induced by thermal expansions and relaxation in the mounting materials, especially the epoxy in the diaphragm frame mounting. Note that equal drifts in two adjacent arms would change the bridge temperature output, but not the pressure output, while equal drifts in opposite arms would change both.

2.3.2.2 Preliminary Tests for Strain Isolation

To minimize the buildup thickness of surface installations configurations B and C (Figures 2-12 and 2-13), it was desirable to minimize the thickness of the flexible RTV layer which is provided for strain isolation. Preliminary tests were conducted in which the strain transfer to a steel metal shim (0.025 mm thick) was measured for four thicknesses of RTV in the range 0.025 mm to 0.25 mm. It was found that the transfer ratio was 0.04 (40$\mu\epsilon$ at shim surface for 1000$\mu\epsilon$ at specimen surface) for all four thicknesses of RTV. A nominal thickness of 0.05 mm of RTV was therefore selected. In this series of tests, carried out with a steel shim cemented to a Hastelloy X test bar, surface strains in excess of 3000$\mu\epsilon$ were applied to some samples (producing yield in the test bar) without failure of the bond.

2.3.2.3 Preliminary Tests of Adhesives

In previous programs, failure of blade mounted transducer installations like Figure 1-2 had been found to occur at the bond between the epoxy and the underside of the shim carrying the transducer. Of several combinations of adhesives tried, the most successful employed was Smooth-On Inc. MT-13 epoxy for retention and Dow-Corning 732 RTV for strain isolation and some contribution to retention.

In the present program, further tests were conducted using additional cleaning and surface priming procedures applied to the surfaces before application of the epoxy and RTV, and adding perforations to the transducer shim to provide pegging. Strength was improved to the point where failure eventually occurred in the epoxy and RTV before the bonds failed. The shear strength of these installations was measured to be 1400 N force in room temperature laboratory tests. Maximum load expected in the spin tests was less than 70 N (based on a mass of 0.06 gm and acceleration of 110,000 G). These materials and procedures were adopted for use in all installations. The materials and procedures are described in detail in Appendix I.

Early in the program it was not known whether direct application of RTV to the diaphragm would produce changes in performance. A decision was made to keep the transducer diaphragm free of contact with RTV throughout the program. A few tests of the effect of exposure to chemical vapors (including fresh RTV) were incorporated in the program later. The results are reported in Section 2.3.2.5; all effects detected were temporary and reversible.

In actual rig and engine tests, it is common practice to apply a 0.025 mm coating of RTV (thoroughly cured) to the diaphragm for erosion protection. Such a layer would be expected to increase the zero drift, but not to affect transducer sensitivity significantly. The results of work at NBS (Reference 6) support these expectations. In addition, the layer would be expected to increase the output signal due to acceleration normal to the diaphragm by an amount proportional to the increased mass. For the transducers used in the present program, the added mass would be about 60 percent. This should be recalled when applying the results of the present tests to engine test data. Finally, a 0.025 mm RTV layer would be expected to alter the frequency response of the transducer in the frequency range above 20 kHz, not covered in the present program.

2.3.2.4 Preliminary Tests for Light Sensitivity

All transducers were sputter coated by the vendor with 1μm of aluminum to eliminate sensitivity to incident light. The output of sample transducers were measured at atmospheric pressure in direct sunlight and in darkness at P&WA during initial calibrations. The difference was found to be equivalent to less than 0.07 kPa compared to 3 kPa for uncoated transducers. Lighting conditions during all other tests in the program were such that any output voltage due to light was certainly less than 0.02 kPa.

2.3.2.5 Preliminary Tests for Chemical Vapor Sensitivity

To check the reported sensitivity of semiconductor strain gage devices to chemical vapors, sample transducers were exposed to a selection of vapors by suspending a calibrated transducer in the air about 1 cm above a liquid surface in a closed container at room pressure and temperature for a time period long enough to establish a steady state condition, and then returning the transducer to clean air. Effects were small in most cases and reversible in all cases, and posed no problem in the conduct of the planned program. The results may be summarized as follows:

	Change In Output Voltage (Equivalent Pressure)		
Chemical	kPa	psi	Remarks
Alcohol	−1.1	−0.16	
Fresh RTV	−0.6	−0.09	
Freon (PMC 9087)	*	*	Output dropped to zero, but returned to normal after re-exposure to clean air.

The effect of the freon was remarkable but not permanent. Use of this transducer type in an atmosphere heavily contaminated with vapors of any kind must be approached with caution.

2.3.3 Test Blades

2.3.3.1 Blade Materials

In accordance with contract requirements, a titanium alloy and a steel alloy were selected, each representative of modern compressor blade material practice. The properties of the two materials are listed in Table 2-II. The titanium alloy was PWA 1202, a Ti8A11V alloy similar to AMS 4928. The steel alloy was CEVRMS 18Ni-300.

2.3.3.2 Thermal Expansion Considerations

Thermal expansion in the blade materials (for temperatures between 21°C and 150°C) were on the order of 1100 microstrain for titanium and 1300 microstrain for steel. The nominal mechanical strain of 1000 microstrain chosen for tensile and bending tests was exclusive of these thermal expansion effects. The strain gage installations were compensated for temperature in accordance with common practice, which includes matching the thermal coefficient of linear expansion of the gage and base material, using three-wire connections to each gage to balance leadwire effects in the bridge circuit, running preliminary tests of residual apparent strain due to temperature, and correcting the indicated strain readings for any remaining effect of temperature. Thus, the strain levels reported during testing are those caused only by the mechanical loads applied to the test specimen. All effects of thermal expansion therefore appear only in the effects of temperature on the pressure transducer and its installation, and are correctly identified as temperature effects in the test results.

2.3.3.3 Test Blades, and Tensile and Bending Strain Calculations

Three titanium blades were instrumented as shown in Figure 2-15 (one each of configuration B, C, and E). The blades were existing Pratt & Whitney Aircraft parts. Figure 2-15 shows details of blade dimensions, as well as locations of the pressure transducer, three strain gages and three thermocouples on each specimen. All instrumentation was located on the same side of the blade as the pressure transducer diaphragm (convex side for C and E, concave side for B.) In the case of configuration E, an additional set of three strain gages was located on the concave side.

Three simulated steel blades were instrumented in the same way as shown in Figure 2-16 (one each of configuration B, C, and E). The blades were twisted flat plates.

The three strain gages permitted measurement of root maximum thickness strain (first bending) and two orthogonal strains on the specimen surface near the pressure transducer. The strain gages were monitored to provide evidence of repeatability from test to test. The strain field in the vicinity of the pressure transducers was complex, due to the machined recess in the surface for configuration C and the machined holes for configurations B and E. Strain distributions along the radial midchord line for an unmachined blade were calculated for each blade type, and compared with measured strain levels at root location (3) and outboard location (1), with an allowance for the effect of stress risers on the measured strain at the outboard location (1). Details of the calculations are presented in Appendix II. The comparison showed agreement with measured strains within the desired tolerance ±100 microstrain. The strain finally used in evaluating strain effect on the pressure transducer was in every case the calculated strain that would be found at the transducer location on the same side of the blade as the transducer diaphragm on a blade with no transducer mounted and no machined hole or recess, for the test load applied. Thus, any stress concentration or stress relief resulting from the machining of the blade or mounting of the transducer was correctly included in the performance of the particular configuration.

A tensile fiber strain is always reported as a positive strain and a compressive strain as negative. In the case of bending tests, the strain calculated is the tensile or compressive fiber strain in the blade surface on the same side of the blade as the diaphragm of the mounted pressure transducer. Then for configurations C and E, the strain on the convex (measured) side is reported. For configuration B the strain on the concave (nonmeasured) side is reported.

Photographs of installations of the pressure transducers, strain gages, and thermocouples are shown in Figures 2-17 through 2-21. No attempt was made to produce smoothly faired surfaces in these test installations, normally accomplished by adding final thin layers of the RTV over the surrounding areas as shown in Figure 1-3 and described in the installation procedures in Appendix I for actual installation on blades to be used in an operating engine. The total buildup of the pressure transducer installtion above the blade surface was held within the dimensions shown in Figures 2-12, 2-13, 2-14.

Figure 2-18 is a particularly striking photograph of configuration B showing the completely unobstructed measured surface. The diaphragm of the back-mounted pressure transducer is visible through the hole in the blade surface.

2.3.4 Instrumentation

2.3.4.1 Instrumentation System and Accuracy

The instrumentation used in the static tests is diagrammed in Figure 2-22, are listed in Table 2-III, along with the accuracy specification for each item, as determined by the P&WA Standards Group. Instrumentation calibration accuracy reported at P&WA is the two-standard-deviation level (2σ), so that 95% of all instruments calibrated fall within the stated accuracy. For purposes of the present program, the stated instrument accuracy was conservatively assumed to be the $1\ \sigma$ level, to allow for differences in instrument performance under field conditions.

The expected effect of instrumentation accuracy on overall uncertainty of static test results is diagrammed in Figure 2-23, in which the error in indicated pressure due to the uncertainty in each type of measurement is identified. Random uncertainties from individual sources are summed in quadrature to produce a final overall uncertainty of ±1.3 kPa.

It should be noted that if the standard deviation of pressure determinations is 1.3 kPa, then the standard deviation of sensitivity (Δmv/ΔkPa) determinations will be:

$$\frac{(\sqrt{2})\ (1.3)}{P_a - P_b} \cdot \phi$$

where ϕ is the sensitivity (ΔmV/ΔkPa) and P_a and P_b are the end points of the pressure interval over which the sensitivity is measured. In the static tests, P_a - P_b was 130 kPa (the intervals were 50 to 180 kPa and 180 to 310 kPa). Then the expected standard deviation of sensitivity determinations was $(\sqrt{2})(1.3)\phi(130) = 0.014\phi$.

Similarly, if the standard deviation of sensitivity determination is 0.014 ϕ, then the expected standard deviation of determinations of changes in sensitivity is $(\sqrt{2})(0.014\phi) = 0.020\phi$.

Short-term repeatability of pressure measurements, over a time period of a few minutes, when pressure or strain was cycled at any constant temperature, was better than ±0.1 kPa since neither the test transducer system nor the reference pressure transducer system displayed any larger zero drift during short periods at constant temperature. Therefore, the zero-shift produced by strain alone, for example, could be documented with an accuracy on the order of ±0.1 kPa.

2.3.4.2 Transducer Calibration History

All blade-mounted transducers were calibrated by the P&WA Instrumentation Standards Facility prior to installation on blades or spin disks. These tests included 6 pressures ascending and 6 pressures descending over the range 7 kPa to 310 kPa at each of two temperatures, 21°C and 150°C. After installation, a calibration of each transducer at 21°C was performed by the Instrumentation Standards Facility to identify the effect of the installation process. Subsequently, the absolute calibration of each transducer was checked from time to time throughout the program, at three pressures at 21°C by comparison with the precision reference transducer P_1 used. A record of changes in sensitivity and zero-shift with time throughout this program for each transducer is presented in the results (Section 3). Since the zero-shifts with time were large and never predictable in direction, a major effort was required to avoid confounding zero-shift effects of time with the zero-shift effects of the controlled variables. Changes in sensitivity with time were modest, generally less than ±3% over the 1 year period of this program, so did not present a major problem in conducting tests or reducing the data.

2.3.5 Test Fixtures

2.3.5.1 Pressure Fixture

To apply precisely known gas pressures to the blade mounted transducers, the system sketch in Figure 2-24 was employed. A pressurized nitrogen supply and a vacuum pump were connected through suitable manifolding and control valves to a length of 1.57 mm diameter hypodermic tubing which terminated in a 19 mm diameter pressure cap cemented to the blade surface. Figure 2-25 is a photograph showing details of the pressure cap. In order to avoid altering the strain field in the blade, the pressure cap was soft-mounted with RTV rubber. The mounting procedure used is described in Appendix I. Figure 2-26 is a general view of another blade specimen instrumented with the pressure cap (and with tensile test pull fixtures, described later, attached to the blade tips). This pressure cap arrangement was used successfully throughout the static tensile and static bending tests, but required modification for vibration tests. Accelerometers mounted on the pressure cap and the blade surface during initial vibration tests revealed slight relative motions due to the soft mounting, which could result in significant pressure oscillations. The pressure cap was therefore removed and reinstalled on each specimen using hard epoxy in place of the soft RTV. The hard mounting undoubtedly reduced the strain levels at the transducer during the vibration tests, but since the strain levels at the transducer were limited for other reasons to rather low values in the vibration tests, the rigid mounting of the pressure cap in this case was not a significant influence on the results.

2.3.5.2 Heating Fixture

To provide rapid and uniform heating to 150°C when required, the blade specimen was wrapped with a flexible strip heater, as shown in Figure 2-27. Some preliminary tests were run using a portable split oven, but the time required to establish a reasonably uniform temperature of about 150°C from root to tip of the blade specimen was several hours. The flexible heater reduced the time to one hour.

2.3.5.2 Tensile and Bending Fixture

A P&WA Structures Laboratory tensile test machine, Figure 2-28, was used to apply static tensile loads to the blade specimens. To grip the blade root, a broach block was made up for each type of root fir tree. (In the case of the steel blade specimens, the root "fir tree" was simply a rectangular block welded to the steel blade). At the blade tip a removable fixture was required since the tip was later to be unrestrained during vibration tests. A removable fixture was therefore provided for each blade specimen using three 0.48 cm diameter bolts through the blade tip to clamp a pair of shaped blocks to the tip. Ceramic cement was applied to the blade tip surfaces before clamping to assure continuous contact over the entire clamped area. Figure 2-29 shows one titanium and one steel specimen with tip fixtures attached. Figure 2-30 shows the locations of the bolt holes and the clamped tip blocks. The broach block mounting is clearly visible in Figures 2-26 and 2-27.

In the tensile tests, the test machine included universal joints and a swivel to permit normal blade untwist as the tensile load was applied. Static friction in the swivel which might lead to nonrepeatability in untwist was checked by attaching four dial gages to a sample specimen during preliminary tests. Return to the same neutral position, after applying and releasing the tensile load, within ±0.2 degrees was accepted as evidence of negligible static friction in the swivel.

In Figure 2-31, a closeup photograph showing application of tensile load to a JT8D fan blade in the tensile test machine, the universal joints and (at top) the swivel are visible.

Tensile loads were applied as nearly as possible along the stacking line of the blade, to minimize bending during tensile tests. A check on how well this was accomplished was available through comparison of the strain gage readings from the two sides of the configuration E blades. The results show that bending of titanium blades during tensile tests was minor, but that bending of the simulated steel blades (whose stacking line was at a considerable angle to the platform) was severe enough to produce strain reversal on one side. The tensile test data thus has different significance for steel and titanium specimens in these tests. Each was subjected to the same tensile load, but the steel specimens were subjected to simultaneous bending. These considerations were taken into account in analyzing the results (Section 3).

In the static bending tests, pure transverse loads were applied to the blade root fir tree broach block, while the tip was held fixed in its bolted and cemented fixture. In these tests the tensile test machine was not used. The tip fixture was clamped to a bench with the blade specimen in a horizontal position, and the load was suspended at the blade root (location X in Figure 2-30).

2.3.5.4 Vibration Fixture

To simulate blade vibration accelerations that would be encountered during flutter in an operating fan or compressor, each instrumented blade was tested on a shaker table, as sketched in Figure 2-32. The root fir tree was clamped to the table using a broach block. The tip was unrestrained (all tip fixtures previously used in static tensile and static bending tests were removed). In addition to the instrumentation already described, a miniature accelerometer was cemented to the blade surface as close to the pressure measuring location as possible, as follows:

Configuration C: concave side of blade, same spanwise and chordwise position

Configuration B and E: concave side of blade, same spanwise position, off-set chordwise by 0.38 cm toward leading edge.

A second identical accelerometer was mounted on the pressure cap to detect any relative motion that would indicate a pumping action due to flexing or translation of the pressure cap. The pressure cap was hard mounted with epoxy cement during the vibrational tests and no relative motion was detected (i.e., less than 0.025 mm peak-to-peak relative motion when the blade motion amplitude was 1.27 mm peak-to-peak).

A vertical sinusoidally varying force was applied by the shaker table. The exciting frequency was gradually raised until the lowest-frequency resonant mode of the blade was encountered (first bending mode). At this frequency the exciting force was increased until the peak-to-peak amplitude indicated by the accelerometers was 1.27 mm. An oscilloscope and a true RMS voltmeter were used to monitor the oscillatory amplitude of the pressure transducer signal and the strain gage signals at each applied steady state pressure, 50, 180, and 310 kPa. ADC voltmeter was used to measure the steady state output voltage of the transducer.

Figure 2-33 shows the shaker table in operation in a previous program, with a compressor blade of about the same size as those tested. The optical telescope shown in Figure 2-33 was not used in the present program.

2.3.6 Test Procedures

2.3.6.1 Test Matrix Development

In the planning stages of the program a statistically designed test matrix was constructed, in which pressure, temperature, and strain would be varied one at a time in random order for each of the six blade specimens. The full factorial program would have required 648 test points (six specimens, 3 test modes, 4 temperatures, 3 presses, 3 strain levels) even without repeat points. Statistical analysis showed that the program could be reduced to

216 test points (including many repeat points) and still retain information on second-order interactions (such as the effect of temperature at various strain levels) provided that repeatability was reasonable (i.e., effects of time not large). Unfortunately this latter requirement could not be met. When the first tensile tests were carried out it became clear that to determine zero-shift effects of strain, random-sequence testing must be abandoned. The reason was that any large change in temperature applied to the blade specimen (say 50°C in 30 minutes) was followed by hours of erratic wandering of the output voltage level. Even though these zero shifts were usually (but not always) monatonic with time at the new temperature and the overall magnitude of the change was not much larger than the manufacturer's specification for unmounted transducers (3% of full scale per 50°C), the random nature of the changes and nonreversability within any predictable time period completely demolished the basis of the statistically designed experiment. This did not suggest that the transducers were unsuitable for measurement of oscillatory pressures on blade surfaces, but only that a different approach was required in the present tests to determine zero-shifts due solely to applied strains and accelerations (as opposed to zero-shifts due to time and temperature history).

As a result the test sequences described in the next three paragraphs were devised. One variable was cycled through its range with all others held constant. This resulted in a total of 328 test points even though the number of temperature levels was reduced to two, the number of strain levels to two, and vibration testing was carried out at room temperature only.

To further define the effect (on zero-shift) of bending strain, which was believed to be the largest contributor to oscillatory zero-shifts in engine tests, an additional several hundred readings of output versus strain were recorded (simply by repeating the two bending strain levels 6 to 20 times in quick succession for each of the specimens tested at each test temperature). These additional readings added only a few days to the test program, but increased the confidence in the results greatly. The test sequence and procedure for each static test mode are described below.

2.3.6.2 Tensile Test Matrix and Procedure

Figure 2-34 shows the matrix of tensile tests performed. For each of four combinations of tensile strain and temperature (0 microstrain, 1000 microstrain, 21°C, 150°C) the applied pressure was cycled through a sequence of five pressures (50, 180, 310, 180, 50 kPa).

The time required to complete each sequence of five pressures was about ten minutes. It was found that the calibration slopes calculated from the ascending portion of the cycle and the descending portion were identical to well within the experimental tolerance. For added confidence, one combination of strain and temperature was repeated for each blade specimen, the one repeated being selected on a random basis. In addition, for one specimen three combinations of strain and temperature were repeated. The entire sequence of 160 tensile test points is charted in Figure 2-34. Note that the chronological order in which strains and temperatures were applied was also selected on a random basis.

The raw data recorded are tabulated in Appendix III, including transducer excitation, (volts) strain gage readings (microstrain), thermocouple readings, and tensile load, all of which were recorded at the beginning and end of each pressure cycle, plus applied gas pressure, and transducer output, mV, which were recorded at each point of each pressure cycle.

The results of these tensile tests were studied at length (see discussion of results in Section 3) before proceeding with bending strain tests described below.

2.3.6.3 Bending Test Matrix and Procedure

The analysis of the tensile tests (Section 3) showed that effects of strain and temperature on transducer sensitivity (mV/kPa) were repeatably established by the test sequence employed, but that the effects of strain on zero-shift (change in output voltage per unit change in strain) were not repeatably established, because of the erratic drifts in output voltage level over the time period of two or more test conditions. Several special tests were conducted to document more thoroughly the nature of the drift. Some tests involved tracking the output voltage over a 24-hour period after a change in applied temperature (also described in Section 3). These tests established that short term strain cycles must be applied if strain effect on zero-shift were to be separated from time effect on zero shift. Since the number of test points threatened to become astronomical if strain cycles were carried out at every level of pressure and temperature for each mode of loading (tensile, bending, vibration), a compromise program was adopted.*

It was decided to document strain effect on zero-shift thoroughly and completely only during the bending tests. One justification was that the only large oscillatory strains ordinarily encountered in fan or compressor operation are the oscillatory bending strains. Very small oscillations in tensile strains can occur due to the oscillations in orientation of the blade in a 100,000 G centripetal acceleration field, but such tensile strain oscillation could never exceed a few microstrain (even for a blade element oscillating through several degrees peak-to-peak in a 100,000 G field at a mean tensile strain of 3000 microstrain, a condition more severe than any actually reported in flutter tests).

Figure 2-35 shows the matrix of bending tests performed. Two separate sequences were carried out, the first to determine the effect of bending strain on transducer sensitivity at room temperature and the second to determine the effect of strain on zero-shift at two temperatures at one pressure (180 kPa).

In the first sequence, for each of two strain levels (0 and approximately 1000 microstrain). the applied pressure was cycled through the sequence of five pressures (50, 180, 310, 180, 50 kPa). Repeat cycles and random order of applied strains were incorporated in the matrix.

In the second sequence, for each of two temperature levels (21°C, 150°C) the strain was alternated between two levels (0 and approximately 1000 microstrain) six to twenty times, all at one pressure (180 kPa). The entire sequence was repeated for the first specimen tested. Repeatability at each temperature was essentially perfect, to the readability of all instrument (3 microstrain, 0.1 kPa).

*The total number of test points would have exceeded 1500, far beyond the planned scope of the program.

The raw data recorded is tabulated in Appendix III, including transducer excitation (volts), strain readings (microstrain), thermocouple readings, applied load, applied pressure, and transducer output (mV). It will be observed in the data tabulation that both positive and negative bending strains were applied in several cases to check for symmetry. In every case the effect of negative bending was equal and opposite to the effect of positive bending. Results are discussed in Section 3.

2.3.6.4 Vibration Test Matrix and Procedure

Figure 2-36 shows the matrix of vibration tests performed. These tests were performed after completion of tensile and bending tests, so the order of magnitude of oscillatory strain effects could be predicted to be very small. The vibration tests served principally to determine the effect of acceleration perpendicular to the transducer diaphragm, and to establish durability of the transducer mounting configurations in the vibration environment at three pressure levels.

For each of two peak deflection levels (0 mm and 0.635 mm zero-to-peak) the applied pressure was cycled through the sequence of five pressures (50, 180, 310, 180, 50 kPa).

The raw data recorded is tabulated in Appendix III, including transducer excitation (volts), strain readings (microstrain) and accelerometer readings, all recorded at the beginning and end of each pressure cycle, plus applied gas pressure and transducer output DC level as observed on the DC digital voltmeter and AC level as observed on an oscilloscope (mV) and a true RMS voltmeter. It will be noted that in Appendix III, the pressure cycle data for two specimens (E, Fe and B, Fe) is missing. These two specimens were tested in the same way as the others, but during the data reduction procedure the transducer DC output raw data vanished. Since it had been observed during the tests that, like all other specimens, the pressures cycles with and without vibration were virtually identical, the tests were not rerun.

2.3.7 Data Reduction Procedures

Data reduction in all static tests was straightforward and self-explanatory in most cases. The primary end quantity was sensitivity (output voltage change divided by corresponding change in applied pressure) as a function of applied pressure, temperature, strain and vibratory acceeleration level. The second end quantity was zero-shift (change in indicated pressure level) as a function of the same variables. In the case of zero-shift calculations the effects of time were eliminated by performing the calculations only on data sets obtained over time intervals of a few minutes, during which one variable was altered and then was returned to its original level, so that negligible zero-shifts with time could be confirmed. The one exception was the case of measurement of zero-shift with temperature; effects of time on zero-shift could not be separated from effects of temperature on zero-shift could not be separated from effects of temperature on zero-shift.

2.3.8 Post Analysis Tests

2.3.8.1 Configuration A Tests

After analysis of all previous test results (discussed in Section 3), it appeared that the rather high strain sensitivities could be largely due to stress concentrations arising from the machining required for each of the three configurations (B, C, E). Therefore, bending strain tests identical with those of Figure 2-35B were carried out with two spare transducers mounted on constant strain bars (Figure 2-37) using configuration A (no machining of the surface, so that the resulting buildup height above the blade surface was 0.38 mm). The data are presented in Appendix III and results are discussed in Section 3.

2.3.8.2 Shelf Life Tests

To determine whether aging of the epoxy and RTV rubber materials used by P&WA resulted in change in strain isolation behavior over extended time periods, the bending strain tests (Figure 2-35B) were repeated at room temperature for the C, Ti specimen only, 6 months after the original tests. The data are included in Appendix III and the results in Section 3.

2.4 SPIN TEST EQUIPMENT AND PROCEDURES

2.4.1 Sensors and Mounting

2.4.1.1 Transducers

The transducers used were the thin transducers specified in Figure 2-3 through 2-7, which are identical with those used in the static tests. Mounting procedures were identical with those used in static tests and described in Appendix I.

2.4.1.2 Mounting Configurations, Material and Orientations

After completion of the static test program, configurations B and $A_{0.005}$ (henceforth designated simply B and A) were selected for spin testing. The number 0.05 is the thickness of the RTV strain isolation pad given in millimeters. Configuration E was eliminated largely on the basis of the difficulty in obtaining a sufficient number of the special cylindrical transducers in the time period available. It was also recognized that configuration E, though attractive aerodynamically, required a large enough through hole in the blade to alarm the blade stress analysts, particularly in cases where multiple installations on a single blade were desired.

PWA 1202 titanium alloy (Table 2-II) was selected as the blade material for spin tests.

Orientations of 0° and 7° were selected, the designation referring to the angle between the plane of the transducer diaphragm and the plane of rotation. Seven degrees was the largest surface angle found in examining representative modern fan and compressor blades.

The leadwork and the reference scribed line provided by the manufacturer on the transducer mounting shim were oriented along a radius of the spin disk, so that the orientation of the semiconductor strain gage bridge elements in the transducer diaphragm surface, relative to the centripetal acceleration vector in the plane of the spin disk, was identical for all units, and was the orientation recommended by the manufacturer in Figure 2-1 for minimum acceleration effect.

Four transducers were mounted for each spin test (B, 0°; B, 7°; A, 0°; A, 7°). In the actual fabrication of hardware, a titanium instrumentation plate (Figure 2-38) carrying all four transducers (two on a 7° ramp) was bolted to a steel spin disk and covered with a sealed housing to form a pressurized cavity. Transducers, strain gages and thermocouples were mounted as shown in Figure 2-39.

2.4.2 Test Hardware

2.4.2.1 Spin Disk

A spin disk was procured with contractor funds, for use in this and other programs. The spin disk itself is shown in Figures 2-40, 2-41, and 2-42. The design substantiation memo for this disk is attached as Appendix IV. The disk places the transducers at a radius of 23.95 cm and its design provided for a 14% burst margin at 20,260 RPM, equivalent to 110,000 G loading at the transducer. After heat treatment of the disk, followed by final machining, it was discovered that the heat treatment had been incomplete and the disk burst strength was low by 18%. The safe loading at the transducer location was therefore 90,000 G. Additional heat treatment was considered but was ruled out on the grounds of the near certainty of resulting distortion. Since dynamic balance of a distorted disk by adding balancing weights is a questionable procedure, and since balancing by remachining the distorted disk could remove enough material to require a reduced load rating on that account, it was decided to accept the disk and limit the spin program to 90,000 G. The replacement cost of the disk was on the order of $7,000.00.

To assure reasonable balance, a dummy instrumentation plate (visible in Figure 2-41) was mounted on the disk rim 180° circumferentially from the transducer location. After all instrumentation and leadwork installations were complete and the disk mounted on its arbor (Figure 2-41), a dynamic balance was carried out (by grinding material from the dummy plate). The instrumented disk was then ready to install in the spin pit.

2.4.2.2 Pressure Transfer Device and Slip Ring

A stainless steel hypodermic tube 0.81 mm OD. x 0.51 mm ID, was cemented into a hole drilled radially through the instrumentation plate of Figure 2-38. This hole communicated (by means of holes drilled perpendicular to the plate into the tube) to the air space above and below the plate, and transmitted pressure to both the configuration A and configuration B pressure transducer diaphragms. In retrospect, it was found to be a troublesome arrangement, prone to plugging.

In a second build, one configuration B transducer was removed to provide a large open channel of communication between top and bottom of the plate.

The hypodermic tube (visible at center in Figure 2-38) was cemented firmly to the disk over its entire length, along with the leadwork from strain gages, thermocouples, and pressure transducers, and led through a slot provided at hub to a splice area and jumped to the arbor bore, as sketched in Figure 2-43.

After the disk and arbor were installed on the spin pit cover (Figure 2-42), a special pressure coupler (Figure 2-44) was slipped down over the leads and bolted to the cover. The hypodermic tube was then brazed to the pressure supply valve and through a tee to a sealed tube containing the rotating reference pressure transducer on the axis of the rotating system.

All leadwork continued up the hollow shaft and was connected to a 200-conductor high-speed miniature slip ring which bolted onto the flange at the top of the pressure coupler in Figure 2-44.

The pressure coupler provided a means for charging the system to any desired pressure level while the system was stationary, through the quick-disconnect pressure supply valve shown (an automobile tire valve), and a means for measuring the pressure on axis when the system was rotating. The pressure coupler device worked flawlessly throughout the program. Desired pressures could be set reasonably quickly and no leakage problems were encountered. This arrangement was considered a lower risk than a high speed rotating seal which, if leaky could abort the entire program plan. The rotating reference pressure transducer was redundant, but proved its worth in permitting zero-speed confidence check points to be carried out without reconnecting the exterior pressure supply.

2.4.3 Instrumentation

2.4.3.1 Disk Instrumentation and Accuracy

The instrumentation used in the spin tests is shown in Figures 2-22 and Table 2-III and is basically identical with the static test instrumentation except for use of the transfer reference pressure transduer (P_2) in the rotating system in addition to the stationary reference (P_1). However, several new sources of error arise due to the rotating environment. Errors are identified and diagrammed in Figure 2-49. Random uncertainties from individual sources are summed in quadrature to produce a final overall uncertainty of ±2.4 kPa. By far the largest error contribution is the uncertainty in the applied pressure, which alone accounts for ±2.1 kPa. The procedures used for determining this pressure and its uncertainty, including centripetal pumping corrections, are examined in the next section.

The second largest error is that due to uncertainty of the applied acceleration (including measurements of speed, radius, and two orientation angles). This error is discussed in a separate section below.

2.4.3.2 Accuracy of Applied Pressure in the Rotating System

The equations relating pressures (P), temperatures (T), volumes (V), rotational speed (ω), and radius (r) in the rotating pressurized system are presented in Figure 2-50.

The test procedure was as follows. A pressure P_1 was established in the closed system at zero RPM and measured accurately with the external stationary reference transducer. The external reference was then disconnected (without altering the pressure in the system). The spin disk was then accelerated to angular velocity ω. Due to centripetal acceleration the pressure at the rim rose to some value P_3, and the pressure on the axis fell to some value P_2.

An equilibrium temperature distribution from axis to rim became established. Temperature measurements were then made in the rotating system at five radii (with thermocouples shown in Figure 2-50). Rotational speed, ω, the radius, r_3, at which the test transducers were located on the rim, the volumes, V_2 and V_3, of the cavities on axis and on the rim, the gas constant, R, and the gravitational constant, G, all were known. Then the pressure ratio P_3/P_2 (rim pressure to axis pressure) was calculated from equation (2) of Figure 2-50.

$$\frac{P_3}{P_2} = e^{\frac{\omega^2}{GR} \int_o^{r_3} \frac{r}{T} dr} \tag{2}$$

by piecewise integration, assuming that the temperature in each interval between thermocouples was constant, i.e.,

$$\frac{P_3}{P_2} = e^{\frac{\omega^2}{2GR} \sum \frac{r_i^2 - r_{i-1}^2}{T_i}} \tag{2a}$$

where T_i is the average temperature in the i^{th} interval, bounded by $r = r_{i-1}$ and $r = r_i$. This was a simple exercise on a hand calculator or small computer. Once P_3/P_2 was determined, the rim pressure was determined by inserting this value of P_3/P_2 into the denominator of the final equation in Figure 2-50:

$$P_3 = P_{20}\left(\frac{T_3}{T_{20}}\right)\left(\frac{1 + (T_{20}/T_{30})(V_3/V_2)}{(T_3/T_2)(P_2/P_3) + (V_3/V_2)}\right) \tag{5}$$

which accounts for the effect of the volume ratio (rim cavity volume to on-axis volume).

In the actual spin tests, the temperature gradients between adjacent thermocouples never exceeded a few degrees C, so the error in the piecewise integration process (2a) was less than 0.5% and was neglected. The error then dependended only on how well the quantities 2GR, ω, r_3, V_3/V_2, T_1, T_2, and T_3 were known. The accuracy tolerances used for estimating error in P_3 were as follows:

Quantity	Value	Tolerance
$2GR_{nitrogen}$	$6 \times 10^6 cm^2/sec^2 \cdot K$	±0.2%
ω	measured (rad/s)	±0.25%
r_3	23.95 cm	±0.13%
V_3/V_2	0.64	±1.0% (note 1)
T_1/T_3	measured	±1.1%
T_3/T_2	measured	±1.1%
T_3	measured	±0.8%

Accuracy of P_3/P_2 was then estimated as follows. Rewriting (3), for constant temperature,

$$\frac{P_3}{P_2} = e^{\frac{\omega^2 r_3^2}{2GRT}}$$

or defining $P_3/P_2 = x$ and $2GR = y$,

$$x = e^{\frac{\omega^2 r_3^2}{yT}}$$

Differentiating and summing the errors in quadrature:

$$\frac{dx}{x} = \frac{\omega^2 r_3^2}{yT} \sqrt{4\left(\frac{d\omega}{\omega}\right)^2 + 4\left(\frac{dr}{r}\right)^2 + \left(\frac{dT}{T}\right)^2 + \left(\frac{dy}{y}\right)^2}$$

Then if:

$$\begin{aligned}
\omega^2 &= [(20000)(2\pi)/(60)]^2 &\approx\ & 4 \text{ X } 10^6 \text{ (rad/sec)}^2 \\
r_3^2 &= (23.95)^2 &\approx\ & 600 \text{ cm}^2 \\
T &= 291\text{K} &\approx\ & 300\text{K} \\
y &= (2)(3000)(980) &\approx\ & 6 \text{ X } 10^6 \text{ cm}^2/\text{sec}^2 \ {}^\circ\text{K}
\end{aligned}$$

and

$$\frac{d\omega}{\omega} = 0.0025, \quad \frac{dr}{r} = 0.0013, \quad \frac{dT}{T} = 0.0110, \quad \frac{dy}{y} = 0.0020$$

then

$$\omega^2 r_3^2/yT \approx 1.33$$

and

$$\frac{dx}{x} = (1.33)(0.013) = 0.017$$

Now, turning to eq. (5), for T = constant, and defining $v \equiv V_3/V_2$,

$$P_3 = XP_{20} \frac{1 + v}{1 + vx}$$

Differentiating, and taking the square root of the sum of the squares of the individual errors, and assuming $dP_{20}/P = 0$ (The error in P_{20} already was reportedly evaluated in Figure 2-49), then

$$\frac{dP_3}{P_3} = \sqrt{\left[\frac{dv}{v}\left(\frac{v}{1+v} - \frac{vx}{1+vx}\right)\right]^2 + \left[\frac{dx}{x}\left(1 - \frac{vx}{1+vx}\right)\right]^2}$$

or, for v = 0.643, x = 3.78, vx = 2.43, and random errors dx and dv,

$$\frac{dP_3}{P_3} = \sqrt{\left(0.292\frac{dx}{x}\right)^2 + \left(0.317\frac{dv}{v}\right)^2}$$

Then for $dx/x = 0.017$ and $dv/v = 0.010$, at $P = 310$ kPa,

$$dP_3 = (310)(0.0059) = 1.8 \text{ kPa.}$$

This is the value entered in the error diagram, Figure 2-49.

The error will be somewhat smaller at low pressure and low rotational speeds. This was taken into consideration in the discussion of results (Section 3).

Note 1: The volume ratio V_3/V_2 was determined experimentally in two ways, first by physical measurements of the cavities and second by measuring the pressure decrement when each cavity was pressurized separately and bled into a precisely known volume. The two measurements agreed within 1.5%. The average of the two volume ratios (0.643) was used and assigned an uncertainty of ±1.0%

2.4.3.3 **Test Error Due to Acceleration Uncertainty**

The centripetal acceleration, a, is:

$$a = \omega^2 r$$

Differentiation yields:

$$\frac{da}{a} = 2\frac{d\omega}{\omega} + \frac{dr}{r}$$

or, for random errors in ω and r:

$$\frac{da}{a} = \sqrt{4\left(\frac{d\omega}{\omega}\right)^2 + \left(\frac{dr}{r}\right)^2}$$

and for $\frac{d\omega}{\omega} = 0.0025$ and $\frac{dr}{r} = 0.0013$:

$$\frac{da}{a} = 0.0051$$

Then at 100,000 G, the uncertainty is da = 510 G

If the zero-shifts of the test transducer due to parallel acceleration and normal acceleration are 0.14 Pa/G and 0.7 Pa/G, respectively, as specified by the manufacturer, the zero-shift due to the two components at 7° inclination is:

$$\frac{dp}{da} = (0.14 \cos 7°) + (0.7 \sin 7°) = 0.22 \text{ Pa/G}$$

and, the uncertainty in pressure is:

$$dp = 0.22 \text{ X } 510 \cong 100 \text{ Pa}$$

This is the value entered in the error diagram of Figure 2-49 for effects of ω and r.

Additional uncertainties due to acceleration effects arise if the orientation angles of the semiconductor strain elements measured in the plane of the spin disk (θ_1) and perpendicular to the spin disk (θ_2) are not exactly known. The design substantiation memo for this spin disk (Appendix IV) states an uncertainty of 0.3° in θ_2 including effects of flexing at maximum rotational speed (90,000 G at the transducer location). The transducer specification requires θ_1 to be identical within 2° for all transducers. The effects on pressure zero axis uncertainty are then as follows(assuming that at worst the effect of changing θ_1 by 90° is to double the effect of parallel acceleration):

For $d\theta_1 = 2°$: $dp = (0.14)(90{,}000)(\sin 2°) \approx 500$ Pa

For $d\theta_2 = 0.3°$: $dp = (0.7)(90{,}000)(\sin 0.3°) \approx 400$ Pa

These values are entered in the error diagram of Figure 2-49 for the effects of θ_1 and θ_2.

2.4.4 Test Facility

Figure 2-45 is a sketch of the spin pit test setup in X-117 Stand at Product & Whitney Aircraft.

In this facility, the drive turbine was steam driven. The turbine was mounted horizontally on the test facility pit cover and the rig to be spun was simply pinned to a drive spindle which extended through the lower portion of the turbine case. The drive spindle was fastened to the top of the turbine bucket wheel with two woodruff keys. No lower support bearings were utilized. Thus the rig was suspended pendulum fashion providing more freedom of movement for finding its own center of rotation. As a result, the entire system had a relatively large tolerance for rig imbalance.

Speed was controlled by remotely operated steam valves and was closely monitored and displayed by an electronic digital counter. Hard copy printout was provided by a mechanical printer. The digital counter and printer are calibrated every three months by the instrument laboratory standards section. The digital counter calibration is done in conjunction with equipment traceable to the National Bureau of Standards. The counter readout was the major item monitored by the test operator during the tests. Two speed signal pickups were used at the turbine. If a five-percent error between pickup signals occurs, the steam supply is automatically shut off as a safety precaution.

In order to satisfy the temperature requirements of the test program a small circular 220-volt Calrod-type resistance heater was used. This was installed above the test rig disk and supported by rods extending from the pit cover. Heater output was controlled by remotely operated variacs from the main control panel. Figure 2-46 shows the control console used.

During normal operation, the spin pit was evacuated to approximately 1 kPa pressure by a vacuum pump.

Figure 2-47 shows a general view of a typical spin rig installation with the pit cover raised. Figure 2-48 is a closer view of the slip ring and pressure coupler installed above the drive turbine on the pit cover in the present program. Accelerometers are visible mounted on two lateral axis at the outboard (top) end of the slip ring installation. Vibration on both axes was continuously monitored. Bearing temperatures in the pressure coupler and in the slip ring were also continuously monitored.

A multipoint temperature recorder, with printout on command, was used to record all disk temperatures.

2.4.5 Test Procedure

2.4.5.1 Spin Test Matrix

The test sequence is diagrammed in Figure 2-51. Run No. 1 and Run No. 2 (to 16,700 RPM 75,000 G, 27°C) were shakedown tests to obtain vibration data for rig safety. A maximum vibration level of 0.15 mm peak deflection was detected at about 8000 RPM (typical of the spin rig). A trim balance was performed and balance weights were adjusted at the slip ring tag board until vibration amplitudes at all operating speeds were below 0.05 mm peak. Run No. 3 was a low speed test of the heaters in the spin pit, and established that an equilibrium temperature of 82°C could be attained in about three hours with air at about atmospheric pressure in the spin pit, and that after subsequent evacuation of the air (to permit operation at high speeds without aerodynamic heating), the temperature could be maintained stably with a low setting of heater controls.

In Runs 4 through 7, pressure transducer output voltages were recorded for applied pressures of 7, 150, and 310 kPa at centripetal acceleration loadings of 27,500, 55,000, 75,000 and 90,000 G at 27°C. Operating problems with leadwork in the bore of the spin drive spindle and at the slip ring tagboard, and with plugging of the small-diameter bleed holes in the pressurization system to the configuration B transducers in the transducer cavity, limited valid data during this sequence to one of the four transducer configurations (B, 0°). In addition, one of the four transducers (A, 7°) was found to have developed a slow pressure leak after installation in the spin pit had begun.

After completion of Run No. 7, the spin disk was removed from the spin pit and several changes were made. The leaking A, 7° transducer was replaced with a new A, 7° transducer. The B, 0° transducer, for which a complete set of spin data at 27°C had now been obtained, was removed completely and not replaced, so that the 1.5 mm hole machined in the instrumentation plate as part of its installation could serve as a bypass for the blocked pressurization system to the B, 7° transducer.

As a piggyback test in subsequent spin testing, a thin transducer was mounted directly on the spin disk using configuration A with one important experimental alteration: no epoxy was used in mounting the shim to the disk. A 0.05 mm layer of RTV rubber between the shim and the disk provided both strain isolation and adhesion. This type of installation, considered a higher mechanical risk, was worth trying for two reasons. First, eliminating the epoxy and its curing procedure simplified the installation technique, and second, the technique offered the option of installing transducers with leadwork and shim in any orientation, rather than limiting the geometry to a shim cantilevered radially outward. (It should be noted that if a transducer were mounted in a different orientation, consideration would have to be given to specifying a different orientation of the semiconductor strain gages on the diaphragm.) In this experimental installation, the usual orientation was used. The leadwork was cemented to the disk as usual, but was not connected to the data acquisition system. The test was designed to evaluate mechanical survival only.

The disk was reinstalled in the spin pit, and the leadwork reconnected to the pressure coupler and slip ring. Runs 8 through 14 (Figure 2-51) were then conducted, in which pressure transducer output voltages were recorded for the same three applied pressures as before (7, 150, 310 kPa) at centripetal acceleration loadings of 27,500, 55,000, 75,000 G successively at 27°C, and then at centripetal acceleration loadings of 27,500, 55,000, 75,000, and 90,000 G successively at 82°C. Leadwork problems in the bore of the drive spindle again limited valid data during this sequence, but this time useful pressure data was obtained with all three active transducers, as follows:

A, 0° All conditions except 90,000 G, 82°C

A, 7° Up to 55,000 G, 27°C only

B, 7° Up to 25,000 G, 27°C only

All transducers including the non-epoxy mounted sample, survived all spin testing, including the 90,000 G, 82°C test.

As a result of the spin program, repeatable pressure data had been obtained for all four types of installation (B, 0°; B, 7°; A, 0°; A, 7°) at three pressures at accelerations to at least 27,500 G, 27°C, and for two of the configurations to 75,000 G, 27° and one to 75,000 G 82°C. A total of six transducers installation had been spun to 90,000 G. The test data conditions are summarized in Figure 2-51. The test data is tabulated in Appendix III.

Post test examinations were conducted, including check calibrations of the mounted transducers, physical inspection of the mountings and leadwork on the disk, and careful step-by-step removal of the B, 7° transducer with inspection of the condition of adhesive, shim, and transducer structure at each step. The discussion of these examinations is included in Section 3.

In addition, the lead wire problems in the drive spindle bore and slip ring tagboard areas were investigated post mortem, and are discussed separately below as problems peculiar to the test fixtures.

2.4.5.2 Spin Test Procedure

In order to account for the zero shifts with time during the course of any one acceleration, stabilization at speed, and deceleration of the spin disk, the 15-step test sequence shown in Figure 2-52 was eventually used during each run of Figure 2-51. This optimum procedure was developed as a result of experience during Runs 4 through 7. In the data summary, Appendix III, it will be noted that the sequence of Figure 2-52 was followed exactly in Runs 8 through 14, but that in the earlier Runs, 4 through 7, a much larger number of repeat points was used to gain the same information.

Before considering the details of the procedure, first note that three reference pressure levels, P_7, P_{150}, P_{310}, were calculated in advance for each run, defined as follows:

P_7 Pressure required in system at 0 RPM to produce 7 kPa at the transducer at speed.

P_{150} Pressure required in system at 0 RPM to produce 150 kPa at the transducer at speed.

P_{310} Pressure required in system at 0 RPM to produce 310 kPa at the transducer at speed.

The calculation could only be approximate since exact temperature distribution was not known in advance. Pressures actually attained at speed were later calculated from the test data. The preliminary calculation provided assurances that pressures reasonably close to the desired levels would be attained.

A minimum procedure for measuring acceleration effects at one speed would have been six steps as follows:

Step	RPM	Procedure
1	O	Set P_7, Read outputs, Disconnect*
2	N	Read outputs
3	O	Set P_{150}, Read outputs, Disconnect*
4	N	Read outputs
5	O	Set P_{310}, Read outputs, Disconnect*
6	N	Read outputs

Two effects would be ignored in this simple sequence. First, the effect of zero-drift with time could be substantial, since the six steps could easily take a half hour to one hour to complete.

Second, any leak in the pressurized system might go undetected. To check for drift effect, three check readings at applied pressure P_{150} were added, one before step 1, one after step 4, and one after step 6. This increased the number of steps to nine. Then to check for leaks, a reading was taken immediately after each deceleration to 0 RPM and before reattaching the external reference system, and this was compared with a reading taken immediately after that when the reference pressure system was reconnected and set to the initial pressure (P_7, P_{150}, P_{310}, as the case might be). This added five steps to the procedure bringing the total to fourteen.

Finally it was realized that this procedure also constituted a complete direct check calibration of each transducer against the transfer-standard stationary transducer during the course of each run, with the exception of pressure near 310 kPa. Therefore, a fifteenth step was added at the end – a reading of each transducer at zero RPM with 310 kPa applied. The complete procedure of Figure 2-52 was thus evolved.

The procedure worked well, and plotting the raw data while the run was in progress instantly identified any nonsensical results (such as misreading the algebraic sign of transducer outputs) and permitted repeat readings on the spot. If the reading pairs (D, E), (H, I), (L, M) were not identical within 1 kPa, the condition was rerun.

If the reading pairs (A, F), (I, N) showed any unusually erratic drift pattern, the whole run was repeated. It will be seen in the data log of Appendix III that a few cases of this kind did occur.

*Disconnect stationary reference supply without altering readings of transducers in the spin disk system.

2.4.6 Spin Test Data Reduction Procedure

From each of the spin test runs (No. 4 through No. 14), five end quantities were desired:

Zero-shift due to rotation at 7 kPa

Zero-shift due to rotation at 150 kPa

Zero-shift due to rotation at 310 kPa

Sensitivity change (7-150 kPa) due to rotation

Sensitivity change (150-310 kPa) due to rotation

The calculation procedure used to reduce the data from any one transducer in one run is summarized in Table 2-IV. The symbols used in Table 2-IV are as follows:

P Actual pressure at the transducer (kPa)

E Transducer output (mV)

ϕ Transducer sensitivity (mV/kPa)

Where a single subscript is used with P or E, the P or E is an actual value obtained at the indicated step of the 15 step test procedure of Figure 2-52. Thus the possible single subscripts are A, B, C, . . ., O.

Where a double subscript is used with E, E is a value of transducer output (mV) corrected for zero-drift with time, and adjusted (in the case of readings at zero RPM, where sensitivity is known) to a corresponding rotating pressure level. The possible subscripts for E_{ij} are:

i =	0 at P = 0 kPa	j =	0 at 0 RPM
	1 at $P = P_C$		N at N RPM
	2 at $P = P_G$		
	3 at $P = P_K$		
	4 at P = 310 kPa		

When a double subscript is used with ϕ, then ϕ is a value of sensitivity calculated from the corrected values of E. Thus

$$\phi_{1N} = \frac{E_{2N} - E_{1N}}{P_G - P_C}$$

and so forth.

Other quantities used in Table 2-IV are defined as they are used.

The five desired final quantities are those calculated on lines 61, 62, 68, 69 and 70 of Table 2-IV.

The results of processing the data of Appendix IV through this calculation procedure are discussed in Section 3.

2.4.7 Operating Problems In the Rotating System

The first build used a miniature liquid-cooled 200-conductor slip ring with a solid shaft. Since the rotating connector hardware usually used with this type of slip ring was not available, a special tagboard was fabricated, with an annular cavity ("cup") provided at the inboard end of the slip ring. Leadwire slack was spiraled into the cup during final assembly. This was a procedure used successfully in the past.

Early in the test, two pressure transducer channels developed open circuits. The tagboard area of the miniature slip ring was suspected as a possible source for the open circuits because it contained many leadwire splices which might be improperly supported. Removal of the slip ring would have been necessary to exposure the tagboard area, but was not done in order to avoid additional damage to the spin-set lead bundle. A slip-ring bearing failure later terminated the test. The slip ring was new and had been bench spin tested to 24,000 RPM, before installation in the spin pit, without distress. Vibration and slip ring bearing temperatures were monitored during the spin pit tests and no unusual conditions were observed. Identical slip rings had been used in ten P&WA programs successfully. There is no explanation available for the bearing failure.

As a result of the slip ring bearing failure, the tagboard cup rubbed against the housing, leadwire burning and prevented a meaningful inspection of the lead splices. Since all leakwork from this point to the disk rim was intact, the original diagnosis was believed to be correct.

Use of the preferred rotating connector hardware or a hollow shaft type of slip ring with exposed tagboard (as in the second spin test) would avoid the type of lead wire problem encountered here.

A conventional hollow-shaft air-cooled slip ring was used in the second build (Figure 2-39).

During installation of the slip ring, one sensor lead was broken inside the drive spindle shaft of the spin rig. Repair was not attempted in order to avoid pulling the rig off the turbine. One open circuit and one short circuit in pressure channels developed during spin testing, although the problems disappeared each time the rig stopped spinning. A teardown inspection showed the otherwise undamaged leads to the severely chafed in three locations between the spin rig drive spindle and tagboard area. The short-circuit problem could be duplicated by pressing the chafed leads together (or against the shaft), but the open circuit could not be located. Since vigorous tugging on the leadwires from the top of the drive spindle to the spin disk produced no open circuit, the problem was believed to be in the slip ring tagboard area.

A method of avoiding the leadwire chafing in a future build of the same rig would be to reduce the lead bundle size by cutting down on the size or number of lead wires and using the space gained for heavy duty protective sleeving. The space available at the top of the drive spindle (Figure 2-43) is limited.

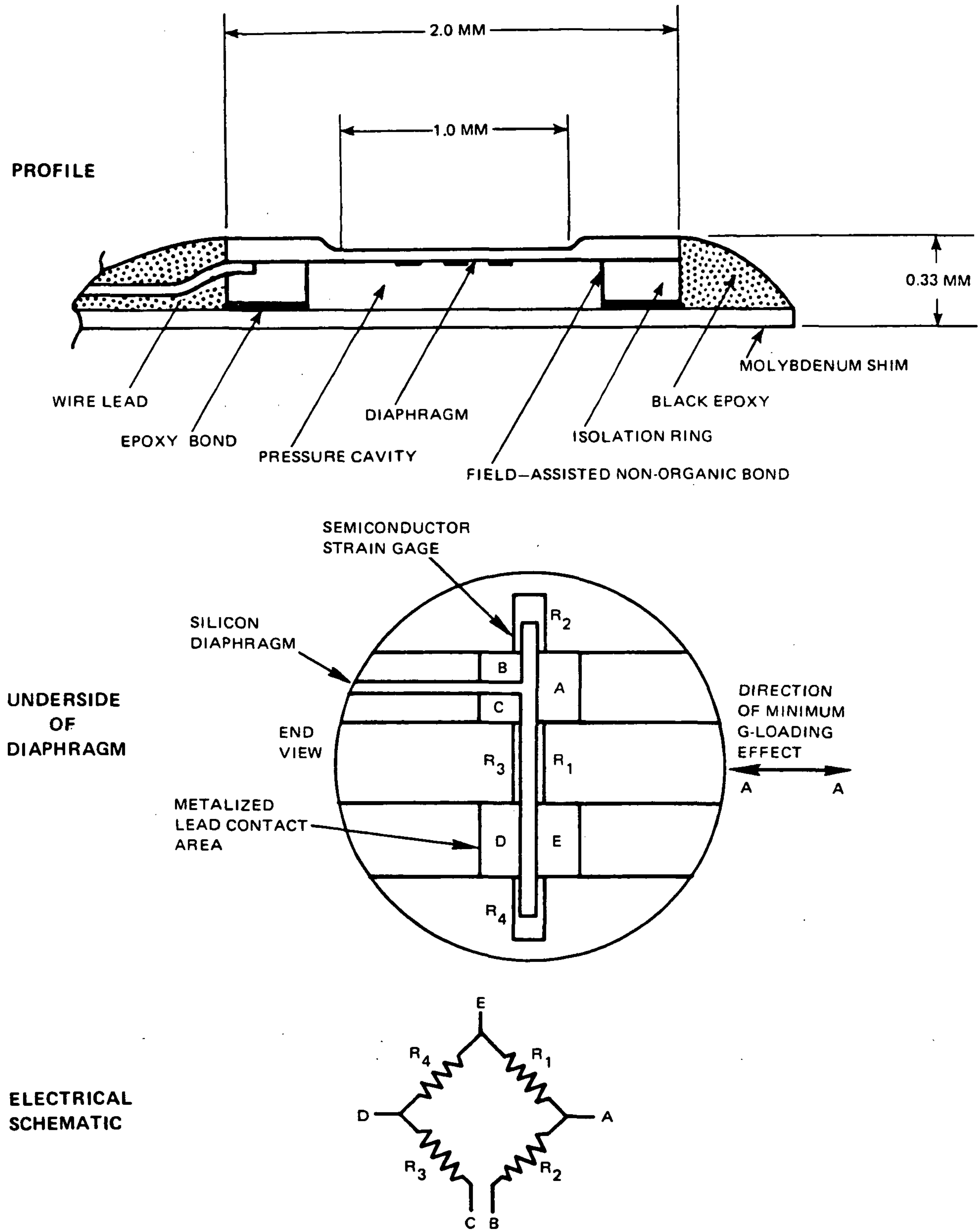

Figure 2-1 *Low-Profile Transducer – Manufacturers have achieved transducer thickness reductions as shown here.*

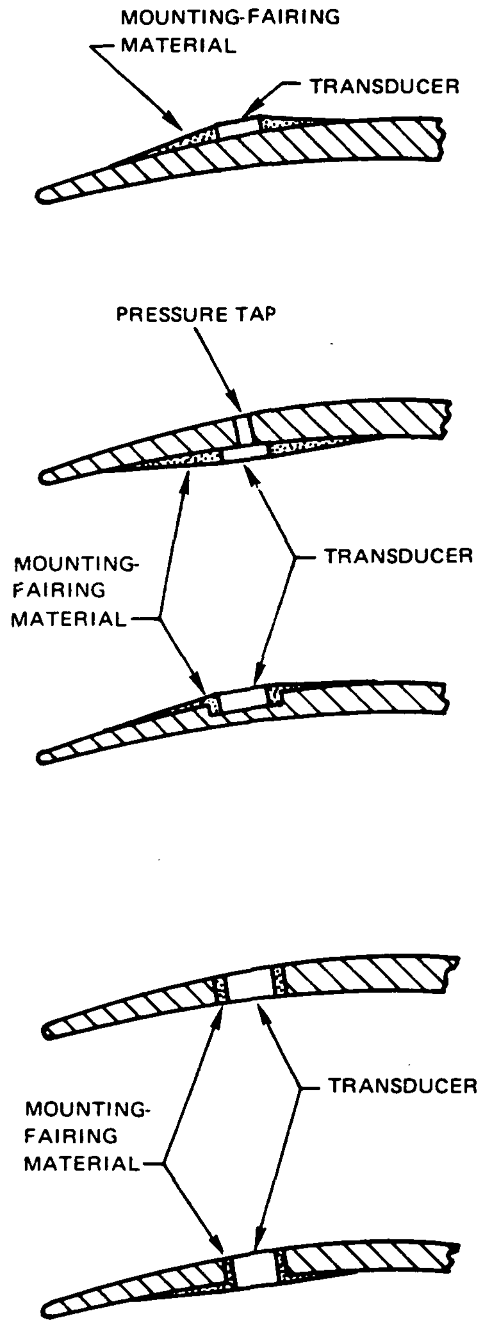

A. SURFACE MOUNTED TRANSDUCER ON THE SUCTION SURFACE.

B. SURFACE MOUNTED TRANSDUCER ON THE PRESSURE SURFACE WITH PRESSURE TAP TO THE SUCTION SURFACE.

C. TRANSDUCER MOUNTED IN AN INDENTATION.

D. TRANSDUCER MOUNTED IN A HOLE.

E. TRANSDUCER MOUNTED IN A HOLE TRANSDUCER EXTENDS BEYOND THE PRESSURE SURFACE.

Figure 2-2 Pressure Transducer Mounting Arrangements

(1) THE SPECIFICATIONS REQUIRED FOR THIS TRANSDUCER ARE THE SAME AS FOR THE LQL-080-25 THIN LINE SERIES GIVEN IN KULITE BULLETIN KPS-LQ-080A EXCEPT AS NOTED BELOW. AND IN ATTACHED FIGURES 2-4, 2-5, 2-6, AND 2-7.

(2) THE TRANSDUCER IS TO BE A 25 PSI UNIT WITH THE INSIDE AIR CAVITY SEALED FROM THE OUTSIDE ATMOSPHERIC PRESSURE. ALL SPECIFICATIONS MUST ALSO APPLY TO A 20 PSI OVERRANGE (I.E., TO 45 PSIA).

(3) THE TRANSDUCER IS TO HAVE A MAXIMUM OPERATING TEMPERATURE OF 350°F

(4) THE TRANSDUCER COMPENSATION RANGE IS TO BE 80°F TO 300°F WITH A MAXIMUM ZERO SHIFT OF 2% F.S./100°F AND A MAXIMUM SENSITIVITY CHANGE OF ±0.025%/°F

(5) THE TRANSDUCER, SHIM STOCK, LEAD WIRE, AND ADHESIVE FILM (THE TRANSDUCER ASSEMBLY) MUST BE THINNER THAN 0.012 INCHES (DIMENSION "A").

(6) THE TRANSDUCER MUST BE MOUNTED ON A 1.0 INCH SQUARE BY 0.001 INCH THICK MOLYBDENUM SHIM PERFORATED THROUGHOUT THE TOTAL SHIM AREA. THE HOLES MUST BE 0.010 TO 0.015 INCHES IN DIAMETER ON 0.035 TO 0.045 INCH CENTERS. THE SHIM STOCK MATERIAL MUST BE FLAT.

(7) ELIMINATE SOLDER TABS BETWEEN GOLD WIRES AND LARGER LEADS, AND USE A WIRE TO WIRE IN LINE SPLICE

(8) THE LEAD REQUIREMENTS ARE:
  A) 2 FEET OF ISONEL 0.005 INCH DIAMETER WIRE FROM THE TRANSDUCER TO A SPLICE
  B) 3 FEET OF AWG 30 - 7/38 ETCHED TEFLON-SHEATHED COPPER WIRE FROM THE SPLICE TO THE COMPENSATION MODULE.
  C) 2 FEET OF AWG 30 - 7/38 ETCHED TEFLON-SHEATHED COPPER WIRE FROM THE COMPENSATION MODULE TO THE WIRE END

(9) KEEP ADHESIVE AREA TO A MINIMUM.

(10) THE TRANSDUCER TOP SURFACE INCLUDING THE DIAPHRAGM IS TO HAVE AN ALUMINUM COATING (1 μm SPUTTERED) TO REDUCE LIGHT SENSITIVITY.

(11) ORIENT THE TRANSDUCER STRAIN ELEMENTS WITH RESPECT TO THE G-LOADING AXIS TO MINIMIZE THE EFFECTS OF HIGH TRANSVERSE G-LOADS. APPLY SCRIBE LINE TO DEFINE WITHIN ± 2° THE ORIENTATION OF TRANSDUCER STRAIN ELEMENTS.

(12) THE COMPENSATION MODULE IS TO BE ENCASED IN STANDARD STEEL TUBE 0.100 INCH DIAMETER X 1.25 INCHES LONG. A TEMPERATURE MEASURING RESISTOR (R_T) IS TO BE INCLUDED IN THE COMPENSATION MODULE. THE VALUE IN OHMS OF R_T IS TO BE KEPT AS CLOSE TO THE ILLUSTRATED VALUE AS POSSIBLE WHILE STILL MEETING STATEMENT (4).

Figure 2-3 Specification for Thin Transducer, Kulite Model LQL-5-080-25S

ORIGINAL PAG
OF POOR QUAI

LQ-080 Specifications

SPECIFICATIONS	LQL-080-25	LQL-080-50	LQL-080-100
Rated Pressure	25 psi	50 psi	100 psi
Maximum Pressure	50 psi	100 psi	300 psi
Nominal Output at Rated Pressure	75 mV	100 mV	100 mv
Bridge Excitation (DC or AC)	5V DC or AC RMS	5V DC or AC RMS	5V DC or AC RMS
Bridge Impedance (nom.)	750 ohms	750 ohms	750 ohms
Zero Balance	±5% FS max.	±3% FS max.	±3% FS max.
Combined Non-Linearity and Hysteresis	±1% FS max.	±1% FS max.	±1% FS max.
Repeatability	±0.5%	±0.5%	±0.5%
Compensated Temperature Range	80°F to 180°F (25°C to 80°C) Any 100°F range within the operating range on request.		
Operating Temperature Range	0°F to 200°F (—20°C to 95°C) Temperatures to 350°F (175°C) available on special order		
Change of Sensitivity with Temp. (constant voltage excitation)		—.06%/°F or ±.025/°F (see Note 1)	
Change of No-Load Output with Temperature	±.03% FS/°F	±0.02% FS/°F	±0.02% FS/°F
Natural Frequency (approx.)	125 KHz	140 KHz	200 KHz
Acceleration Sensitivity: (perpendicular) (transverse)	0.0004% FS/g 0.00008% FS/g	0.0003% FS/g 0.00006% FS/g	0.0002% FS/g 0.00004% FS/g
Resolution	Infinite	Infinite	Infinite

Note 1: ±.025%/°F obtained by using constant voltage excitation (15V) with a 1500 ohm resistance in series with the transducer.

LQ-080 Series Outline

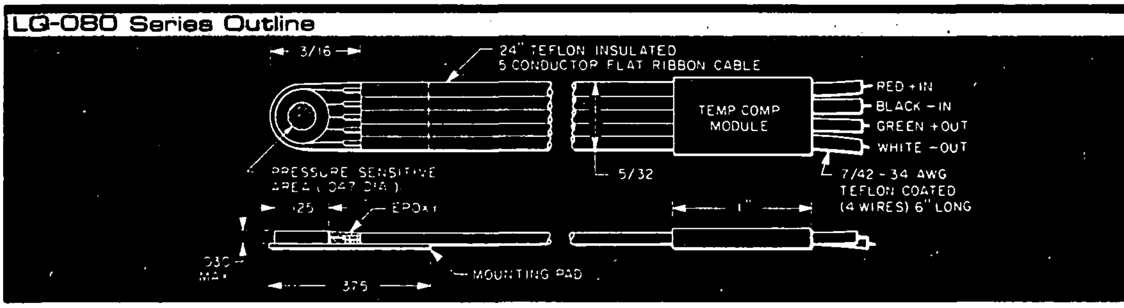

Transducer Circuit

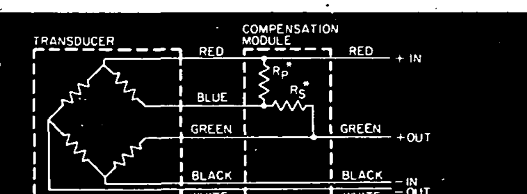

* These resistors are sometimes connected in the lower leg between the BLACK, GREEN and BLUE wires.

Bulletin KPS-LQ-080A

Figure 2-4 *Manufacturer's Specification for Thin Transducer, Kulite Model Series LQL-080-25*

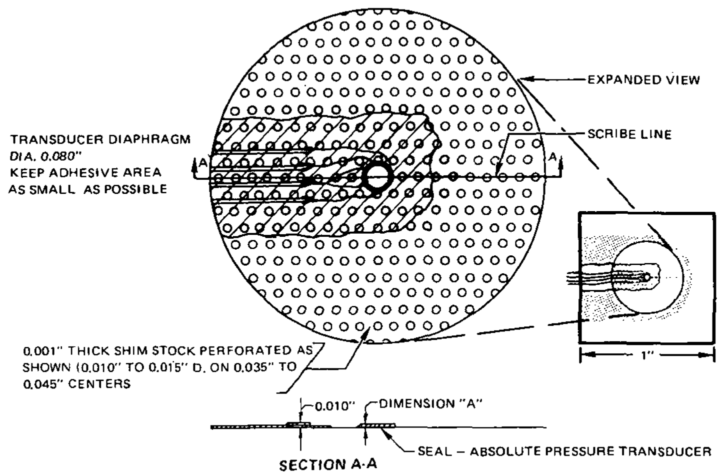

Figure 2-5 Thin Surface Mount Transducer, P&WA Requirements

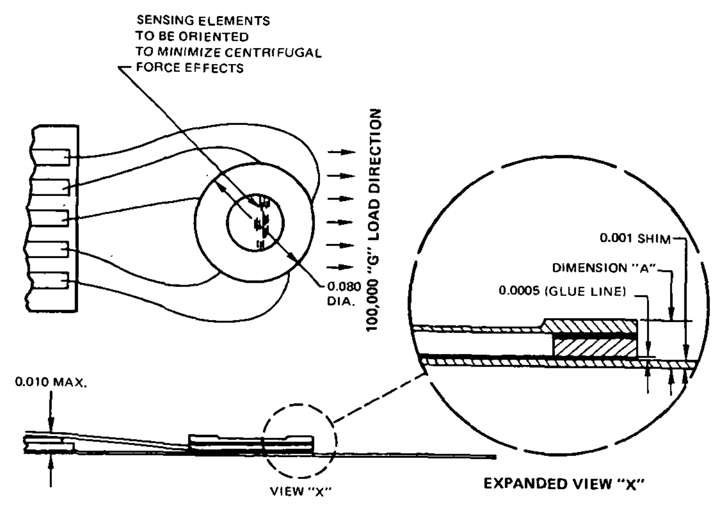

Figure 2-6 Transducer Diaphragm Detail – Thin Surface Mount Transdı

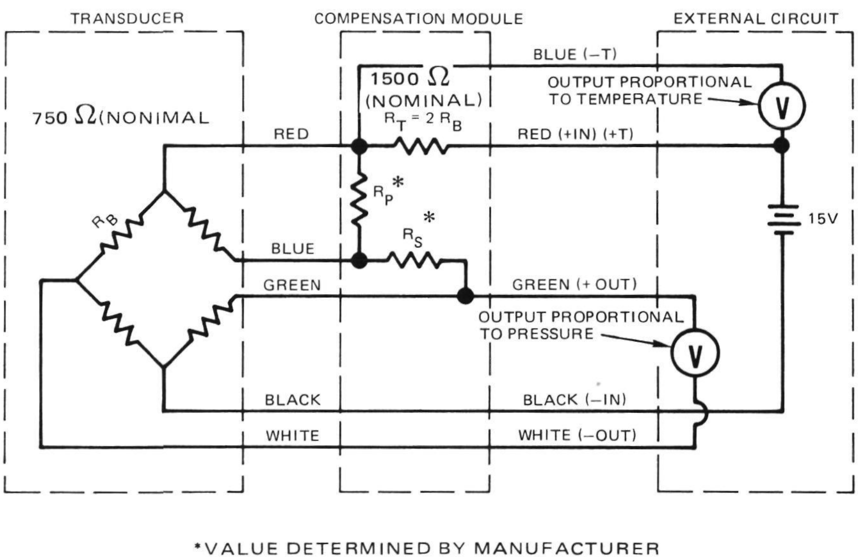

Figure 2-7 Test Transducer Wiring Diagram

B

A

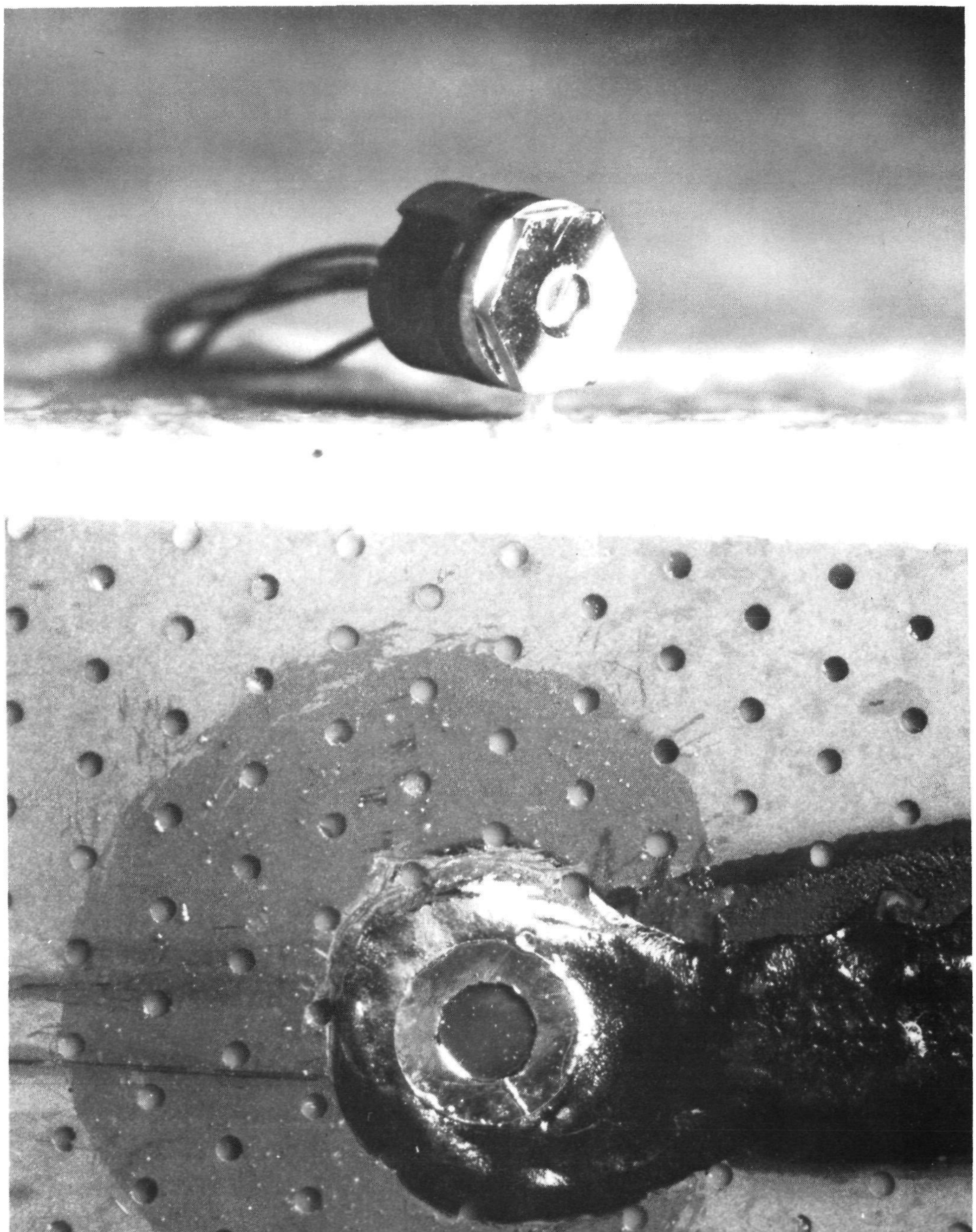

Figure 2-8 *Transducers As Received From Manufacturer. (A) Thin transducer. (B) Cylindrical transducer.*

(1) THE SPECIFICATIONS REQUIRED FOR THIS TRANSDUCER ARE THE SAME AS THE CQL-080-25S SERIES GIVEN IN KULITE BULLETIN KPS CQ-080 EXCEPT AS NOTED BELOW, AND IN ATTACHED FIGURES 2-7, 2-10, AND 2-11.

(2) THE TRANSDUCER IS TO BE A 25 PSI UNIT WITH THE INSIDE AIR CAVITY SEALED FROM THE OUTSIDE ATMOSPHERIC PRESSURE. ALL SPECIFICATIONS MUST ALSO APPLY TO A 20 PSI OVERRANGE (I.E., TO 45 PSIA).

(3) THE TRANSDUCER IS TO HAVE A MAXIMUM OPERATING TEMPERATURE OF 350°F.

(4) THE TRANSDUCER COMPENSATION RANGE IS TO BE 80°F TO 300°F WITH A MAXIMUM ZERO SHIFT OF 2% F.S./100°F AND A MAXIMUM SENSITIVITY CHANGE OF ±0.025%/°F

(5) THE TRANSDUCER HOUSING AND ADHESIVE MUST BE NO LONGER THAN 0.080 INCHES OVERALL.

(6) THE LEAD REQUIREMENTS ARE:

A) 2 FEET OF ISONEL 0.005 INCH DIAMETER WIRE FROM THE TRANSDUCER TO A SPLICE

B) 3 FEET OF AWG 30 - 7/38 ETCHED TEFLON-SHEATHED COPPER WIRE FROM THE SPLICE TO THE COMPENSATION MODULE

C) 2 FEET OF AWG 30 - 7/38 ETCHED TEFLON-SHEATHED COPPER WIRE FROM THE COMPENSATION MODULE TO THE WIRE END

(7) THE TRANSDUCER TOP SURFACE INCLUDING THE DIAPHRAGM IS TO HAVE AN ALUMINUM COATING (1 μm SPUTTERED) TO REDUCE LIGHT SENSITIVITY.

(8) MARK TRANSDUCER HOUSING WITH A SCRIBE LINE INDICATING G LOAD DIRECTION FOR MINIMUM EFFECT OF TRANSVERSE G LOADS. SCRIBE LINE MUST BE LOCATED WITHIN AN ACCURACY OF ± 2 DEGREES.

(9) THE COMPENSATION MODULE IS TO BE ENCASED IN STANDARD STEEL TUBE 0.100 INCH DIAMETER X 1.25 INCHES LONG. A TEMPERATURE MEASURING RESISTOR (R_T) IS TO BE INCLUDED IN THE COMPENSATION MODULE PER FIGURE 5. THE VALUE IN OHMS OF R_T IS TO BE KEPT AS CLOSE TO THE ILLUSTRATED VALUE AS POSSIBLE WHILE STILL MEETING STATEMENT (4).

Figure 2-9 Specification for Cylindrical Transducer, Kulite Model LQL-14-080-25S

CQ-080 Specifications

SPECIFICATIONS	CQL - 080-25	CQL - 080-50	CQL - 080-100	CQL - 080-200	CQL - 080-500
Rated Pressure	25 psi	50 psi	100 psi	200 psi	500 psi
Maximum Pressure	50 psi	100 psi	200 psi	400 psi	1000 psi
Output—Nominal at Rated Pressure	75 mv	90 mv	100 mv	100 mv	100 mv
Bridge Excitation	5v nom. 7.5v max. AC or DC				
Bridge Impedance	750 ohms (nominal)	750 ohms (nominal)	750 ohms (nominal)	750 ohms (nominal)	750 ohms (nominal)
Zero Balance	±3% FS max.	±3% FS max.	±3% FS max.	±3% FS max.	±3% FS max.
Combined Non-Linearity and Hysteresis	±1.0% FS max.	±1.0% FS max.	±1.0% FS max.	±1.0% FS max.	±1.0% FS max.
Repeatability	0.5%	0.5%	0.5%	0.5%	0.5%
Compensated Temperature Range	80°F to 180°F (25°C to 80°C) Any 100°F range within the operating range on request.				
Operating Temperature Range	0°F to 250°F (−20°C to 120°C) Temperatures to 350°F (175°C) available on special order.				
Change of Sensitivity with Temperature	±2.5%/100°F when excited as in note 1.				
Change of No-Load Output with Temperature	±2% FS/100°F (max.)	±2% FS/100°F (max.)	±2% FS/100°F (max.)	±2% FS/100°F (max.)	±2% FS/100°F (max.)
Natural Frequency (approx.)	125 KHz	150 KHz	210 KHz	280 KHz	420 KHz
Acceleration Sensitivity: Perpendicular Transverse	0.0003% FS/g 0.00006% FS/g	0.0002% FS/g 0.00004% FS/g	0.0001% FS/g 0.00002% FS/g	0.00009% FS/g 0.000018% FS/g	0.00005% FS/g 0.00001% FS/g
Resolution	Infinite	Infinite	Infinite	Infinite	Infinite

Note 1.....When using a 15v constant voltage source with 1500 ohms in series with the transducer.

CQ-080 Series Outline

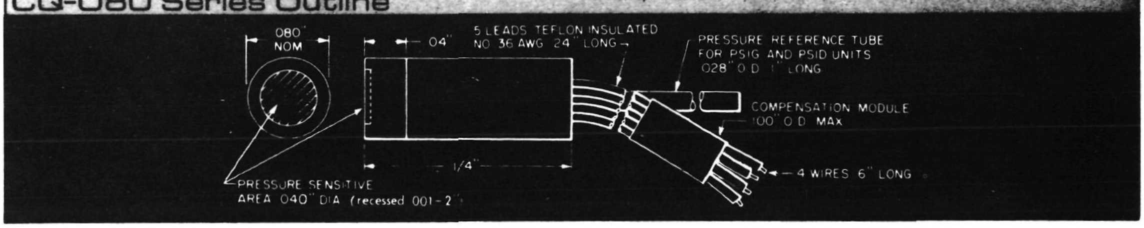

Transducer Circuit

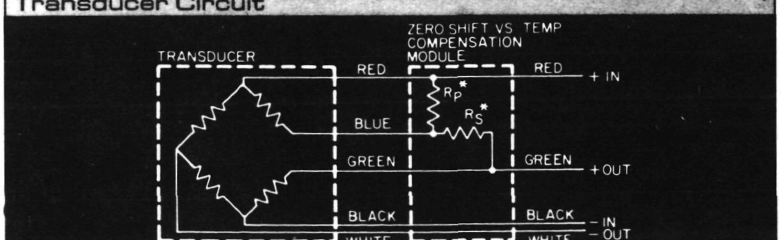

* These resistors are sometimes connected in the lower leg between the BLACK, GREEN and BLUE wires

Typical Installation

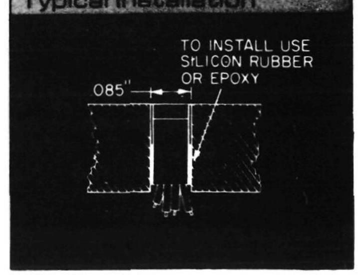

Bulletin KPS-CQ-080

Figure 2-10 Manufacturer's Specification for Kulite CQL-080 Series Cylindrical Transducers

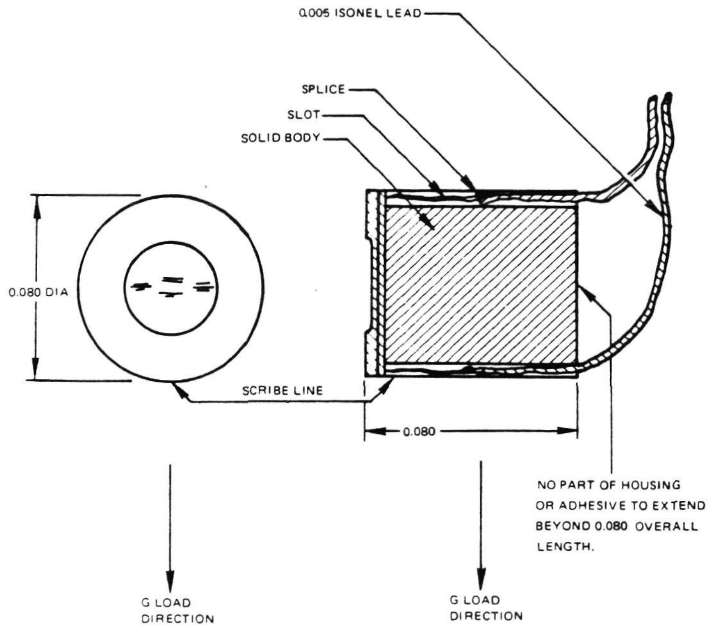

Figure 2-11 Kulite LQL-14-080-25S Transducer

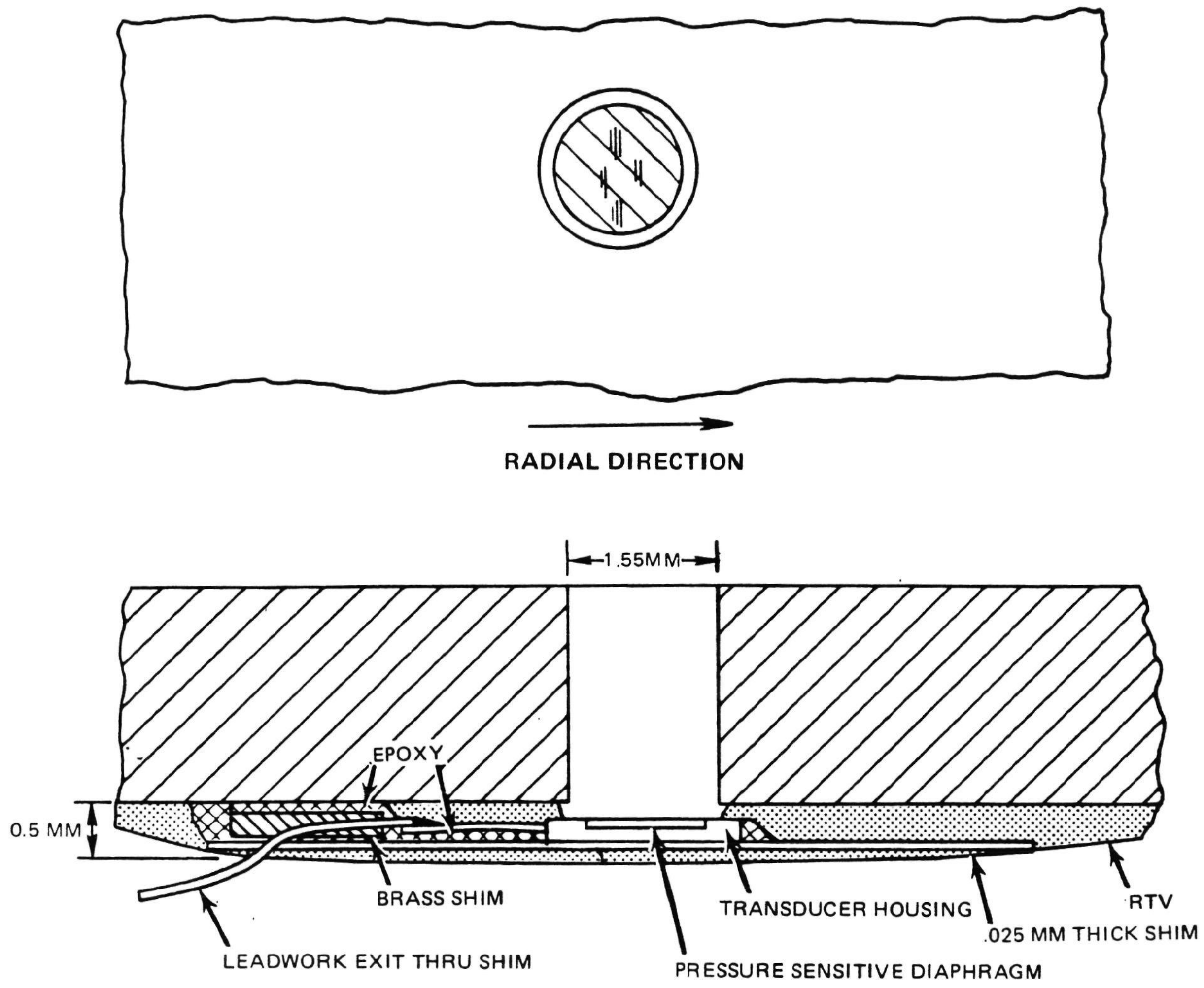

Figure 2-12 Transducer Mounting – Configuration "B"

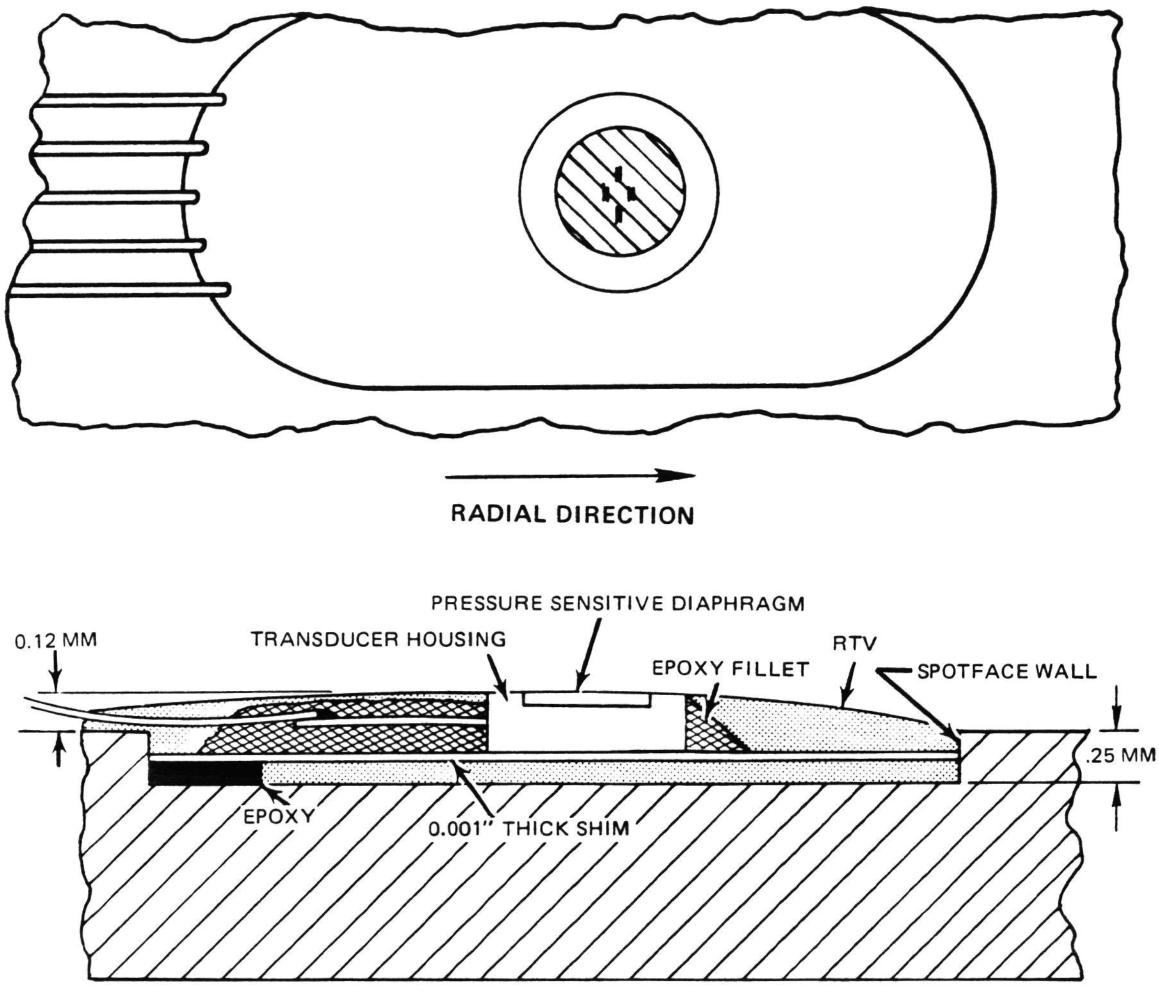

Figure 2-13 Transducer Mounting – Configuration "C"

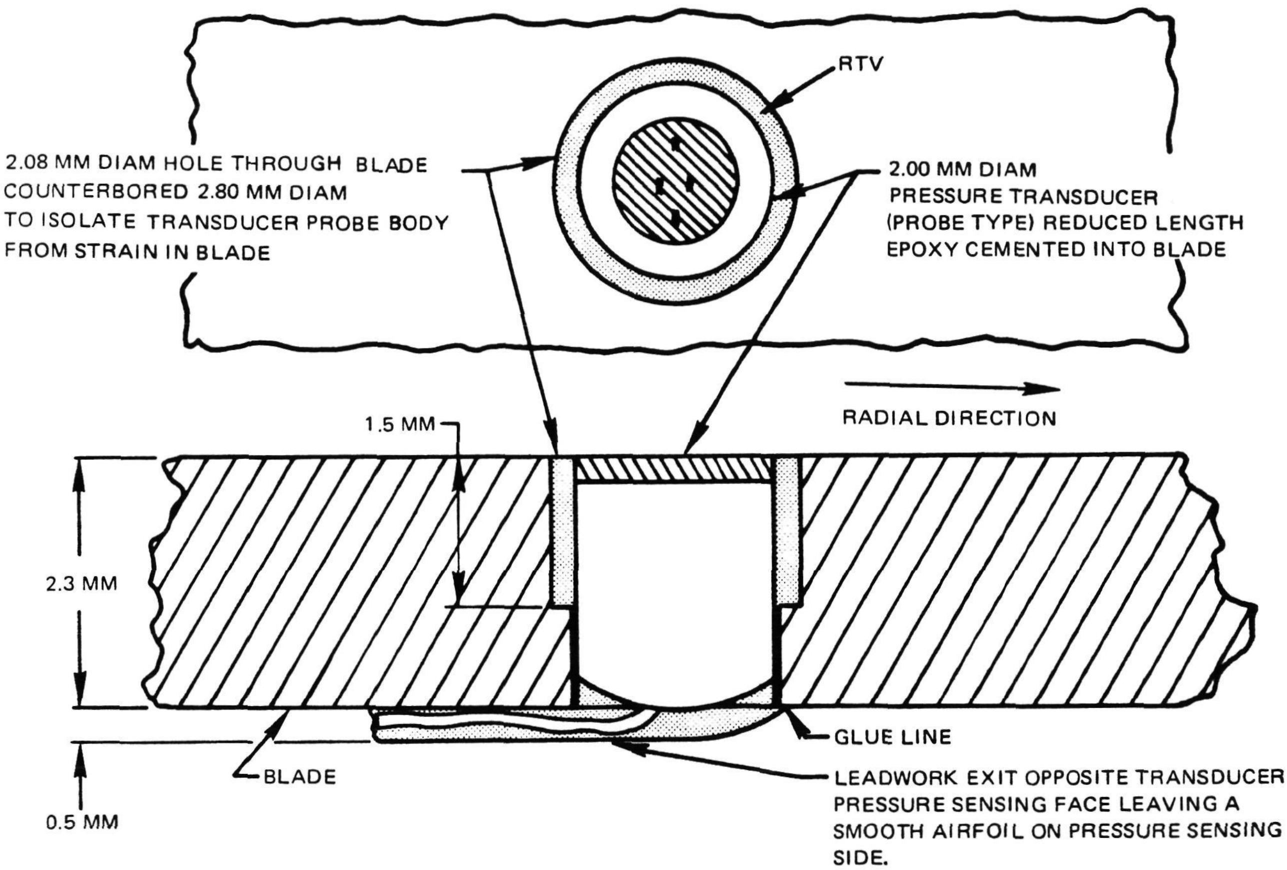

Figure 2-14 Transducer Mounting – Configuration "E"

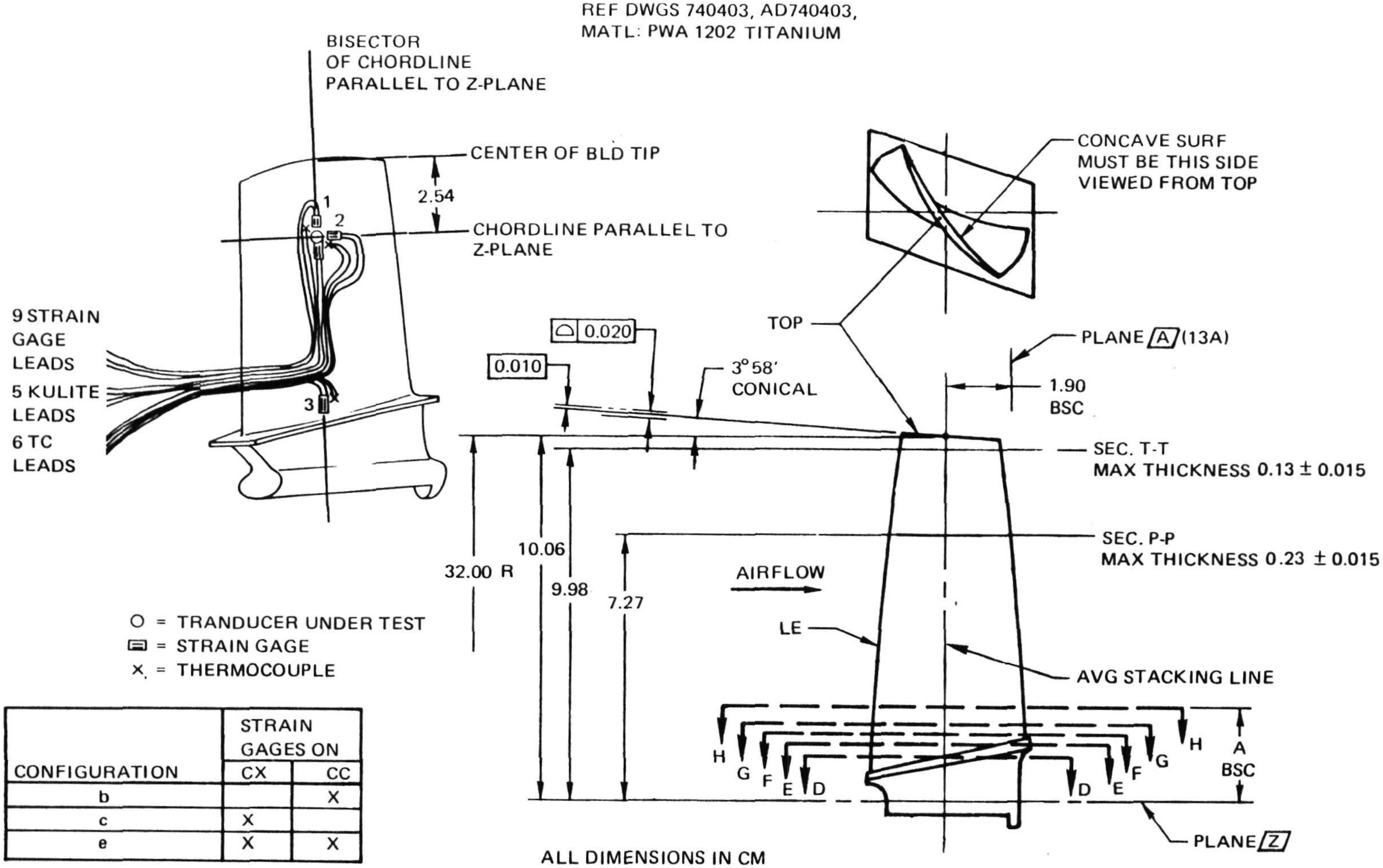

O = TRANDUCER UNDER TEST
▭ = STRAIN GAGE
X = THERMOCOUPLE

CONFIGURATION	STRAIN GAGES ON	
	CX	CC
b		X
c	X	
e	X	X

NOTE: ONE SET OF S/G'S (CX OR CC) ONLY WILL BE USED FOR ANALYSIS.

Figure 2-15 Titanium Test Specimen for Static Test

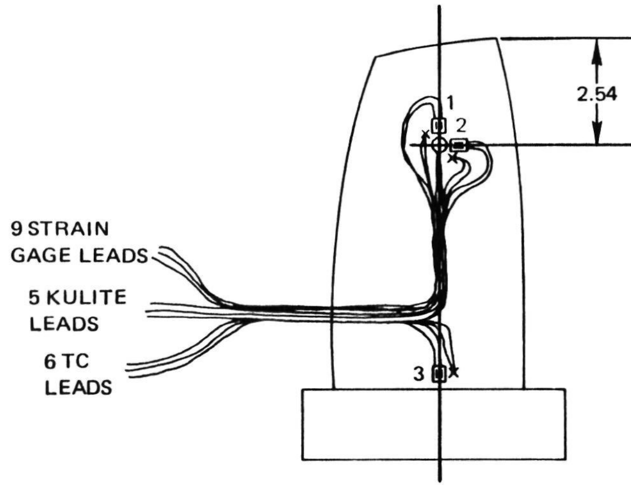

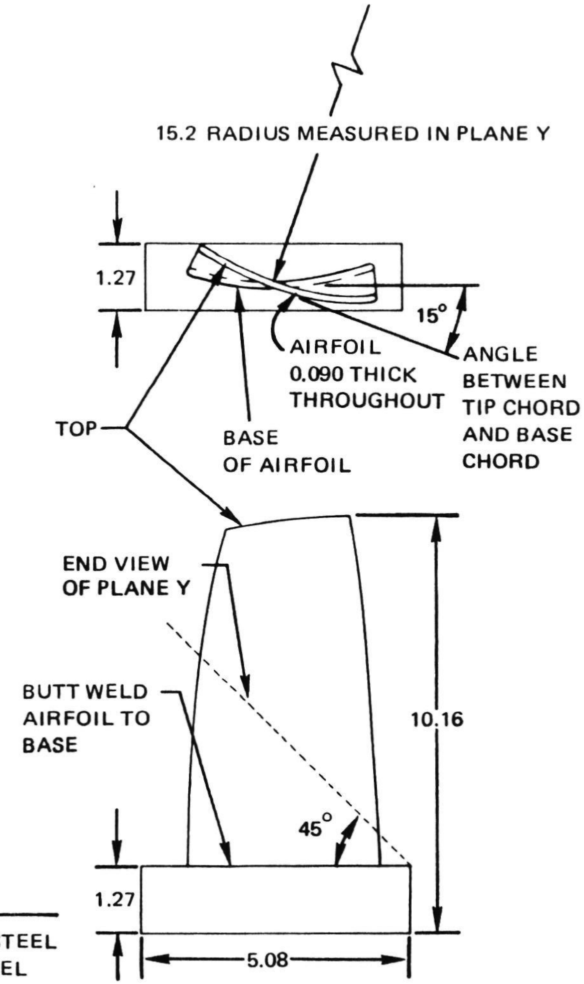

○ = TRANSDUCER UNDER TEST
⊟ = STRAIN GAGE
x = THERMOCOUPLE

CONFIGURATION	GAGES ON	
	CX	CC
b		X
c	X	
e	X	X

NOTE: ONE SET OF S/G'S ONLY (CX OR CC) USED FOR ANALYSIS

MATERIAL

AIRFOIL: 18 Ni 300 STEEL
BASE: AMS 5610 STEEL

ALL DIMENSIONS IN CM

Figure 2-16 Steel Test Specimen for Static Test

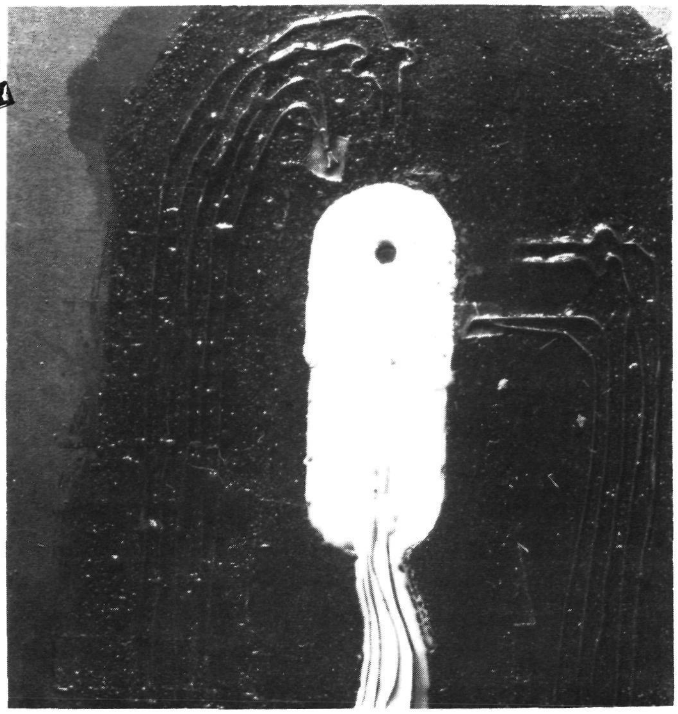

Figure 2-17 *Steel Test Specimen For Static Test With Transducer Mounting Configuration "C". View of Transducer area on measured surface.* *(77-444-9063-A)*

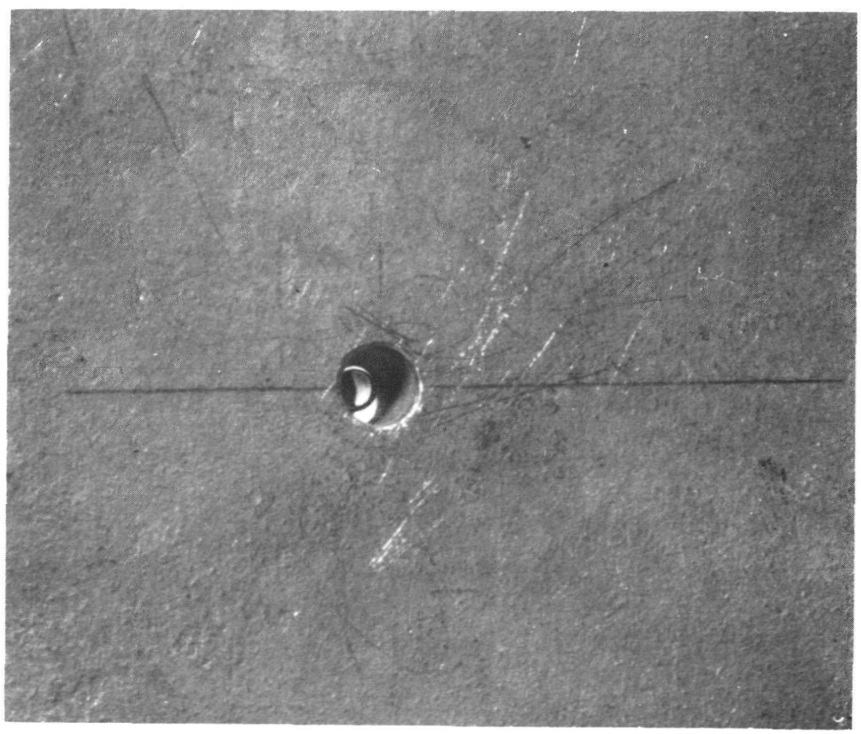

Figure 2-18 *Steel Test Specimen for Static Test With Transducer Mounting Configuration "B". View of transducer area on measured surface.* *(77-444-9063-C)*

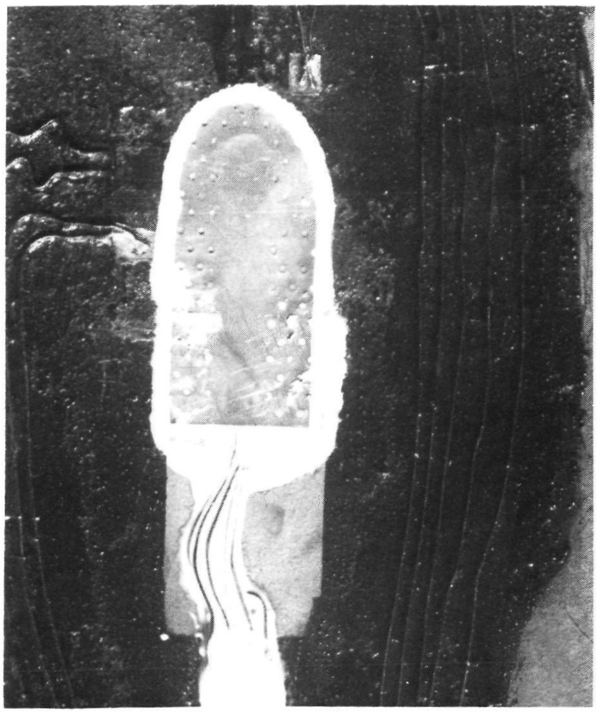

Figure 2-19 *Steel Test Specimen for Static Test With Transducer Mounting Configuration "B". View of transducer area on non-measured surface.* *(77-444-9063-B)*

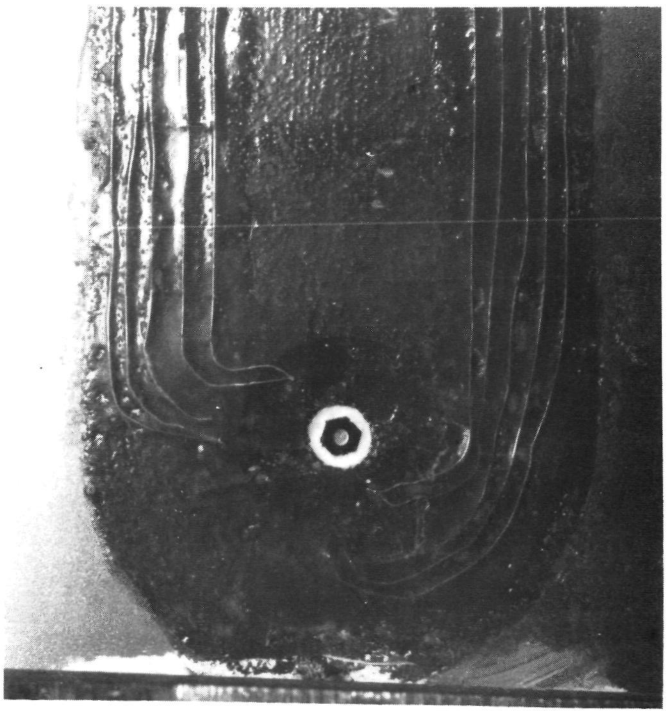

Figure 2-20 *Titanium Test Specimen for Static Test with Transducer Mounting Configuration "E". View of transducer area on measured surface.* *(77-441-9559-A)*

ORIGINAL PAGE IS
OF POOR QUALITY

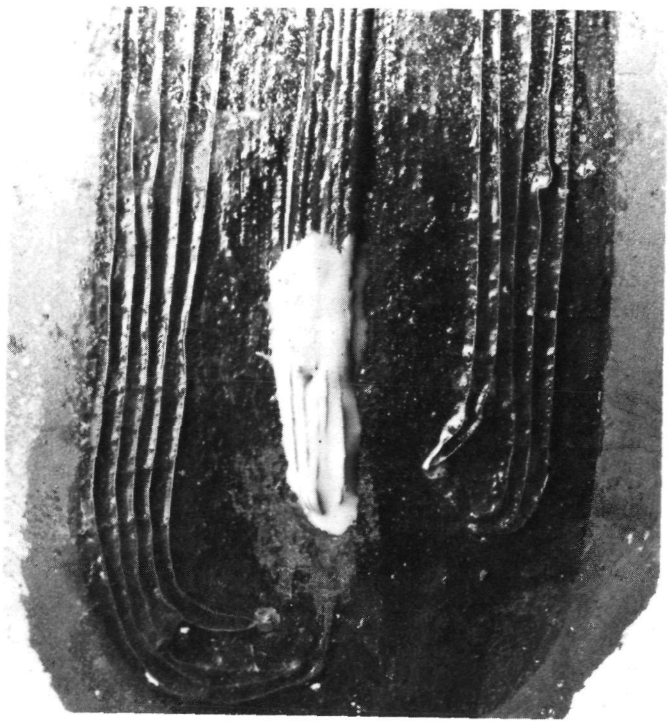

Figure 2-21 *Titanium Test Specimen for Static Test With Transducer Mounting Configuration "E". View of transducer area on unmeasured surface.* *(77-441-9559-B)*

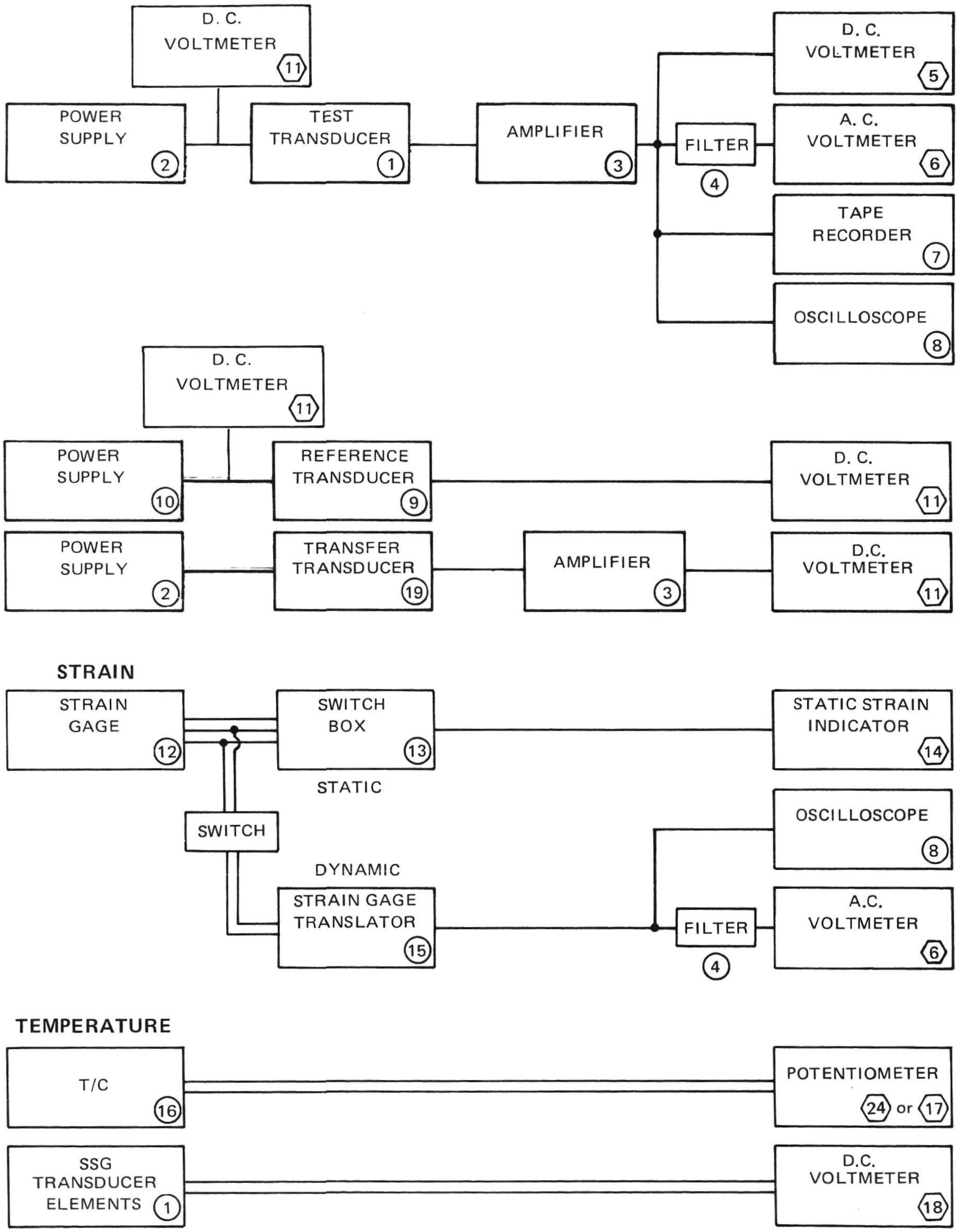

NOTE: SEE TABLE 2-III FOR INSTRUMENT LIST

Figure 2-22 Instrumentation Layout

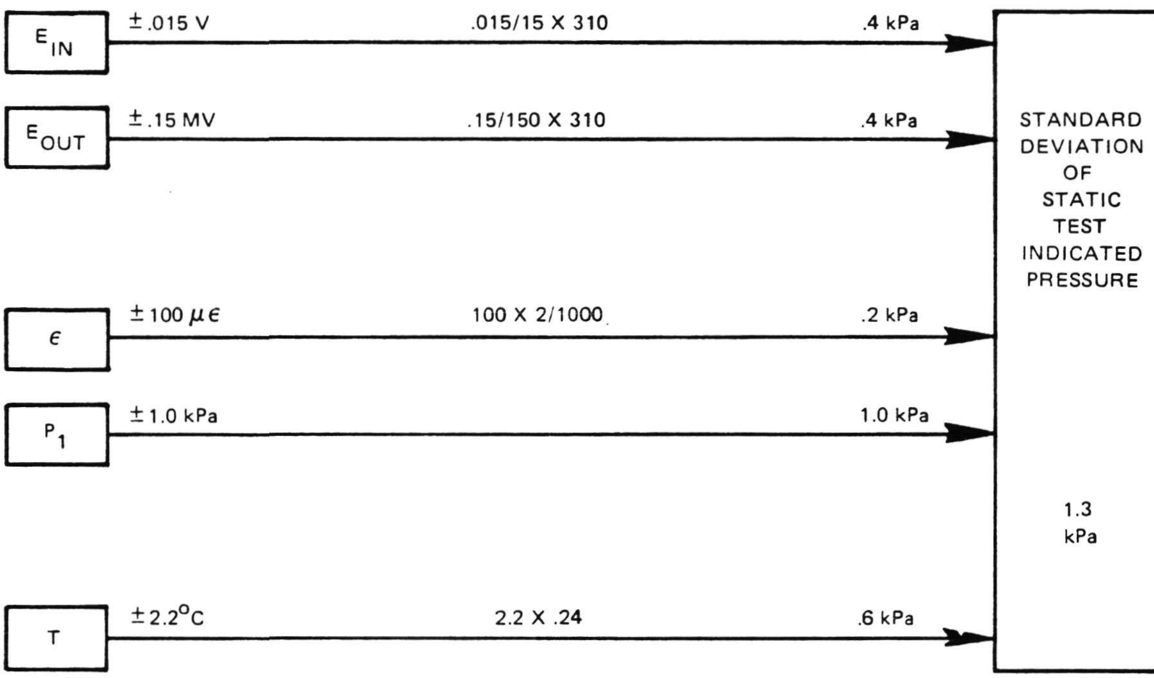

Figure 2-23 Static Test Error Diagram

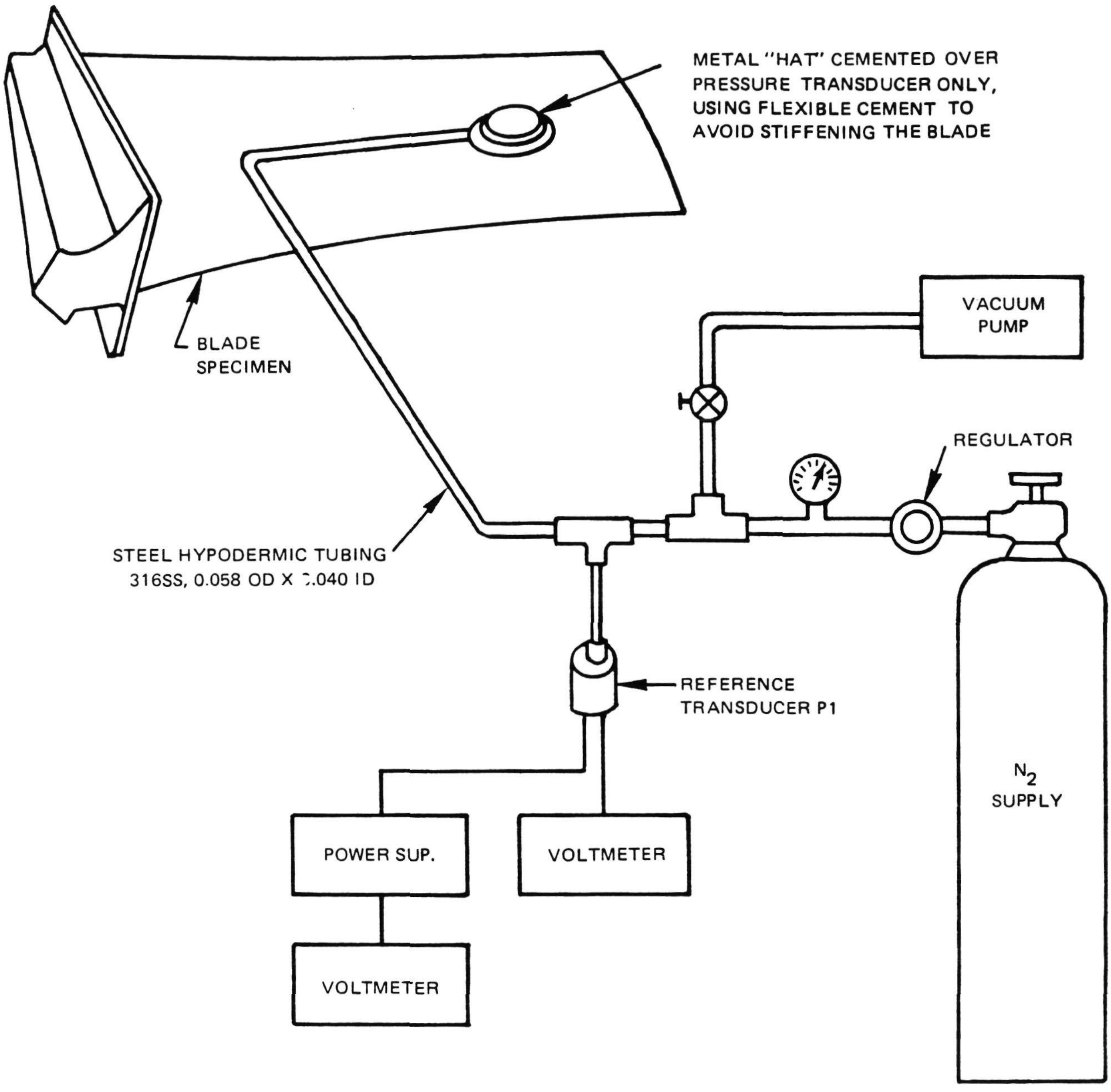

Figure 2-24 Pressure System for Static Tests

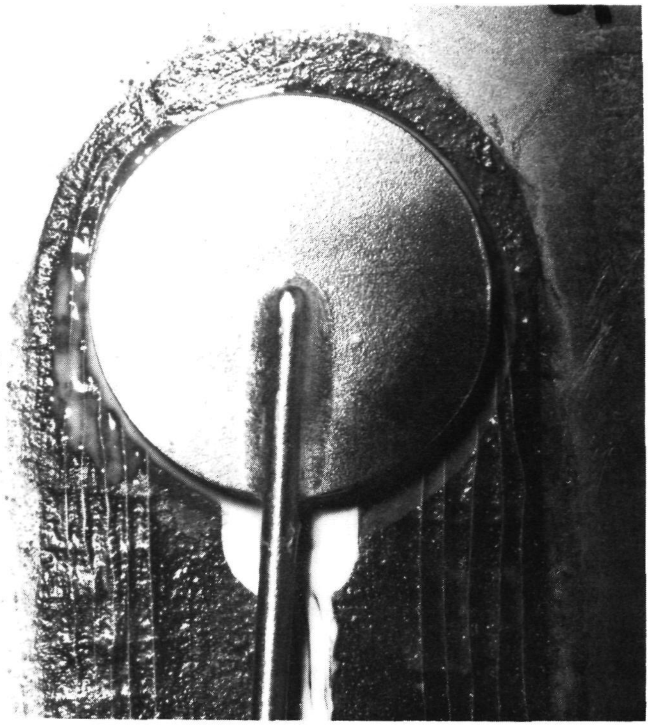

Figure 2-25 *Titanium Test Specimen for Static Test With Transducer Mounting Configuration "C". View of transducer area on measured surface with pressure cap installed. Cap diameter is 19 mm and tube diameter is 1.57 mm* (77-441-9321-A)

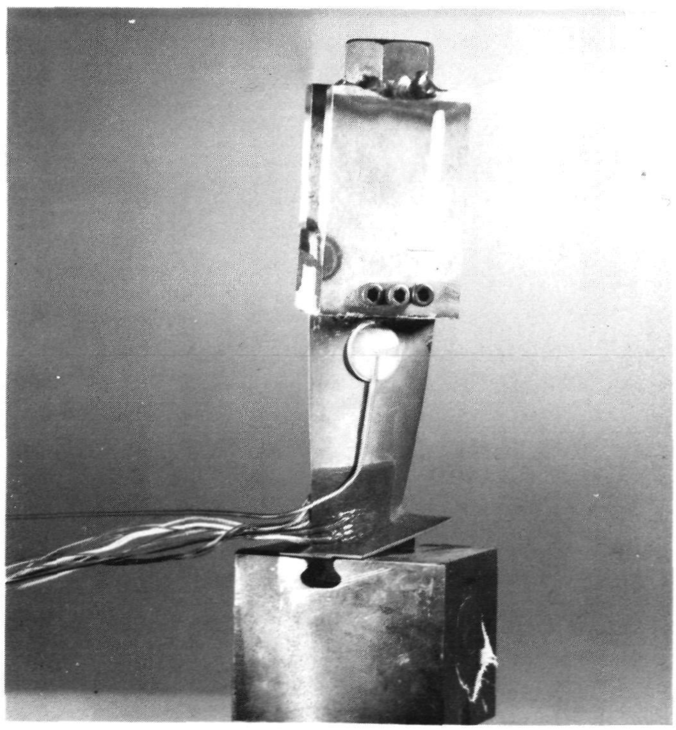

Figure 2-26 *Titanium Test Specimen With Fixtures for Tensile Test, Without Heating Tape* (77-441-9586-B)

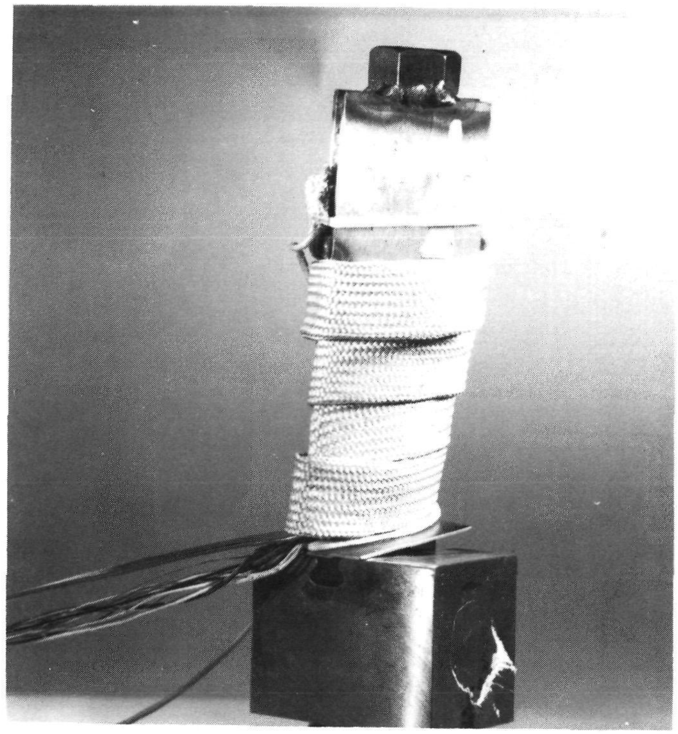

Figure 2-27 Titanium Test Specimen With Fixtures for Tensile Test, With Heating Tape (77-441-9586-D)

Figure 2-28 Tensile Test Facility (76-6323)

Figure 2-29 *Titanium (L) and Steel (R) Test Specimens for Static Test With Transducer Mounting Configuration "E". Oblique view with tip fixtures installed.* *(77-441-9559-G)*

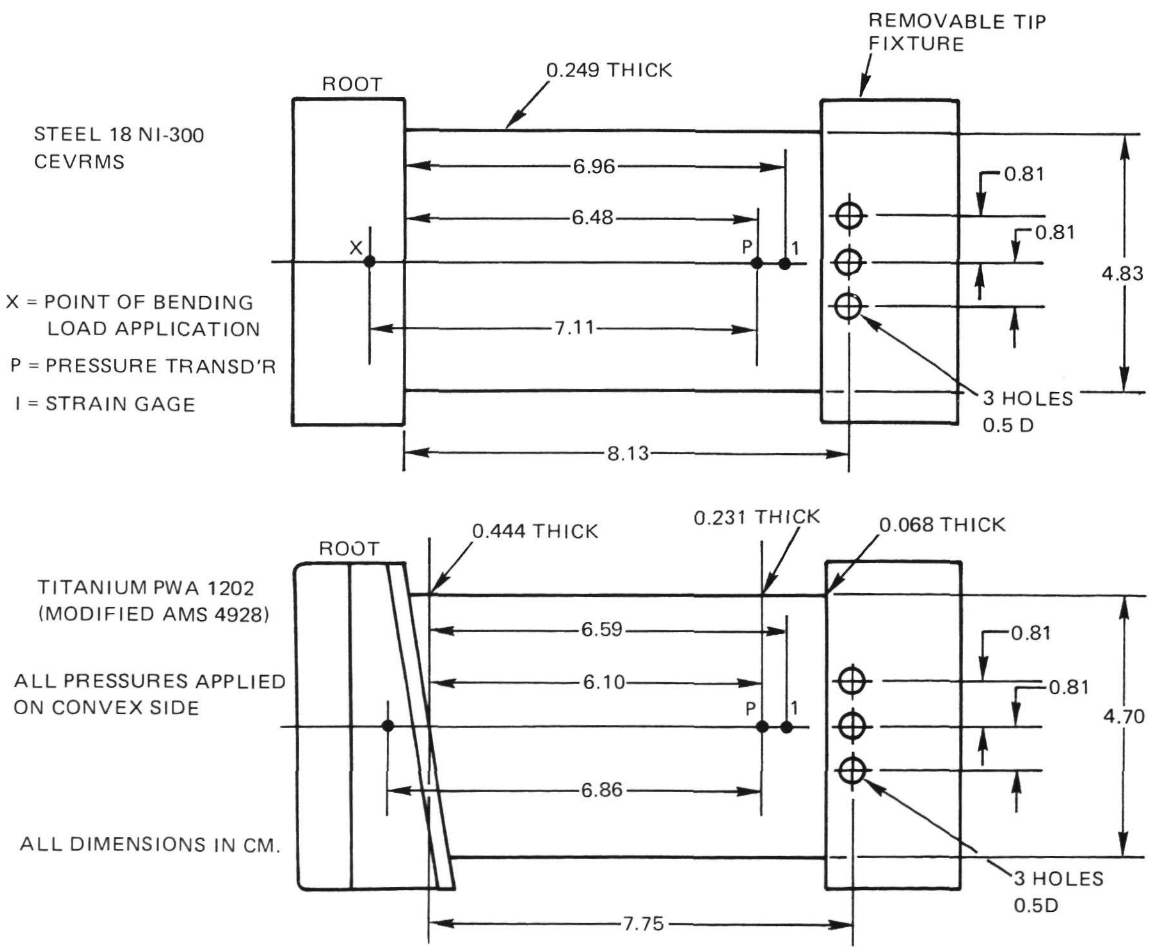

Figure 2-30 *Static Test Specimens*

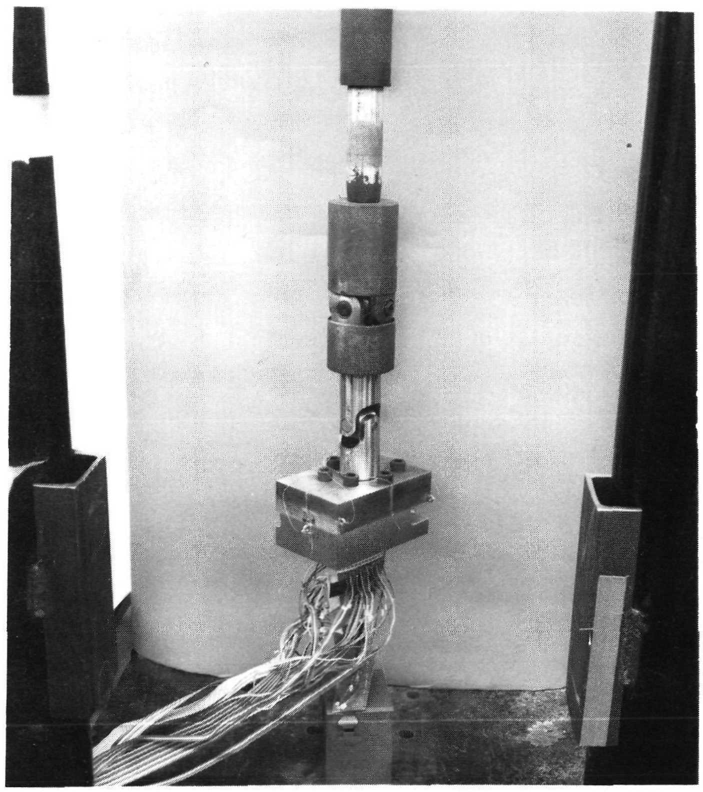

Figure 2-31 JT8D-109 First Fan Blade Pull Test (Z-53716)

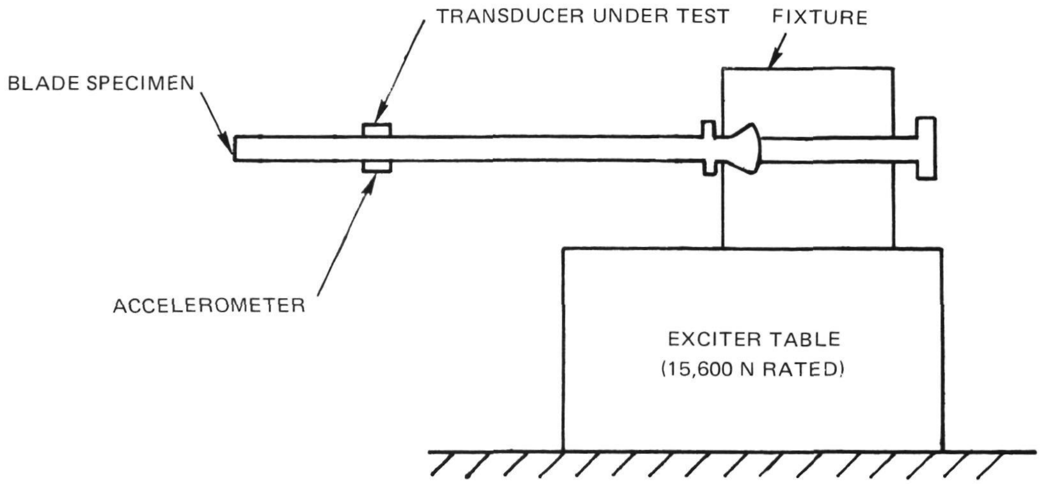

LOCATION; VIBRATION RIG ROOM AT PRATT & WHITNEY AIRCRAFT
FREQUENCY OF VIBRATION; BLADE FIRST BENDING MODE

Figure 2-32 Vibration Test Configuration

ORIGINAL PAGE IS
OF POOR QUALITY

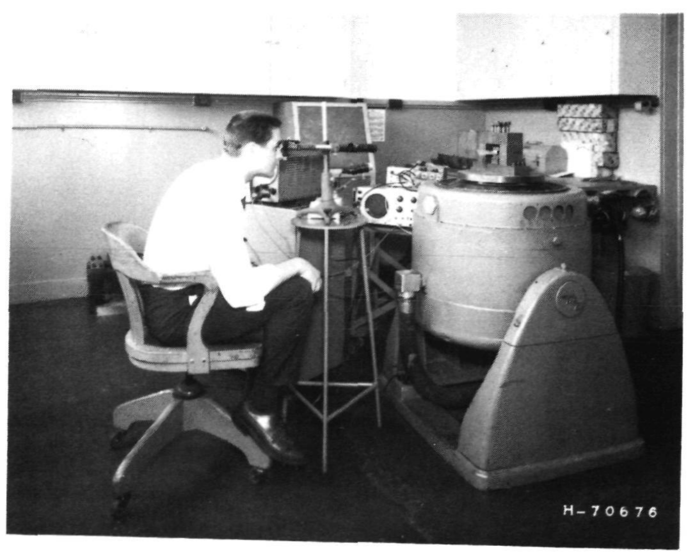

Figure 2-33 Shaker Table (H-70676)

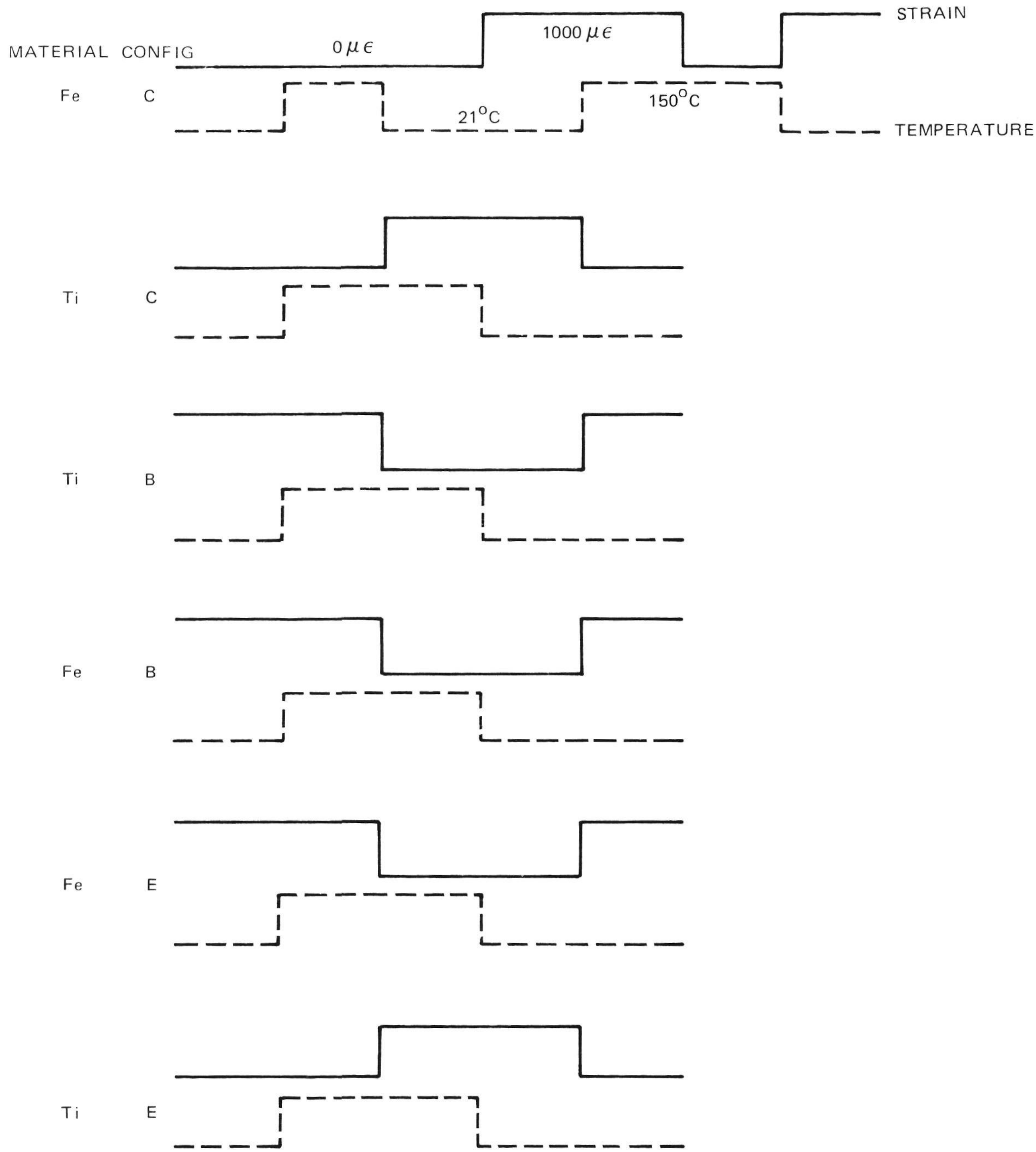

PLUS REPEATS

AT EACH CONDITION OF STRAIN AND TEMPERATURE, MEASURE TRANSDUCER OUTPUT AT 50, 180, 310, 180, 50 kPa APPLIED PRESSURE

Figure 2-34 Tensile Test Matrix

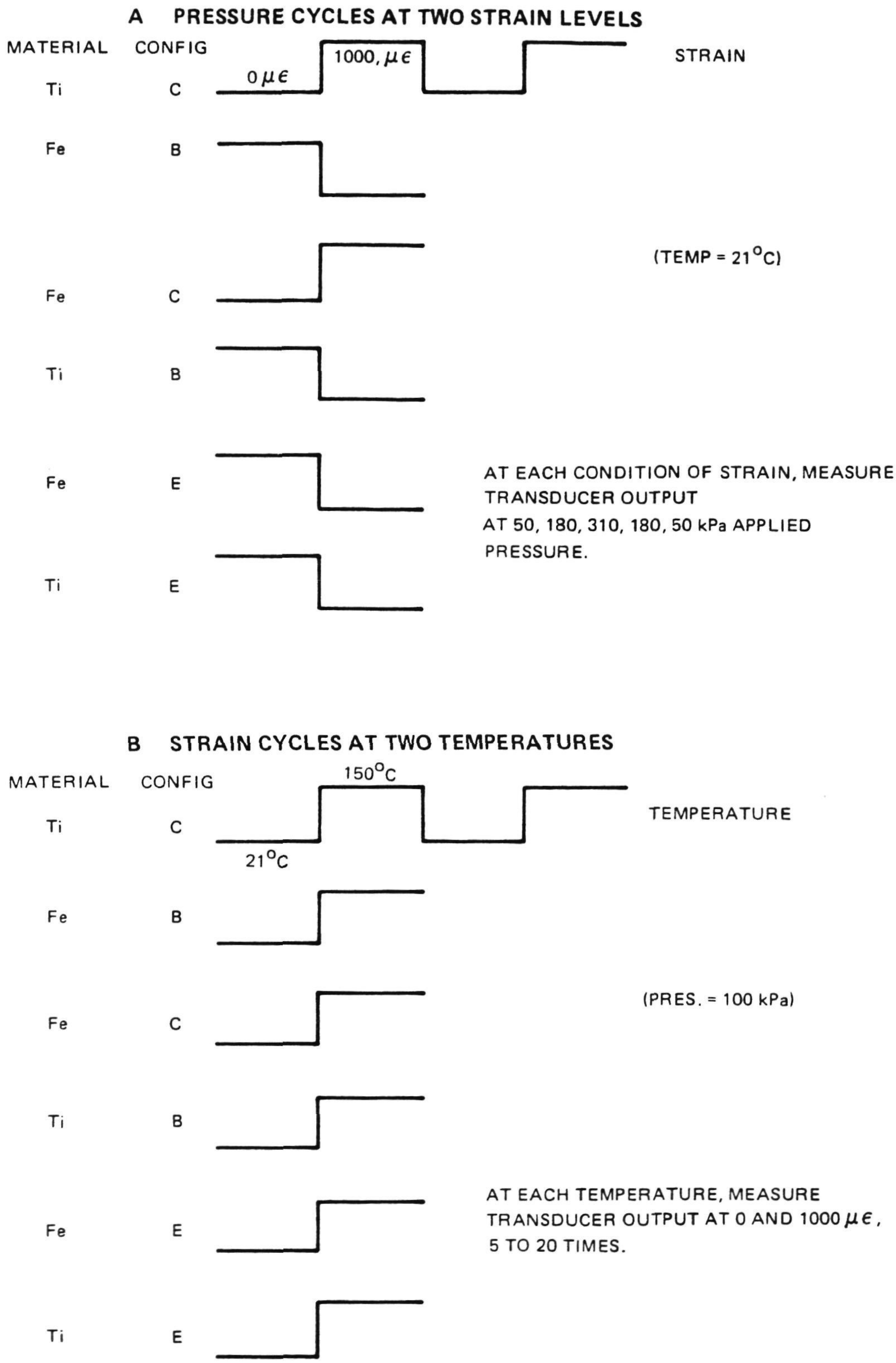

Figure 2-35 Bending Test Matrix

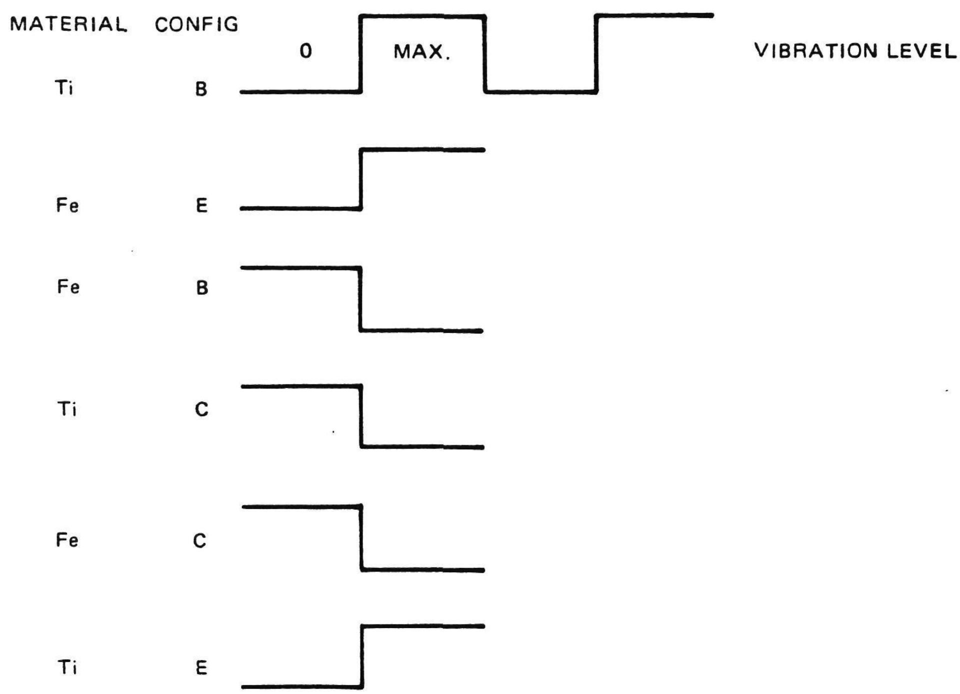

AT EACH CONDITION OF VIBRATION MEASURE TRANSDUCER OUTPUT
AT 50, 180, 310, 180, 50 kPa APPLIED PRESSURE

VIBRATION TEST CONDITIONS

	STEEL	TITANIUM
FREQUENCY	240 HZ	510 HZ
PEAK ACCEL. AT XDCR	144 G	650 G
PEAK DEFLECTION AT XDCR	0.635 MM	0.635 MM
PEAK STRAIN AT XDCR	$< 100\,\mu\epsilon$	$< 100\,\mu\epsilon$
PEAK ROOT STRAIN	$400\,\mu\epsilon$	$400\,\mu\epsilon$

Figure 2-36 Vibration Test Matrix

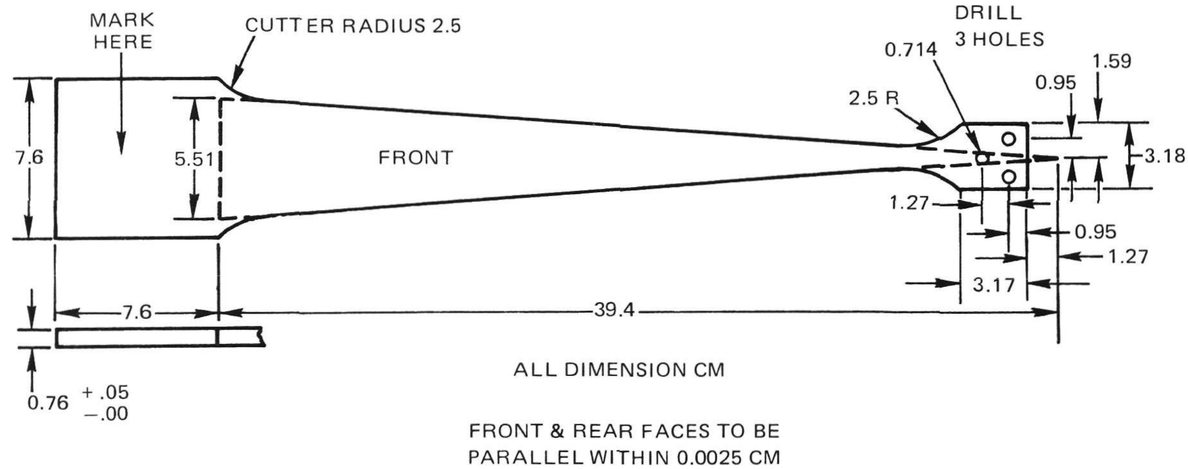

Figure 2-37 Constant Stress Test Beam

ORIGINAL PAGE IS
OF POOR QUALITY

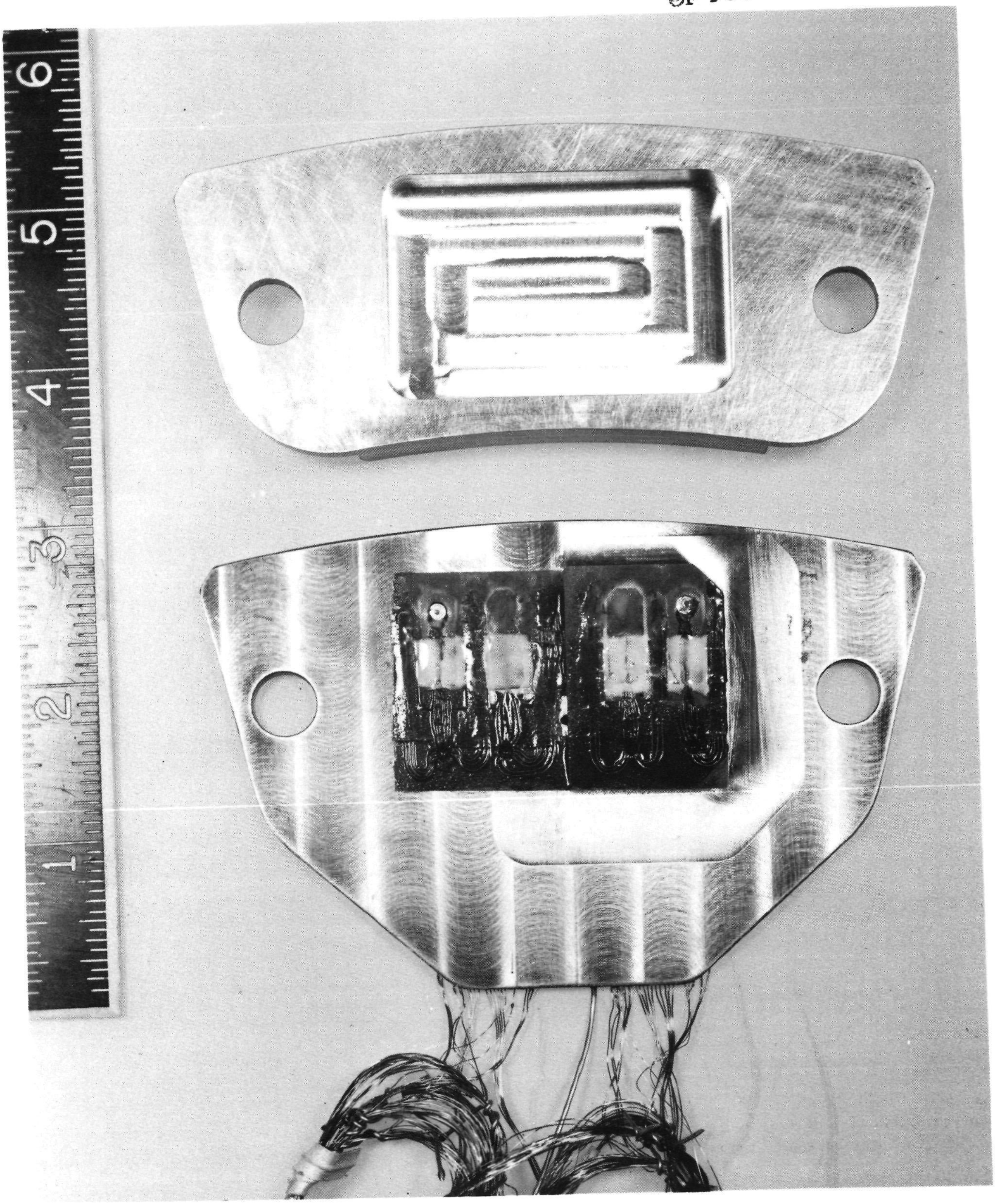

Figure 2-38 *Instrumentation Plate, With Cover, Before Installation on Disk. View of inside surfaces of pressure chamber. Rig 16273-1.* *(77-441-9839-E)*

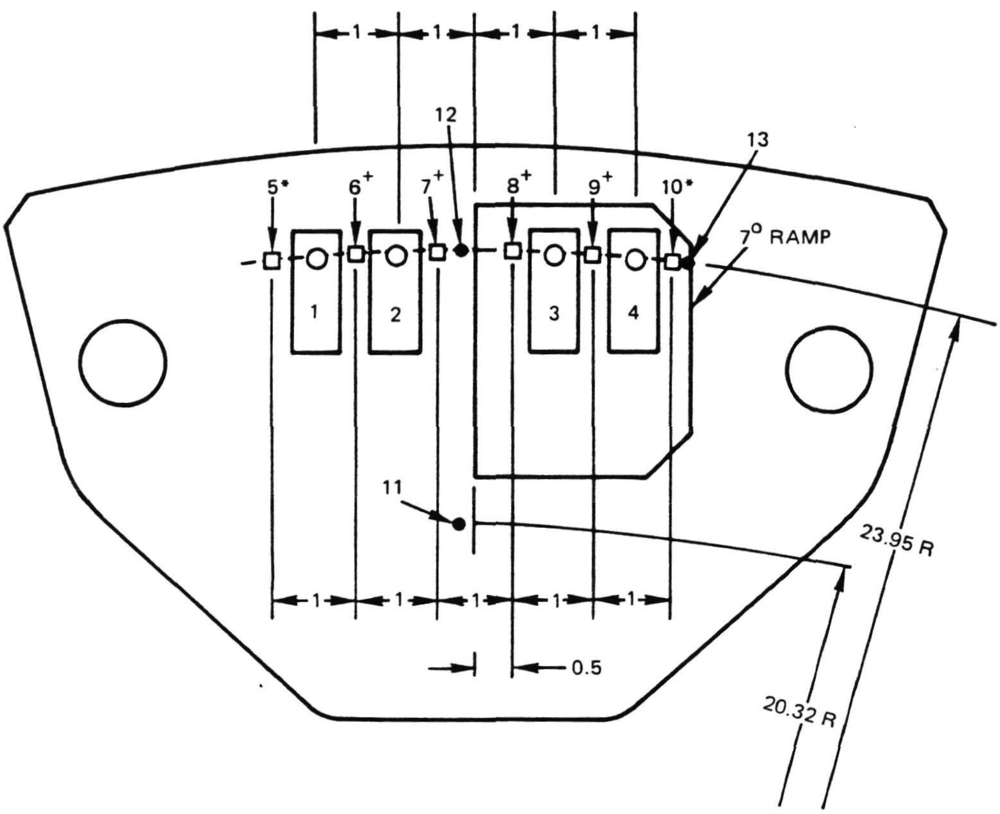

NOTES: LOCATIONS 1 THROUGH 4 ARE PRESSURE TRANSDUCERS. LOCATIONS 5 THROUGH 10 ARE STRAIN GAGES. LOCATIONS 11 THROUGH 13 ARE THERMOCOUPLES.
ALL DIMENSIONS CM

* TRANSVERSE STRAIN GAGE

+ RADIAL STRAIN GAGE

Figure 2-39 Location of Transducers on Spin Disk

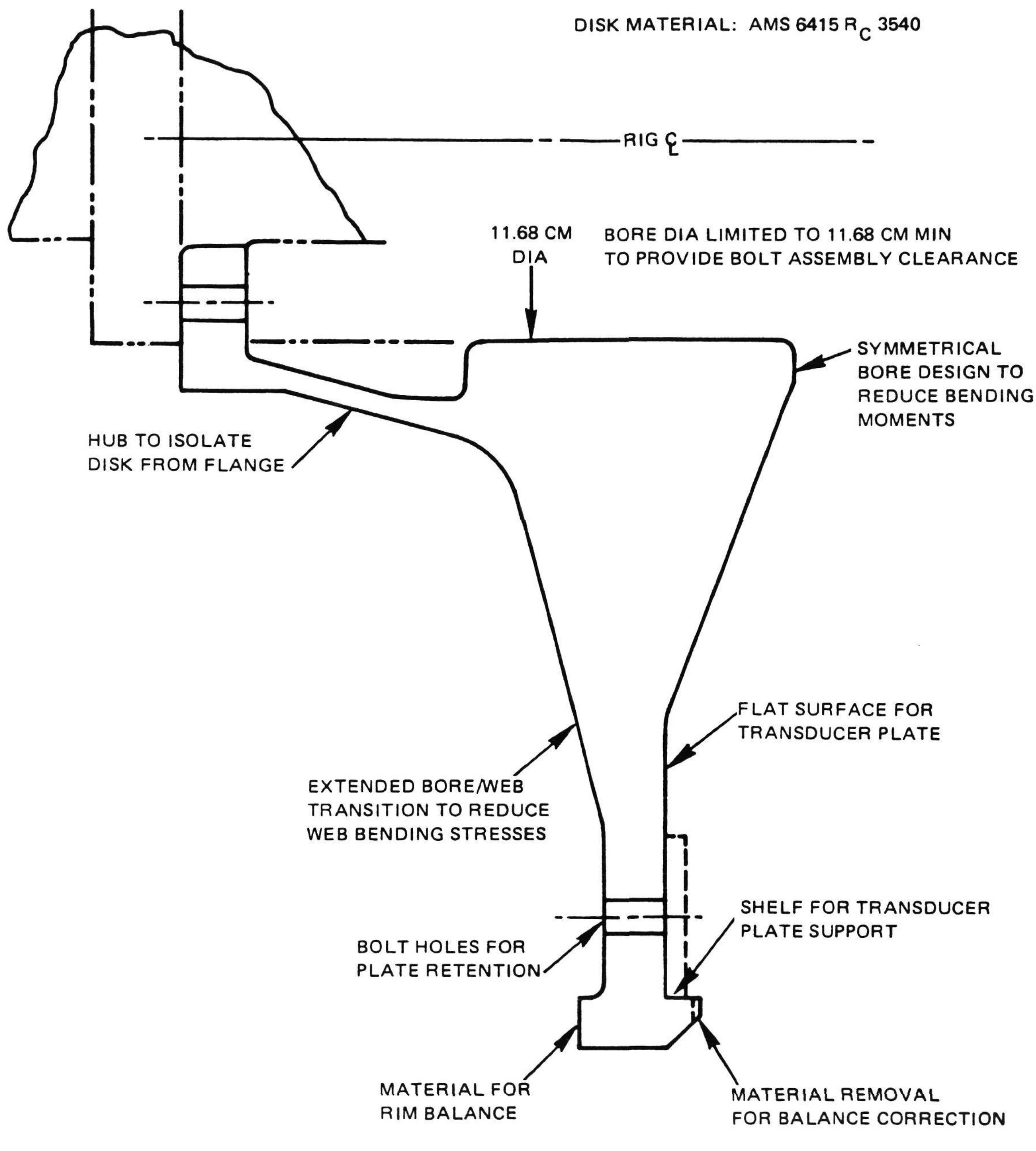

Figure 2-40 Spin Test Disk Special Features

Figure 2-41 *Rig 16273-1, Instrumented Disk, Before Spin Test. Instrumentation plate on right side. (77-444-4203-A)*

Figure 2-42 *Rig 16273-1, Mounted on Pit Cover at X-117 Stand. Heater is visible above the disk. (77-444-4236-B)*

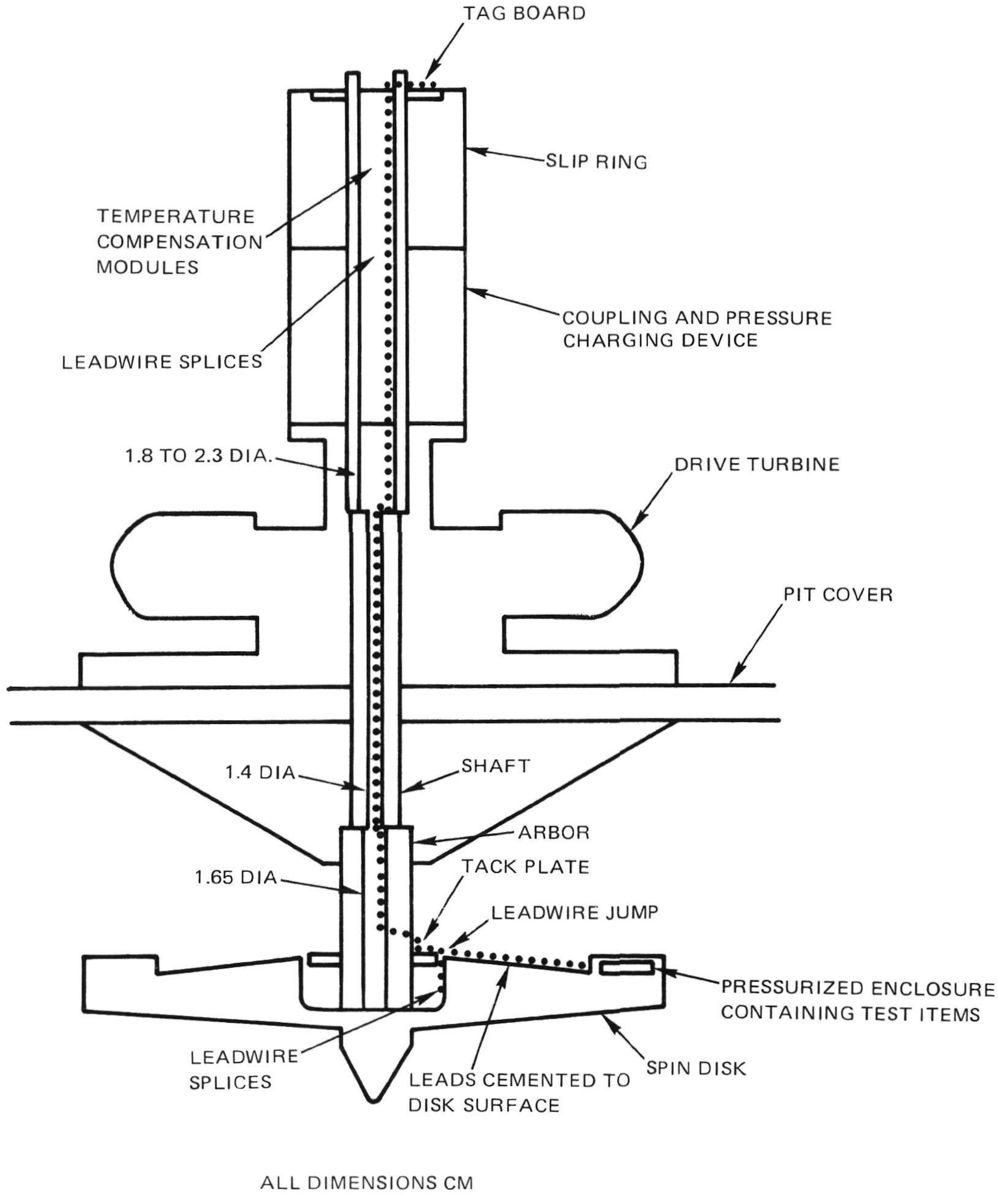

Figure 2-43 Spin Test Setup Showing Path of Rotating Leadwires

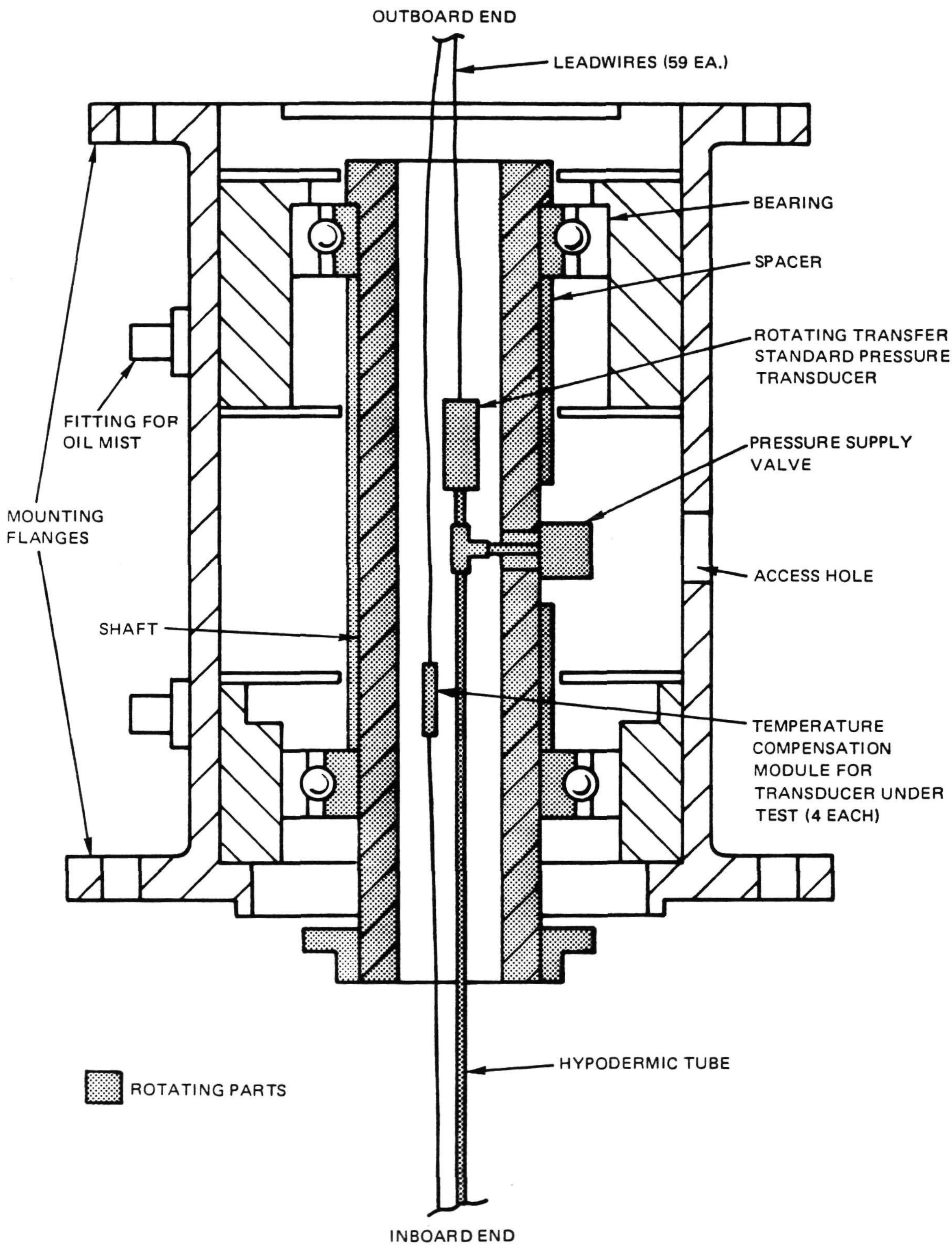

Figure 2-44 Coupling and Pressure Charging Device (Conceptual Drawing)

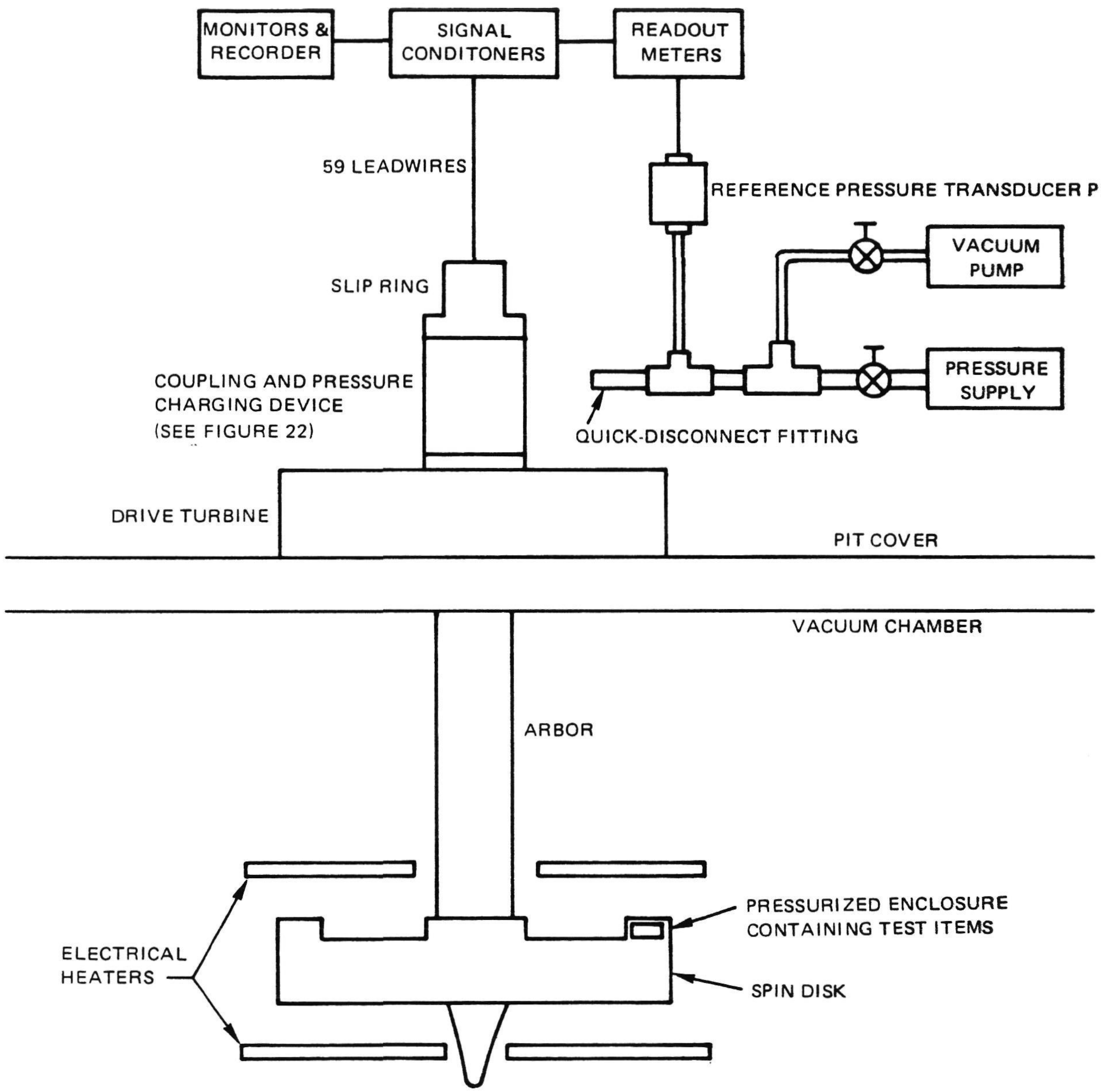

Figure 2-45 Test Setup for Spin Test

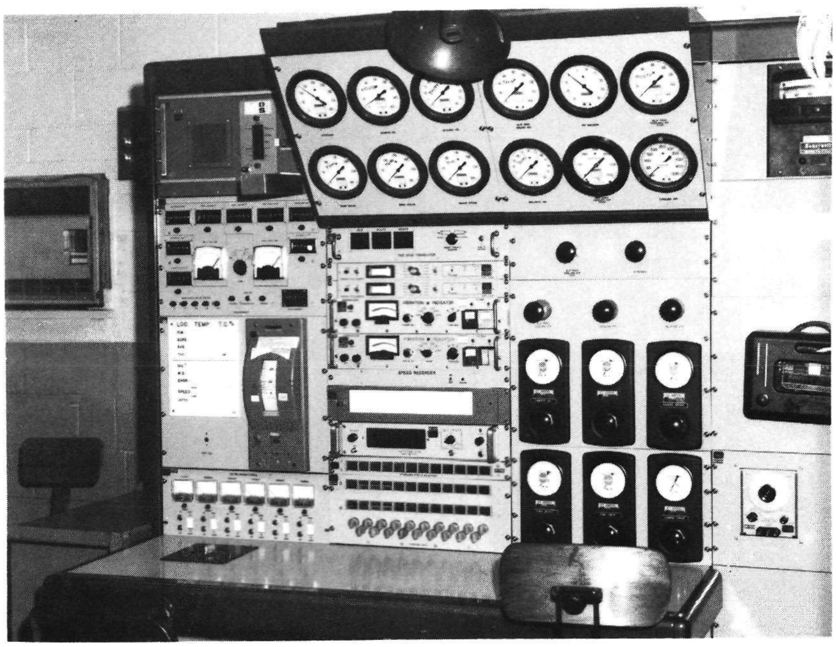

Figure 2-46 Spin Test Stand Control Console (X-32931)

ORIGINAL PAGE IS
OF POOR QUALITY

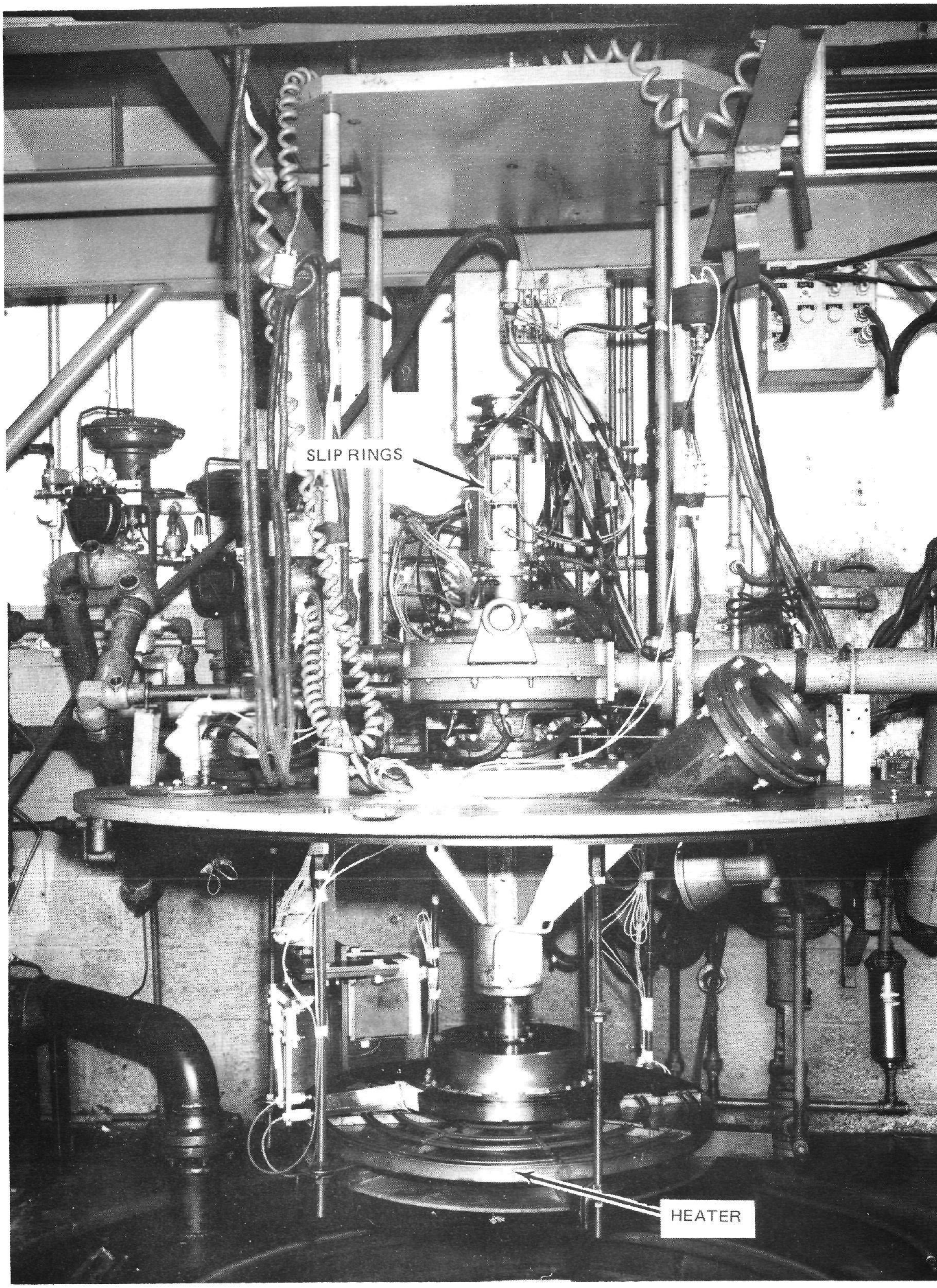

Figure 2-47 Typical Spin Rig Installation (X-36099)

ORIGINAL PAGE IS
OF POOR QUALITY

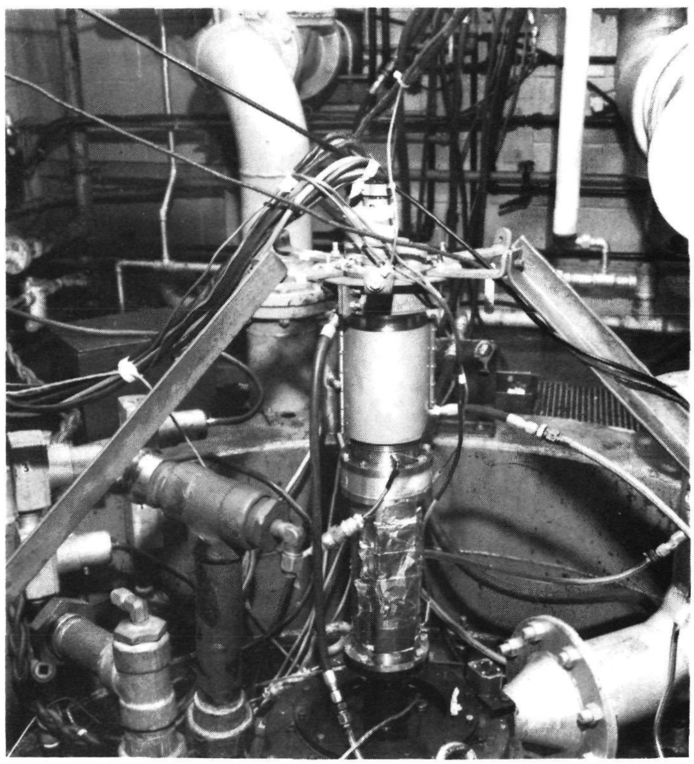

Figure 2-48 *Rig 16273-1, X-117 Stand. Slip ring and pressure coupler with associated plumbing and wiring, mounted on turbine, during spin test.* *(77-444-4236-C)*

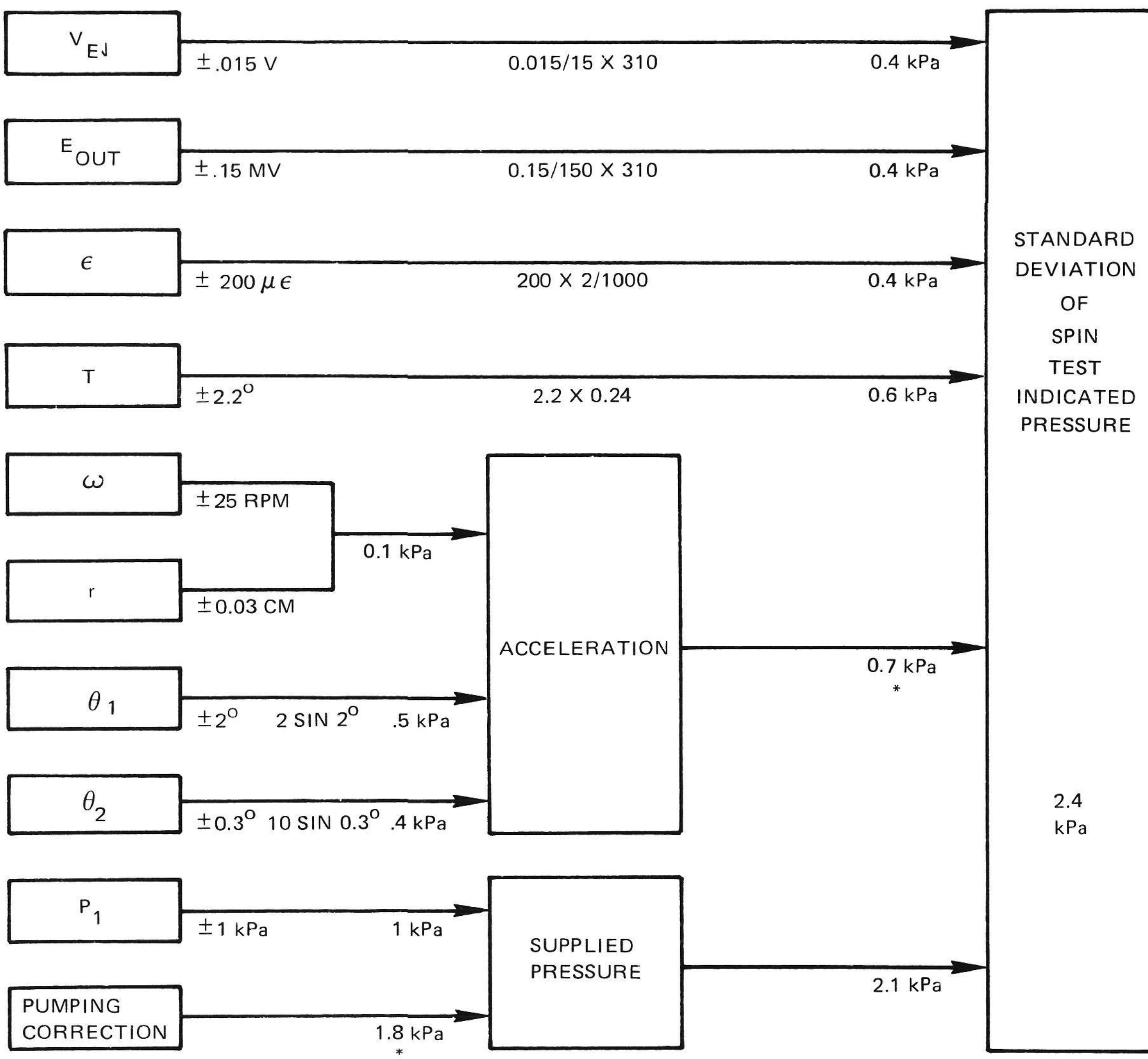

*SEE TEXT FOR CALCULATION PROCEDURE

Figure 2-49 Spin Test Error Diagram

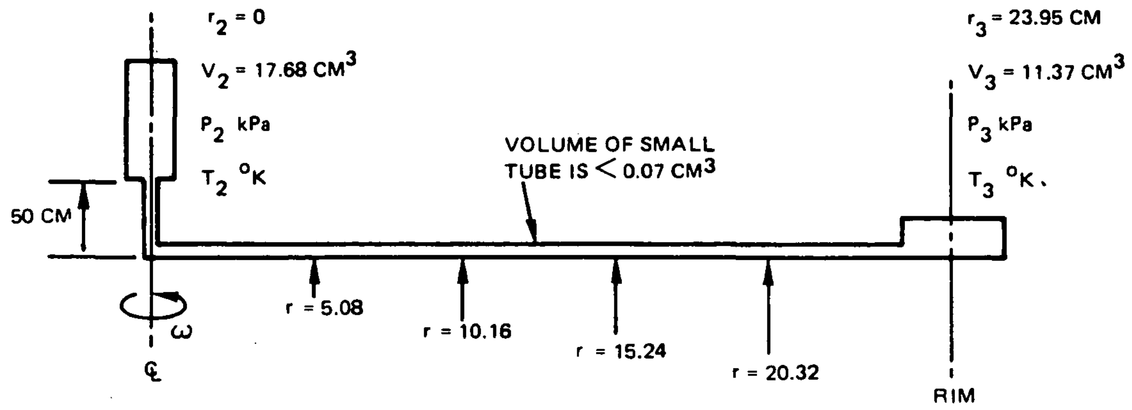

THERMOCOUPLE LOCATIONS

At $\omega = 0, P_{20} = P_{30}$ = pressure measured with stationary reference.
At $\omega \neq 0$, Newton's Laws require that, in the small tube, $AdP = \rho\ Adr\ \omega^2\ r/G$ or

$$dP/dr = P\omega^2\ r/GRT \tag{1}$$

Which integrates to

$$P_3/P_2 = \exp\left[(\omega^2/GR) \int_{r_2}^{r_3} (r/T)dr\right] \tag{2}$$

or, if T = constant from axis to rim,

$$P_3/P_2 = \exp\left[\omega^2\ r_3^2 / 2GRT\right] \tag{3}$$

Also, from conservation of mass, if the volume of the small tube is negligible, then for any temperature distributions,

$$P_{20}\ V_2 + P_{30}\ V_3 = P_2\ V_2 + P_3\ V_3 \tag{4}$$

or

$$P_3 = P_{20}\left(\frac{T_3}{T_{20}}\right)\left[\frac{1 + (T_{20}/T_{30})\,(V_3/V_2)}{(P_2/P_3)\,(T_3/T_2) + (V_3/V_2)}\right] \tag{5}$$

where P_2/P_3 is determined from Equation (2) for any known temperature distribution or from Equation (3) if temperature is constant from axis to rim.

Figure 2-50 Pressure Relationships in the Rotating System

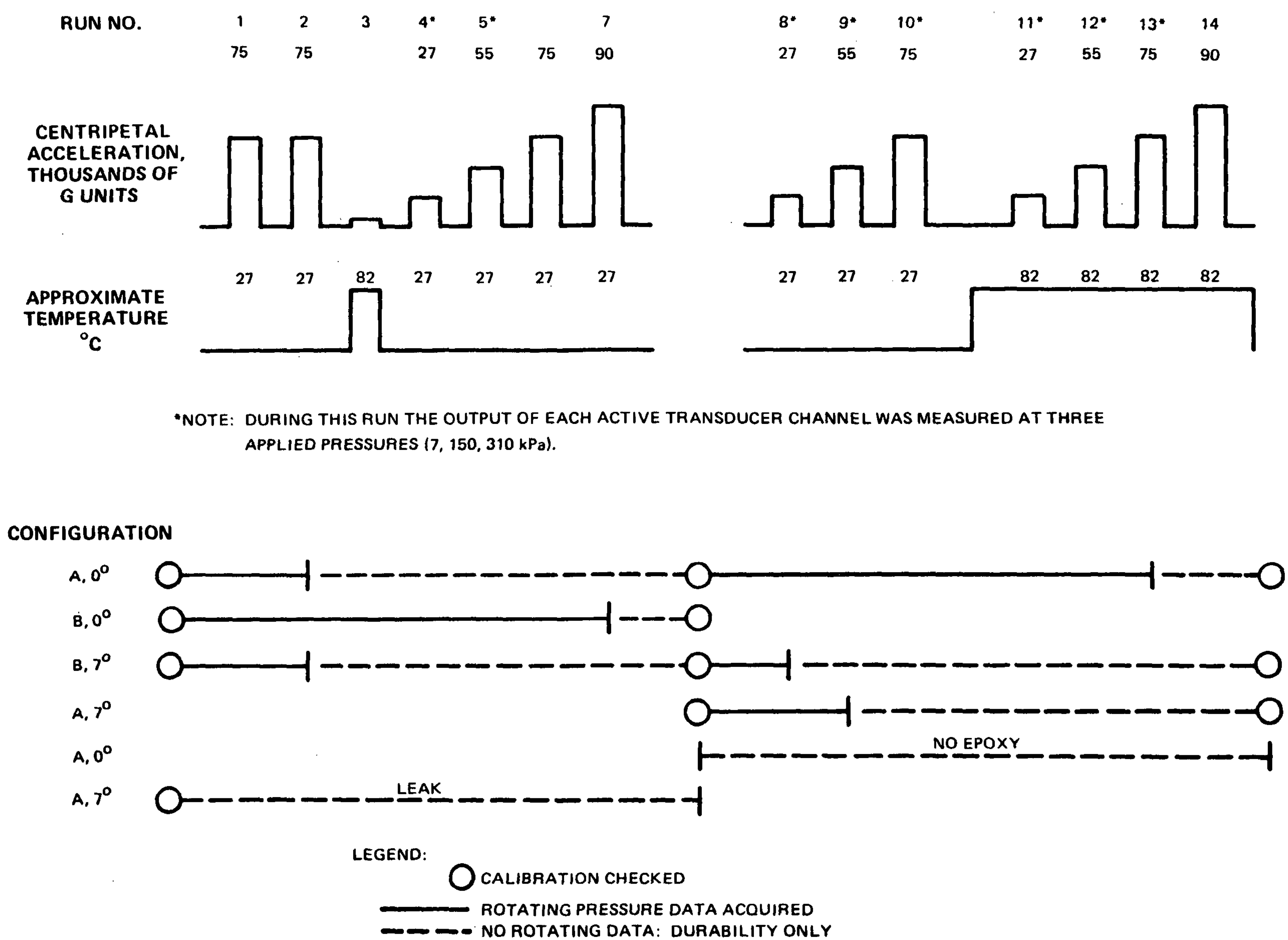

Figure 2-51 *Spin Test Program*

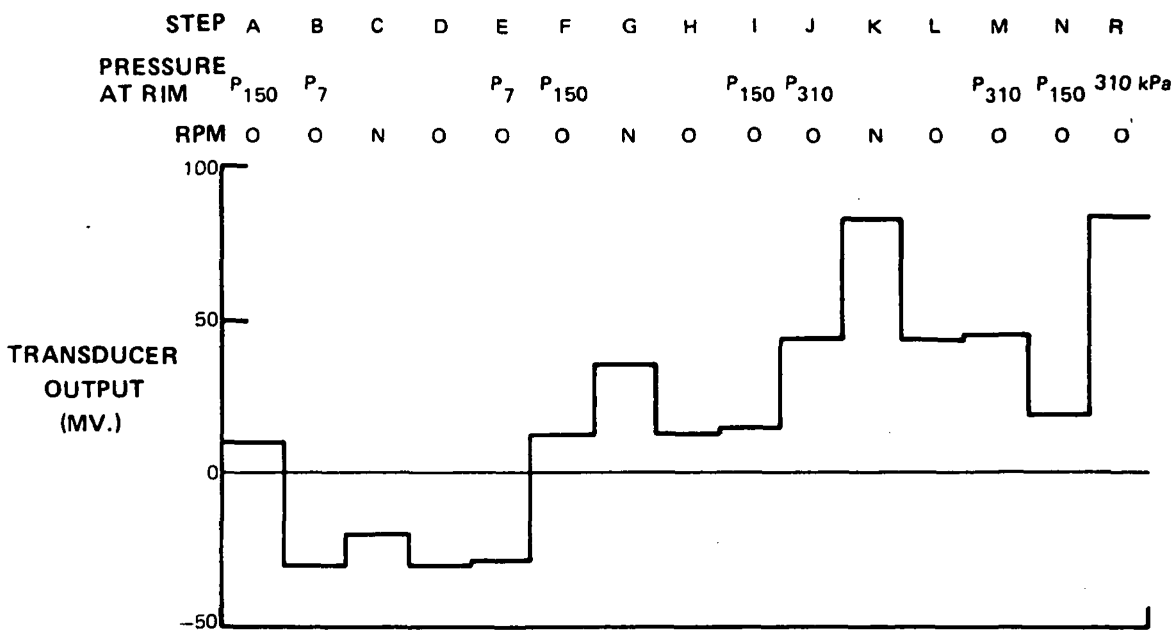

Figure 2-52 Spin Test Procedure

TABLE 2-I

EXAMPLE OF ACCELERATIONS*

Direction of Acceleration	Steady-State Component	Peak-to-Peak Value of Time-Varying Component: Vibration Alone	Peak-to-Peak Value of Time-Varying Component: Vibration plus Centripetal Contribution
Parallel to Blade Surface in Spanwise Direction	110,700 G	0 G	10 G
Normal to Blade Surface	9,700 G	250 G	360 G
Parallel to Blade Surface in Chordwise Direction in a Circumferential Plane	0 G	0 G	0 G

* Accelerations experienced at a radius of 25 cm at 20,000 rpm with blade surface at an average inclination of 5 degrees from radial plane and the blade vibrating in easywise pure bending at 500 Hz through a 0.25 mm peak-to-peak amplitude.

TABLE 2-II

PROPERTIES OF BLADE MATERIALS

		Titanium PWA 1202 38°C	Titanium PWA 1202 315°C
Composition:	Al	8	
	V	1	
	Mo	1	
	C	0.08	
	Fe	0.3	
	0	0.12	
	N	0.05	
	H	0.015	
	Ti	Bal.	
MPa. 0.2% Yield Strength		790	500
MPa. 0.1% Creep, 10 Hr.			480
MPa, 10 Hr. Stress Rupture			620
MPa, Fatigue 10^8 Cycles, Reversing			360
(1) kPa X 10^6 Young's Modulus		126	110
(2) kPa X 10^6 Shear Modulus		48	
Poisson Ratio		0.35	
gm/cm^3 Density		4.66	
Magnetic Properties		Non-Magnetic	
Temp. Coef. of Linear Expansion, ppm/°C		8.5	9.0

		Consumable Electrode Vacuum Remelt Maraging Steel 18 Ni-300 R.T.	Consumable Electrode Vacuum Remelt Maraging Steel 18 Ni-300 315°C
Composition:	C	0.03 Max	
	Si	0.10 Max	
	Mn	0.10 Max	
	S	0.010 Max	
	P	0.010 Max	
	Mo	4.80	
	Ni	18.50	
	Co	9.00	
	Ti	0.60	
	Al	0.10	
	B	0.003	
	Zr	0.02	
	Fe	Bal.	
MPa. 0.2% Yield Strength		2130	1690
Creep Properties		N/A	
MPa, Ultimate Tensile Strength			1770
MPa, Fatigue 10^8 Cycles		800	
kPa X 10^6, Young's Modulus		190	
kPa X 10^6 Shear Modulus		73	
Poisson Ratio		0.30	
gm/cm^3 Density		8.00	
Magnetic Properties		Magnetic	
Temp. Coef. of Linear Expansion, ppm/°C			10.1

TABLE 2-III

INSTRUMENTATION LIST

Instrument	No.	Mfg. Model No.	PWA Model No.	Range	Uncertainty Per Mfr Spec
Pressure Transducer, Kulite	1	LQL-14-080-25S LQL-5-080-25S		345 kPa	3.45 kPa max.
Power Supply, SRC/Moxon	2	3564		15 VDC	N.A.
Amplifier, Neff	3	128		X1,X10,X100	0.01%
Filter, Kron-Hite	4	330N		75Hz-5KHz	N.A.
DC Voltmeter, FLUKE	5	8120A		200mV	0.02% Rdg +0.01% Range
AC Voltmeter, FLUKE	6	8120A		100mvrms	0.2% Rdg + 0.05% Range
Tape Recorder, Precision Instrument	7	2100		500mvrms	2% Rdg
Oscilloscope, Tektronix	8	535A	646-8	N.A.	N.A.
Pressure Transducer, MB	9	151-DBA-1		345 kPa	0.7 kPa max.
Power Supply, PWA	10		840-21	N.A.	N.A.
DC Voltmeter, FLUKE	11	8000A (4 Digits)		200mv	0.1% Rdg + 1 Digit
Strain Gage, Micro-Measurements	12	EA-05-062AQ-350		4000$\mu\epsilon$	50$\mu\epsilon$
Strain Gage, Micro-measurements	12A	EA-06-062AQ-350		4000$\mu\epsilon$	50$\mu\epsilon$
Switch Box, Vishay Instmts	13	SB-1	2042-2	N.A.	N.A.
Strain Indicator, Vishay Instmts	14	P-350	1452-1	4000$\mu\epsilon$	0.1% Range
S.G. Translator, PWA	15		1563-12	4000$\mu\epsilon$	2.3% Rdg
CA Thermocouple, Sigmund-Cohn	16		SKH8290B, 8750B	150°C	2.2°C
Temp. Potentiometer, Leeds & Northup	17	8692-2	1135-5	150°C	0.3°C
Ohmmeter, FLUKE	18	8120A		1000Ω	0.05% Rdg & .01% Range
Pressure Transducer, Kulite, Rot. Std	19	CQL-080-25		345 kPa	3.45 kPa
Accelerometer, Endevco, with Amplifier, Ithaco 125M44	20	2226C		20-1000 Hz	1.5% Rdg
Frequency, General Radio	22	1150-B and 1151 APSI		200-1000Hz	2 counts
Slip Ring, Poly-Scientific	23	BN2288		N.A.	N.A.
Temperature Indicator, Doric	24	400		150°C	1.1°C

TABLE 2-IV
DATA REDUCTION PROCEDURE FOR SPIN TESTS

RUN NO.______
RUN DATE______
RPM______
NOM. TEMP.______

GIVEN: $P_A, P_B, P_C, P_F, P_G, P_I, P_K, P_N, P_R$
AND CLOCK TIME OF EACH MEASUREMENT

ITEM	DESCR.	SOURCE	UNITS	
1	E_A	DATA	MV	
2	E_B			
3	E_C			
6	E_F			
7	E_G			
9	E_I			
11	E_K			
14	E_N			
15	E_R			
35	ϕ_{10} EST	(1 - 2) ÷ (P_A - P_B)	MV/PSI	
36	ϕ_{20} EST	(15 - 14) ÷ (P_R - P_N)	MV/PSI	
37	X_A	1 + 35 (22.00 - P_A)	MV	
38	X_F	6 + 35 (22.00 - P_F)		NOTE 1
39	X_I	9 + 35 (22.00 - P_I)		
40	X_N	14 + 35 (22.00 - P_N)		
41	$X_A - X_B$	INTERPOLATE FROM GRAPH		
42	$X_A - X_G$			
43	$X_A - X_R$			
44	$X_B - X_C$			
45	$X_B - X_R$			NOTE 2
46	$X_C - X_G$			
47	$X_G - X_K$			
48	$X_K - X_R$			
49	$E_{2N} - E_{1N}$	7 - 3 - 46		
50	$E_{3N} - E_{2N}$	11 - 7 - 47		
51	E'_{10}	2 + 35 (P_C - P_B)		
52	E'_{20}	1 + 35 (P_G - P_A)		NOTE 3
53	E'_{30}	15 + 36 (P_K - P_R)		
54	E'_{00}	2 - 35 P_B		
55	$E_{20} - E_{10}$	52 - 51 + 41		
56	$E_{30} - E_{20}$	53 - 52 - 43		
57	ϕ_{1N}	49 ÷ (P_G - P_C)	MV/PSI	
58	ϕ_{2N}	50 ÷ (P_K - P_G)		
59	ϕ_{10}	55 ÷ (P_A - P_B)		
60	ϕ_{20}	56 ÷ (P_R - P_N)		
61	$(\phi_{1N} - \phi_{10})/\phi_{10}$	(57 - 59) ÷ 59	—	NOTE 4
62	$(\phi_{2N} - \phi_{20})/\phi_{10}$	(58 - 60) ÷ 59	—	
63	$E_{1N} - E_{10}$	3 - 51 - 44	MV	
64	$E_{2N} - E_{20}$	7 - 52 - 42		
65	$E_{3N} - E_{30}$	11 - 53 + 48		
66	E'_{40}	15 + 36 (45.00 - P_R)		NOTE 3
67	$E_{40} - E_{00}$	66 - 54 - 43		
68	$(E_{1N} - E_{10})/(E_{40} - E_{00})$	63 ÷ 67	—	
69	$(E_{2N} - E_{20})/(E_{40} - E_{00})$	64 ÷ 67	—	NOTE 4
70	$(E_{3N} - E_{30})/(E_{40} - E_{00})$	65 ÷ 67	—	

NOTES

1. OUTPUT ADJUSTED FOR DEVIATION FROM 22.00 PSI
2. ADJUSTMENT FOR DRIFT IN OUTPUT WITH TIME, INTERPOLATED FROM A GRAPH OF ITEMS 37 THROUGH 40 PLOTTED VS. TIME
3. PRIMED QUANTITIES ARE UNCORRECTED FOR DRIFT
4. DESIRED FINAL QUANTITY

3.0 RESULTS AND DISCUSSION

3.1 STATIC TEST RESULTS

3.1.1 Sensitivity Data

Accurate calculations of transducer sensitivity (mV/kPa) could be made whenever the static test data acquisition sequence included a 5-point pressure sequence (50, 180, 310, 180, 50 kPa) which was completed within 10 to 20 minutes with no significant change in temperature. The static test data log in Appendix III contains 69 such cycles, representing 44 different combinations of 3 configurations (B, C, E), 2 materials (Ti, Fe), 2 temperatures (21°C, 150°C), 2 strains (0, 1000 $\mu\epsilon$ nominal), and 3 test modes (tensile, bending, vibration). There are 25 repeat cycles taken at random times. Each pressure cycle permits calculation of two sensitivities (50 to 180 kPa, 180 to 310 kPa), designated low range sensitivity (L) and high-range sensitivity (H). Furthermore, each cycle permits two calculations of each sensitivity, one ascending and one descending. Inspection of the raw data (Appendix III) shows that there is no noticeable hysteresis effect; ascending sensitivities are not more than 1 percent different from descending sensitivities. The data from each of the 69 cycles was therefore averaged in each range to produce two sensitivity figures, L and H. Further inspection shows that the repeatability of sensitivity (in those cases where repeat cycles were run) is within the ±1.4 percent standard deviation expected. Therefore, all repeat runs were averaged.

The result is the matrix of 44 pairs of sensitivity values (L, H) presented in Table 3-I.

Certain performance features stand out clearly in the tabulated sensitivities of Table 3-I. It is obvious that strain effects are small (difference between the two sensitivity values in each small box), and that the total range of all sensitivity values is quite large for some specimens (0.4227 mV/kPa to 0.3944 mV/kPa for the E, Ti specimen).

To sort out the predominant influences on sensitivity quantitatively, it was found useful to focus attention on the differences due solely to strain, solely to temperature, and solely to pressure for each of the six specimens in each test mode. Strain effects are summarized in Table 3-II, temperature effects in Table 3-III, and pressure effects (linearity) in Table 3-IV.

These are discussed in order below.

3.1.1.1 Effect of Strain on Sensitivity

The percentage change in sensitivity (Δ_ϵ) resulting from applying strain was calculated directly from the data of Table 3-I, using the definition:

$$\Delta_\epsilon = 100 \text{ X } \frac{(\text{mV/kPa})_{\text{strain } 2} - (\text{mV/kPa})_{\text{strain } 1}}{(\text{mV/kPa})_{\text{strain } 1}}$$

for each test mode, configuration, material, temperature, and pressure. The results are tabulated in Table 3-II. The strain levels for each test made are also identified in Table 3-II.

"Strain 2" was at least 1000 $\mu\epsilon$ in every case, and "Strain 1" was xero in every case. Note that the values of Δ_ϵ are not normalized to "per unit strain".

Strain effect on sensitivity is clearly insignificant for all cases. It will be recalled that for the steel specimens, the tensile test actually subjected the specimens to combined tensile and bending strains. Even these tests show no significant effect of strain on sensitivity in Table 3-II.

The average effect of the applied strain on sensitivity for any one specimen is less than 0.5 percent, the standard deviation for any one specimen is less than 1 percent, and the worst single determination showed only a 2.5 percent effect on sensitivity. The average of all determinations is 0.03 percent and the standard deviation of the sensitivity change due to strain is only 0.42 percent relative.

It should be commented that for brevity, the effect of vibration level on sensitivity is included in Table 3-II, with vibration level simply replacing strain level in the definition of Δ_ϵ. If any significant "strain" effects on sensitivity had appeared in this test mode, a careful analysis of the combined strain and acceleration condition would have been required. The same condensation of parameters is used later is discussing effects of pressure level on sensitivity (nonlinearity).

The conclusion is that the effect of 1000$\mu\epsilon$ on sensitivity is zero, with an experimental uncertainty of less than 0.5 percent, for all specimens.

3.1.1.2 Effect of Temperature Sensitivity

The percentage change in sensitivity (Δ_T) resulting from the change in temperature was calculated directly from the data of Table 3-I, using the definition:

$$\Delta_T = 100 \text{ X } \frac{(\text{mV/kPa})_{\text{temp 2}} - (\text{mV/kPa})_{\text{temp 1}}}{(\text{mV/kPa})_{\text{temp 1}}}$$

for each case in which temperature was changed.

The results are tabulated in Table 3-III. The conclusion is clearcut. There are significant effects of temperature. The effects depend strongly on configuration and blade material, but only slightly on pressure level or strain level. Configuration C is worst on either material (about 6 percent per 100°C). Configuration B is much better on either material (about -3 percent per 100°C). Configuration E is poor on Fe (-4 percent) but excellent on Ti (-1 percent). The scatter of the results is well within the ±2 percent expected.

3.1.1.3 Effect of Pressure on Sensitivity

It will be recalled that the average pressure sensitivity was determined in the low range of operation (50 - 180 kPa) and again in the high range of operation (180 - 310 kPa). The results were tabulated in Table 3-I. The difference between these two determinations, expressed as a percentage of the first, is the percent change in sensitivity due to pressure (Δ_P), i.e.,

$$\Delta_P = 100 \text{ X } \frac{(\text{mV/kPa})_H - (\text{mV/kPa})_L}{(\text{mV/kPa})_L}$$

This quantity was calculated from the data of Table 3-I for every case available. The results are tabulated in Table 3-IVA and B.

Note that the low range of operation is the manufacturer's specified full scale range. The high range includes pressures about twice the manufacturer's stated full scale range.

There are nonlinearities of several percent. The nonlinearity depends strongly on configuration and, oddly enough, test mode, but less strongly on material, temperature, or strain level. The scatter of the results is larger than that of the strain and temperature results of Tables 3-II and 3-III. It is assumed that there were random linearity changes with time which contributed to this scatter.

The grand average and standard deviation of all data for each specimen are presented in Table 3-IVB. The conclusions are as follows:

a) Configuration E is quite nonlinear on either titanium (-2.2%) or steel (-3.9%).

b) Configuration C is the most linear on titanium (0.5%), but is poor on steel (-2.6%).

c) Configuration B is linear on either titanium (0.8%) or steel (1.45%).

d) Linearity uncertainty from day to day is on the order of ±2%.

e) There is some evidence that temperature affects linearity, but the effect is not strong. Strain level has little effect on linearity.

3.1.2 Zero-Shift Data

In scanning the static test data of Appendix III, it is easy to see that run-to-run zero-shifts at identical test conditions are large. For example, between May 13 and May 16, 1977, the zero reading at room temperature and zero strain of the C, Fe specimen wandered over a range of about 3.5 mV, equivalent to more than 8 kPa or 2.6 percent of maximum applied pressures (310 kPa). During this time period, pressure cycles were run at two strain levels (0 and 1000 $\mu\epsilon$) and two temperatures (21°C and 150°C). Attempts to separate zero-shifts due to strain (order of 1 kPa) in this data from zero-shifts due to time and temperature history (order of 8 kPa) were fruitless.

To examine the drift behavior further, the test shown in Figure 3-1 was run. Here the output voltage of the C, Ti specimen at a constant pressure of 103 kPa and constant temperature of 150°C was recorded every few minutes over a 20-minute period, with a 1000 $\mu\epsilon$ bending load applied and removed alternately. The specimen had initially been at temperature for an hour. The drift with time was still so rapid (and unsteady) that determination of zero-shift due to applied strain was not possible. The distance between the curves for the loaded and unloaded specimens in Figure 3-1 varies from 0 to 0.15 mV equivalent to about 0.4 kPa scatter. The drift rate is about 0.25 kPa/minute.

Finally a specimen (B, Ti) was monitored for 24 hours after raising the temperature from 21°C to 150°C. Output voltage vs. time is shown in Figure 3-2. At least 12 hours elapses before the drift rate stabilizes at a low value (about 0.002 kPa/min). After 24 hours, the drift is still progressing at this low rate. Strain cycles carried out after the 12-hour stabilization produced data repeatable to within the readability of the instruments. All strain-induced zero-shift tests subsequently were run after a 12-hour to 24-hour stabilization period at constant temperature.

It should be remarked that the drifts observed were all small percentages of full scale pressure, but they became prohibitive when compared to the anticipated signals in the present application.

3.1.2.1 Effect of Time and Temperature on Zero-Shift

It was found to be impossible to separate the effects of time and temperature on zero-shift of the blade-mounted transducers. The most useful observation during the tests was that in no case did sudden exposure of any specimen to a 129°C air temperature change result in zero-shift rate as large as 4 kPa per minute. From this observation, the maximum possible oscillatory zero-shifts due to an oscillatory temperature condition can be estimated as follows:

Since the thermal time constant of the transducer diaphragm is on the order of 100 milliseconds, it is safe to assume that the $<$ 4 kPa changes observed over a period of 1 minute or more required at least 100 milliseconds to occur. But the longest time interval of interest in the measurement of oscillatory pressure in the frequency range above 75 Hz is about 3 milliseconds (the rise time of a 75 Hz sinusoid). In this time interval, the zero-shift due to the 129°C step change could not exceed about 3/100 of 4 kPa. Then the oscillatory zero-shift due to an oscillatory temperature condition can never exceed about 1 Pa (peak-to-peak) per °C (peak-to-peak). The figure is reassuringly small; this effect of temperature can safely be ignored in flutter studies, for example, when the smallest pressure signals to be measured are on the order of 1 kPa (peak-to-peak), and the temperature fluctuations are generally only a few °C (peak-to-peak).

In judging the usefulness of blade mounted transducers for steady-state pressure measurements, the conclusion from inspection of data in Appendix III is that an uncertainty of about ±14 kPa must be accepted due to zero-shifts with time and temperature history. This uncertainty cannot be "calibrated out" due to the unpredictable nature of the effect of time. In some temperature cycling tests for example, a positive zero-shift occurred when temperature was raised to 150°C and held there for several hours, and then a further positive shift occurred when the temperature was reduced to 21°C and held there for several hours.

3.1.2.2 Effect of Strain on Zero-Shift

The calculation procedure and results of the cyclic bending strain tests of Figure 2-35 are tabulated in Table 3-V. The results are summarized here in condensed form:

Specimen	21°C Pa/$\mu\epsilon$	150°C Pa/$\mu\epsilon$
C, Fe	–2.65	–0.56
C, Ti	–1.38	–0.18
B, Fe	–1.27	–0.85
B, Ti	–1.15	–0.57
E, Fe	–0.20	
E, Ti	–0.38	
$A_{0.125}$, H	–0.43	
$A_{0.025}$, H	–0.51	
A_0, H	–8.55	

Each data entry represents the average of six to twenty determinations. The mean deviation of the determinations for each test condition was less than 0.05 kPa. A 12 to 24 hour stabilization at temperature preceded each strain sequence.

The three preliminary strain-isolation test items (designated configuations A_0H; $A_{0.025}H$; $A_{0.125}H$, where the subscript indicates the thickness of RTV used for strain isolation, in mm) were tested at 21° C and the results are included in the tabulations. The raw data is included in Appendix III.

Six important conclusions may be derived from the table of results. The first five deal with behavior at room temperature.

1) Strain effects on zero-shift are quite large, ranging from 0.2 Pa per microstrain to 2.6, not counting the hard-mounted reference, A_0, at 8.5.

2) Configuration $A_{0.025}$ and $A_{0.125}$, at 0.5, are about equal, confirming that using more than 0.05 mm thickness RTV does not provide increased strain isolation.

3) Configuration A provides better strain isolation than B or C by a factor of more than two, indicating that stress concentrations due to machining holes or recesses in the blade surface seriously increases strain-induced error.

4) Configuration E is best of all at about 0.2 on the steel specimen and 0.4 on titanium. The effect of stress concentration due to machining is offset by the excellent strain isolation, by locating the transducer near the neutral axis, and by the relative rigidity of the cylindrical transducer compared with the thin transducer.

5) Configuration C is worst, and its behavior is worst of all on the steel specimen, at 1.4 on titanium and 2.6 on steel. It is quite probable that the performance difference between the two specimens is more due to geometry than material, even though the configurations were supposedly the same. The airfoil contour of the titanium blade required less removal of material in machining to provide the necessary recess, than the relatively flat contour of the steel simulated blade. The conceptual sketch in Figure 3-3 shows that not only is more material removed from the steel specimen, but also the resulting 4-sided recess places regions of higher stress concentration adjacent to the transducer shim edges. The C, Ti and C, Fe specimens must be regarded as different configurations in this regard.

6) The effect of temperature on response to strain is surprisingly large. The effect of strain on zero-shift drops dramatically at high temperature. The greatest change occurs in the C configuration, which was worst at room temperature; so great is the improvement that C becomes better than B at 150°C, at 0.2 Pa/$\mu\epsilon$. The improvement is presumably due to a reduction in the stiffness to the RTV rubber used for strain isolation. E was not tested at 150°C but presumably is still superior to all others at the higher temperature.

The algebraic sign of all zero-shifts is negative, including that, as expected, increased tension has the same effect as a reduced pressure. Note again that the convention used in reporting strains in the blade results in tension in the blade surface (on the same side of the blade as the pressure transducer diaphragm), being reported as positive. The algebraic sign of the strain effect is therefore the same for all configurations.

Though all the strain-cycle tests were carried out at a pressure of one atmosphere, it is believed that the results would be nearly identical at any other pressure within the range of the static test. The deflection of the diaphragm at full scale pressure of 310 kPa for example, is only about 0.03 mm, and this amount of distortion could hardly change the transducer geometry enough to change the strain effect on zero-shift.

3.1.2.3 Effect of Vibration Acceleration on Zero-Shift

The vibration tests provided the only data in either phase of the program on the effect of pure acceleration perpendicular to the transducer diaphragm. During the initial vibration tests of the six specimens, the output voltage was monitored on an oscilloscope with a resolution equivalent to 300 Pa, and the maximum acceleration was 650 G. Peak-to-peak output was below the 300 Pa threshhold, so the tests indicated only that the effect was less than 0.5 Pa/G. To obtain a better measurement, the three titanium specimens were retested at atmospheric pressure. (This time only the E specimen had a cup installed over the pressure transducer.) An oscilloscope with resolution of 0.6 Pa and a sensitive true RMS voltmeter was used.

The oscilloscope signals were clean undistorted sine waves. The oscilloscope peak reading and the peak reading calculated from $\sqrt{2}$ X RMS reading agreed within 10 percent. The peak reading calculated from RMS measurement was accepted as the more accurate, and the following results were obtained:

Configuration	Zero-Shift Due to Normal Acceleration Pa/G	Uncertainty Pa/G
B, Ti	0.16	0.01
C, Ti	0.34	0.01
E, Ti	0.32	0.01

For the C and E configurations it was therefore found that the effect of normal acceleration was about equal to the predicted 0.4 Pa/G, but for the B configuration the measured effect was less than one-half the predicted effort. The much lower effect of acceleration on the B configuration was a surprise, and has not been explained. The vibration test was repeated and the transducer pressure calibration was rechecked carefully, with the same result.

It might be concluded that the B configuration provides vibration isolation, because of the much larger thickness of RTV rubber employed in the B configuration (about 0.48 mm, compared with 0.05 mm for the other two configurations). As a check on this conjecture, the compliance of the B, Ti mounting was measured by pressing on the back of the transducer with a force gage, and measuring the force required for a displacement of 0.05 mm. The resulting stiffness was 20 N/mm, several orders of magnitude too large to provide vibration isolation. (The inertial forces on the transducer during the vibration test were on the order of only 0.05 n.)

It is also obvious that aerodynamic damping in the hole and cavity which the transducer faces is negligible.

The surprisingly small effect of acceleration on the B, Ti specimen remains unexplained, and the result is regarded with suspicion. Testing of additional samples in the B, Ti configuration would be required to resolve the question.

3.2 SPIN TEST RESULTS

3.2.1 Spin Test Data

Spin test data is tabulated in Appendix III. Table 3-VI presents a summary table of transducer sensitivity shift (low range and high range) and zero shift (at 7, 150, 310 kPa) vs. centripetal loading, configuration, orientation, and temperature. The data reduction procedure described in Section 3 was used in calculating the results of Table 3-VI.

The results are plotted in Figure 3-4, Percent Sensitivity Change vs. Centripetal Loading, and Figure 3-5, Zero-Shift vs. Centripetal Loading, with other parameters indicated by keyed symbols. In these plots, the effects of strain and acceleration loading are not separated.

Strain was monitored continuously during the spin test of the first build, and the strain data is included in Appendix III. The maximum strain observed and the estimated zero-shift due to strain at each centripetal acceleration are plotted in Figure 3-6. The strain is compressive because the instrumentation plate was restrained by the outer rim of the spin disk. Strain is found to be linearly proportional to acceleration. The separation of the strain effects of Figure 3-6 from the combined strain and acceleration effects in Figures 3-4 and 3-5 are discussed below.

3.2.1.1 Effect of Centripetal Acceleration on Sensitivity

Sensitivity change (percent) versus centripetal acceleration is presented in Figure 3-4a. The general trend (ignoring details of configuration, orientation, temperature) is an increase in sensitivity of about 3.5 percent per 100,000 G, an impressively small effect.

The solid line in Figure 3-4a is the least-square-error best fit straight line for the entire set of 22 data points (including one data point at zero acceleration). The zero intercept of this straight line is close to zero change in sensitivity (0.387 percent). At 100,000 G, the best straight line indicates a 3.447 percent effect on sensitivity.

The standard deviation (σ) of the data set is 3.84 percentage points (from the best straight line). On the basis of random error, a σ of about 2.4 percentage points would have been expected. This expectation is based on a σ of about 2.4 kPa in pressure determinations (Figure 3-6), on a 145 kPa interval for sensitivity determinations (and hence a σ of $(100)(\sqrt{2})(2.4)/145 \approx 2.4$ percent in sensitivity determinations).

On statistical grounds, the conclusion is that the effect of other parameters (configuration, orientation, temperature) in the spin tests was slight, within the accuracy of these experiments. Configuration, orientation, and temperature are identified by keyed symbols in Figure 3-4. Inspection of the sets of keyed symbols presents no evidence to contradict the conclusion reached on statistical grounds. Each set is scattered randomly around the trend line. The 82°C data are in the same range as the 21°C data. No effect of tilting the transducer by 7° is evident. The B and A configurations results are not noticeably different from each other.

It would be expected that scatter would be less at lower pressure levels because the pumping correction is a smaller fraction of the pressure internal used. In Figure 3-4b and 3-4c the subsets of data for low pressure range and high pressure range are plotted separately, superimposed on the overall trend line of Figure 3-4a. Although the largest scatter does occur in the high pressure range, the difference is not striking, and both sets of data appear to follow the overall trend.

It would also be expected that scatter would be less at low acceleration levels. This expectation is not borne out by Figure 3-4. In fact, the few points obtained at highest acceleration (75,000 G) happen to show the least scatter.

Finally, it should be observed that although strain and acceleration effects are not separated in Figure 3-4, no effect of strain in sensitivity is expected. The evidence of Table 3-II (static strain effect on sensitivity) has already shown that the effect of strain on sensitivity is not significant.

It may be concluded with confidence that the trend line in Figure 3-4 represents the effect of acceleration alone, and that the trend is about the same for both configurations, both orientations, and both temperatures.

3.2.1.2 Effect of Centripetal Acceleration on Zero-Shift

Zero-shift (kPa) versus centripetal acceleration is presented in Figure 3-5a. The general trend of this data shows a positive zero-shift of about 12 kPa per 100,000 G, ignoring details of configuration, orientation, temperature, pressure and strain.

The solid line in Figure 3-5a is the least-square-error best straight line calculated by applying linear regression to the entire set of 33 data points (including one data point at zero acceleration). The zero-acceleration intercept of this straight line is very close to zero kPa (-0.04 kPa). At 100,000 G the best straight line indicates a 12.14 kPa zero-shift.

The standard deviation (σ) of the data set is 5.43 kPa (from the best straight line). On a random error basis, σ of about 3.4 kPa would have been expected. This expectation is based on a σ of 2.4 kPa in pressure determinations from Figure 3-6, and therefore a σ of $\sqrt{2} \times 2.4 = 3.4$ kPa for differences between pressure determinations.

On a statistical basis, then, it would appear that some parameter other than centripetal acceleration is significant in this set of data. The other parameters are configuration, orientation, temperature, pressure, strain and time.

Strain effects can be accounted for readily. Figure 3-6 shows maximum measured strain during the spin tests (fiber strain in the plate surface in the radial direction) versus centripetal acceleration and the resulting expected zero-shift due to strain for the A, Ti configuration, based on the static test results of Table 3-V. The expected zero-shift due to strain accounts for 15 percent of the zero-shift indicated by the trend line in Figure 3-5a. For the B, Ti configuration, the expected zero-shift due to strain accounts for 12.6 percent of the total indicated by the trend line of Figure 3-5a. This contribution is not negligible and will be taken into account in the process of drawing formal conclusions from the spin tests. It may be ignored for the moment in examining the relative zero-shifts due to configuration, orientation, temperature, and pressure. Note that the strain increases the zero-shift in the spin tests because the strain is compressive. On an unrestrained fan blade (unshrouded) the fiber strain would be tensile and the zero-shift due to strain would be negative, tending to cancel the effect of acceleration.

Configuration, orientation and temperature are identified by keyed symbols in Figure 3-5a. The effects of pressure are examined separately in Figures 3-5b, c, d where the subsets of data points for 7, 150, 310 kPa are each plotted superimposed on the overall trend line of Figure 3-5a. The effect of each of the parameters may therefore be examined separately.

Pressure. Figures 3-5 b, c, d show that the scatter of the zero-shift data is larger at higher pressure as expected, due to the large pumping correction at high pressure. The overall trend line fits reasonably well with the ten or eleven data points at each pressure level. There is no evidence that zero-shift with acceleration varies with pressure.

Temperature. The scatter of measurements of zero-shift with acceleration at high temperature is remarkably small. The six data points follow the overall trend line closely. There is no strong evidence that zero shift with acceleration varies with temperature. The smaller effect of strain at high temperature (Reference: Section 3.1.2.2) would be expected to cause the high-temperature points in Figure 3-5 to fall slightly lower, but either the effect is too small to be observed or is concealed by a possible slightly higher effect of acceleration at high temperature.

Orientation. It would be expected that the A, 7° orientation would show a more positive zero-shift with acceleration, since the transducer diaphragm is face up on the 7° slope and is therefore deflected in the direction of high pressure reading by the normal component of the inertial force on the diaphragm. The parallel component of acceleration is negligibly different for the two orientations. The predicted difference between A, 7° and A, 0° would be about +1 kPa at a centripetal acceleration of 27,000 G based on the vibration test result of 0.3 Pa/G for normal acceleration (G_n) and G_n of 27,000 Sin 7° = 3300 G.

In Figure 3-5a, each of the three measurements at 27,000 G indicate a negative shift, from –0.8 kPa to –8.3 kPa (relative to the trend line for all data). Since the expected effect was only about one fith of the standard deviation of the measurements, at least thirty test points at 7° orientation would be required to determine whether the expected trend existed. The only conclusions permissable are that the effect of the added normal component of acceleration is certainly within an order of magnitude of that observed in the vibration tests, and that the build-in uncertainty of the spin test measurement prevents a more quantitative statement because of the small data sample obtained.

Configuration. Examination of the subsets of data for the A, 0° (15 points) and B, 0° (14 points) configurations in Table 3-VI shows no significant difference in acceleration effect. Of course, there is no reason to expect any difference. The diaphragms of these two transducers are ostensibly identical, and at the same orientation. The conclusion is that mounting configuration does not affect steady-state zero-shift due to steady-state parallel acceleration.

Time. It is concluded that the larger scatter than expected is due to random zero-shifts with time not completely eliminated from the calculated results despite the elaborate procedures used in testing and data reduction to do so.

3.2.1.3 Effect of Temperature and Time on Zero-Shift

It was remarked that the effects of temperature and time on zero-shift could not be separated in the static test data. The same kind of observation applies to the spin test data. For example, Figure 3-7 is a plot of the series of reference readings of the B, 0° and A, 0° output voltage levels corrected to the reference pressure of 151.7 kPa at zero RPM during the entire period of the spin tests, including several different days in October for B, 0° and several different days in December for A, 0°. This type of plot was generated for every transducer for use in applying zero shift drift corrections in the spin test data reduction procedure (calculation steps 41 to 48 in Table 2-IV). It should be noted that the zero-shifts with time at constant temperature were on the order of 6 mV (e.g. run 11 and run 12) and that zero-shifts with 55°C temperature change (e.g. run 10 and run 11) were the same order of magnitude. (The typical shift from one check reading to the next on any one day was less than 0.2 mV so the accuracy of the correction procedure was thought to be adequate.) It must be concluded that for blade mounted transducers, with the configurations and materials used in this program, the overall uncertainty due to time and temperature is about ±14 kPa in steady-state zero output level. These blade-mounted configurations are therefore not suitable for measurement of steady-state pressure on rotating blades if higher accuracy is required.

3.2.1.4 Post-Test Examination of Transducers

After post-test calibrations were completed (discussed in the next section) the B, 7° transducer was carefully loosened from the instrumentation plate on the spin disk by sliding a razor blade along the surface under the RTV rubber, and peeling it back for inspection. The two photographs in Figure 3-8 show the transducer before and after peeling back. The entire installation was found to be in excellent condition, with no detectable migration or distortion of the RTV or epoxy. The A, 7° transducer, also visible in Figure 3-8, and the A, 0° transducer could be inspected without removal, and both installations were in excellent condition as well.

3.3 Calibration History

The calibration history of each transducer used in the program is tabulated in Table 3-VII. Six-level primary calibrations (starred items in Table 3-VII) were carried out by the P&WA Instrumentation Standards Group, using a pressure standard directly traceable to NBS. Three-level secondary calibrations were carried out using the transfer standard P1 of Figure 2-24 (±1.0 kPa). The sensitivity reported is the average over the entire pressure range 0 to 310 kPa.

All transducers were within specification at room temperature when accepted from the manufacturer and introduced into the test program (±1 percent F.S. combined linearity and hysteresis, ±0.014 percent/°C). Table 3-VII shows that the subsequent change in sensitivity due to mounting varied from +9.1 percent to −15.5 percent. For the mounted transducers the total further change in sensitivity during static tests or spin tests varied from −2.9 percent to +19.9 percent, but more detailed examination of Table 3-VII shows that the behavior is less alarming than these two extreme figures would indicate. All six static test items changed sensitivity by less than 3 percent throughout the entire program of tensile, bending, and vibration tests (average 1.7 percent).

During the spin program, four different transducers were active and the sensitivity changes were as follows:

Serial No.	Sensitivity Change During First Build Tests	Sensitivity Change During Second Build Tests
3	N.A.	+ 4.7%
8	–0.9%	N.A.
9	+2.7%	+19.9%
15	+6.7%	+ 2.5%

Thus during the first build, the greatest change in sensitivity was +6.7 percent (Serial No. 15); in the second build the sensitivity of this particular transducer changed by only +2.5 percent. It does not appear that the Serial No. 15 transducer is deteriorating. Serial No. 9 changed +2.7 percent during the first build and +19.9 percent during the second. The latter change is rather large. Examination of the data (Appendix III) shows that virtually all of the change occurred during the initial 27,500 G test of the second build, and that changes thereafter (including exposure to 90,000 G and 82°C) were small. Apparently some unique event during the 27,500 G test, such as an inadvertent overpressure, produced the major change. There is no evidence of progressive deterioration thereafter.

The other two transducers (Serial Nos. 3 and 8) experienced only modest changes in sensitivity during the spin tests.

The conclusion is that the stability of sensitivity during the torture tests of the program was excellent. It is evident that in actual use in an engine program, a sensitivity calibration (mV/kPa) of each transducer must be carried out after mounting, and that the calibration should be repeated from time to time to check for change due to exposure to the engine environment.

3.4 SUMMARY OF ACCURACY OF ROTATING PRESSURE MEASUREMENTS USING BLADE-MOUNTED TRANSDUCERS

Table 3-VIII summarizes the effects on sensitivity of temperature, pressure, strain, parallel and normal acceleration, and time for each configuration tested. Table 3-IX summarizes the effects of these parameters on zero-shift for each configuration tested. In each case the uncertainty of the determination is stated. The summaries can be used in assessing the accuracy in specific applications. Examples of applications using these results are presented in the next section.

3.5 APPLICATION OF RESULTS

3.5.1 JT15D Fan

In the JT15D Engine Fan Noise Static Test Program at P&WA and the NASA Lewis Research Center, and the JT15D Engine Fan Noise Flight Test Program at the NASA Langley Research Center, fan-blade-mounted pressure transducers were proposed for acoustic surveys. P&WA was asked to provide an assessment of accuracy of oscillatory pressure measurements of blade mounted pressure transducers for these programs, based on the results of the present test program. The assessment is summarized in Table 3-X. The conclusion was that when an allowance was made for ±5 percent uncertainty in calibrations performed at frequencies up to 7500 Hz in the field, the overall error would not exceed 5.88 percent ±0.074 kPa in the operating engine. The error includes the effects of pressure, temperature, oscillatory strain, and steady-state and oscillatory accelerations, using configuration A, including the estimated increase in effect of normal acceleration due to a 0.025 mm RTV coating.

Durability for at least 15 hours up to 75,000 G was required. Experience in the previous engine program (including flight tests) and in the present transducer development program showed this to be a safe bet, the only real threat being the possibility of foreign object damage. For this reason, it was recommended that the transducer diaphragm be overcoated with about 0.025 mm thickness of RTV rubber and that one set of spare blades be instrumented.

3.5.2 TS22 Fan

Sixteen fan-blade-mounted transducers of Configuration A and one of Configuration B were used in the Subsonic/Transonic Stall Flutter Program at Pratt & Whitney Aircraft in 1977 under Contract NAS3-20606. The TS22 fan rotor was used. A library of previous flutter data was available for this fan.

Operating conditions and expected accuracy were essentially the same as those for the JT15D (Table 3-X).

The transducers were mounted on the surfaces of several blades at selected chordwise and spanwise locations. The Configuration A transducer diaphragms were overcoated with about 0.025 mm of RTV. A.C. and D.C. signals were amplified (using electronic amplifiers in the rotating system) and the signals transmitted through a 200-ring miniature liquid-cooled slip ring to a multichannel tape recording system. Two-minute tape recordings of each signal were obtained at each of approximatley 250 operating points (including many repeats). Other rotating instrumentation included one strain gage on each of the 32 blades, a number of blade-mounted hot films, and blade-mounted mirrors for optical determinations of blade deflections in twisting and bending during flutter.

From the huge mass of recorded data available, four pressure transducers (on three blades) and three strain gages (one on each of these blades) were selected for analysis under the present contract to evaluate the performance of the Configuration A and B blade-mounted pressure transducers.

Each signal was analyzed at each of six fan operating points (one point in flutter and one point out of flutter at each of three operating speeds). The operating points are shown in Figure 3-9.

The locations of the selected pressure transducers were as follows:

Transducer No.	Configuration	Blade No.	Chordwise Location (Convex Side)	Radius (cm.)	Spanwise Location % Span	Spanwise Location % Tip Radius
116	A	3	40%	36.8	83	90
111	B	6	50%	36.8	83	90
816	A	3	65%	36.8	83	90
179	A	5	65%	36.8	83	90

The pressure was measured on the convex side of the airfoil in each case; the Configuration B transducer was therefore mounted on the concave side and all others on the convex side.

The strain gages were mounted on each blade on the convex airfoil surface at maximum thickness position (near 50% chord) just above a shroud at 65% span. Enough data reduction had already been completed to provide steady and oscillatory (amplitude and phase) strain, deflection and acceleration values at each pressure transducer location at each of the six fan operating points. Great care was taken to preserve phase information (relative to a reference strain gage) for all sensor signals.

For the purposes of the present study the selected data were reduced to the following form:

a) Sample oscillograph recordings of each of 36 oscillatory signals (24 pressure, 12 strain),

b) Power spectrum density plots of each of 36 oscillatory signals,

c) Steady state indicated pressures for each of the 24 pressure transducer records.

From the power spectrum plots, the broad-banded RMS levels of indicated oscillatory pressures and strains were calculated, and, at the in-flutter operating points, narrow-band RMS level at the flutter frequency and at the first harmonic of flutter frequency. The results are presented in Figures 3-10, 3-11, 3-12, and 3-13, and in Tables 3-XI and 3-XII.

Figure 3-10 presents the 36 power spectra of pressure transducer and strain gage signals. The outstanding features are the following:

(a) Pressure signal spectra of Configuration A and B transducers are qualitatively the same. At no-flutter operating points, the oscillatory pressure levels are very low (10^{-4} kPa^2/Hz) except for small peaks (10^{-3} kPa^2/Hz) at rotor frequency (120 Hz to 136 Hz) and at all multiples of rotor frequency. In flutter there is a significant level of broad band energy (10^{-3} kPa^2/Hz) plus a prominent peak (10^{-2} kPa^2/Hz) at flutter frequency (about 620 Hz). Small peaks at rotor frequency and at some multiples of rotor frequency are evident during flutter, but the peak at flutter frequency dominates. In addition there is a significant peak at twice flutter frequency.

(b) All of the strain spectra are characterized by a distinct background pattern of peaks at rotor frequency and several multiples of rotor frequency; this background pattern is much the same in flutter and out of flutter. At all operating points in flutter, however, an extremely large peak at flutter frequency appears. This peak is 10 to 30 times higher than any of the background peaks and clearly dominates the oscillatory strain behavior.

(c) The strain level on Blade 6 is much lower than on Blade 3 or Blade 5 (not shown), at all operating points. (The strain pattern for the whole rotor shows a variation in blade oscillatory strain level vs. blade position on the rotor.

In Table 3-XI the measured rms pressure fluctuations at flutter frequency (plus the energy at twice flutter frequency) are tabulated. Also tabulated are the corrections required to each rms level due to oscillatory strains and accelerations at flutter frequency, calculated from the independently known strains and blade deflections. The calculation procedure is shown in the table. Note that the phase of the strains and accelerations is taken into account. The results are graphed in Figure 3-11 showing rms pressure amplitude, corrected and uncorrected, versus chordwise position for each of the six operating points. The outstanding features of Figure 3-11 are as follows:

(a) Corrections are small, ranging from -5% to +5% for oscillatory strains and -2% to +10% for oscillatory accelerations.

(b) In the case of the Configuration B transducer (#111) the strain and acceleration effects tend to cancel, so that the total correction is less than +3%.

(c) The indicated pressure fluctuation amplitude varies smoothly with chordwise position, as would be expected. Again there is no indication that transducer mounting configuration alters the blade flutter response or the pressure fluctuation character in flutter or out of flutter.

Figures 3-12 and 3-13 and Table 3-XII summarize the average (D. C.) pressure measurements obtained with the four transducers at the six operating points. It will be recalled that random drifts on the order of ±14 kPa were to be expected, on the basis of laboratory tests of Article 3.1.2 and 3.2.1. To this must be added the possible drift in TS22 rotating amplifier zero levels and gains, and drift in excitation voltages. These contributions were judged to be less than ±1 kPa. The total expected random scatter of the data was thus about ±15 kPa. At first glance (Figure 3-12) it would appear that the TS22 scatter was nearer ±100 kPa, but when the readings of each transducer are zero-adjusted by subtracting the average of all readings obtained with that particular transducer, then (Figure 3-13) it is evident that the largest scatter occurred only during the first day of the program. Spread of zero-adjusted readings during the last two days presented in Figure 3-13, October 27 and November 2, is ±30 kPa. Part of this spread is systematic with operating point on the fan performance map. The spread at any one operating point is ±20 kPa. The conclusion is that the expected ±14 kPa drift is increased to about ± 20 kPa under real fan operating conditions. (The even larger spread on the first day of the program is unexplained and can be blamed on possible data system problems.) It is unfortunate that reference readings of transducer D. C. output in each channel were not recorded at zero rpm (or a low idle speed) each day to provide a better base line than the overall average for each transducer. Even so, there is little hope that the resulting scatter would have been reduced to less than ±15 kPa.

The 17 blade mounted transducers in the TS22 program all survived the entire program and the great majority provided reliable oscillatory pressure measurements throughout the program. The capability for such measurements was demonstrated up to 50,000 G (11000 rpm/14.5" radius) during this TS22 program.

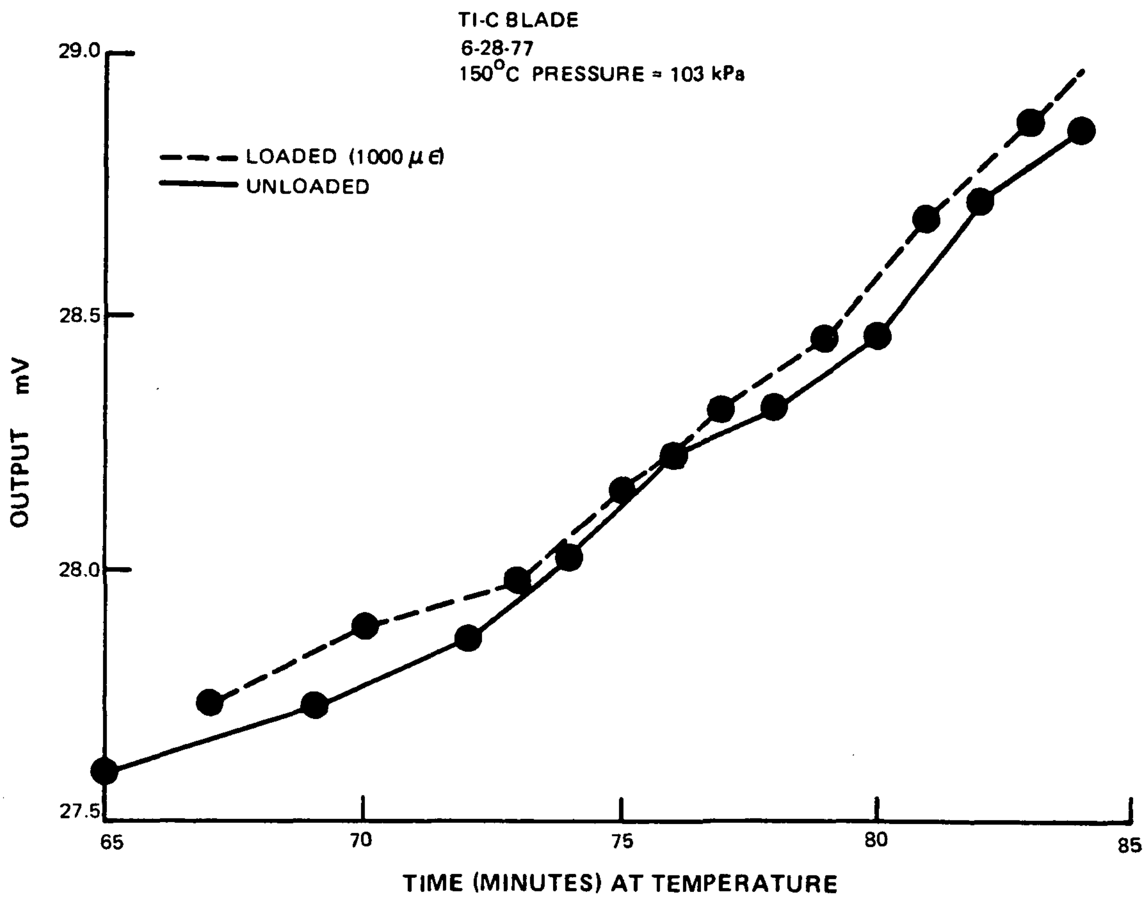

Figure 3-1 *Output Due to Bending Strain*

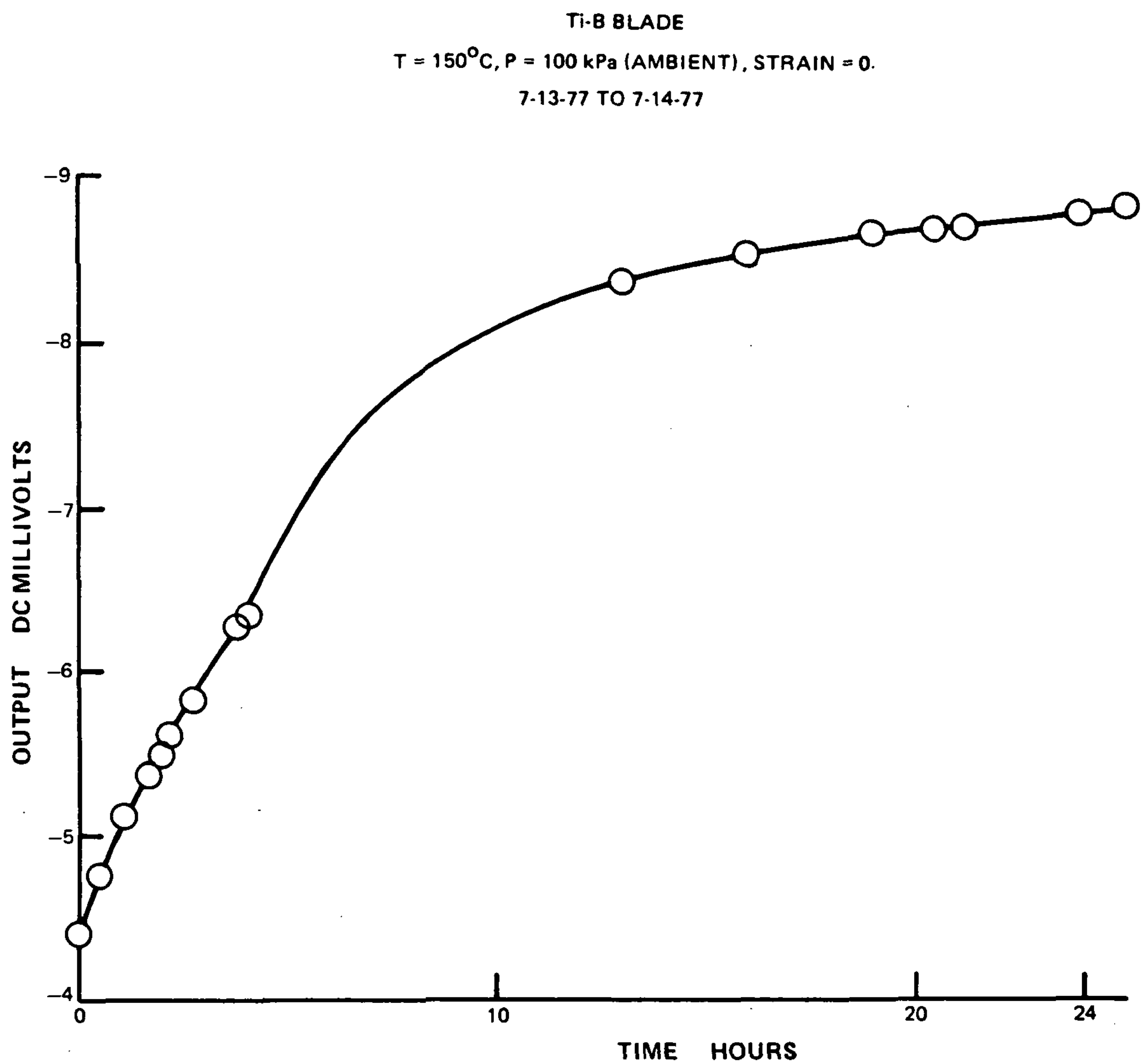

Figure 3-2 Effect of Time at Temperature

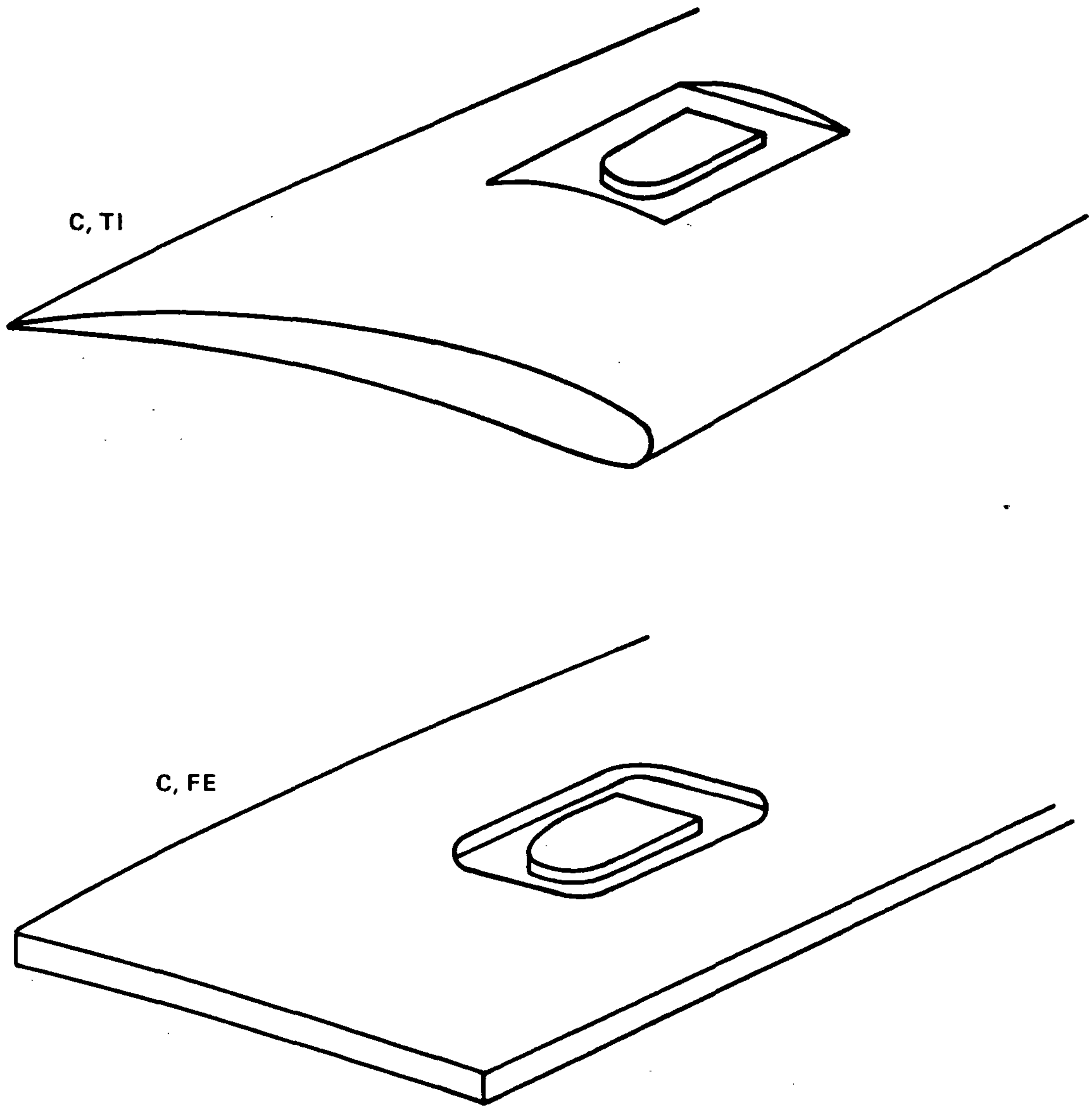

Figure 3-3 *Comparison of Machining of Configuration "C" Titanium and Steel Blade Specimens (Not to Scale)*

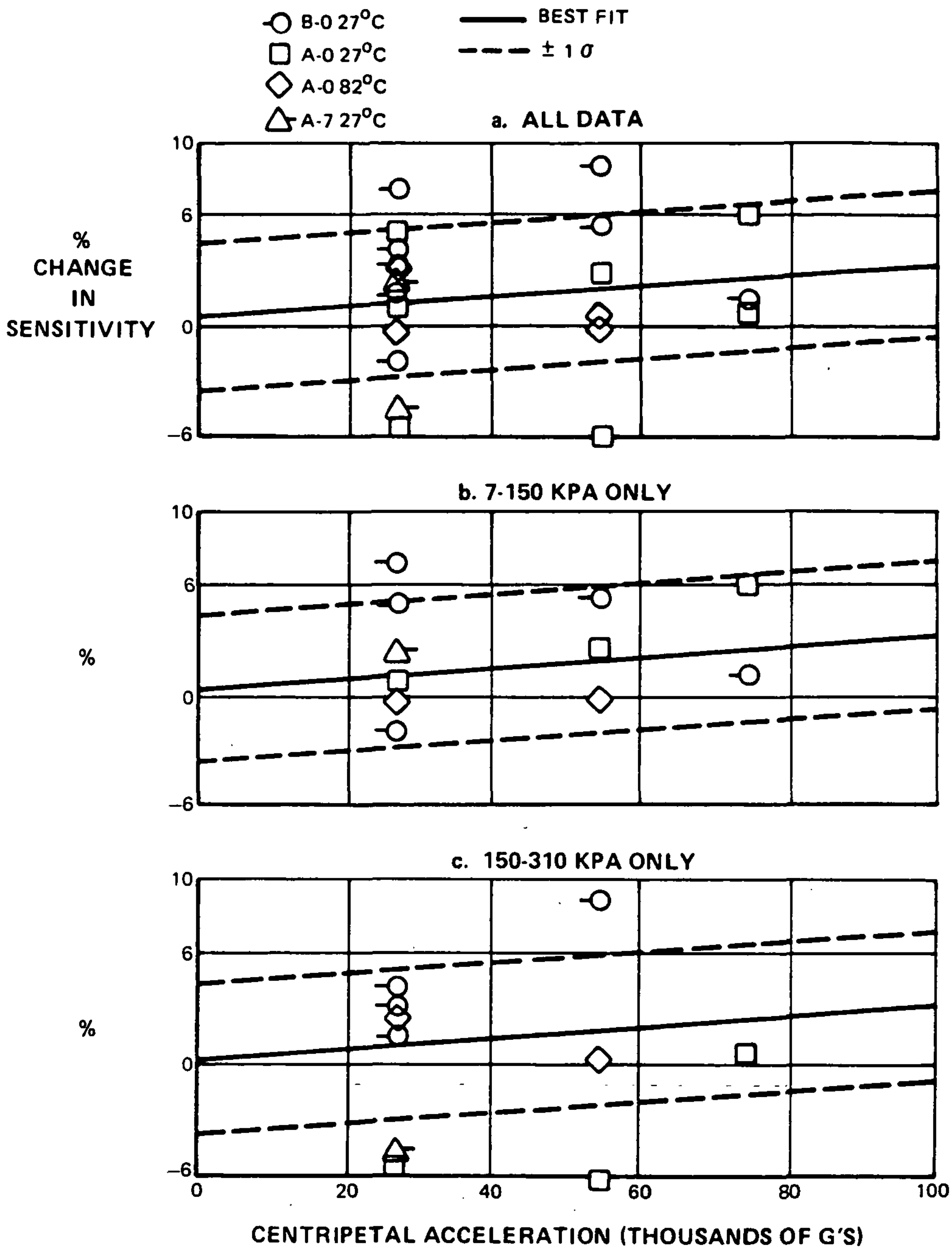

Figure 3-4 Effect of Centripetal Acceleration on Sensitivity

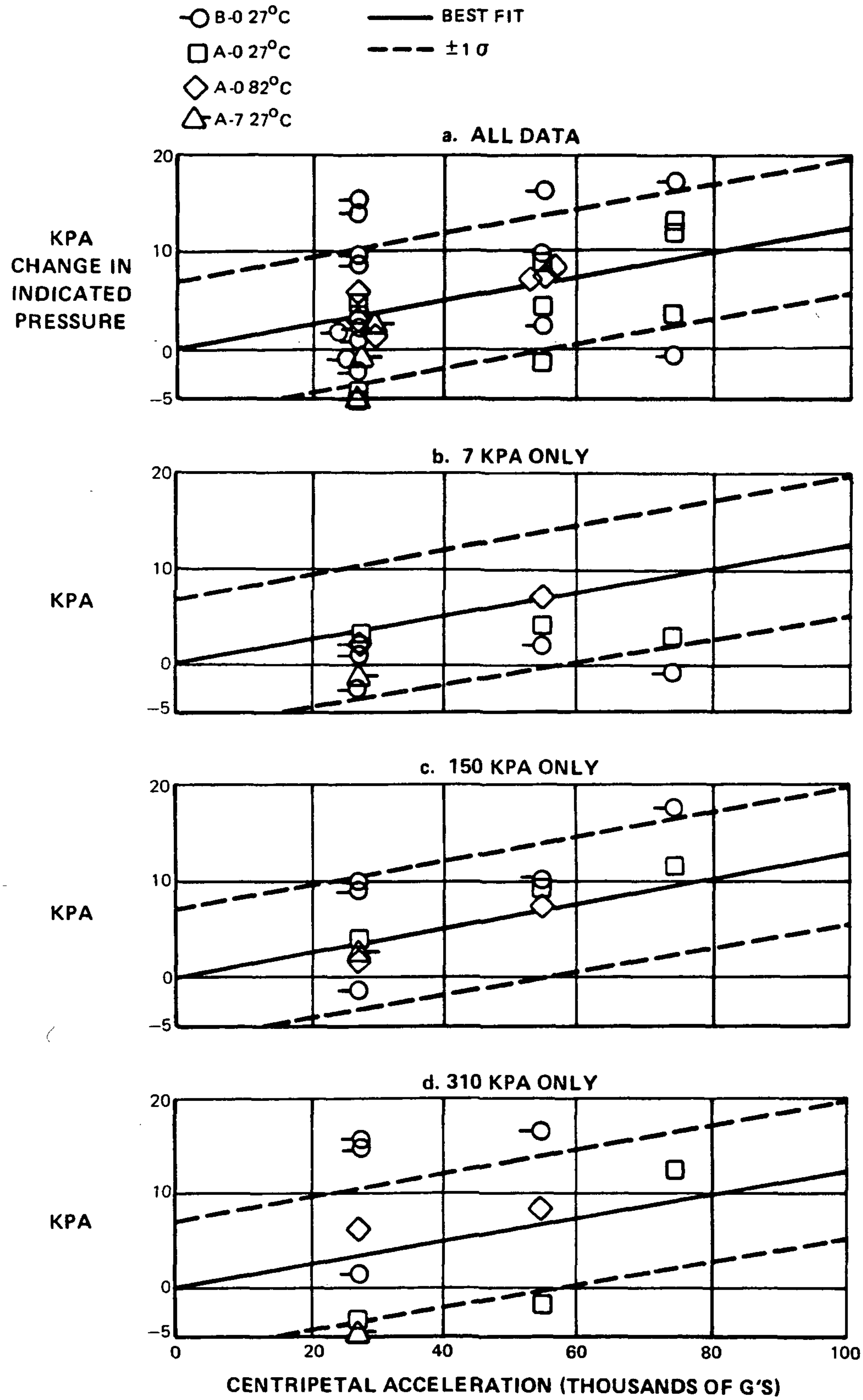

Figure 3-5 Effect of Centripetal Acceleration on Zero Shift

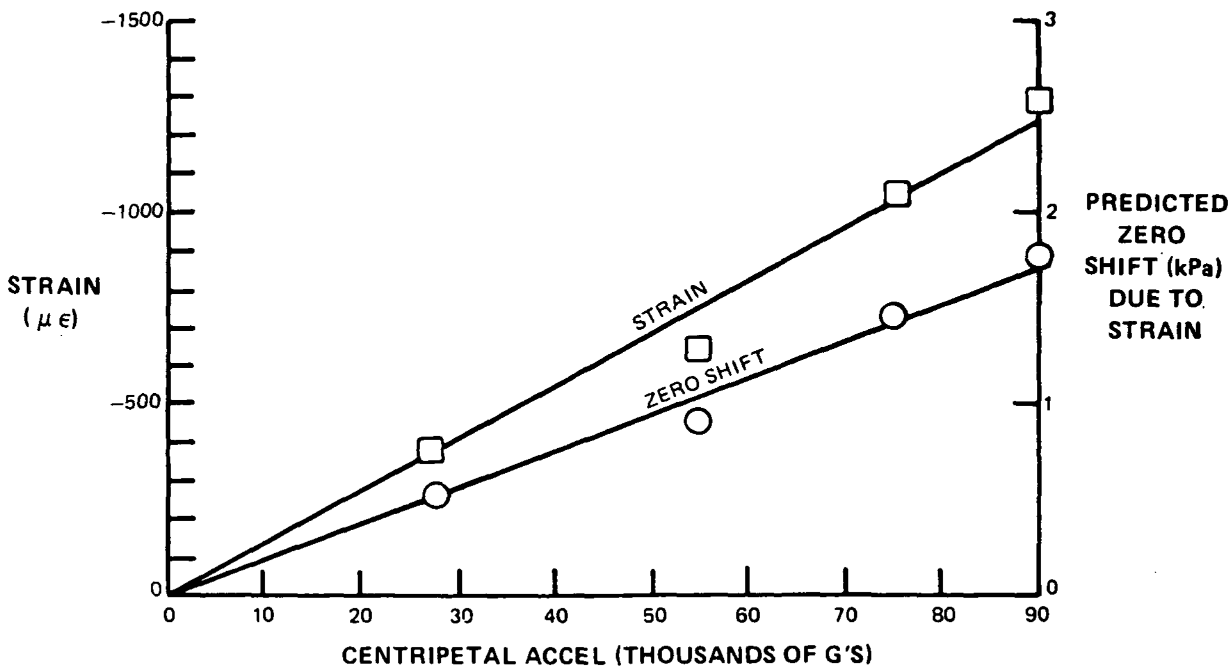

Figure 3-6 *Predicted Zero Shift Due to Strain During Spin Tests for Configuration "A"*

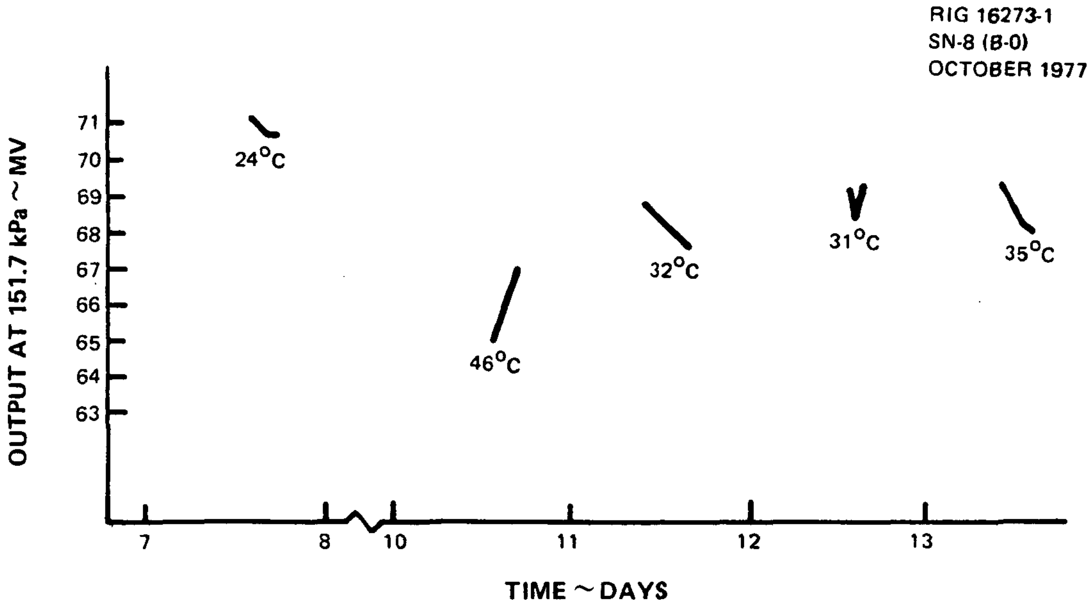

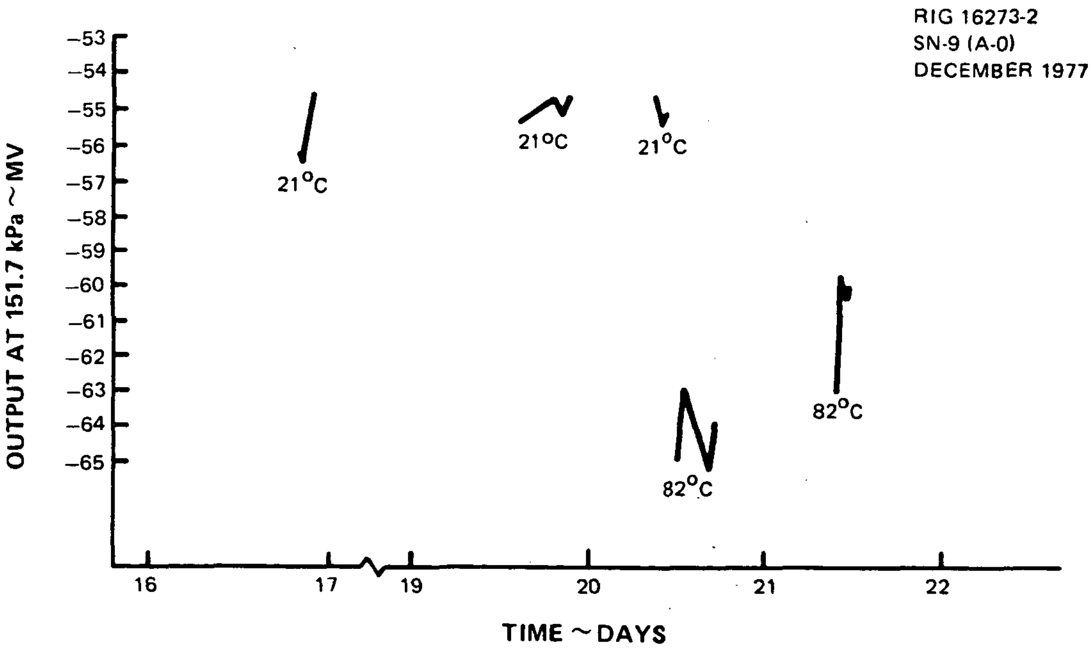

Figure 3-7 Drift of Output With Time

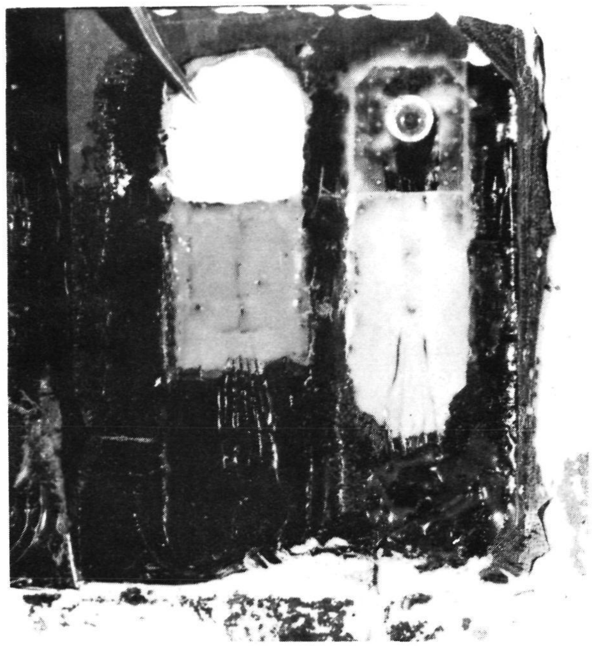

A) B, 7 Transducer Installation Ready for Peel Back of RTV Mounting From Instrumentation Plate (78-441-0056-E)

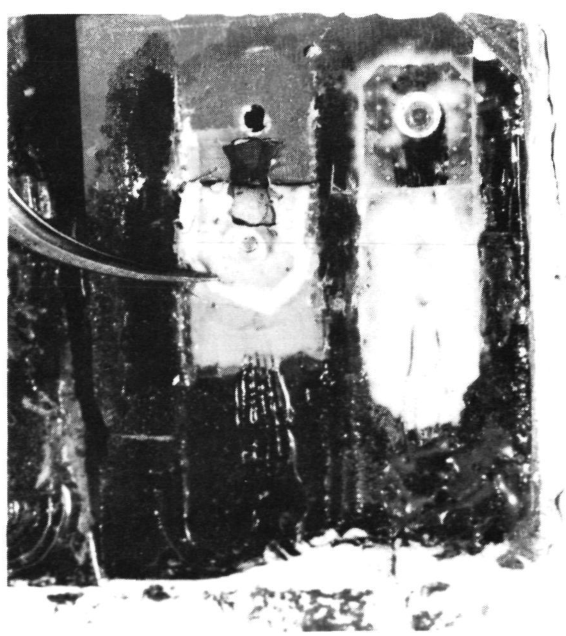

B) B, 7 Transducer Ready for Inspection (78-441-0056-F)

Figure 3-8 *Post Spin Test Inspection of Transducers B, 7° (Left) and C, 7° (Right) – Both transducers were unaffected by the spin test.*

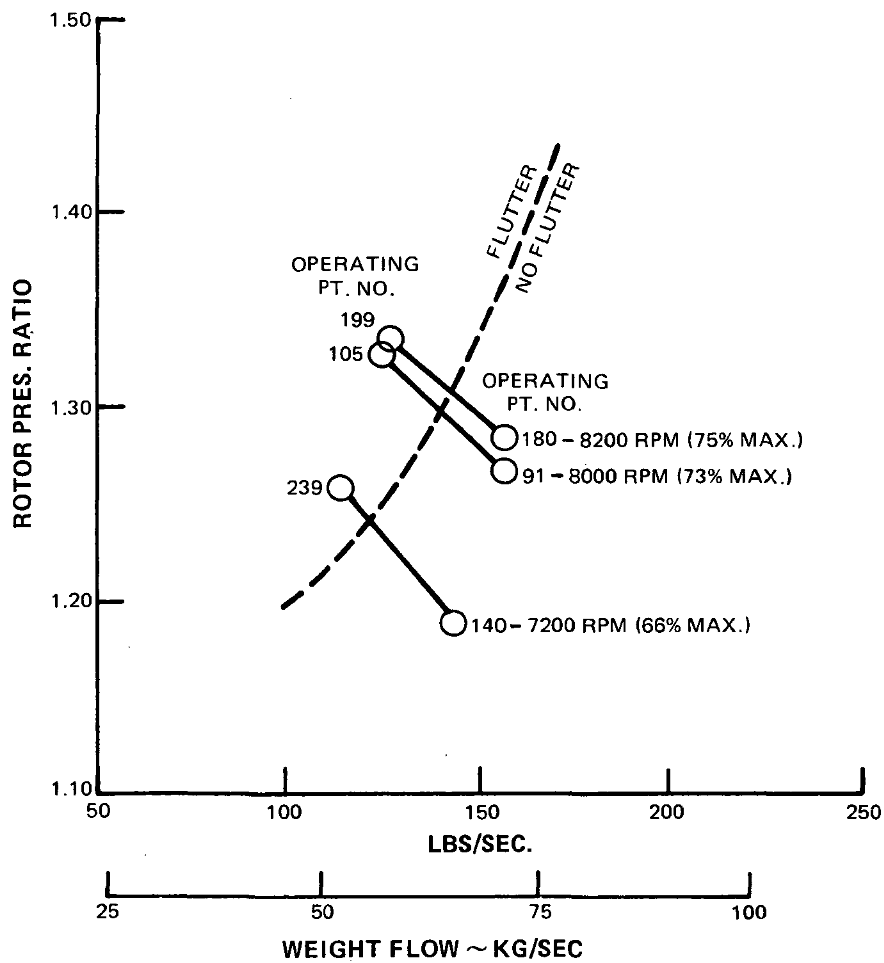

Figure 3-9 *TS22 Fan Performance Map*

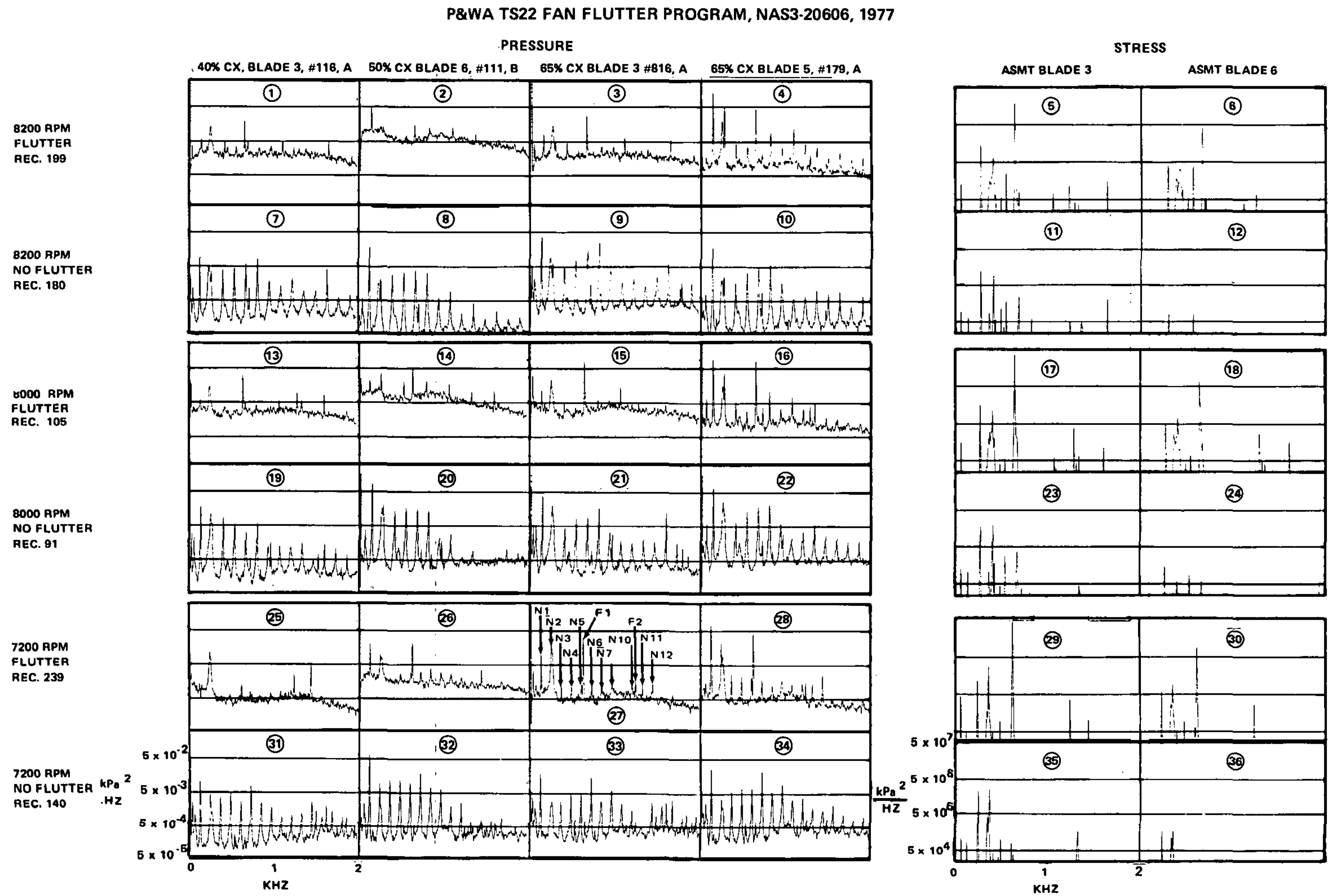

NOTES: ASMT = ABOVE SHROUD, MAXIMUM THICKNESS, CX SIDE, RADIUS = 12", 55% SPAN, 75% TIP RADIUS
ALL PRESSURE TRANSDUCERS AT RADIUS = 14.5", 83% SPAN, 90% TIP RADIUS. LETTER A OR B INDICATES MOUNTING CONFIGURATION

Figure 3-10 Blade-Mounted Pressure Transducer and Strain Gage Power Spectra

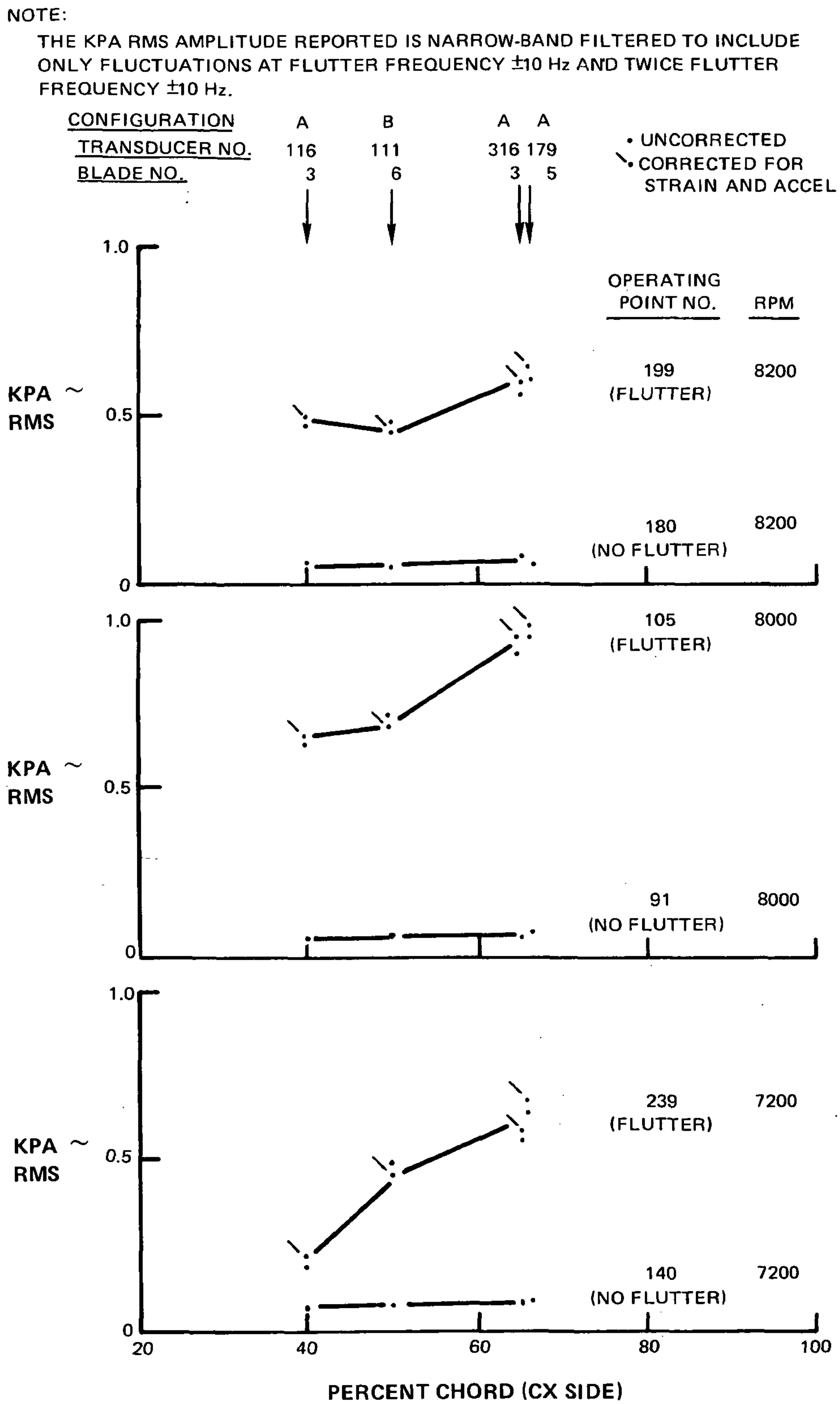

Figure 3-11 Surface Pressure Fluctuation Amplitude (KPA rms) Versus Chordwise Position on Convex Side of TS22 Fan Blade

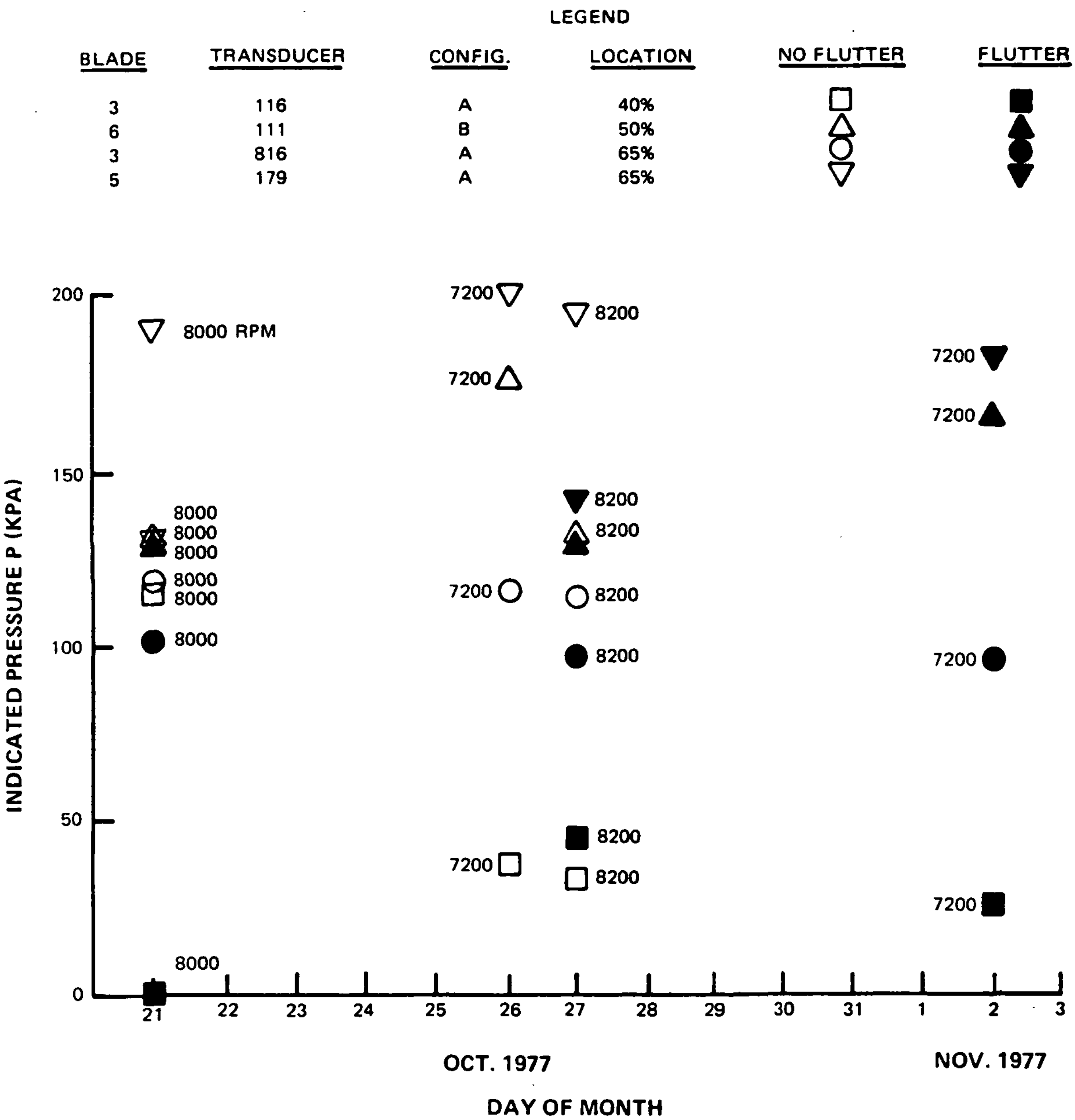

Figure 3-12 *Steady State Pressure Measurements: Blade-Mounted Pressure Transducers on TS22 Fan*

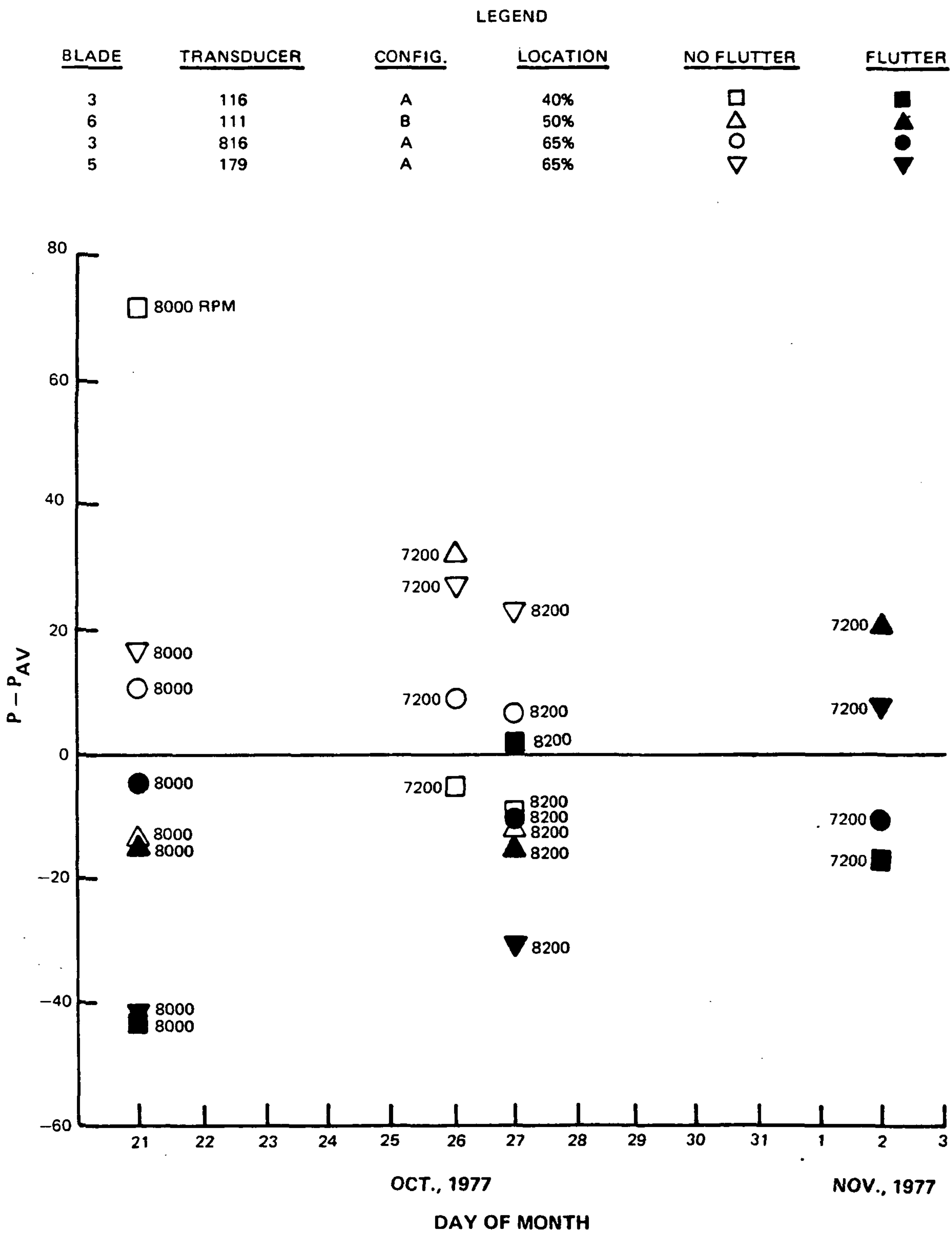

Figure 3-13 *Zero-Adjusted Steady State Pressure Measurements: Blade-Mounted Pressure Transducers on TS22 Fan*

TABLE 3-I

SUMMARY OF SENSITIVITY DATA (MV/kPa)

Tensile Tests	Fe Low	Fe High	Ti Low	Ti High
Config. E, Temp. 1, Strain 1	0.41421	0.40274	0.40819	0.39855
1 2	0.41624	0.40315	0.41840	0.39443
2 1	0.40386	0.37878	0.40867	0.39778
2 2	0.41009	0.37759	0.40725	0.39797
Config. B, Temp. 1, Strain 1	0.36331	0.37034	0.36510	0.37560
1 2	0.36612	0.37089	0.36310	0.37153
2 1	0.36032	0.36626	0.35479	0.35659
2 2	0.35868	0.36420	0.35806	0.35414
Config. C, Temp. 1, Strain 2	0.38740	0.37349	0.41500	0.42155
2 1	0.41414	0.40294	0.44802	0.45514
2 2	0.40615	0.40223	0.44853	0.45691

Temp. 1 = 21°C Strain 1 = 0
Temp. 2 = 150°C Strain 2 = 1000 $\mu\epsilon$

Bending Tests	Fe Low	Fe High	Ti Low	Ti High
Config. E, Strain 1	0.41391	0.40362	0.41471	0.40532
2	0.41044	0.40641	0.42271	0.40422
Config. B, Strain 1	0.36286	0.36728	0.37020	0.36286
2	0.36362	0.36753	0.36831	0.36347
Config. C, Strain 1	0.38297	0.37597	0.42567	0.42532
2	0.38307	0.37226	0.42742	0.42758

Strain 1 = 0 Strain 2 (Fe) = 1170 $\mu\epsilon$ Strain 2 (Ti) = 1680 $\mu\epsilon$

Vibration Tests	Fe Low	Fe High	Ti Low	Ti High
Config. E, Vib. 1			0.39521	0.40334
2			0.40120	0.40277
Config. B, Vib. 1			0.35708	0.36595
2			0.35678	0.36502
Config. C, Vib. 1	0.38041	0.36918	0.42663	0.42525
2	0.38022	0.36922	0.42541	0.42586

Vib. 1 = 0
Vib. 2: See Figure 2-36

In All Tests: Low = 50 to 180 kPa
High = 180 t 310 kPa

TABLE 3-II

CHANGE IN SENSITIVITY DUE TO STRAIN

$$\Delta_\epsilon (\%) = \frac{(mV/kPa)_{strain 2} - (mV/kPa)_{strain 1}}{(mV/kPa)_{strain 1}} \times 100$$

Mode	Config.	Material	Temp.	Pressure	Δ_ϵ (%)	Avg.	Std. Dev.	$\mu\epsilon$ Strain 2-Strain 1
Tensile	E	Fe	1	L	0.40			
				H	0.10	0.432	0.69	1000
			2	L	0.54			
				H	−0.31			
		Ti	1	L	2.50			
				H	−1.03	0.290	1.33	1000
			2	L	−0.35			
				H	0.04			
	B	Fe	1	L	0.77			
				H	0.15	−0.022	0.53	1000
			2	L	−0.45			
				H	−0.56			
		Ti	1	L	−0.55			
				H	−1.08	−0.350	0.76	1000
			2	L	0.92			
				H	−0.69			
	C	Fe	1	L	−0.01			
				H	−0.58	−0.735	0.85	1000
			2	L	−2.17			
				H	−0.18			
		Ti	1	L	−1.90			
				H	0.10	−0.325	0.92	1000
			2	L	0.11			
				H	0.39			
Bending	E	Fe	1	L	−0.84	−0.075	0.76	1170
				H	0.69			
		Ti	1	L	1.93	0.830	1.10	1680
				H	−0.27			
	B	Fe	1	L	0.21	0.135	0.08	1170
				H	0.06			
		Ti	1	L	−0.51	−0.170	0.34	1680
				H	0.17			
	C	Fe	1	L	0.03	−0.480	0.51	1170
				H	−0.99			
		Ti	1	L	0.41	0.470	0.06	1680
				H	0.53			
Vibration	E	Fe	1	L				
				H				< 100
		Ti	1	L	1.52	0.690	0.83	< 100
				H	−0.14			
	B	Fe	1	L				
				H				< 100
		Ti	1	L	−0.08	−0.165	0.08	< 100
				H	−0.25			
	C	Fe	1	L	−0.05	−0.020	0.03	< 100
				H	0.01			
		Ti	1	L	−0.28	−0.070	0.14	< 100
				H	0.14			

Grand Avg.	Std. Dev.
0.03	0.42

Levels of Temperature, Pressure and Strain are the same as those listed in Table 3-I. "Strain 1" is zero in every case.

TABLE 3-III

CHANGE IN SENSITIVITY DUE TO TEMPERATURE

$$\Delta_T\ (\%) = \frac{(\mathrm{mV/kPa})_{\mathrm{temp}\ 2} - (\mathrm{mV/kPa})_{\mathrm{temp}\ 1}}{(\mathrm{mV/kPa})_{\mathrm{temp}\ 1}} \times 100$$

Mode	Config.	Material	Pressure	Strain	Δ_T (%)	Avg.	Std Dev.
			L	1	−2.59		
		Fe		2	−1.48	−4.09	2.10
			H	1	−5.95		
	E			2	−6.34		
			L	1	0.12		
		Ti		2	−2.66	−0.46	1.33
			H	1	−0.19		
				2	0.90		
			L	1	−0.82		
		Fe		2	−2.03	−1.44	0.49
			H	1	−1.10		
Tensile	B			2	−1.80		
			L	1	−2.82		
		Ti		2	−1.39	−3.49	1.48
			H	1	−5.06		
				2	−4.68		
			L	1	7.15		
		Fe		2	4.84	6.74	1.11
			H	1	7.26		
	C			2	7.70		
			L	1	5.91		
		Ti		2	8.08	7.62	0.99
			H	1	8.08		
				2	8.39		

Levels of Temperature, Pressure and Strain are the same as those listed in Table 3-I. "Strain 1" is zero in every case.

TABLE 3-IVA

CHANGE IN SENSITIVITY DUE TO PRESSURE

$$\Delta_p(\%) = \Delta_p(\%) = \frac{(mV/kPa)_H - (mV/kPa)_L}{(mV/kPa)_L} \times 100$$

Mode	Config.	Material	Temp.	Strain	Δ_p (%)	Avg.	Std. Dev.
			1	1	−2.86		
		Fe		2	−3.15	−5.04	2.12
			2	1	−6.21		
	E			2	−7.92		
			1	1	−2.36		
		Ti		2	−5.73	−3.26	1.43
			2	1	−2.66		
				2	−2.88		
			1	1	1.94		
		Fe		2	1.30	1.61	0.23
			2	1	1.65		
Tensile	B			2	1.54		
			1	1	2.88		
		Ti		2	2.32	1.16	1.56
			2	1	0.51		
				2	−1.09		
			1	1	−3.04		
		Fe		2	−3.59	−2.63	1.00
			2	1	−2.94		
	C			2	−0.96		
			1	1	−0.45		
		Ti		2	1.58	1.14	0.93
			2	1	1.59		
				2	1.86		
		Fe	1	1	−2.48	−1.73	0.75
	E		1	2	−0.98		
		Ti	1	1	−2.26	−3.32	1.06
			1	2	−4.37		
		Fe	1	1	1.22	1.14	0.07
Bending	B		1	2	1.07		
		Ti	1	1	−1.98	−1.65	0.33
			1	2	−1.32		
		Fe	1	1	−1.83	−2.32	0.50
	C		1	2	−2.82		
		Ti	1	1	−0.08	−0.02	0.05
			1	2	0.03		
		Fe	1	1			
	E		1	2			
		Ti	1	1	2.06	1.22	0.84
			1	2	0.39		
		Fe	1	1			
			1	2			
Vibration	B	Ti	1	1	2.48	2.40	0.09
			1	2	2.31		
		Fe	1	1	−2.95	−2.92	0.03
	C		1	2	−2.89		
		Ti	1	1	−0.32	−0.11	0.21
			1	2	0.10		

Levels of Temperature, Pressure and Strain are the same as those listed in Table 3-I. "Strain 1" is zero in every case.

TABLE 3-IVB

CHANGE IN SENSITIVITY DUE TO PRESSURE

$$\Delta_P(\%) = \frac{(mV/kPa)_H - (mV/kPa)_L}{(mV/kPa)_L} \times 100$$

Config.	Material	ΔP (%) Grand average all data	Std. Dev.
E	Fe	–3.93	2.37
	Ti	–2.15	2.20
B	Fe	1.45	0.29
	Ti	0.76	1.72
C	Fe	–2.63	0.78
	Ti	0.54	0.90

TABLE 3-V

ZERO SHIFT DUE TO BENDING STRAIN (Pa/$\mu\epsilon$)*

Config.	21°C					150°C				
	Δ mV	mV/kPa	Δ kPa	Δ ($\mu\epsilon$)	Pa/$\mu\epsilon$	Δ mV	mV/kPa	Δ kPa	Δ ($\mu\epsilon$)	Pa/$\mu\epsilon$
C, Fe	−1.20	0.387	−3.10	1170	−2.65	−0.27	0.415	0.65	1170	−0.56
C, T1	−0.98	0.423	−2.32	1680	−1.38	−0.14	0.448	0.31	1680	−0.18
B, Fe	−0.54	0.362	−1.49	1170	−1.27	−0.36	0.360	1.00	1170	−0.85
B, Ti	−0.71	0.365	−1.94	1680	−1.15	−0.34	0.355	0.96	1680	−0.57
E, Fe	−0.09	0.400	−0.23	1170	−0.20					
E, Ti	−0.25	0.397	−0.63	1680	−0.38					
$A_{.125}$, H	−0.10	0.234	−0.43	1000	−0.43					
$A_{.025}$, H	−0.12	0.234	−0.51	1000	−0.51					
A_0, H	−2.00	0.234	−8.55	1000	−8.55					

* The strain reported is tensile fiber strain in an unmachined specimen on the same side of the blade as the transducer diaphragm. The numerical subscript (0, 0.025, 0.125) is the thickness of the RTV pad under the transducer in mm

F_e = Steel
T_i = Titanium
H = Hastelloy X

TABLE 3-VI

EFFECT OF CENTRIPETAL ACCELERATION ON SENSITIVITY SHIFT AND ZERO SHIFT

Accel. KG	27.5	27.5	27.5	55	75	27.5	27.5	55	75	27.5	55
Temp. °C	24	46	32	31	35	21	21	21	21	82	82
Run No.	4	4	4	5	6	8	8	9	10	11	12
Ser. No.	8	8	8	8	8	9	3	9	9	9	9
Configuration	B, 0°	B, 0°	B, 0°	B, 0°	B, 0°	A, 0°	A, 7°	A, 0°	A, 0°	A, 0°	A, 0°
Sens. Shift (%) 7 - 150 kPa	5.3	−1.9	7.7	5.7	1.3	1.0	2.4	2.8	6.1	−0.4	−0.1
Sens. Shift (%) 150 - 310 kPa	4.2	1.8	3.4	9.0	N.A.	−5.6	−4.9	−6.1	0.9	2.7	0.3
Zero Shift (kPa) 7 kPa	1.24	1.58	−2.21	1.86	−0.62	2.83	−0.96	4.34	2.83	2.48	7.45
Zero Shift (kPa) 150 kPa	8.69	−0.96	9.03	9.65	17.72	4.07	2.48	8.76	11.17	1.86	7.17
Zero Shift (kPa) 310 kPa	15.51	1.58	14.00	16.75	N.A.	−4.34	−4.96	−1.24	12.41	5.93	7.79

Sensitivity Best Straight Line: $100\ \Delta\phi/\phi = (0.306)\ (KG) + (0.387)$
Zero Shift Best Straight Line: $\Delta P = (0.1214)\ (KG) - (0.041)$ kPA

TABLE 3-VII

TRANSDUCER SENSITIVITY HISTORY

Ser. No.	Test Item	Sensitivity (mV/kPa) 21°C Unmounted *	150°C Unmounted *	21°C Mounted *	After Tensile	After Bending	After All Tests	Percent Change Due to Mounting	Percent Change During Test Final - Initial
				Static Tests					
98-7-62	B, Ti	0.347	0.348	0.360	0.360	0.370	0.357	+3.7	−0.8%
98-7-68	B, Fe	0.352	0.351	0.364	0.362	0.364	0.358	+3.4	−1.6%
98-7-65	C, Ti	0.415	0.420	0.431	0.434	0.426	0.420	+3.9	−2.5%
98-7-58	C, Fe	0.378	0.384	0.374	0.399	0.383	0.371	−1.1	−0.8%
28-18-32	E, Ti	0.390	≠	0.405	0.412	0.412	0.397	+3.8	−2.0%
28-18-34	E, Fe	0.394	0.399	0.412	0.410	0.418	0.400	+4.6	−2.9%
				Spin Tests, First Build					
99-4-9	A, 0°	0.380	N.A.	0.376			0.386	−1.1	+2.6%
99-4-8	B, 0°	0.316	N.A.	0.307			0.304	−2.8	−1.0%
99-4-15	B, 7°	0.319	0.323	0.326			0.348	+2.2	+6.7%
				Spin Tests, Second Build					
99-4-9	A, 0°	0.380	N.A.	0.386			0.463	+1.6	+19.9%
99-4-15	B, 7°	0.319	0.323	0.348			0.357	+9.1	+2.6%
99-4-3	C, 7°	0.328	N.A.	0.277			0.290	−15.5	+4.7%

Notes: * 11-point calibrations by P&WA Standards Group; others are 5-point calibrations by Development Group.

≠ Excessive drift at 150°C; did not complete the calibration.

N.A. calibration omitted.

TABLE 3-VIII

CHANGE IN SENSITIVITY [Δ (mV/kPa)/(mV/kPa)] DUE TO CHANGE IN TEMP., PRES., STRAIN, ACCELERATION, AND TIME

	Mfr. Spec. Not Mounted	Measured, NAS3-20296						
		Config. B		Config. E		Config. C		
		Ti	Fe	Ti	Fe	Ti	Fe	A
%/100°C, 21°C to 150°C, Comp.	±4.5	−3.5 ± 1.5	−1.4 ± 1.0	−0.5 ± 1.9	−4.1 ± 2.1	7.6 ± 1.0	6.7 ± 1.1	–
%/100°C, 21°C to 150°C, Uncomp.	±10.8	–	–	–	–	–	–	–
% Nonlinear, 50-180 to 180-310 kPa	±1.0	0.8 ± 1.7	1.4 ± 0.3	−2.2 ± 2.2	−3.9 ± 2.4	0.5 ± 0.9	−2.6 ± 0.8	–
%/1000 $\mu\epsilon$, 0 to 1000 $\mu\epsilon$	–	0 ± 0.5	0 ± 0.5	0 ± 0.5	0 ± 0.5	0 ± 0.5	0 ± 0.5	–
Parallel acceleration %/1000 G, 0 to 75,000 G	–	.04 ± 0.4	–	–	–	–	–	.04 ± .04
Acceleration at 7° %/1000 G, 0 to 75,000 G	–	–	–	–	–	–	–	.04 ± .04
Normal acceleration %/1000 G, 0 to 1000 G	–	0 ± 0.6	0 ± 0.6	0 ± 0.6	0 ± 0.6	0 ±0.6	0 ± 0.6	–
% Change in 8 mos.	–	± 3.0	± 3.0	± 3.0	± 3.0	± 3.0	± 3.0	± 3.0

TABLE 3-IX

ZERO SHIFT DUE TO TEMPERATURE, STRAIN, ACCELERATION, AND TIME

	Mfr. Spec. Not Mounted	Measured, NAS3-20296						
		Config. B		Config. E		Config. C		A
		Ti	Fe	Ti	Fe	Ti	Fe	
kPa/100°C, 21°C to 150°C	5.2	±14	±14	±14	±14	±14	±14	±14
Pa/$\mu\epsilon$ Bending, 21°C	–	−1.2 ± .1	−1.3 ± .1	−.4 ± .1	−.2 ± .1	−1.4 ± .1	−2.6 ± .1	−.5 ± .1
Pa/$\mu\epsilon$ Bending, 150°C	–	−.6 ± .1	−.8 ± .1	–	–	−.2 ± .1	−.6 ± .1	–
Parallel Acceleration Pa/G, 0 to 75000 G	0.14	.11 ± .04	–	–	–	–	–	.10 ± .04
Acceleration at 7° Pa/G, 0 to 27500 G	0.16	–	–	–	–	–	–	.10 ± .04
Normal Acceleration Pa/G, 0 to 500 G	0.70	.16 ± .02	–	.32 ± .02	–	.34 ± .02	–	–
kPA Drift in 8 Months	–	±14	±14	±14	±14	±14	±14	±14

TABLE 3-X

JT15D FAN BMT ERROR ESTIMATES

	Environment	
	Static	Oscillatory (20 Hz - 20 kHz)
Temperature	21 to 77°C	± 0°C
Pressure	100 to 140 kPa	± 7 kPa
Strain	0 to 1000 $\mu\epsilon$	± 100 $\mu\epsilon$
Parallel Acceleration	0 to 74,000 G	± 10 G
Normal Acceleration	0 to 8000 G	± 100 G

Error Analysis

	Configuration B on Ti Blade			Configuration A on Ti Blade		
	Sensitivity Uncorrected Max %	Sensitivity Corrected %	Noise kPa	Sensitivity Uncorrected %	Sensitivity Corrected %	Noise kPa
Calibration (20 - 7500 Hz)	± 5	± 5	–	± 5	± 5	–
Calibration (20 - 20,000 Hz)	±15	±15	–	±15	±15	–
Pressure Nonlinear	± 0.2	± 0.2	–	± 0.2	± 0.2	–
Temperature	± 2.0	± 0.8	–	± 3.3	± 0.5	–
Strain	± 0.5	± 0.5	±0.12	± 0.5	± 0.5	±0.05
Parallel Acceleration	± 6.0	± 3.0	±0.001	± 6.0	± 3.0	±0.001
Normal Acceleration	–	–	±.026	–	–	±.054
Σ 20 - 7500 Hz	± 8.08	± 5.91	±.123	± 8.50	± 5.88	±.074
Σ 20 - 20,000 Hz	±16.28	±15.34	±.123	±16.50	±15.31	±.074

SECTION 4.0

CONCLUSIONS AND RECOMMENDATIONS

1. The capability for measuring the oscillatory component of the pressure on the surface of compressor and fan blades during engine operation was established, using blade-mounted transducers, for oscillatory pressure amplitudes of 1 kPa or more, absolute pressures to 310 kPa, temperatures to 150°C, static strains to $2000\mu\epsilon$, oscillatory strains to $\pm 1000\mu\epsilon$, parallel accelerations to at least 90,000 G, and oscillatory normal accelerations to at least 650 G. The blade-mounted transducers tested are the miniature semiconductor strain gage type known to provide good frequency response to at least 30 kHz, with a resonance frequency of 125 kHz. Sensing area is 1 mm in diameter.

2. Accuracy of measurement of the oscillatory component of pressure is degraded typically by about ±3%, due to the rotating blade environment. Noise signals due to oscillatory acceleration (vibration) and oscillatory strains are generally below ±0.1 kPa (±0.015 psi).

3. Selection of one mounting configuration over another is therefore based on the significant differences in surface buildup, and the significant differences in zero shift due to strain among the three presently developed configurations (A, B, C).

4. Configuration A (thin transducer mounted on a 0.05 mm layer of adhesive on the unmachined surface of the measured side of the blade) provides the best strain isolation of A, B, or C, but requires a surface buildup of RTV rubber on the measured surface of 0.38 mm. Strain effect is -0.5 $Pa/\mu\epsilon$. This configuration is the best for flutter studies where oscillatory strains are large.

5. Configuration B (thin transducer mounted upside down on the non-measured surface, facing a 1 mm diameter hole through the blade to the measured surface) provides moderate strain isolation, requires no buildup on the measured surface, but requires 0.5 mm buildup on the non-measured surface. Strain effect is -1.2 $Pa/\mu\epsilon$.

6. Configuration C (same as A, except the mounting is in a 0.25 mm recess in the blade surface) provides moderate strain isolation. Surface buildup on the measured surface is only 0.13 mm. Measured strain effect is -1.4 $Pa/\mu\epsilon$ and would probably be reduced if the recess is carefully faired to minimize stress concentrations.

7. Configuration E, a fourth configuration not fully developed (special cylindrical transducer mounted entirely within the blade in a 2 mm diameter through hole, with leadwork on the unmeasured surface) provides excellent strain isolation and no buildup on the measured surface. Strain effect is -0.4 $Pa/\mu\epsilon$. This configuration was not spin tested. (See Item 11 for comment on development of the special cylindrical transducers.)

8. The average sensitivity changes due to mounting was 4.4%. An initial sensitivity calibration in the as-mounted condition on the non-rotating blade is therefore required, and a recheck of sensitivity on the non-rotating blade from time to time during an extended test program is recommended.

9. Error of measurement of the steady-state component of pressure is about ±14 kPa (±2 psi) for the blade-mounted transducers, due to random unpredictable zero-shifts with time and temperature. The accuracy cannot ordinarily be improved significantly by calibration before and after an engine test, because shifts of this order of magnitude can occur in a few hours. Maintaining the transducer and blade at an absolutely constant temperature (±2°C), for 24 hours reduces the drift rate to less than 2 Pa/hr, but unpredictable drifts of ±14 kPa may again occur as soon as the blade is exposed to a new environment in which there exist significant temperature gradients or temperature changes.

10. Durability of thin-shim-mounted transducer installations using techniques developed in this program is excellent. In the four installations subjected to static tests (to 310 kPa nitrogen pressure, 150°C, 1000 to 3000 $\mu\epsilon$ surface strain, ±500 to ±650 G vibration) and the four installations subjected to spin tests (to 310 kPa nitrogen pressure, 82°C, 1000$\mu\epsilon$ surface strain, 90,000 G parallel acceleration) there were no separations, failures, or unreasonable changes in transducer sensitivity. One other thin-shim-mounted transducer developed a pressure leak after installation and before spin tests began. Three other thin-shim-mounted transducers were tested for static strain effects in slightly modified installations (to ±1000 $\mu\epsilon$, 150°C) with no failures.

11. Durability of special cylindrical transducers designed for mounting inside a 2.5 mm thick blade was marginal, early in the program. These transducers were made to a P&WA specification requiring 2.0 mm diameter and 2.0 mm length. Two installations were eventually successfully subjected to static tests (to 310 kPa, 150°C, 2000 $\mu\epsilon$ strain, 650 G vibration), but several others were rejected because of gas leaks. None were spin tested because development was completed too late in the program. Further evaluation would be desirable because this type is least affected by strain and permits zero surface buildup on the measured surface and minimum buildup (leadwork only) on the non-measured surface.

12. Three of the configurations developed (A, B, C), all using thin-shim-mounted transducers, are entirely acceptable for the purpose intended. The fourth (E), using the special cylindrical transducer, is potentially the best of all, but is not yet fully developed.

13. Sensitivity changes due to strains in the blade surface are negligible for all four configurations (A, B, C, E).

14. Sensitivity changes due to temperature and pressure changes are small and documented for all four configurations (A, B, C, E).

15. Zero shift due to acceleration parallel with the transducer diaphragm is the same (small and documented) for all three presently developed configurations (A, B, C).

16. The effect on zero shift of a change in orientation of 7° in spin tests could not be detected, since it was smaller than the 5 kPa random scatter of the data.

17. The effect of changing the orientation of the acceleration component lying in the plane of the diaphragm was not determined. All transducers were oriented with the semiconductor strain gage bridge (on the diaphragm) oriented in the same way relative to the centripetal acceleration component in the plane of the diaphragm.

18. Zero shift due to acceleration perpendicular to the diaphragm was about 0.33 Pa/G for the transducers in the C and E configurations, as would be predicted from the known thickness and density of the diaphragm. Zero shift for one sample of the same type of transducer tested twice in the B configuration was only 0.22 Pa/G, a result which can not be explained on any theoretical basis. Additional samples should be tested before accepting this result for the B configuration.

19. Blade material has no important effect on the performance of blade-mounted transducers. The small corrections required for the effects of temperature, pressure, and acceleration on sensitivity are only slightly different for the two-blade materials tested (steel and titanium). The effect of strain on sensitivity is negligible for both materials. The small corrections required for the effects of accelerations on zero shift are the same for both materials. The effect of strain on zero-shift is the same for both materials. (An apparent difference in strain effect on zero shift for the two materials in the C configuration specimens tested was judged to be in fact attributable to large difference in the shape of the machined recess in the blade surface for the two specimens, and was therefore a configuration effect, not a material effect.)

20. A simplified thin-shim installation of configuration A, eliminating epoxy and using only RTV, proved as durable (in one spin test to 90,000 G, 82°C) as the more difficult installation techniques employing both RTV and epoxy.

21. Zero-shifts due to strain are reduced sharply at high temperature, and can be increased sharply by any machining performed in the vicinity of the transducer (holes or recesses for the purpose of reducing surface buildup and resulting aerodynamic disturbance).

22. Shelf life of blade-mounted transducer installation is at least six months. No change in strain isolation characteristics was found after aging for this period.

23. Zero shift due to change in incident light intensity is reduced to an acceptable level (<0.07 kPa from darkness to full sunlight) by the 1 μm metallic aluminum coating provided by the manufacturer as an option. Without the coating, zero shift may be a much as 3 kPa from shadow to sunlight. Even with the aluminum coating, care should be excerised to avoid exposing the transducer to strong oscillatory lighting such as that which would occur from light-chopping by upstream guide vanes in a sunlit engine inlet.

24. All laboratory tests were conducted without any erosion-protective overcoat on the transducer diaphragm (other than the 1 μm aluminum), but it is recommended that an overcoat of 0.025 mm of RTV rubber be applied in actual engine tests. Several engine test programs at P&WA and Boeing have proved the value of this coating in preventing foreign object damage. It is estimated that the 0.025 mm of RTV will in 0.53 Pa/G effect of acceleration normal to the transducer diaphragm, rather than the 0.33 Pa/G found for the uncoated transducers.

APPENDIX I

MOUNTING PROCEDURES

Pressure Transducer Installation: Configuration C or A,
Using Kulite LQL-5-080-25S Thin Transducer

Sign-off initial

1. Machine slot or recess in blade per drawing, approximately 0.64 cm (.25") wide by 1.75 cm (0.68") long by .025 cm (.010") deep, located as required[a] ______
2. Degrease the part by washing in Trichloroethylene, then acetone, then Freon, and then baking at 200C (400 F) for 1 hour. ______
3. Grit blast (120 grit aluminum oxide, Al_2O_3) all surfaces to be instrumented with leadwork. ______
4. Install trunk leadwork. Use an overcoat of GA-60 cement. Cure 3 hours at 135C (275 F). GA-60 is a product of Micro-Measurements Div. of Vishay, Romulus, Michigan. ______
5. Trim transducer shim to fit into slot with approximately .04 cm. (.015") space all around. ______
6. Mask instrumented areas and grit blast (120 grit Al_2O_3) area of pressure transducer installation. ______
7. Grit blast (50 micron Al_2O_3) back side of transducer shim very lightly and very carefully. ______
8. Apply RTV primer (DC1200) to the sensor half of the perforated shim, both surfaces. RTV is a product line of Dow Corning Corp., Midland, Michigan. ______
9. Apply RTV primer (DC1200) to the corresponding part of the slot surface. Allow 1 hour minimum cure at room temperature. ______
10. Apply a <u>thin</u>[b] coat of epoxy (Smooth-on MT-13, a product of Smooth-on Inc., Gillette, N.J.) to the bottom side of the perforated shim, lead wire end (the unprimed half). ______
11. Apply a <u>thin</u>[b] coat of MT-13 epoxy to the corresponding part of the blade surface. ______
12. Install transducer onto blade insuring that any excess epoxy squeezes out around shim side or toward leadwork end, <u>not</u> toward transducer end. ______
13. Tape and clamp under load of about 50 KN/M^2 (7 psi), again keeping epoxy away from transducer end. Check that the overall height of the installation is within the tolerance specified in the job order. Cure 16 hours at room temperature. ______
14. Splice trunk leadwork to transducer leadwork. Perform continuity check. ______

15. Apply a thin coat of epoxy (Smooth-on MT-13) to splices and any leadwork not already cemented to blade. Cure 16 hours at room temperature. ______

16. Lift diaphragm end of transducer shim slightly and apply RTV (DC 732) under shim and toward epoxy bond. RTV penetration can be gaged by observing rubber escaping around shim edges and through holes. ______

17. Remove the excess rubber and apply a clamp. The clamp should apply a pressure of 40 kN/m^2 (6 psi) against a 6 mm thick piece of foam rubber placed over the transducer and separated from it with a piece of 0.06 mm (2.5 mil) teflon tape. Cure in high humidity (in a plastic bag with a damp cloth) 16 hours at room temperature. ______

18. Perform transducer electrical continuity check. ______

19. Trim away rubber protruding above airfoil surface. ______

20. Blend transducer installation in slot area with a self-leveling RTV (DC 734) for as smooth an airfoil as possible. Cure same as DC 732. ______

21. Perform transducer electrical continuity check. ______

a. For **A** configuration, omit step 1.

b. Final epoxy installed thickness will be .0025 cm (.001") to .0075 cm (.003") after squeezing out excess and clamping in Step 13. Avoid excess amounts in Steps 10 and 11.

Pressure Transducer Installation: Configuration B, using Kulite LQL-5-080-25S Thin Transducer

Sign-off initial

1. Machine a 0.157 cm. (.062") hole through blade, located as required. The hole must be sharp-edged, free from burrs, and perpendicular ± 2° to the blade surface on which pressure is to be measured (not the surface on which the transducer is to be mounted). ______

2. Degrease the part by washing in Trichloroethylene, then acetone, then Freon, and then baking at 200C (400 F) for 1 hour.

3. Grit blast (120 grit aluminum oxide, Al_2O_3) all surfaces to be instrumented with leadwork. ______

4. Install trunk leadwork. Use an overcoat of GA-60 cement. Cure 3 hours at 135C (275 F). GA-60 is a product of Micro-Measurements Div. of Vishay, Romulus, Michigan. ______

5. Trim transducer shim so that leadwork and diaphragm area is approximately 0.64 cm. (0.25") wide and 1.6 cm. (0.62") long. Round corners to approximately 0.16 cm. (.062") radius ______

6. Mask instrumented areas and grit blast area of transducer installation with 50 micron aluminum oxide. ______

7. Apply RTV Primer (DC 1200) on the transducer side of blade in an area of 0.8 cm. (0.31") radius around hole. RTV is a product line of Dow Corning Corp., Midland, Michigan. Cure 1 hour at room temperature. ______

8. Mask a 0.5 cm (0.1875") dia. Circle centered on transducer diaphragm and very lightly grit blast shim and epoxy with 50 micron aluminum oxide grit. The mask as made from 0.09 mm (3.5 mil) Scotch 5480TFE tape with a smaller circle of 0.05 mm (2.5 mil) Scotch 8403 Mylar Tape stuck against its sticky side. The mask is placed over the diaphragm and pressed down using a piece of soft foam rubber. ______

9. Apply RTV primer (Dow Corning 1200) to diaphragm end of transducer shim (1/2 of shim). Cure 1 hour at room temperature. ______

10. Apply a 0.005 cm. (0.002") coat of RTV (DC 732) 0.25 cm. (0.100") dia. centered on hole on transducer side of blade. Allow to cure in high humidity (in a plastic bag with a damp cloth) 16 hours at room temperature. ______

11. Cut two 5-mil brass shims to fit at lead end of perforated shim. Grit blast brass shims with 50 micron aluminum oxide. ______

12. Cement brass shims in place on the blade with a thin coat of epoxy (Smooth-on MT-13 a product of Smooth-on Inc., Gillette, N.J.). Clamp and cure 16 hours at room temperature. ______

13. Clean brass shim area and grit blast with 50 micron aluminum oxide. ________

14. Apply a thin coat of epoxy (Smooth-on MT-13) to the pressure transducer side, leadwork end, of the perforated shim (approximately half the area) and also to the corresponding area on the blade. The epoxy will be cured in Step 17. ________

15. Apply a very thin coat of RTV (DC 732) to transducer diaphragm ring but not to diaphragm itself, and also to the corresponding area on the blade. ________

16. Install transducer on blade surface being careful to position transducer correctly so that minimal movement is required after contact is made. ________

17. Tape, clamp and cure in high humidity 16 hours. ________

18. Apply RTV (DC 732) into any areas that require it; apply small additional amounts to smooth airfoil. ________

19. Clamp and cure in high humidity 16 hours. ________

20. Splice trunk leadwork to transducer leadwork. Perform electrical continuity check. ________

21. Coat leadwork splices and any leadwork not already cemented to blade with a thin coat of epoxy (Smooth-on MT-13). Cure 16 hours at room temperature ________

Pressure Transducer Installation: Configuration "E",
Using Kulite LQL-14-080-25S Cylindrical Transducer

Sign-off initial

1. Machine a 0.208 cm (.082") dia. hole through blade; counter bore 0.28 cm. (0.109") dia X 0.15 cm (0.06") deep on pressure sensing side, located as required. ______

2. Degrease the part by washing in Trichlorethylene, then acetone, then Freon, and then baking at 200 C (400 F) for 1 hour. ______

3. Grit blast (120 grit aluminum oxide) all surfaces to be instrumented with leadwork. ______

4. Install trunk leadwork. Use an overcoat of GA-60 cement. Cure 3 hours at 135C (275 F). GA-60 is a product of Micro-Measurements Div. of Vishay, Romulus, Michigan. ______

5. Check transducer fit into mounting hole. Perform electrical countinuity check. ______

6. Mask surface around hole and grit blast wall of hole with 50 micron aluminum oxide. ______

7. Carefully mask leadwork exiting transducer. Don't leave any leadwork exposed. Slide transducer (pressure sensing end) into some snug-fitting tube (Tygon) just past diaphragm ring. Grit blast lightly with 50 micron aluminum oxide. Remove masking without touching grit blasted surface. leave tube on for easy handling and diaphragm protection. ______

8. Apply a very small bead of epoxy (smooth-on MT-13, a product of Smooth-on Inc., Gillette, N.J.) around leadwork end of transducer. Slide transducer carefully into counter bored end of hole leadwork first. Avoid touching counter bored area with epoxy. When transducer begins to enter the through hole continue insertion with a twisting motion (for uniform epoxy distribution) until diaphragm is in position and check for any epoxy bridges in counter bored area between transducer and wall, it may be necessary to remove transducer and clean the area with acetone if bridges exist. Inspect installation frequently during epoxy cure and correct any transducer position shifts. Cure 16 hours at room temperature. ______

9. Prime transducer O.D. and counter bore wall with RTV Primer (DC-1200) allow 1 hour minimum cure. RTV is a product line of Dow-Corning Corp. Midland, Michigan. ______

10. Fill void (counter bore) with RTV (DC-734); avoid RTV on transducer diaphragm. Clean off any excess with toluene, to achieve a smooth airfoil surface. Cure in high humidity (in plastic bag with a damp cloth) for 16 hours at room temperature.

11. Solder transducer leads to trunk wiring. ______

12. Perform electrical continuity check. ______

13. Coat leadwork splices and any leadwork not already cemented to blade with a thin coat of epoxy (smooth-on MT-13). Cure 16 hours at room temperature. ______

PRESSURE CAP INSTALLATION

1. Mask a 0.95 cm (0.375") diameter circle centered over transducer pressure sensing diaphragm.

2. Punch a 2.2 cm (0.875") diameter hole in a piece of tape and apply the tape to the blade such that two circles are concentric.

3. Very lightly grit blast annular area between tape with 50 micron aluminum oxide.

4. Resistance weld a length of 0.025 cm (0.010") diameter stainless steel wire to the face of the cap (facing blade) at a diameter of approximately 1.3 cm (0.520"). Tack all around. Leave gaps at leadwire areas.

5. Apply DC 1200 RTV primer to cap face and grit blasted surface of blade. Cure 1 hour at room temperature.

6. Apply PWA-404 Silicone Rubber Compound (supplied by H. S. Bancroft Corp. of Cherry Hill, NJ) to cap face and primed blade surface. Use enough compound to fill the 0.025 cm (0.010") gap but not so much that the compound squeezes over transducer area. Install cap onto blade.

7. Clamp and cure (16 hours at room temp., and 1 hour at 150°C (300°F)).

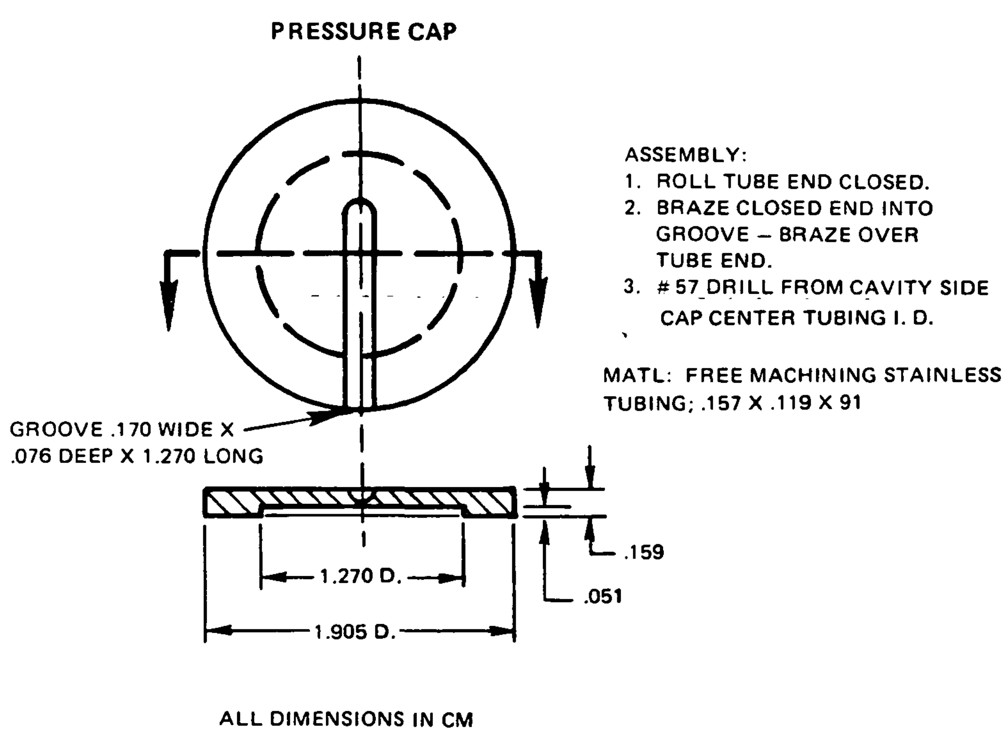

APPENDIX II
CALCULATION OF BENDING STRAIN AND TENSILE STRAIN IN UNMACHINED BLADE SPECIMENS

Calculation of Strain Due to Bending

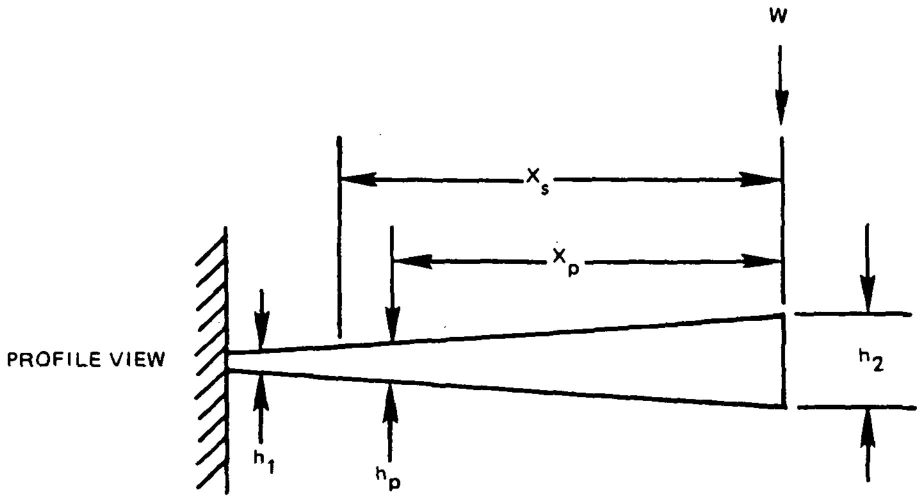

At point P, the fiber strain ϵ_p (cm/cm) is

$$\epsilon_p = \frac{Wxc}{IE} \tag{1}$$

where: W = load (N)

x = moment arm (cm.)

c = distance from neutral axis (cm.)

I = moment of inertia of cross-section (cm^4)

E = Young's modulus (N/cm^2)

and for a rectangular cross-section

$$I = b_p h_p^3 / 12 \tag{2}$$

where: b_p = width (cm) at point P

h_p = thickness (cm) at point P

For the titanium blade (Fig. 2-30)

$$W = 66.8 \text{ N}$$
$$h_p = .231 \text{ cm}$$
$$c_p = .116 \text{ cm}$$
$$x_p = 6.86 \text{ cm}$$
$$E = 12.6 \times 10^6 \text{ N/cm}^2$$

and because the cross-section is airfoil shaped rather than rectangular it seems reasonable to use an effective width b_p in equ. (2) equal to the cross-section area (0.562 cm^2) divided by the thickness (0.231 cm). Hence,

$$b_p = 2.43 \text{ cm}$$

then, $$I = (2.43)(.231)^3/12 = .00250 \text{ cm}^4$$

and $$\epsilon_p = \frac{(66.8)(6.86)(.116)}{(.0025)(12.6)(10^6)} = .001680 \text{ cm/cm}$$

or $$\epsilon_p = 1680 \text{ microstrain}$$

Measured strain at point S for the three configurations was:

B: 1318 $\mu\epsilon$
c: 1210 $\mu\epsilon$
E: 839 $\mu\epsilon$

These values are lower than the calculated value of strain at point P by about the amount expected due to stress reduction from the machining plus the reduced value of c at Point S due to the blade taper. Note that configuration B would indeed be expected to produce the least stress change (from the unmachined condition) and configuration E the most.

Conclusion: Use ϵ_p = 1680 microstrain as the nominal strain proved by the 66.8 N bending force used on titanium blades.

For the steel blade (Fig. 2-30)

$$W = 156 \text{ N}$$

$$h_p = 0.249 \text{ cm}$$

$$c_p = 0.124 \text{ cm}$$
$$x_p = 7.11 \text{ cm}$$
$$E = 19.0 \times 10^6 \text{ N/cm}^2$$
$$b_p = 4.83 \text{ cm}$$
$$I = (4.83)(0.249)^3/12 = .00621 \text{ cm}^4$$

and $$\epsilon_p = \frac{(156)(7.11)(.124)}{(.00621)(19)(10^6)} = .001170 \text{ cm/cm}$$

or $$\epsilon_p = 1170 \text{ microstrain}$$

Measured values at point S were

B: 1066 $\mu\epsilon$
c: 1155 $\mu\epsilon$
E: 1180 $\mu\epsilon$

It appears that on the stiffer, untapered steel specimen, the stress change from point P (on an unmachined blade) to point S (on a machined blade) is small.

Conclusion: Use $\epsilon_p = 1170$ microstrain as the nominal strain produced by the 156 N bending force on the steel blades.

Note: The effect of the twist in all blades and the camber in the titanium blades was ignored. The crudity of the model, in this respect and others, suggests an uncertainty of about ±20% in the calculated nominal values finally used. This amount of uncertainty has negligible effect on the conclusions reached in static and spin tests, since it was found that strain had no significant effect on transducer sensitivity and – for the recommended configuration – only modest effect on zero-shift.

Calculation of Tensile Strain

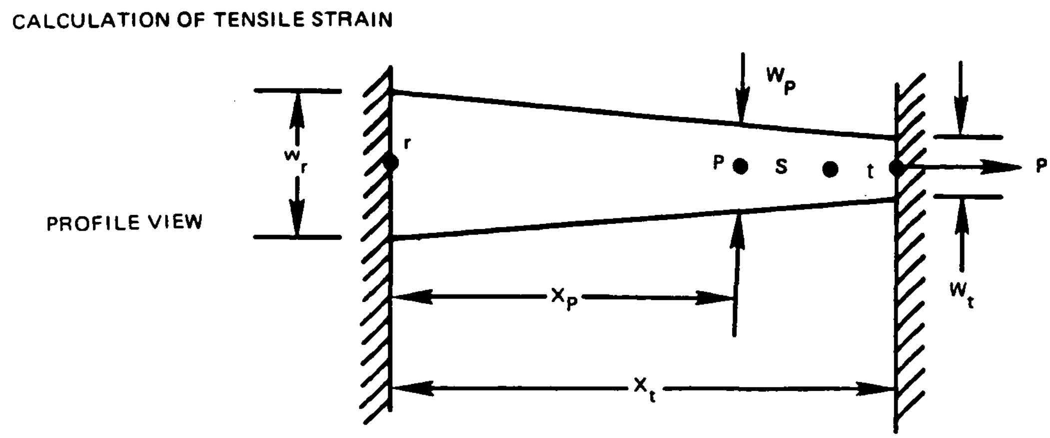

At point P the fiber strain ϵ_p is

$$\epsilon_p = \frac{P}{w_p h_p E}$$

where P is the tensile load (N), w_p is width (cm) and h_p (cm) is thickness at point P, and E (N/cm^2) is Young's Modulus. Note that the load is applied by means of three bolts at the tip (see Fig. 2-30), so that the effective loaded width w_t at the tip is approximately 2.13 cm on all specimens. The effective loaded width w_p, at the transducer location P is therefore about

$$w_p = w_r - (x_p/x_t)(w_r - w_t)$$

For the titanium blades (Fig. 2-30)

P	=	7120 N	(This value was selected during preliminary tests and used throughout the program. The detailed analysis was carried out later.)
E	=	12.6×10^6 N/cm^2	
h_p	=	0.231 cm	
w_r	=	4.67 cm	
w_t	=	2.13 cm	
x_p	=	6.10 cm	
x_t	=	7.75 cm	

so $w_p = 4.67 - (.787)(2.54) = 2.67$ cm

$$\text{and } \epsilon_p = \frac{7120}{(2.67)(.231)(12.6)(10^6)} = 0.000916$$

For the steel blade (Fig. 2-30)

P = 13350 N (This value was selected during preliminary tests and used throughout the program. The detailed analysis was carried out later.)

$E = 19 \times 10^6 \text{ N/cm}^2$

$h_p = 0.249$ cm

$w_r = 4.83$ cm

$w_t = 2.13$ cm

$x_p = 6.48$ cm

$x_t = 8.13$ cm

so $w_p = 4.83 - (0.797)(2.70) = 2.68$ cm

$$\text{and } \epsilon_p = \frac{13350}{(2.68)(.249)(19)(10^6)} = 0.001053$$

Conclusion: Use ϵ_p = 1000 microstrain as the nominal tensile strain produced at the transducer location by the 7120 N tensile load used in testing the titanium blades and by the 13350 N tensile load used in testing the steel blades.

Note: Actual measured tensile strains were found to be different on the front and back of the blade specimens, since some bending was introduced during tensile tests due to the complicated shapes of the blades. When the readings of strain gages on front and back of machined specimens were averaged, and compared with calculated tensile strain at the location of the gages, the measured strain was low by 4% at the root and 11% at the outboard strain gage location (point S). The latter disagreement is reasonable considering the stress reduction effects of the machining and the crudity of the model used for calculations in this area. Again, as in the bending strain tests, uncertainties in strain of this order of magnitude have no significant effect on the conclusions reached from the test program.

APPENDIX III

DATA LOG; STATIC TESTS AND SPIN TESTS

STATIC TEST DATA

NOTE 1: POWER SUPPLY VOLTAGE 15 ± .010 ON TEST XDCR. AND 10 ± .005 ON STD. XDCR.
NOTE 2: STD. XDCR. SENSITIVITY = .5934 mV/PSI, ZERO = .1490 mV

TEST POINT	DATE / TIME	TEST SPECIMEN	TYPE LOAD	LOAD (LB)	NOMINAL T (°F)	NOMINAL P (PSIA)	NOMINAL STRAIN	TEST XDCR. OUTPUT (mvDC)	STD XDCR. OUTPUT (mvDC)	TEMP. (°F) Loc. 1	TEMP. (°F) Loc. 2	MEASURED STRAINS (με) Loc. 1	Loc. 2	Loc. 3	Loc. 4	Loc. 5	Loc. 6
	5-13-77																
1 - A	1000	Fe - C	TENSILE	0	70	7	0	-23.35	4.30	76.2	76.3	0	0	0	N.A.	N.A.	N.A.
1 - B						26		+26.61	15.64	76.2	76.4						
1 - C						45		+75.14	26.95	76.2	76.4						
1 - D						26		+27.13	15.68	76.2	76.4						
1 - E	1010					7		-23.21	4.30	76.2	76.4						
2 - A	1100	Fe - C	TENSILE	0	300	7	0	-21.70	4.31	295.6	309.8	0	0	0	N.A.	N.A.	N.A.
2 - B						26		+30.90	15.68	297.9	311.6						
2 - C						45		+83.47	27.12	299.7	313.2						
2 - D						26		+31.02	15.67	300.7	313.8						
2 - E	1110					7		-23.72	3.81	294.9	306.8						
3 - A	1400	Fe - C	TENSILE	0	70	7	0	-24.14	4.29	80.2	80.6	0	0	0 -	N.A.	N.A.	N.A.
3 - B						26		+26.54	15.71	80.1	80.5						
3 - C						45		+75.33	27.04	80.1	80.4						
3 - D						26		+26.65	15.65	80.0	80.4						
3 - E	1410					7		-23.30	4.30	80.0	80.3						
4 - A	1430	Fe - C	TENSILE	3000	70	7	MAX	-22.97	4.35	79.4	79.7	+478	-85	+618	N.A.	N.A.	N.A.
4 - B						26		+26.97	15.67	79.4	79.6						
4 - C						45		+75.59	27.07	79.4	79.7						
4 - D						26		+27.04	15.65	79.4	79.6						
4 - E	1440					7		-23.05	4.32	79.4	79.6						
5 - A	1530	Fe - C	TENSILE	3000	300	7	MAX	-22.93	4.32	293.2	305.0	-280	+215	+380	N.A.	N.A.	N.A.
5 - B						26		+29.72	15.68	293.8	305.6						
5 - C						45		+82.11	27.09	294.2	306.0						
5 - D						26		+30.13	15.74	294.5	306.4						
5 - E	1535					7		-22.84	4.29	295.9	307.8						
6 - A	1600	Fe - C	TENSILE	0	300	7	0	-22.96	4.26	305.6	315.6	0	0	0	N.A.	N.A.	N.A.
6 - B						26		+30.47	15.75	306.9	316.9						
6 - C						45		+82.93	27.09	304.4	312.9						
6 - D						26		+30.65	15.66	307.4	317.3						
6 - E	1605					7		-21.51	4.33	301.0	309.0						
	5-16-77																
7 - A	0905	Fe - C	TENSILE	3000	70	7	MAX	-20.63	4.34	75.8	75.9	+255	-66	+437	N.A.	N.A.	N.A.
7 - B						26		+26.34	15.66	75.7	75.9						
7 - C						45		+75.40	27.11	75.6	75.7						
7 - D						26		+26.78	15.67	75.4	75.6						
7 - E	0920					7		-23.58	4.31	75.2	75.4	+220	-66	+422			
	5-19-77																
15 - A	1130	Ti - B	TENSILE	1600	70	7	MAX	-19.32	4.42	76.0	76.0	+792	-260	+592	N.A.	N.A.	N.A.
15 - B						26		+26.66	15.66			+796	-260	+604			
15 - C						45		+74.90	27.10								
15 - D						26		+27.04	15.67								
15 - E	1140					7		-19.65	4.30			+792	-262	+605			

Strain Gage and Thermocouple Locations
Same side of blade as diaphram

1. Spanwise S/G outboard (toward top) from transducer
2. Chordwise S/G beside transducer
3. Spanwise S/G at root

Opposite side of blade

4. Same as 1
5. Same as 2
6. Same as 3

STATIC TEST DATA

TEST POINT	DATE/ TIME	TEST SPECIMEN	TYPE LOAD	LOAD (LB)	NOMINAL T(°F)	NOMINAL P(PSIA)	NOMINAL STRAIN	TEST XDCR. OUTPUT DCMV.	STD. XDCR. OUTPUT DC.MV.	TEMP. (°F) LOC 1	TEMP. (°F) LOC. 2	MEASURED STRAINS (με) LOC. 1	LOC 2	LOC 3	LOC 4	LOC 5	LOC 6
	5-19-77																
16-A	1340	Ti-B	TENSILE	1600	300	7	MAX	-19.43	4.30	293.2	305.5	+794	-214	+192	+607	N.A.	N.A.
16-B		↓	↓	↓	↓	26	↓	26.90	15.50	↓	↓	↓	↓	↓	↓	↓	↓
16-C		↓	↓	↓	↓	45	↓	74.00	27.12	↓	↓	↓	↓	↓	↓	↓	↓
16-D		↓	↓	↓	↓	26	↓	28.23	15.74	↓	↓	↓	↓	↓	↓	↓	↓
16-E	1350	↓	↓	↓	↓	7	↓	-17.73	4.33	301.2	313.5	+784	-218	+188	+605	↓	↓
17-A	1355	Ti-B	TENSILE	0	300	7	0	-17.18	4.33	301.6	313.8	0	0	0	0	N.A.	N.A.
17-B		↓	↓	↓	↓	26	↓	28.93	15.70	↓	↓	↓	↓	↓	↓	↓	↓
17-C		↓	↓	↓	↓	45	↓	75.46	27.10	↓	↓	↓	↓	↓	↓	↓	↓
17-D		↓	↓	↓	↓	26	↓	29.46	15.74	↓	↓	↓	↓	↓	↓	↓	↓
17-E	1405	↓	↓	↓	↓	7	↓	-16.82	4.27	300.8	312.3	↓	↓	↓	↓	↓	↓
18-A	1540	Ti-B	TENSILE	0	80	7	0	-17.20	4.30	80.7	80.9	0	0	0	0	N.A.	N.A.
18-B		↓	↓	↓	↓	26	↓	30.06	15.73	↓	↓	↓	↓	↓	↓	↓	↓
18-C		↓	↓	↓	↓	45	↓	78.82	27.10	↓	↓	↓	↓	↓	↓	↓	↓
18-D		↓	↓	↓	↓	26	↓	30.16	15.72	↓	↓	↓	↓	↓	↓	↓	↓
18-E	1550	↓	↓	↓	↓	7	↓	-17.78	4.28	80.6	80.7	↓	↓	↓	↓	↓	↓
19-A	1555	Ti-B	TENSILE	1600	80	7	MAX	-17.83	4.29	80.5	80.6	+778	-226	+170	+611	N.A.	N.A.
19-B		↓	↓	↓	↓	26	↓	29.90	15.71	↓	↓	↓	↓	↓	↓	↓	↓
19-C		↓	↓	↓	↓	45	↓	78.71	27.13	↓	↓	↓	↓	↓	↓	↓	↓
19-D		↓	↓	↓	↓	26	↓	30.13	15.74	↓	↓	↓	↓	↓	↓	↓	↓
19-E	1600	↓	↓	↓	↓	7	↓	-17.79	4.28	80.6	80.7	+781	-224	+174	+611	↓	↓
	5-20-77																
20-A	0855	Fe-B	TENSILE	0	80	7	0	-22.84	4.30	76.0	76.0	76.0	0	0	N.A.	N.A.	N.A.
20-B		↓	↓	↓	↓	26	↓	24.06	15.68	↓	↓	↓	↓	↓	↓	↓	↓
20-C		↓	↓	↓	↓	45	↓	72.05	27.10	↓	↓	↓	↓	↓	↓	↓	↓
20-D		↓	↓	↓	↓	26	↓	24.25	15.70	↓	↓	↓	↓	↓	↓	↓	↓
20-E	0905	↓	↓	↓	↓	7	↓	-22.51	4.33	↓	↓	↓	↓	↓	↓	↓	↓
21-A	0955	Fe-B	TENSILE	0	300	7	0	-41.38	4.29	297.7	303.3	0	0	0	N.A.	N.A.	N.A.
21-B		↓	↓	↓	↓	26	↓	5.83	15.60	↓	↓	↓	↓	↓	↓	↓	↓
21-C		↓	↓	↓	↓	45	↓	54.60	27.10	↓	↓	↓	↓	↓	↓	↓	↓
21-D		↓	↓	↓	↓	26	↓	2.54	15.70	↓	↓	↓	↓	↓	↓	↓	↓
21-E	1005	↓	↓	↓	↓	7	↓	-38.54	4.30	302.7	306.7	↓	↓	↓	↓	↓	↓
22-A	1010	Fe-B	TENSILE	3000	300	7	MAX	-34.74	4.30	303.0	306.3	+2169	-960	+1182	N.A.	N.A.	N.A.
22-B		↓	↓	↓	↓	26	↓	12.87	15.70	↓	↓	↓	↓	↓	↓	↓	↓
22-C		↓	↓	↓	↓	45	↓	59.90	27.10	↓	↓	↓	↓	↓	↓	↓	↓
22-D		↓	↓	↓	↓	26	↓	12.69	15.66	↓	↓	↓	↓	↓	↓	↓	↓
22-E	1020	↓	↓	↓	↓	7	↓	-33.37	4.30	302.1	304.8	↓	↓	↓	↓	↓	↓
23-A	1050	Fe-B	TENSILE	3000	80	7	MAX	-22.02	4.30	81.6	81.7	+1420	-505	+1089	N.A.	N.A.	N.A.
23-B		↓	↓	↓	↓	26	↓	25.55	15.70	↓	↓	↓	↓	↓	↓	↓	↓
23-C		↓	↓	↓	↓	45	↓	73.79	27.10	↓	↓	↓	↓	↓	↓	↓	↓
23-D		↓	↓	↓	↓	26	↓	25.62	15.70	↓	↓	↓	↓	↓	↓	↓	↓
23-E	1055	↓	↓	↓	↓	7	↓	-21.98	4.30	80.8	81.2	↓	↓	↓	↓	↓	↓

ORIGINAL PAGE IS
OF POOR QUALITY

STATIC TEST DATA

TEST POINT	DATE/ TIME	TEST SPECIMEN	TYPE LOAD	LOAD (LB)	NOMINAL T(°F)	NOMINAL P(PSIA)	NOMINAL STRAIN	TEST XDCR OUTPUT DC.MV.	STD. XDCR OUTPUT DC.MV.	TEMP. (°F) LOC. 1	TEMP. (°F) LOC. 2	MEASURED STRAINS (με) LOC. 1	LOC. 2	LOC. 3	LOC. 4	LOC. 5	LOC. 6
	5-20-77																
24-A	1100	Fe-B	TENSILE	0	80	7	0	-22.58	4.30	80.9	81.2	0	0	0	N.A.	N.A.	N.A.
24-B						26		24.90	15.70								
24-C						45		73.34	21.10								
24-D						26		24.85	15.70								
24-E	1105					7		-22.52	4.30	80.1	80.5						
	5-23-77																
8-A	0855	Ti-C	TENSION	0	80	7	0	-3.24	4.30	79.4	79.4	0	0	0	N.A.	N.A.	N.A.
8-B						26		52.63	15.70								
8-C						45		108.53	27.10								
8-D						26		52.79	15.70								
8-E	1000					7		-3.17	4.30	79.4	79.3						
13-A	1330	Fe-C	TENSILE	0	80	7	0	-23.80	4.30	81.0	81.0	0	0	0	N.A.	N.A.	N.A.
13-B						26		25.70	15.70								
13-C						45		74.00	27.10								
13-D						26		25.97	15.70								
13-E	1335					7		-23.73	4.30								
14-A	1430	Fe-C	TENSILE	0	300	7	0	-49.43	4.30	302.9	302.0	0	0	0	N.A.	N.A.	N.A.
14-B						26		2.53	15.70								
14-C						45		55.60	27.14								
14-D						26		2.75	15.56								
14-E	1435					7		-47.86	4.27	303.3	302.4						
	5-24-77																
8-A	1100	Ti-C	TENSILE	0	80	7	0	-3.38	4.30	86.1	85.5	0	0	0	N.A.	N.A.	N.A.
8-B						26		51.41	15.70								
8-C						45		105.92	27.10								
8-D						26		51.62	15.70								
8-E	1105					7		-3.33	4.30	85.4	84.9						
9-A	1145	Ti-C	TENSILE	0	300	7	0	-11.74	4.30	293.0	312.2	0	0	0	N.A.	N.A.	N.A.
9-B						26		46.61	15.70								
9-C						45		106.05	27.10								
9-D						26		47.18	15.70								
9-E	1150					7		-10.83	4.30	295.4	314.0						
10-A	1200	Ti-C	TENSILE	1600	300	7	MAX	-2.82	4.30	297.0	313.6	+933	-365	+540	N.A.	N.A.	N.A.
10-B						26		55.40	15.70								
10-C						45		115.10	27.10								
10-D						26		56.03	15.70								
10-E	1205					7		-2.34	4.30	297.9	314.3	+938	-368	+544			
11-A	1337	Ti-C	TENSILE	1600	80	7	MAX	-8.84	4.28	86.4	86.4	+830	-318	+498	N.A.	N.A.	N.A.
11-B						26		44.20	15.70								
11-C						45		99.19	27.10								
11-D						26		44.60	15.70								
11-E	1342					7		-10.33	4.30	85.7	85.7	+840	-322	+499			

STATIC TEST DATA

TEST POINT	DATE / TIME	TEST SPECIMEN	TYPE LOAD	LOAD (LB)	NOMINAL T(°F)	NOMINAL P(PSIA)	NOMINAL STRAIN	TEST XDCR. OUTPUT DC MV	STD XDCR OUTPUT DC MV	TEMP.(°F) LOC 1	TEMP.(°F) LOC 2	MEASURED STRAINS (με) LOC 1	LOC 2	LOC 3	LOC 4	LOC 5	LOC 6
	5-24-77																
12-A	1345	Ti-C	TENSILE	0	80	7	0	-10.20	4.30	85.6	85.6	0	0	0	N.A.	N.A.	N.A.
12-B		↓	↓	↓	↓	26	↓	44.90	15.70	↓	↓	↓	↓	↓	↓	↓	↓
12-C		↓	↓	↓	↓	45	↓	99.98	27.10	↓	↓	↓	↓	↓	↓	↓	↓
12-D		↓	↓	↓	↓	26	↓	44.94	15.70	↓	↓	↓	↓	↓	↓	↓	↓
12-E	1350	↓	↓	↓	↓	7	↓	-10.14	4.30	85.6	85.6	↓	↓	↓	↓	↓	↓
35-A	1425	Ti-C	BEND	0	80	7	0	-7.95	4.30	87.0	87.0	0	0	0	N.A.	N.A.	N.A.
35-B		↓	↓	↓	↓	26	↓	47.40	15.70	↓	↓	↓	↓	↓	↓	↓	↓
35-C		↓	↓	↓	↓	45	↓	102.63	27.10	↓	↓	↓	↓	↓	↓	↓	↓
35-D		↓	↓	↓	↓	26	↓	47.38	15.70	↓	↓	↓	↓	↓	↓	↓	↓
35-E	1430	↓	↓	↓	↓	7	↓	-7.82	4.30	87.0	87.0	↓	↓	↓	↓	↓	↓
36-A	1435	Ti-C	BEND	15	80	7	MAX	-7.35	4.30	87.0	87.0	-1220	+226	-70	N.A.	N.A.	N.A.
36-B		↓	↓	↓	↓	26	↓	48.74	15.70	↓	↓	↓	↓	↓	↓	↓	↓
36-C		↓	↓	↓	↓	45	↓	105.07	27.10	↓	↓	↓	↓	↓	↓	↓	↓
36-D		↓	↓	↓	↓	26	↓	49.01	15.70	↓	↓	↓	↓	↓	↓	↓	↓
36-E	1440	↓	↓	↓	↓	7	↓	-7.75	4.30	87.0	87.0	↓	↓	↓	↓	↓	↓
37-A	1445	Ti-C	BEND	0	80	7	0	-8.25	4.30	87.0	87.0	0	0	0	N.A.	N.A.	N.A.
37-B		↓	↓	↓	↓	26	↓	46.94	15.70	↓	↓	↓	↓	↓	↓	↓	↓
37-C		↓	↓	↓	↓	45	↓	102.01	27.10	↓	↓	↓	↓	↓	↓	↓	↓
37-D		↓	↓	↓	↓	26	↓	46.98	15.70	↓	↓	↓	↓	↓	↓	↓	↓
37-E	1450	↓	↓	↓	↓	7	↓	-8.30	4.29	87.0	87.0	↓	↓	↓	↓	↓	↓
	5-25-77																
35R-A	0830	Ti-C	BEND	0	80	7	0	-3.64	4.30	78	78	0	0	0	N.A.	N.A.	N.A.
35R-B		↓	↓	↓	↓	26	↓	51.60	15.70	↓	↓	↓	↓	↓	↓	↓	↓
35R-C		↓	↓	↓	↓	45	↓	107.00	27.10	↓	↓	↓	↓	↓	↓	↓	↓
35R-D		↓	↓	↓	↓	26	↓	51.80	15.70	↓	↓	↓	↓	↓	↓	↓	↓
35R-E	0835	↓	↓	↓	↓	7	↓	-3.58	4.30	78	78	↓	↓	↓	↓	↓	↓
36R-A	0840	Ti-C	BEND	15	80	7	MAX	-4.13	4.30	78	78	+1355	-277	+73	N.A.	N.A.	N.A.
36R-B		↓	↓	↓	↓	26	↓	50.30	15.70	↓	↓	↓	↓	↓	↓	↓	↓
36R-C		↓	↓	↓	↓	45	↓	105.45	27.10	↓	↓	↓	↓	↓	↓	↓	↓
36R-D		↓	↓	↓	↓	26	↓	50.70	15.70	↓	↓	↓	↓	↓	↓	↓	↓
36R-E	0845	↓	↓	↓	↓	7	↓	-4.23	4.30	78	78	↓	↓	↓	↓	↓	↓
37R-A	0900	Ti-C	BEND	0	80	7	0	-3.60	4.30	78	78	0	0	0	N.A.	N.A.	N.A.
37R-B		↓	↓	↓	↓	26	↓	51.87	15.70	↓	↓	↓	↓	↓	↓	↓	↓
37R-C		↓	↓	↓	↓	45	↓	107.50	27.10	↓	↓	↓	↓	↓	↓	↓	↓
37R-D		↓	↓	↓	↓	26	↓	52.07	15.70	↓	↓	↓	↓	↓	↓	↓	↓
37R-E	0905	↓	↓	↓	↓	7	↓	-3.52	4.30	78	78	↓	↓	↓	↓	↓	↓
41-A	1010	Fe-C	BEND	0	80	7	0	-24.00	4.30	78.8	78.9	0	0	0	N.A.	N.A.	N.A.
41-B		↓	↓	↓	↓	26	↓	25.65	15.70	↓	↓	↓	↓	↓	↓	↓	↓
41-C		↓	↓	↓	↓	45	↓	74.70	27.10	↓	↓	↓	↓	↓	↓	↓	↓
41-D		↓	↓	↓	↓	26	↓	26.02	15.70	↓	↓	↓	↓	↓	↓	↓	↓
41-E	1015	↓	↓	↓	↓	7	↓	-23.88	4.30	79.0	79.1	↓	↓	↓	↓	↓	↓

STATIC TEST DATA

TEST POINT	DATE/ TIME	TEST SPECIMEN	TYPE LOAD	LOAD (LB)	T(°F)	NOMINAL P(PSIA)	NOMINAL STRAIN	TEST XDUCR OUTPUT DCMV	STD. XDUCR OUTPUT DCMV	TEMP. (°F) LOC.1	TEMP. (°F) LOC.2	MEASURED STRAINS (με) LOC 1	LOC 2	LOC 3	LOC 4	LOC 5	LOC 6
	5-25-77																
42-A	1020	Fe-C	BEND	35	80	7	MAX	-23.82	4.30	79.1	79.2	-1158	+0268	-0287	N.A.	N.A.	N.A.
42-B						26		26.15	15.70								
42-C						45		24.75	27.10								
42-D						26		26.40	15.70								
42-E	1025					7		-23.71	4.30	79.2	79.5	-1160	+0271	-0286			
42R-A	1030	Fe-C	BEND	35	80	7	-MAX	-24.23	4.30	79.6	79.7	+1162	-0190	+0241	N.A.	N.A.	N.A.
42R-B						26		25.16	15.70								
42R-C						45		23.66	27.10								
42R-D						26		25.58	15.70								
42R-E	1036					7		-24.10	4.30	79.9	79.9	+1162	-0191	+0260			
39-A	1120	Fe-B	BEND	35	80	7	MAX	-22.09	4.30	81.3	81.0	+1066	-0323	+0188	N.A.	N.A.	N.A.
39-B						26		25.10	15.70								
39-C						45		23.46	27.10								
39-D						26		25.70	15.70								
39-E	1127					7		-21.88	4.30	81.4	82.8	+1070	-0327	+0187			
40-A	1255	Fe-B	BEND	0	80	7	0	-22.35	4.30	82.9	82.8	0	0	0	N.A	N.A.	N.A.
40-B						26		21.87	15.70								
40-C						45		22.36	27.10								
40-D						26		21.78	15.70								
40-E	1300					7		-22.32	4.30	83.1	83.1						
39R-A	1302	Fe-B	BEND	35	80	7	-MAX	-22.76	4.30	83.4	83.1	-0989	+0223	-0194	N.A.	N.A.	N.A.
39R-B						26		24.30	15.70								
39R-C						45		21.85	27.10								
39R-D						26		24.33	15.70								
39R-E	1308					7		-22.78	4.30	83.4	83.4	-0998	+0215	-0193			
43-A	1330	Ti-B	BEND	15	80	7	MAX	-19.31	4.30	84.8	84.8	+1318	-0191	+0049	-0071	N.A	N.A.
43-B						26		28.59	15.70								
43-C						45		26.00	27.10								
43-D						26		28.57	15.70								
43-E	1340					7		-19.19	4.30	85.1	85.3	+1324	-0196	+0047	-0070		
44-A	1343	Ti-B	BEND	0	80	7	0	-19.88	4.30	85.2	85.3	0	0	0	0	N.A.	N.A.
44-B						26		28.27	15.70								
44-C						45		25.47	27.10								
44-D						26		28.35	15.70								
44-E	1347					7		-19.73	4.30	85.5	85.7						
13R-A	1353	Ti-B	BEND	15	80	7	-MAX	-20.38	4.30	85.5	85.6	-1656	+0570	-0055	+0076	N.A	N.A
13R-B						26		27.42	15.70								
13R-C						45		24.53	27.10								
13R-D						26		27.52	15.70								
13R-E	1359					7		-20.50	4.30	85.7	85.9	-1672	+0573	-0056	+0076		

STATIC TEST DATA

TEST POINT	DATE/ TIME	TEST SPECIMEN	TYPE LOAD	LOAD (LB)	NOMINAL T(°F)	P(PSIA)	STRAIN	TEST XDCR OUTPUT (DC MV)	STD XDCR OUTPUT (DC MV)	TEMP. (°F) LOC. 1	LOC 2	MEASURED STRAINS (μE) LOC 1	LOC 2	LOC 3	LOC 4	LOC 5	LOC 6
	5-25-77																
49-A	1410	Ti-C	BEND	0	80	7	0	-76.20	4.30	85.0	84.8	0	0	0	N.A.	N.A.	N.A.
49-B						26		-20.00	15.70								
49-C						45		+32.00	27.10								
49-D						26		-19.95	15.70								
49-E	1415					7		-76.25	4.30	85.5	85.5						
50-A	1500	Ti-C	BEND	15	80	7	MAX	-73.60	4.30	86.6	86.6	-1213	+0223	-0069	N.A.	N.A.	N.A.
50-B						26		-15.60	15.70								
50-C						45		+36.85	27.10								
50-D						26		-15.15	15.70								
50-E	1505					7		-73.62	4.30	86.7	86.7	-1216	+0226	-0069			
50R-A	1510	Ti-C	BEND	15	80	7	-MAX	-74.80	4.30	86.8	86.8	+1341	-0281	+0073	N.A.	N.A.	N.A.
50R-B						26		-18.20	15.70								
50R-C						45		+37.70	27.10								
50R-D						26		-18.10	15.70								
50R-E	1525					7		-74.55	4.30	87.0	87.0	+1349	-0281	+0073			
	5-26-77																
13-A	1115	Fe-C	TENSILE	0	80	7	0	-24.15	4.30	76.1	76.1	0	0	0	N.A.	N.A.	N.A.
13-B						26		+27.48	15.70								
13-C						45		+74.97	27.10								
13-D						26		+28.88	15.70								
13-E	1130					7		-24.10	4.30	76.1	76.2						
14-A	1340	Fe-C	TENSILE	0	300	7	0	-37.22	4.30	300.5	299.5	0	0	0	N.A.	N.A.	N.A.
14-B						26		+16.40	15.70								
14-C						45		+67.65	27.10								
14-D						26		+16.54	15.70								
14-E	1345					7		-36.97	4.30	300.7	299.8						
	6-8-77																
15-A	0910	Fe-E	BEND	35	80	7	MAX	-23.86	4.30	74.6	74.5	-1180	+0214	-0250	+1124	-0285	+0170
15-B						26		+29.57	15.70								
15-C						45		+82.62	27.10								
15-D						26		+29.66	15.70								
15-E	0925					7		-23.86	4.30	74.4	74.5	-1173	+0214	-0242	+1131	-0284	+0173
16-A	0930	Fe-E	BEND	0	80	7	0	-23.84	4.30	74.6	74.8	0	0	0	0	0	0
16-B						26		+29.99	15.70								
16-C						45		+82.46	27.10								
16-D						26		+30.01	15.70								
16-E	0935					7		-23.75	4.30	74.6	74.6						
15R-A	0940	Fe-E	BEND	-35	80	7	-MAX	-23.59	4.30	74.8	74.9	+1145	-0245	+0273	-1119	+0282	-0209
15R-B						26		+29.61	15.70								
15R-C						45		+82.78	27.10								
15R-D						26		+29.64	15.70								
15R-E	0945					7		-23.59	4.30	75.0	75.0	+1145	-0233	+0275	-1118	+0282	-0205

STATIC TEST DATA

TEST POINT	DATE/ TIME	TEST SPECIMEN	TYPE LOAD	LOAD (LB)	NOMINAL T(°F)	NOMINAL P(PSIA)	NOMINAL STRAIN	TEST XDCR OUTPUT DCMV	STD XDCR OUTPUT DCMV	TEMP.(°F) LOC 1	TEMP.(°F) LOC 2	MEASURED STRAINS (με) LOC 1	LOC 2	LOC 3	LOC 4	LOC 5	LOC 6
	6-8-77																
47-A	1015	Ti-E	BEND	0	80	7	0	-23.37	4.30	74.9	—	0000	0000	0000	0000	0000	0000
47-B						26		+30.45	15.70								
47-C						45		+83.23	27.10								
47-D						26		+30.65	15.70								
47-E	1020					7		-23.33	4.30	75.0							
48-A	1025	Ti-E	BEND	15	80	7	MAX	-23.84	4.30	75.1	—	-0839	+0182	-0086	+1221	-0210	+0048
48-B						26		+30.15	15.70								
48-C						45		-83.50	27.10								
48-D						26		+30.45	15.70								
48-E	1030					7		-23.35	4.30	74.4		-0838	+0182	-0082	+1222	-0208	+0048
48R-A	1035	Ti-E	BEND	-15	80	7	-MAX	-24.50	4.30	74.8	—	+1060	-0350	+0081	-1549	+0476	-0046
48R-B						26		+31.29	15.70								
48R-C						45		+83.32	27.10								
48R-D						26		+31.60	15.70								
48R-E	1042					7		-24.58	4.30	75.5		+1065	-0352	+0090	-1555	+0481	-0047
25-A	1455	Fe-E	TENSION	3000	80	7	MAX	-23.45	4.30	80	80	+0703	-0033	+0220	+0978	-0457	+0764
25-B						26		+31.39	15.70								
25-C						45		+83.48	27.10								
25-D						26		+31.38	15.70								
25-E	1505					7		-23.26	4.30	79	79	+0641	+0004	+0188	+1042	-0486	+0773
26-A	1536	Fe-E	TENSION	3000	300	7	MAX	-48.54	4.30	306	315	-0150	+0380	+0116	+1829	-0914	+0884
26-B						26		-7.37	15.70								
26-C						45		+57.36	27.10								
26-D						26		-9.20	15.70								
26-E	1543					7		-48.49	4.30	306	310	-0157	+0384	+0114	+1937	-0914	+0890
27-A	1545	Fe-E	TENSION	0	300	7	0	-38.33	4.30	306	310	-0040	+0041	-0014	+0047	-0021	+0008
27-B						26		+14.70	15.70								
27-C						45		+64.33	27.10								
27-D						26		+15.50	15.70								
27-E	1552					7		-36.45	4.30	306	310	-0042	+0042	-0018	+0050	-0021	+0002
28-A	1610	Fe-E	TENSION	0	80	7	0	-22.95	4.30	86	84	0000	0000	0000	0000	0000	0000
28-B						26		+31.09	15.70								
28-C						45		+83.40	27.10								
28-D						26		+31.02	15.70								
28-E						7		-22.71	4.30	80	80	-0008	-0002	0000	-0002	-0006	+0007
29-A	1615	Fe-E	TENSION	3000	80	7	MAX	-22.37	4.30	80	80	+0263	+0052	+0070	+1170	-0580	+0897
29-B						26		+31.27	15.70								
29-C						45		+84.05	27.10								
29-D						26		+31.43	15.70								
29-E	1625					7		-21.85	4.30	84	84	+0232	+0073	+0061	+1197	-0527	+0803

ORIGINAL PAGE IS
OF POOR QUALITY

STATIC TEST DATA

TEST POINT	DATE/ TIME	TEST SPECIMEN	TYPE LOAD	LOAD (LB)	NOMINAL T(°F)	NOMINAL P(PSIA)	NOMINAL STRAIN	TEST XDCR OUTPUT DCMV	STD XDCR OUTPUT DCMV	TEMP (°F) LOC 1	TEMP (°F) LOC 2	MEASURED STRAINS (με) LOC 1	LOC 2	LOC 3	LOC 4	LOC 5	LOC 6	TIP MILS
	6-9-77																	
30-A	0850	Ti-E	TENSION	0	80	7	0	-29.03	4.30	77	75	0000	0000	0000	0000	0000	0000	N.A
30-B						26		+24.35	15.70									
30-C						45		+76.09	27.10									
30-D						26		+24.80	15.76									
30-E	0900					7		-28.13	4.30	77	76	+0007	0000	0000	-0003	0000	-0005	
31-A	1005	Ti-E	TENSION	0	300	7	0	-21.99	4.30	300	319	0000	0000	0000	0000	0000	0000	N.A.
31-B						26		+31.30	15.70									
31-C						45		+83.35	27.10									
31-D						26		+32.00	15.70									
31-E	1010					7		-20.94	4.30	299	318	0000	0000	0000	0000	0000	0000	
32-A	1015	Ti-E	TENSION	1600	300	7	MAX	-20.15	4.30	302	319	+0620	-0214	+0608	+0794	-0234	+0351	N.A
32-B						26		+32.93	15.70									
32-C						45		+84.88	27.10									
32-D						26		+33.38	15.76									
32-E	1060					7		-19.40	4.30	302	320	+0615	-0213	+0610	+0789	-0232	+0338	
33-A	1330	Ti-E	TENSION	1600	80	7	MAX	-29.54	4.30	79	79	+0601	-0201	+0527	+0749	-0212	+0377	N.A
33-B						26		+24.65	15.70									
33-C						45		+76.13	27.10									
33-D						26		+25.08	15.70									
33-E	1337					7		-29.49	4.30	78	79	+0605	-0201	+0537	+0740	-0210	+0368	
34-A	1339	Ti-E	TENSION	0	80	7	0	-29.96	4.30	78	79	0000	0000	0000	0000	0000	0000	N.A.
34-B						26		+22.78	15.70									
34-C						45		+75.18	27.10									
34-D						26		+23.41	15.70									
34-E						7		-29.75	4.30			0000	0000	0000	0000	0000	0000	
	6-10-77																	
59-A	1115	Ti-C	VIBRATION	N.A.	70	7	MAX	-2.30	4.30	—	72.5	6	14	322	N.A.	N.A.	N.A	25
59-B						26		+53.36	15.70									
59-C						45		+109.10	27.10									
59-D						26		+53.26	15.70									
59-E	1130					7		-2.54	4.30									
60-A	1122	Ti-C	VIBRATION	N.A	70	7	0	-2.73	4.30	—	72.5	0	0	0	N.A.	N.A.	N.A.	0
60-B						26		+53.12	15.70									
60-C						45		+108.46	27.10									
60-D						26		+53.18	15.70									
60-E	1125					7		-2.75	4.30									
61-A	1325	Fe-C	VIBRATION	N.A.	70	7	MAX	-24.82	4.30	—	73.0	NEAR 0	NEAR 0	360	N.A.	N.A.	N.A.	25
61-B						26		+25.51	15.70									
61-C						45		+73.94	27.10									
61-D						26		+25.71	15.70									
61-E						7		-24.18	4.30									

STATIC TEST DATA

TEST POINT	DATE/ TIME	TEST SPECIMEN	TYPE LOAD	LOAD (LB)	NOMINAL T(°F)	NOMINAL P(PSIA)	NOMINAL STRAIN	TEST XDCR OUTPUT DCMV	STD XDCR OUTPUT DCMV	TEMP. (°F) LOC 1	TEMP. (°F) LOC 2	MEASURED STRAINS (με) LOC 1	MEASURED STRAINS (με) LOC 2	MEASURED STRAINS (με) LOC 3	MEASURED STRAINS (με) LOC 4	MEASURED STRAINS (με) LOC 5	MEASURED STRAINS (με) LOC 6	TIP ±MILS
	6-10-77																	
62-A	1345	Fe-C	VIBRATION	N.A.	70	7	0	-24.23	4.30	—	73.0	0	0	0	N.A.	N.A.	N.A.	0
62-B						26		+25.55	15.70									
62-C						45		+74.00	27.10									
62-D						26		+25.72	15.70									
62-E						7		-24.17	4.30									
63-A	1403	Ti-E	VIBRATION	N.A.	70	7	0	-32.07	4.30	—	73.0	0	0	0	0	0	0	0
63-B						26		+20.61	15.70									
63-C						45		+73.28	27.10									
63-D						26		+20.97	15.70									
63-E						7		-32.00	4.30									
64-A	1405	Ti-E	VIBRATION	N.A	70	7	MAX	-32.17	4.30	—	73.0	6	11	380	78	20	296	25
64-B						26		+20.40	15.70									
64-C						45		+73.34	27.10									
64-D						26		+20.75	15.70									
64-E						7		-31.90	4.30									
65-A	1425	Ti-B	VIBRATION	N.A.	70	7	0	-20.63	4.30	—	73.0	0	0	0	N.A.	N.A.	N.A.	0
65-B						26		+26.21	15.70									
65-C						45		+74.15	27.10									
65-D						26		+26.21	15.70									
65-E						7		-20.51	4.30									
66-A		Ti-B	VIBRATION	N.A	70	7	MAX	-20.52	4.30	—	73.0	10	—	337	N.A.	N.A.	N.A.	25
66-B						26		+26.21	15.70									
66-C						45		+74.06	27.10									
66-D						26		+26.27	15.70									
66-E						7		-20.48	4.30									

ADDITIONAL STATIC TEST DATA

NOTE: TRUE STRAIN LEVEL = 1680με AT A 15 LB LOAD FOR Ti SPECIMENS AND 1170με AT A 35 LB LOAD FOR Fe SPECIMENS.
NOTE: A POSITIVE LOAD PRODUCES POSITIVE STRAIN (TENSION) ON THE CC SIDE. NOTE: THE INDICATED με IS ALWAYS ON THE SAME SIDE AND NEAR THE XDCR.

TEST POINT	DATE/TIME	TEST SPECIMEN	TYPE LOAD	LOAD (LB)	T (°F)	P(PSIA)	INDICATED MICRO-STRAIN	TEST XDCR. OUTPUT DCMV	EXCITATION DCV	STRAIN EFFECT ΔMV	STRAIN EFFECT Δ PSI	UNTWIST ANGLE (DEG.)	TEST XDCR. S/N	TEST XDCR. SENS. (μV/psi)	STRAIN SENS. (PSI/με)	COMMENTS
1	5-16-77	Fe - C	TENSILE	3000	70	14.7	—	—	—	—	—	0.63	N.A.	N.A.	N.A.	BLADES RETURNED TO ZERO ANGLE WHEN LOAD REMOVED.
2	5-16-77	Fe - C	↓	3000	260	↓	—	—	—	—	—	0.63	↓	↓	↓	
3	6-1-77	Ti - C	↓	1600	70	↓	—	—	—	—	—	0.13	↓	↓	↓	
4	6-6-77	↓	↓	1600	300	↓	—	—	—	—	—	0.29	↓	↓	↓	
5	6-7-77	↓	↓	1600	300	↓	—	—	—	—	—	0.80	↓	↓	↓	
1	6-16-77	Ti - C	BENDING	15	68	14.7		19.77	15	0.98	0.33	N.A.	2498-7-65	2.97	-0.20	
1	6-17-77	BAR	BENDING	N.A.	70	14.7	+50	-20.76	15	-0.08		N.A.	2499-4-1	1.61		XDCR. MOUNTED TO HASTELLOY CONSTANT STRAIN BAR WITH EASTMAN 910 CEMENT. REFERENCE STRAIN GAGE MOUNTED NEAR XDCR.
2	↓	↓	↓	↓	↓	↓	+100	-20.87	↓	-0.20		↓	↓	↓		
3	↓	↓	↓	↓	↓	↓	-50	-20.57	↓	+0.10		↓	↓	↓		
4	↓	↓	↓	↓	↓	↓	-100	-20.47	↓	+0.21		↓	↓	↓		
5	↓	↓	↓	↓	↓	↓	+200	-21.30	↓	-0.39		↓	↓	↓		
6	↓	↓	↓	↓	↓	↓	+300	-21.49	↓	-0.58		↓	↓	↓		
7	↓	↓	↓	↓	↓	↓	+400	-21.66	↓	-0.76		↓	↓	↓		
8	↓	↓	↓	↓	↓	↓	+500	-21.83	↓	-0.94		↓	↓	↓		
9	↓	↓	↓	↓	↓	↓	-500	-19.88	↓	+1.00	0.62	↓	↓	↓	-1.24	
1	6-21-77	BAR	BENDING	N.A.	70	14.7	-1000	-25.79	15	+0.10	0.06	N.A.	2499-4-1	1.61	-0.06	MOUNTED WITH 5-MIL SHIM OF 732 RTV.
2	6-21-77	BAR	BENDING	N.A.	70	14.7	+1000	-26.01	15	-0.10	0.06	N.A.	2499-4-1	1.61	-0.06	
1	6-21-77	BAR	BENDING	N.A.	70	14.7	+50	+14.80	15	-0.20		N.A.	2500-1-102	2.57		XDCR. MOUNTED WITH EASTMAN 910 CEMENT.
2	6-21-77	↓	↓	↓	↓	↓	0	+15.00	↓		AVG =	↓	↓	↓		
3	6-21-77	↓	↓	↓	↓	↓	+50	+14.88	↓	- .12	0.06	↓	↓	↓	-0.93	
1	6-22-77	Ti - C	BENDING	15	68	14.7	-1352	18.66	15	+1.05	0.35	N.A.	2498-7-65	2.97		
1	6-24-77	BAR	BENDING	N.A.	70	14.7	+500	-27.68	15	-0.06		N.A.	2499-4-1	1.61	-0.07	XDCR. MOUNTED WITH ONE MIL THICKNESS OF 732 RTV.
2	6-24-77	↓	↓	↓	↓	↓	+1000	-27.74	↓	-0.12	0.07	↓	↓	↓	↓	
3	6-24-77	↓	↓	↓	↓	↓	-500	-27.54	↓	+0.06		↓	↓	↓	↓	
4	6-24-77	↓	↓	↓	↓	↓	-1000	-27.47	↓	+0.12	0.07	↓	↓	↓	↓	
1	6-29-77	Ti - C	BENDING	+15	303	14.7		37.35	15	+0.14	0.05	N.A.	2498-7-65	2.97	-0.03	AFTER 24-HR SOAK AT 300F
2	6-29-77	Ti - C	BENDING	-15	298	14.7		36.94	15	-0.15	0.05	N.A.	↓	↓	-0.03	
3	6-29-77	Ti - C	BENDING	-15	73	14.7		18.61	15	-0.98	0.33	N.A.	↓	↓	-0.20	
1	6-29-77	BAR	CHEMICAL	AIR	73	14.7	0	27.64	15	—	—	N.A.	2499-4-1	1.61	N.A.	
2	1400	↓	↓	↓	↓	↓	↓	27.66	↓	—	—	↓	↓	↓	↓	
3	1424	↓	↓	↓	↓	↓	↓	27.62	↓	—	—	↓	↓	↓	↓	
4	1427	↓	↓	RTV	↓	↓	↓	27.46	↓	—	—	↓	↓	↓	↓	DOW CORNING 732 SILASTIC
5	1442	↓	↓	↓	↓	↓	↓	27.50	↓	—	—	↓	↓	↓	↓	
6	1454	↓	↓	↓	↓	↓	↓	27.54	↓	—	—	↓	↓	↓	↓	
7	1457	↓	↓	ALCOHOL	↓	↓	↓	27.55	↓	—	—	↓	↓	↓	↓	2 PROPANOL = $CH_3CHOHCH_3$
8	1500	↓	↓	↓	↓	↓	↓	27.57	↓	—	—	↓	↓	↓	↓	
9	1524	↓	↓	↓	↓	↓	↓	27.27	↓	—	—	↓	↓	↓	↓	
10	1527	↓	↓	FREON	↓	↓	↓	0	↓	—	—	↓	↓	↓	↓	FREON TF = PMC 9087

ADDITIONAL STATIC TEST DATA

TEST POINT	DATE/TIME	TEST SPECIMEN	TYPE LOAD	LOAD (LB)	T (°F)	P(PSIA)	INDICATED MICRO-STRAIN	TEST XDCR. OUTPUT DC mV	EXCITATION DCV	STRAIN EFFECT Δ mV	Δ PSI	UNTWIST ANGLE (DEG.)	TEST XDCR. S/N	TEST XDCR. SENS. (mV/PSI)	STRAIN SENS. (PSI/1000 με)	COMMENTS
11	1535	BAR	CHEMICAL	AIR	73	14.7	0	27.62	15	—	—	N.A.	2499-4-1	1.61	N.A.	
12	1603	BAR	CHEMICAL	AIR	73	14.7	0	27.71	15	—	—		2499-4-1	1.61	N.A.	
1	7-12-77	Ti-B	BENDING	-15	74	14.7	-1486	+3.78	15	+0.71	0.29		2498-7-62	2.48	-0.17	
1	7-13/1626	Ti-B	BENDING	0	76	14.7	0	+3.20	15	—	—		2498-7-62	2.48	N.A	
2	1940				291			-4.42		—	—					
3	2345				300			-6.37		—	—					
4	7-14/1940				297			-8.78		—	—					
5				-15	302		-1741	-8.40		+0.34	0.14				-0.08	
6	2115			-15	76		-1567	-2.95		+0.63	0.25				-0.15	
7	7-15-77			15	77		+1395	-3.67		-0.65	0.26				-0.15	
8	1635			0	77		0	-3.02		—	—				N.A.	
1	7-15-77	Fe-B	BENDING	15	76	14.7	+487	+4.59	15	-0.23	0.09		2498-7-68	2.51	-0.08	
2	7-18-77			35	78		+1148	+4.40		-0.54	0.22				-0.19	
3	1900			0	77		0	+4.97		—	—				N.A.	
4	2100				297			+46.21		—	—					
5	2230				302			-0.60		—	—					
6	7-19/2230				304			-5.91		—	—					
7				35	304		+1210	-6.26		-0.36	0.14				-0.12	
8	7-20/1355			0	300		0	-6.94		—	—				N.A.	
9	1645			35	296		+1232	-9.80		-0.37	0.15				-0.13	
10	1700			0	293		0	-9.34		—	—				N.A.	
11				35	79		+1140	-1.02		-0.53	0.21				-0.18	
12	2020			0	80		0	-0.49		—	—				N.A.	
1	8-8-77	Fe-C	BENDING	35	81	14.7	-1012	+1.20	15	+1.20	0.47		2498-7-58	2.58	-0.40	USING SPECIAL ADJUST-ABLE COMPENSATION MODULE ON XDCR.
2	8-10-77				300		-1235	13.27		+0.27	0.10				-0.09	
3	8-15-77				78		-1036	13.34		+1.28	0.50				-0.43	
1	8-15-77	Ti-C	BENDING	15	78	14.7		1.00	15	1.00	0.34		2498-7-65	2.97	-0.20	
2	8-18-77				300			134.04		0.14	0.05				-0.03	
3	8-22-77				75			131.68		0.96	0.32				-0.19	
1	1-12-78	Ti-C	BENDING	15	77	14.7		8.71	15	0.97	0.33		2498-7-65	2.97	-0.20	

ADDITIONAL VIBRATION TEST DATA

TEST POINT	DATE	TEST SPECIMEN	TYPE LOAD	T (°F)	P (PSIA)	(a) NOISE mV rms @ 0 g	(b) SIGNAL PLUS NOISE mV rms @ 500 g	(c) TRUE SIGNAL mV rms	(d) AMPLIFIER GAIN	(e) EXCITATION DURING CAL DCV	(f) EXCITATION DURING TEST DCV	(g) SENSITIVITY mV/PSI	(h) VIBRATION LEVEL PEAK g	CALCULATED PSI/g	(i) CALCULATED Pa/g	(j) CALCULATED %FSO/g
1	5-9-78	T_i - B	VIBRATION	70	14.7	2.25	4.90	6.16	326	15	7.17	2.48	500	3.18×10^{-5}	0.22	.00013
2	↓	T_i - C	↓	↓	↓	2.25	24.10	33.94	326	5	7.17	2.97	500	4.89×10^{-5}	0.34	.00020
3	↓	T_i - E	↓	↓	↓	2.25	7.60	10.27	326	15	7.17	2.84	500	4.64×10^{-5}	0.32	.00019

NOTE :

$$i = \frac{6895 \times \sqrt{2} \times \sqrt{b^2 - a^2} \times e}{d \times f \times g \times h}$$

$$c = \sqrt{2} \times \sqrt{b^2 - a^2}$$

j is based on a FSO of 25 psi

BENDING STRAIN TESTS OF E CONFIGURATION BLADES

JL & WM

DATE	TIME	SAMPLE	LOAD (LB)	DC MV OUTPUT	TEMP (°F)	LOAD DIRECTION	SENS (MV/PSI)	NOMINAL STRAIN LEVEL (με)	PSI/Kμε	SUPPLY VOLTS
5-16-78	1540	Ti-E	0	-7.54	73	CC-UP	2.74	1680		15
			15	-7.30				@15lb		
			0	-7.55						
			15	-7.31						
			0	-7.55						
			15	-7.28						
			0	-7.56						
			15	-7.31					0.054	
			0	-7.57						
			15	-7.31						
			0	-7.57						
			15	-7.31						
			0	-7.57						
5-16-78	1550	Fe-E	0	-4.41	73	CC-UP	2.76	1170		15
			35	-4.29				@35lb		
			0	-4.40						
			35	-4.31						
			0	-4.40						
			35	-4.31					0.028	
			0	-4.40						
			35	-4.31						
			0	-4.39						
			35	-4.31						
			0	-4.39						
			35	-4.31						
			0	-4.39						

☐ Run No.

DEFINITIONS: P_s = Pressure at rim of spin disk; P_m = Pressure at middle of spin disk; P_o = Pressure in spin disk plumbing at zero RPM.

NOTE: P_o pressures were set using the centerline xdcr. as a transfer standard.

SPIN TEST DATA (RIG 16273-1)

		NOMINAL			OUTPUT IN MILLIVOLTS				RIG SPEED	TEMPERATURES (°F)								STRAIN (με)						CALCULATED		
					A-0	B-0	B-7	℄																		
TEST POINT	DATE/TIME	T (°F)	P (PSIA)	G's	SN-9	SN-8	SN-15	SN-53	(RPM)	R=0	R=2	R=4	R=6	R=8	R=9.43	CAPSULE TOP	CAPSULE BOTTOM	LOC. 5	LOC. 10	LOC. 6	LOC. 7	LOC. 8	LOC. 9	P (PSIA)	P_s/P_m	P_s/P_o
1-1-C	10-3-77	80	1	0	-37.66	+18.92	-32.26	-29.74	0					80	80			0 ↓	0 ↓	0 ↓	0 ↓	0 ↓	0 ↓	1.04	-	-
-H	1610	80	22	0	+17.25	+65.27	+20.49	+15.91	0					80	80									22.02	-	-
1-2-C	10-5-77 1012	80	1	0	-36.949	+21.240	-32.010	-30.282	0					78	78									1.15	-	-
-H		80	22	0	+17.883	+67.180	+20.777	+15.250	0					78	78									22.02	-	-
-M	1042	80	45	0	+86.368	+126.910	+86.030	+71.300	0					78	78									47.78	-	-
-Q	1103	80	1	0	-36.499	+22.100	-31.371	-29.993	0					78	78											
2-1-C	10-5-77 1811	180	1	0	-42.73	N.A. ↓	N.A. ↓	-30.90	0					187	187									0.85	-	-
-H	1825	180	22	0	+14.85			+15.24	0					183	183									22.02	-	-
-M	1835	180	45	0	+77.96			+64.63	0					179	179									44.84	-	-
-Q	1843	180	1	0	-40.48			-30.50	0					175	175									0.99	-	-
2-2-C	10-6-77 2100	110	1	0	N.A. ↓	+17.44	-32.29	-30.28	0					110	110									0.98	-	-
-H	2112	110	22	0		+66.40	+20.32	+15.83	0					109	109									22.07	-	-
-M	2124	110	45	0		+121.50	+79.39	+65.97	0					108	108									45.24	-	-
-Q	2140	110	1	0		+17.79	-32.60	-30.24	0					108	108									0.97	-	-
2-3-C	10-6-77	110	1	0		+17.79	-32.60	-30.24	0					108	108									0.97	-	-
-H	2152	110	22	0		+66.86	+20.40	+15.85	0					107	107									22.06	-	-
-M		110	45	0		+120.84	+78.60	+65.21	0					106	106									44.86	-	-
5-1-C	10-7-77	70	1	0		+24.22	-32.39	N.A. ↓	0					73	73									1.00	-	-
-H		70	22	0		+71.48	+20.29		0					72	72									21.98	-	-
-M		70	45	0		+124.46	+78.89		0					72	72									44.96	-	-
-Q		70	1	0		+27.06	+29.29		0					72	72									2.09	-	-
5-2-C	10-7-77 1038	70	1	0		+26.47	-30.132	-28.768	0					72	72									1.72	-	-
-H		70	22	0		+71.78	+21.091	+15.616	0					72	72									21.99	-	-
-M		70	45	0		+124.78	+79.429	+65.240	0					72	72									44.93	-	-
-Q	1103	70	1	0		+27.16	-30.124	-28.544	0					73	73									1.77	-	-
6-1-C	10-7-77 1516	80 ↓		0	$\boxed{4}$	+24.238	N.A. ↓	-30.703	0	71.8	72.5	72.8	72.9	72.8	73.1	70.4	70.2							0.93	-	-
-D	1559		1	27.5K		+24.915		-30.292	10,132	104.0	74.3	71.4	72.7	73.1	73.5	93.7	102.5	+35	-25	-320	-338	+155	+70	1.135	1.4622	1.220
-E	1626			0		+23.440		-29.910	0	94.2	81.7	75.8	76.0	76.4	76.4	96.8	104.6							1.29	-	-
-H				0		+60.193		+5.257	0						76.7	86.9	95.1							17.30	-	-
-I			22	27.5K		+70.935		+0.135	10,132	104.9	79.8	73.6	74.6	74.8	74.9	87.6	93.9	+35	-25	-335	-354	+142	+60	20.826	1.4600	1.204
-J				0		+60.229		+5.543	0						78.4	97.2	102.0							17.43	-	-
-M				0		+102.644		+45.103	0						78.7	90.3	98.1							35.87	-	-
-N			45	27.5K		+123.980		+35,070	10,132	104.1	83.1	75.5	76.6	76.2	75.8	90.1	99.9	+30	-10	-357	-380	+125	+50	42.992	1.4581	1.199
-O				0		+103.500		+45.750	0						78.6	99.7	107.0							36.17	-	-
-Q				0		+23.480		-30.130	0						79.9	99.2	106.9							0.99	-	-

☐ Run No.

SPIN TEST DATA (RIG 16273-1)

TEST POINT	DATE/TIME	NOMINAL T (°F)	NOMINAL P (PSIG)	NOMINAL G'S	OUTPUT IN MILLIVOLTS A-O SN-9	B-O SN-8	B-7 SN-15	℄ SN-53	RIG SPEED (RPM)	TEMPERATURES (°F) R=0	R=2	R=4	R=6	R=8	R=9.43	CAPSULE TOP	CAPSULE BOTTOM	STRAIN (με) LOC. 5	LOC. 10	LOC. 6	LOC. 7	LOC. 8	LOC. 9	CALCULATED P (PSIA)	P_0/P_m	P_b/P_c
7-1-C	10-10-77 1405	115		0	[4] N.A.	+14.623	N.A.	-31.271	0						118.2	79.7	88.3							0.45	1	1
-D	1420		1	27.5K		+15.539		-31.271	10,132	113.7	105.7	112.3	113.2	113.6	113.9	85.7	96.4	+45	-15	-330	-352	+158	+65	0.579	1.4244	1.287
-E	1427			0		+14.538		-30.986	0						116.3	95.5	101.0							0.67	1	1
-H	1502			0		+58.218		+8.725	0						113.5	86.8	95.0							18.91	1	1
-I	1521		22	27.5K		+69.818		+3.822	10,132	121.1	104.8	110.5	111.3	110.7	111.4	92.6	102.6	+19	-31	-337	-366	+148	+61	23.889	1.4263	1.263
-J	1538			0		+59.069		+8.947	0						112.3	99.2	105.7							19.02	1	1
-M	1612			0		+105.391		+50.580	0						110.5	88.7	97.0							38.41	1	1
-N	1659		45	27.5K		+129.270		+41.687	10,132	128.6	105.2	107.3	107.6	108.9	109.4	104.6	116.0	+22	-25	-338	-363	+143	+55	47.865	1.4283	1.246
-O	1717			0		+107.970		+51.640	0						110.4	107.8	113.8							38.90	1	1
-Q			1	0		+17.669		-30.360	0						108.1	90.8	97.7							0.84	1	1
9-1-C	10-11-77 1006	90		0		+21.238		-30.621	0						78.6	74.9	83.2							0.87	1	1
-D	1112		1	27.5K		+20.776		-30.334	10,132	118.5	88.1	83.3	83.9	86.1	87.0	105.5	117.1	+4	-28	-371	-368	—	+93	1.056	1.4495	1.214
-E	1126			0		+19.442		-29.985	0						88.1	110.9	116.8							1.16	1	1
-H				0		+60.980		+8.355	0						87.2	76.2	78.8							18.85	1	1
-I	1414		22	27.5K		+73.609		+4.213	10,132	117.8	90.4	88.1	88.9	91.1	91.8	108.2	116.1	0	-21	-368	-370	—	+90	23.149	1.4450	1.228
-J				0		+62.366		+9.891	0						92.5	113.9	116.7							19.55	1	1
-M				0		+105.148		+49.612	0						91.5	89.6	100.1							38.05	1	1
● -N	1607		45	27.5K		+128.390		+39.320	10,132	120.8	93.4	89.8	89.8	91.3	93.4	107.8	118.3	+7	-28	-304	-385	—	+82	46.028	1.4439	1.210
-O	1623			0		+107.623		+51.037	0						92.8	117.9	122.4							38.71	1	1
-Q	1734			0		+102.023		+30.235	0						92.4	87.8	100.1							0.99	1	1
10-1-C	10-12-77 1438	90		0	[5]	+20.416		-31.300	0						78.6	79.1	85.0							0.24	1	1
-D	1458		1	55K		+21.003		-31.111	14,330	102.7	78.2	76.2	77.9	80.9	81.0	100.5	120.1	+138	-35	-700	-622	—	+172	0.346	2.1198	1.440
-E				0		+19.082		-30.739	0						83.9	115.2	122.8							0.50	1	1
-H	1537			0		+43.656		-8.206	0						82.7	101.1	112.3							10.89	1	1
-I	1559		15	55K		+56.894		-14.337	14,330	121.0	87.0	81.9	83.9	87.0	87.6	113.2	128.4	+162	-32	-728	-631	—	+161	15.256	2.1013	1.401
-J				0		+43.169		-7.735	0						87.9	121.8	126.1							11.11	1	1
-M	1633			0		+68.603		N.A.	0						87.1	116.8	108.6							21.76	1	1
-N	1707		30	55K		+94.530			14,330	121.5	92.4	86.0	88.8	92.5	93.4	114.7	135.0	+150	-28	-745	—	—	+165	30.369	2.0869	1.396
-O	1721			0		+69.757			0						94.8	130.8	137.2								1	1
20-1-C	10-13-77 1025	90		0	[6]	+21.574			0						78.7	71.4	73.1							1.00	1	1
-D	1052		1	75K		+22.687			16,734	110.6	76.4	78.3	82.4	89.1	89.5	106.1	117.6	+489	-38	-995	—	—	+248	1.631	2.7589	1.631
-E	1107			0		+19.737			0						89.7	120.5	122.2								1	1
-H	1335			0		+34.305			0						85.9	76.5	81.6							7.06	1	1
-I	1357		11	75K		+46.513			16,734	116.3	84.4	85.4	89.8	95.6	90.1	107.3	117.9	+285	-55	-1020	—	—	+242	11.421	2.7267	1.618
-J	1414			0		+33.469			0						98.0	119.8	123.5								1	1
-M	1500			0		+50.803			0						94.1	90.1	100.8							14.71	1	1
-N	1532		22	75K		+76.190			16,734	130.5	94.2	96.0	100.0	106.0	99.7	113.0	127.6	+302	-46	-1048	—	—	+242	23.473	2.6770	1.596
-O	1551			0		+50.995			0						108.1	124.4	129.4								1	1
● 15-1-C	10-17-77 0951	70		0	[7]	+21.352			0	75.2	75.6	75.8	75.8	75.8	76.1	72.3	72.4							0.17	1	
-D	1046	70	1	90K		N.A.			19,330	107.8	72.0	71.9	113.8	83.2	71.1	99.1	111.9	+452	-196	-1287	—	—	—	—	3.3607	

DEFINITIONS: P_s = Pressure at r.m of spin disk; P_m = Pressure at middle of spin disk; P_o = Pressure in spin disk plumbing at zero RPM.

☐ Run No. SPIN TEST DATA (RIG 16273-2)

		NOMINAL			OUTPUT IN MILLIVOLTS			RIG SPEED	TEMPERATURES (°F)								CALCULATED		
					A-0	A-7	REF.												
TEST POINT	DATE / TIME	T (°F)	P (PSIA)	G's	SN-9	SN-3	SN-10	(RPM)	R=0	R=2	R=4	R=6	R=8	R=9.43	CAPSULE TOP	CAPSULE BOTTOM	P(PSIA)	P_s/P_m	P_s/P_o
	12-16-77		8																
1-1-A	2045	70		0	-67.888	+70.496	10.775	0									17.915		
-B	2051			0	-119.037	+39.245	0.656	0						72.1	75.2	74.5	0.851		
-C	2056		1	27.5K	-117.200	+39.390	—	10,133	83.8	75.4	69.7	70.1	70.2	70.3	79.1	90.6	1.062	1.465	1.249
-D	2100			0	-119.020	+38.850	—	0											
-E	2113			0	-87.998	+57.684	0.658	0									.854		
-F	2120			0	-68.108	+70.536	10.774	0						70.7	87.0	103.0	17.913		
-G	2130		22	27.5K	-53.700	+78.602	—	10,133	84.5	77.0	70.9	71.0	71.7	71.9	90.1	118.5	22.244	1.463	1.242
-H	2133			0	-68.094	+70.307	—	0											
-I	2139			0	-67.915	+69.623	10.768	0									17.903		
-J	2209			0	-9.120	+106.673	21.705	0						72.3	89.2	103.5	36.347		
-K	2219		45	27.5K	+17.530	+121.842	—	10,133	89.8	81.9	74.4	70.5	70.2	70.3	96.3	128.6	45.390	1.463	1.249
-L	2225			0	-8.427	+104.635	—	0											
-M	2237			0	-7.758	+105.448	21.782	0									36.477		
-N	2243			0	-66.431	+69.443	10.747	0									17.868		
-O	2248		45	0	+19.123	+122.501	26.846	0									45.016		
	12-19-77																		
2-1-A	1415	70	9	0	-77.835	+64.030	8.888	0											
-B	1429			0	-96.532	+52.841	0.613	0											
-C	1438		1	55K	-73.620	—	—	14,330											
-D	1443			0	-91.188	+55.680	—	0											
-E	1454			0	-121.248	+37.093	0.648	0											
-F	1456			0	-78.340	+63.544	8.881	0						70.4	104.4	123.0			
-G	1504		22	55K	-52.973	—	—	14,330	89.4	78.8	153.0	71.0	72.0	72.0	112.0	154.0	21.634	2.102	1.470
-H	1507			0	-77.490	+65.220	—	0											
-I	1510			0	-78.230	+64.722	8.880	0											
-J	1541			0	-30.507	+93.533	18.206	0						71.4	100.1	116.2			
-K	1611		45	55K	+20.048	—	—	14,330	87.8	86.4	113.6	72.1	73.6	73.8	145.0	165.7	45.823	2.114	1.505
-L	1615			0	-29.084	+94.834	—	0											
-M	1652			0	-27.501	+95.451	18.273	0											
-N	1655			0	-77.778	+64.692	8.902	0											
-O	1705		45	0	+18.075	+123.664	26.820	0											
	12-19-77																		
3-1-A	1953	70	10	0	-82.099	+62.109	8.093	0											
-B	2004			0	-122.322	+37.543	0.596	0						75.9	77.0	76.9			
-C	2017		1	75K	-119.541	—	—	16,734	90.2	81.7	118.0	72.4	74.3	75.2	109.8	151.5	1.267	2.771	1.689
-D	2021			0	-122.131	+37.796	—	0											
-E	2031			0	-122.553	+37.296	0.600	0											
-F	2049			0	-82.823	+61.397	8.051	0						78.9	107.4	123.0			
-G	2103		22	75K	-50.637	—	—	16,734	92.2	82.1	100.8	75.9	77.5	79.4	125.5	157.2	21.793	2.772	1.636
-H	2107			0	-81.606	+62.577	—	0											
-I	2114			0	-82.783	+61.937	8.060	0											
-J	2119			0	-38.134	+89.208	16.378	0						81.2	121.6	144.3			
-K	2136		45	75K	+21.998	—	—	16,734	94.9	93.0	99.5	77.8	81.8	83.3	133.7	156.6	44.106	2.755	1.612
-L	2141			0	-38.110	+89.271	—	0											
-M	2156			0	-37.164	+87.985	16.430	0											
-N	2201			0	-82.244	+60.056	8.054	0											
-O	2206		45	0	+18.960	+122.728	26.721	0											

☐ Run No. SPIN TEST DATA (RIG 16273-2)

		NOMINAL			OUTPUT IN MILLIVOLTS			RIG SPEED	TEMPERATURES (°F)								CALCULATED		
					A-0	A-7	REF												
TEST POINT	DATE/TIME	T (°F)	P (PSIA)	G'S	SN-9	SN-3	SN-10	(RPM)	R=0	R=2	R=4	R=6	R=8	R=9.43	CAPSULE TOP	CAPSULE BOTTOM	P(PSIA)	P_s/P_m	P_s/P_a
	12-20-77																		
2-2-A	0905	70	9	0	-77.240	+64.880	8.920										14.787		
B	0935			0	-121.70	+38.06	.527							73.4	68.7	68.7	0.634		
C	0949		1	55K	-18.875	—	—	14.330	85.4	80.0	137.7	72.1	70.8	73.4	92.8	133.9	0.962	2.108	1.518
D	0953			0	-121.350	+38.160	—												
E	0957			0	-121.64	—	.514										0.612		
F	1001			0	-78.09	+63.384	8.916							73.9	91.6	114.2	14.780		
G	1016		22	55K	-51.000	—	—	14.330	91.5	86.2	115.0	75.2	75.6	75.0	112.0	162.0	22.103	2.108	1.495
H	1019			0	-76.461	+65.035	—												
I	1021			0	-77.82	+63.750	8.920										14.787		
	12-20-77		11																
4-1-A	1247	180		0	-76.03	+73.12	11.10										18.463		
B	1250			0	-131.34	+38.39	0.65							186.2	102.7	119.1	.841		
C	1302		1	27.5K	-129.08	—	—	10,133	144.3	150.0	177.0	168.2	169.0	168.5	122.7	151.6	1.033	1.381	1.229
D	1306			0	-130.34	+37.49	—												
E	1317			0	-127.53	+38.26	0.57										.706		
F	1321			0	-74.42	—	11.12							164.5	112.3	129.6	18.497		
G	1331		22	27.5K	-60.785	—	—	10,133	137.6	143.7	171.4	163.5	163.6	162.0	116.6	140.5	22.488	1.385	1.216
H	1335			0	-76.683	+72.390													
I	1340			0	-72.49	+73.10	11.37										18.919		
J	1357			0	-51.72	—	20.75										34.736		
K	1414		45		-32.750	—	—												
L	1418			0	-51.600	+87.180													
M	1426			0	-73.68	—	22.10										37.013		
N	1430			0	-83.23	—	11.33										18.851		
O			45	0	-22.20	—	26.99										45.859		
	12-20-77																		
5-1-A	1715	180	12	0	-84.483	+68.105	9.503										15.770		
B	1721			0	-130.700	+39.165	.601							193.6	106.6	126.7	.758		
C	1736		1	55K	-127.857	—	—	14,330	138.6	156.0	194.0	178.9	178.2	177.2	120.4	163.7	1.090	1.887	1.458
D	1739			0	-130.482	-0.276	—												
E	1750			0	-130.456	+39.010	.606										.767		
F	1802			0	-82.705	+68.482	9.556							178.8	115.5	134.3	16.658		
G	1816		22	55K	-57.694	—	—	14,330	138.4	156.9	185.2	182.5	183.6	179.6	131.2	165.6	25.953	1.883	1.446
H	1820			0	-82.513	+68.956	—												
I	1828			0	-82.905	—	9.537										15.827		

☐ Run No. SPIN TEST DATA (RIG 16273-2)

NOMINAL					OUTPUT IN MILLIVOLTS A-0	A-7	REF.	RIG SPEED	TEMPERATURES (°F)								CALCULATED		
TEST POINT	DATE/TIME	T (°F)	P (PSIA)	G'S	SN-9	SN-3	SN-10	(RPM)	R=0	R=2	R=4	R=6	R=8	R=9.43	CAPSULE TOP	CAPSULE BOTTOM	P(PSIA)	P_s/P_m	P_s/P_a
	12-21-77																		
4-2-I	1015	180	11	0	-74.370	+75.923	11.055	0									18.387		
J	1022			0	-10.902	+114.670	22.433	0						202.2	96.8	114.1	37.575		
K	1029		45	27.5K	-17.856	—	—	10,133	145.6	157.6	183.4	185.0	186.8	185.5	85.8	149.7	45.294	1.371	1.219
L	1032			0	-9.070	+115.612	—	0											
M	1045			0	-9.550	+114.830	22.33	0									37.401		
N	1051			0	-70.93	+76.462	11.06	0									18.396		
O	1056		45	0	+15.565	—	26.92	0									45.141		
	12-21-77	180	12																
5-2-I	1102			0	-78.940	—	9.490	0									15.715		
J	1106			0	-26.66	+103.530	19.850	0						175.8	93.9	109.1	32.207		
K	1112		45	55K	+24.930	—	—	14,330	137.6	146.5	183.2	169.4	170.0	170.5	100.9	155.2	46.997	1.903	1.459
L	1116			0	-23.733	+105.430	—	0											
M	1120			0	-25.882	+104.214	19.25	0									32.207		
N	1125			0	-79.202	+71.323	9.49	0									15.748		
O	1149		45	0	+14.10	—	26.60	0									46.602		
	12-21-77		14																
6-1-C	1812	150	45	90K	—	—	—	18,330											

PRECEDING PAGE BLANK NOT FILMED

APPENDIX IV

SPIN DISK DESIGN

Preceding page blank

INTRODUCTION

Contract NAS3-20296 required a spin test program with possible loads of 110,000 G's on pressure transducer configurations. Relatively simple spin fixtures, such as flat plates, investigated by P&WA would not support the high loads encountered.

CONCLUSION

The disk (ref. P&WA drawing L-108485), made of AMS 6415 has 15% burst margin over 20,750 RPM redline speed at an average disk temperature of 150°F and has the required features for the transducer test (see Figures IV-1 and IV-2 for summary).

RECOMMENDATIONS

1. The disk is recommended to support the pressure transducer at 110,000 G forces.

2. Quality inspections, sonic test, etc. specified on the layout are recommended for the raw material and final machined disk to insure the integrity of the disk.

3. Titanium material for the transducer support plate and aluminum for the cover are required to insure reduced bending moments, stresses and slope at the bolt circle of the disk web.

4. Plate retention bolt and nut strengths equivalent to or greater than AMS 6304 Rc 35-40 is required to insure adequate shear and tensile capability at the rig redline speed.

5. Disk is not coated to prevent rusting because of short duration of test, however, it should be inserted in some protective covering when stored.

6. A chamfer of 0.030-0.040 at the edge of the bearing surface on the transducer support plate should be provided to clear the 0.020-0.030 fillet radius on the disk shelf.

7. Monitor vibration during running to insure that the test rig does not operate at critical resonant speeds.

8. The transducer support plate unbalance should be counterbalanced with a weight located 180° from the plate.

DISCUSSION

The pressure transducer spin test program consists of possible test points at temperature up to 150°C (300°F), pressures up to 310 kPa (45 psi) and forces up to 110,000 G's.

The following criteria are provided to insure the structural integrity of the disk and to permit successful test objectives.

1. 15% burst margin over redline speed
2. 150°C maximum environment temperature at the area of the transducer
3. 110,000 G load at the transducer mount plate retention bolt area
4. ±0.3° slope from radial at the disk web face
5. Spin pit testing

The disk meets the test and structural requirements (Figures IV-1 and IV-2).

Figure IV-1 indicates the special features on the disk to insure structural integrity and test requirements.

Figure IV-2 summarizes the slopes and axial deflections at critical locations, and lists burst margins of the disk at different disk average temperatures.

Special features and reasons for providing these features on the spin disk are as follows (Figure IV-1):

1. Shelf for transducer support: A shelf is provided at the rim of the disk to support the transducer plate and cover. The axial induced moment of the shelf, plate and cover is high and must be balanced by adding material at the front side of the rim to reduce the bending stresses in the web and to keep the web radial slope to within 0.3° at the plate bolt area.

2. Symmetrical disk: The disk has a symmetrical bore feature whereby the bore and web radial centerlines line up. A flat radial surface at the rear of the disk web is provided to insure that the transducer plate seats properly against the web without interference with the bore/web transition radius.

   The bore to web transition surface at the front of the disk is extended radially beyond that of the rear transition to reduce the web bending stresses.

3. Bolt holes: Holes are provided in the web for the retention bolts of the transducer plate. A set of holes located 180° from the plate holes allows the addition of counterweights to balance the plate.

4. Rotor balance: The rotor can be balanced by providing a balance weight at a location 180° from the transducer plate.

   Additonal balance correction can be done by machining a 2.5 mm groove at the rear lip of the transducer support shelf.

5. Hub: A hub between the disk and support flange is provided with the proper length to insure that the flange is isolated from the influence of the disk and not susceptable to excessive radial growth and loads induced by the disk.

6. Bore diameter limitation: The bore diameter is limited to 11.7 cm to allow clearance for the assembly of the disk retention bolts.

7. Material selection: The material used for the spin disk is AMS 6415 Rc 35-40. Raw material with the required stock is available in stores. AMS 6415 would require a coating to prevent rusting, however, because of the short duration of the tests, coating is not provided. When stored the disk should be provided a protective covering to minimize rusting.

The disk and rig assembly were not analyzed for resonant or critical speed vibration. The rig should be monitored during operation to insure that it does not operate at speeds where vibration exists.

Unsymmetrical Disk Design Study

A disk configuration with a straight radial surface at the back of the disk from the bore to the plate support shelf was investigated to facilitate the bonding of and reduce the centrifugal pull on the instrumentation wires. Analysis indicates hoop bending stresses in the bore of 8.6×10^5 kPa (125,000 psi). The web radial slope at the plate retention area was calculated to be 0.8° which is 0.5° more than that of the symmetrical disk. Further iterations were therefore abandoned.

Transducer Support Plate and Cover

The titanium plate and aluminum cover were analyzed for bearing and buckling capability. The support plate with a maximum chamfer of 0.040 has a maximum bearing stress of 5.8×10^5 kPa with an allowable .2% yield strength of 6.2×10^5 kPa (90,000 psi) at 150°C (300°F). The cover has a bearing stress of 1.6×10^5 kPa (23,500 psi) with an allowable .2% yield strength of 2.8×10^5 kPa (40,000 psi) at 150°C (300°F).

Both the plate and cover have a buckling margin of 2 at a free unrestrained condition.

Plate and Cover Retention Bolts

Two bolts (0.375-24 UNF) are used to retain the support plate and cover. The strength of the material should be equivalent to or stronger than AMS 6304 Rc 35-40.

Shear stress in bolt due to the nut and bolt protrusion is calculated to be 3.0×10^5 kPa (43,700 psi) at 20.750 RPM with an allowable shear strength of 4.3×10^5 kPa (62,700 psi) at 150°C (300°F) for AMS 6304.

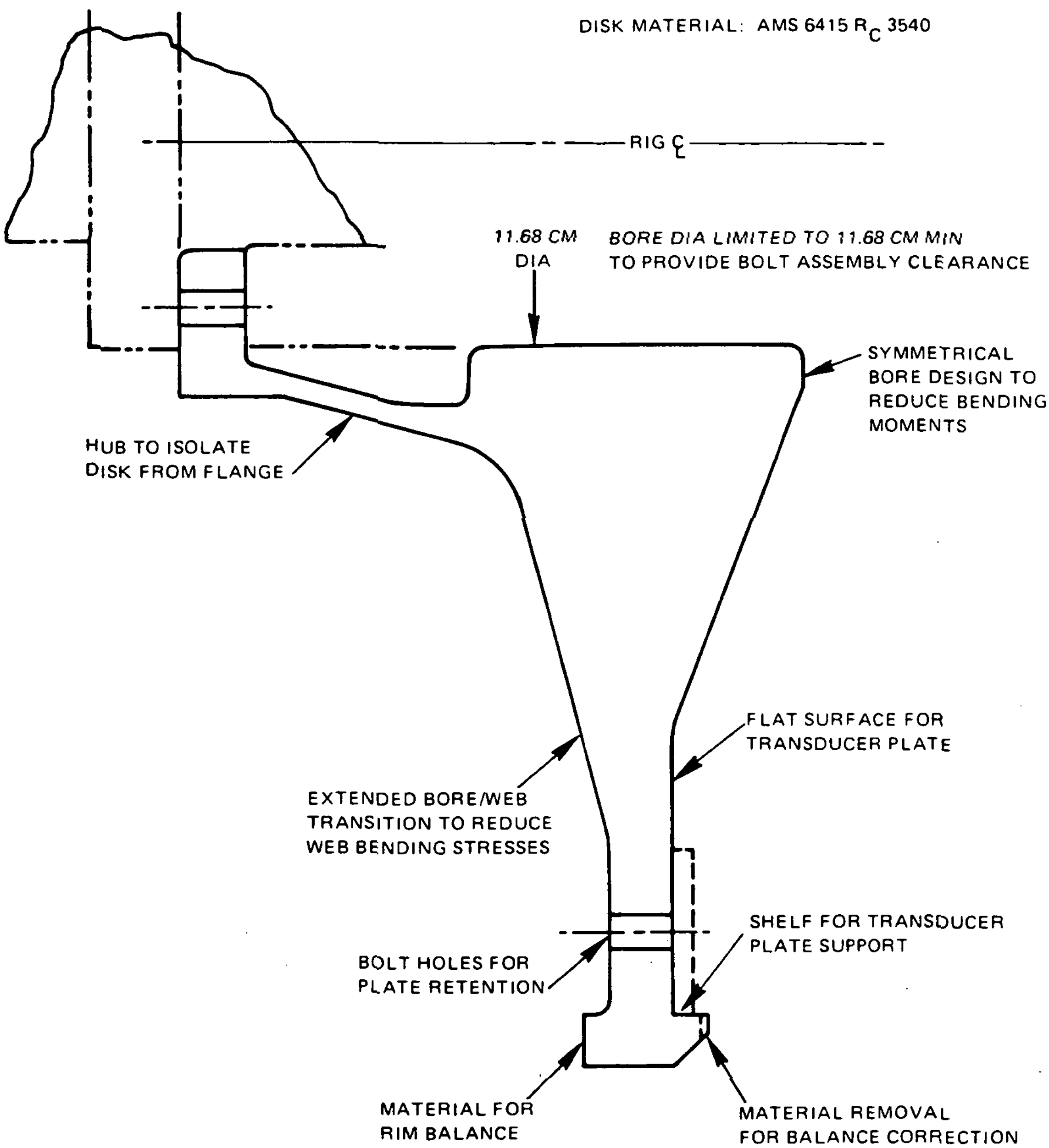

Figure IV-1 Spin Test Disk Special Features

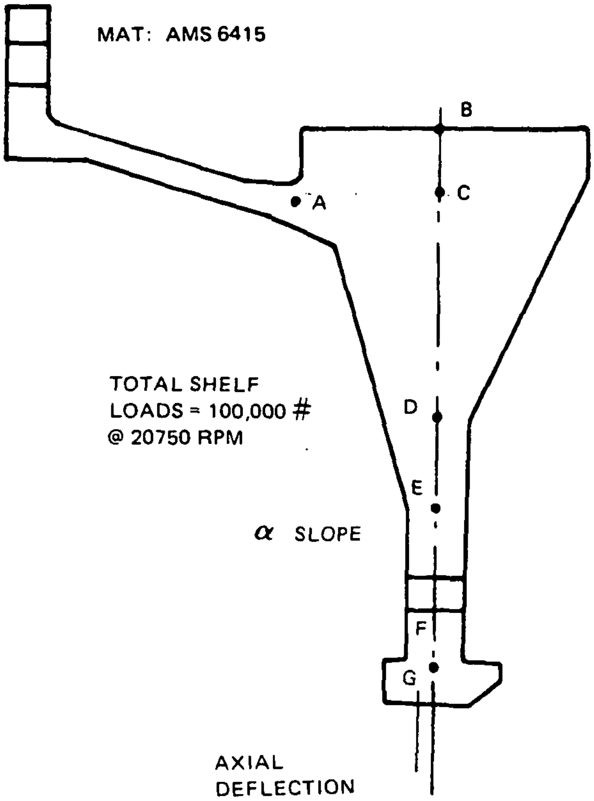

- RED LINE SPEED = 20750 RPM
- BURST MARGIN REQD. = 15%
- BURST SPEED = 23860 RPM
- LCF LIFE >1000 CYCLES AT RED LINE

BURST MARGIN AT DIFFERENT TEMPERATURES

TEMP.	B.M.
38°C (100°F)	1.154
93 (200)	1.147
150 (300)	1.140
204 (400)	1.128
260 (500)	1.102

LOC	RADIUS CM (IN)	SLOPE α DEGREE	AXIAL DEFLECTION CM (IN)
A	8.8 (3.45)	–	–
B	5.8 (2.30)	–	–
C	7.4 (2.90)	–	0
D	17.0 (6.70)	–	0.30 (0.012)
E	20.3 (8.00)	–	0.41 (0.016)
F	23.5 (9.24)	.28°	0.41 (0.016)
G	25.4 (10.00)	.28°	0.43 (0.017)

Figure IV-2 Spin Disk Summary

NOMENCLATURE

SI units are used throughout the main text of this report. The work was accomplished using customary engineering units. The raw data presented in Appendix III are therefore expressed in customary units. Also, the calculations procedure used to convert raw data to dimensionless ratios is presented in Table 2-IV in terms of customary units.

A	Area	(cm^2)
a	Centripetal acceleration	(cm/s^2)
E or E_{out}	Output voltage form pressure transducer	(volts)
E_{in}	Input voltage to pressure transducer	(volts)
G	Standard acceleration due to gravity, equal to 980.665 m/s^2	(m/s^2)
N	Angular velocity	(rpm)
P	Pressure	(kPa)
R	Gas Constant in $p=\rho RT$	(cm)
r	Radius	(cm)
T	Temperature	(K)
V	Volume	(cm^3)
$\Delta\epsilon$	Percent change in sensitivity due to applied strain	(percent)
$\Delta\rho$	Percent change in sensitivity due to 130 kPa change in pressure	(percent)
Δ_T	Percent change in sensitivity due to 129°C change in temperature	(percent)
ϕ	Transducer sensitivity	(mV/kPa)
ϵ	Strain, m/m, equal to fractional increase in length due to applied tensile load	(dimensionless)
$\mu\epsilon$	Microstrain, equal to a strain of a X 10^{-6}	(dimensionless)
ω	Angular velocity	(rad./sec)
θ_1	Angle between plane of pressure transducer diaphragm and radial plane of spin disk	(degrees)
θ_2	Angle between axis A-A of the semiconductor strain gage array (Figure 2-1) and the centripetal acceleration vector, measured in the plane of the diaphragm	(degrees)
ρ	Weight per unit volume	(N/cm3

REFERENCES

1. Carroll, J. T., "Dynamic Flow Studies by Application of Pressure and Velocity Sensors on Axial Flow Fan Blades," Instrumentation for Airbreathing Propulsion, *Progress in Astronautics and Aeronautics*, Vol. 34, 1973, The MIT Press, Cambridge, Massachusetts.

2. Hanson, D. B., "Application of Rotor Mounted Pressure Transducers to Analysis of Inlet Turbulence", Paper No. 9, AGARD 46th Propulsion and Energetics Panel Meeting, Monterey, Cal., Sept. 22-26, 1975.

3. Carta, F. O., *Unsteady Surface Flow Behavior on a Cascade of Airfoils Oscillating Below Stall,* United Technologies Research Center Report R75-912083-3, September 1975.

4. Fleeter, S., Novick, A. S., Riffel, R. E., and Caruthers, J. E., *An Experimental Determination of the Unsteady Aerodynamics in a Controlled Oscillating Cascade,* ASME Paper No. 76-GT-17, April, 1976.

5. Minkin, H. L., "Performance of Some Miniature Pressure Transducers Subjected to High Rotational Speeds and Centripetal Accelerations", NASA TMX-71791, NASA LeRC.

6. Hilten, J. S.; Vezzetti, C. F; Mayo-Wells, J. F.; and Lederer, P. S.; NBS Inter Agency Transducer Project, Progress Report No. 5, NBSIR 76-1144, Nov. 1, 1976.

DISTRIBUTION LIST

Address	No. of Copies
NASA Lewis Research Center Attn: David R. Englund (MS 77-1) 21000 Brookpark Road Cleveland, OH 44135	15
NASA Lewis Research Center Attn: John E. Dilley (MS 500-305) 21000 Brookpark Road Cleveland, OH 44135	1
NASA Scientific and Technical Information Facility Attn: Acquisitions Branch P. O. Box 33 College Park, MD 20740	10
NASA Lewis Research Center Attn: Library (MS 60-3) 21000 Brookpark Road Cleveland, OH 44135	2
NASA Lewis Research Center Attn: Report Control Office (MS 5-5) 21000 Brookpark Road Cleveland, OH 44135	1
General Electric Company Aircraft Engine Group Attn: Wayne Shaffernocker (MS H 78) Evendale, OH 45215	1
Kulite Semiconductor Products, Inc. Attn: John C. Kicks 1039 Hoyt Avenue Ridgefield, New Jersey 07657	1
Bolt Beranek and Newman, Inc. Attn: Richard E. Hayden 50 Moulton Street Cambridge, Massachusetts 02138	1
Arnold Engineering Development Center Attn: Marshall Kingery Arnold Air Force Station, TN 37389	1

Address	No. of Copies
Air Force Aero Propulsion Laboratory Attn: Joseph Batka/TBC Wright Patterson Air Force Base Dayton, Ohio 45433	1
Air Force Aero Propulsion Laboratory Attn: Everett E. Bailey Wright Patterson Air Force Base Dayton, Ohio 45433	1
Naval Post Graduate School Attn: Prof. R. P. Shreeve Department of Aeronautics (Code 67) Monterey, CA 93940	1
Math Sciences Northwest Attn: John Zumdieck P. O. Box 1887 Bellevue, Washington 98009	1
NASA Langley Research Center Attn: Vernie Knight (MS 477) Hampton, Virginia 23665	1
Pratt & Whitney Aircraft Palm Beach Gardens Facility Attn: John T. Carroll Bldg 30 (MS R 23) West Palm Beach, FL 33402	1
Teledyne CAE Attn: Walter Dindoffer 1330 Lasked Road Toledo, Ohio 43601	1
Garrett - AiResearch Attn: Robert Olive P. O. Box 5217 Phoenix, AZ 85010	1
Pennsylvania State University Applied Research Laboratory Attn: Frank S. Archibold P. O. Box 30 State College, PA 16801	1

DISTRIBUTION LIST (Cont'd)

Address	No. of Copies	Address	No. of Copies
Virginia Polytechnic Institute and State University Attn: W. F. O'Brien Jr. Mechanical Engineering Department Blacksburg, Virginia 24061	1	AVCO-Lycoming Division Attn: Michael S. Saboe, V. P. Engineering 550 South Main Stratford, Connecticut 06497	1
Detroit Diesel-Allison Attn: Robert L. Jay W-16 Box 894 Indianapolis, Indiana 46206	1	Detroit Diesel-Allison Attn: Thomas Bueher S-6 Box 894 Indianapolis, Indiana 46206	1
William Research Attn: Edward Worth, Head, Aero Dept. 2280 W. Maple Rd. Walled Lake, Michigan 48088	1	Williams Research Attn: Henry Moore, Head, Instr. Dept. 2280 W. Maple Rd. Walled Lake, Michigan 48088	1